Hyperpolarization in Coupled Multi-Spin Systems

Dissertation

zur Erlangung des akademischen Grades des Doktor der Naturwissenschaften eingerecht im Fachbereich Physik der Freien Universität Berlin

von

Sergey Evgen'evich

KORCHAK

aus Chabarowsk (Russland)

Mai 2010

1. Erstgutachter: Prof. Dr. Hans-Martin Vieth

2. Zweitgutachter: Prof. Dr. Robert Bittl

Tag der mündlichen Prüfung: 21 Juni 2010

Zusammenfassung

Kernspinresonanz-Experimente an skalar gekoppelten Vielspinsystemen wurden erstmals bei Variation des äußeren Magnetfelds in Kombination mit hoher spektraler Auflösung durchgeführt. Schwerpunkt dabei war die Untersuchung von hyperpolarisierten Kernspin-zuständen in den gekoppelten Systemen als Funktion der Feldstärke, um feldabhängige Effekte von feldunabhängigen zu unterscheiden und den Polarisationsgrad zu optimieren. Die experimentelle Realisierung der Feldvariation basiert auf schnellem mechanischen Transfer der Spins zwischen Positionen unterschiedlicher Feldstärke: für die gewünschte Spinevolution im variablem Feld bzw. den optimierten Nachweis im konstanten Hochfeld. Umfangreiche apparative Verbesserungen der Feldzyklisierung werden beschrieben, die insbesondere zu einer erheblichen Verbesserung der Auflösung und zur Erhöhung der Transfer-Geschwindigkeit bei genauerer Kontrolle des zeitlichen Ablaufs geführt haben. Zu diesem Zweck wurde unter anderem ein neuartiges Kompositmaterial mit verschwindender magnetischer Suszeptibilität entwickelt und für einen NMR-Probenkopf verwendet, dessen Metallteile zudem reduziert waren, um Wirbelstrom-Effekte beim Feldschalten zu unterdrücken. Außerdem wurde die Rechnersteuerung des Spektrometers komplett erneuert.

Dadurch gelang es die Signale der unterschiedlichen Spinpositionen im Molekül bei zeitlich genau gesteuerter Feldvariation im Bereich zwischen 100 μT und 7T mit einer Auflösung von 10^{-9} nachzuweisen. Alle Untersuchungen fanden an flüssigen Proben statt, wo die Wechselwirkungung unter den Spins durch skalare Kopplung gegeben ist, die in niederviskosen Flüssigkeiten im Gegensatz zu dipolarer Kopplung nicht ausgemittelt ist. Die Messungen zeigen, dass die skalare Kopplung trotz ihrer geringen Stärke große Auswirkungen auf die Evolution von Spinpolarisation hat, insbesondere wenn die Spinzustände Populationsverteilungen fernab vom thermischen Gleichgewicht aufweisen. Bei ausreichend kleiner externer Feldstärke wird der sogenannte Fall starker Kopplung erreicht, bei dem die Spin-Spin-Kopplung dominant wird und alle Hyperpolarisations- und Relaxationsexperimente beeinflusst.

So führt bei der Magnetfeldabhängigkeit der Spin-Gitter-Relaxation, der sogenannten Relaxationsdispersion (NMRD) die skalare Kopplung dazu, dass in Vielspinsystemen bei starker Kopplung sich die Relaxationsraten einander annähern, selbst wenn im Fall schwacher Kopplung die Raten der einzelnen Spins deutlich verschieden sind. Darüber hinaus wurden scharfe Strukturen in den Dispersionskurven nachgewiesen, die bei Feldern in der Nähe von Niveaukreuzungen (level anti-crossings) auftreten. Der Effekt der starken Spinkopplung konnte

von dem feldabhängigen Einfluss paramagnetischer Metallionen auf die Relaxationsdispersion diskriminiert werden.

In einer weiteren Gruppe von Experimenten wurden verschiedene Methoden zur Erzeugung von Hyperpolarisation untersucht: Chemisch induzierte dynamische Kernspinpolarisation (CIDNP), Parawasserstoff-induzierte Polarisation (PHIP) und dynamische Kernspinpolarisation vom Overhauser-Typ (DNP). Diese Experimente hatten das Ziel die Hyperpolarisation durch Steuerung von Spinkohärenzen zu manipulieren sowie die im Polarisationsprozess verschlüsselte Information für analytische Zwecke zu nutzen. In diesem Zusammenhang ließ sich nachweisen, dass sich die Hyperpolarisation auf alle gekoppelten Spins verteilt, wenn der Fall starker Kopplung gegeben ist. Die Untersuchungen ergaben, dass dieser Verteilungsprozess von kohärenter Natur ist und sich in Oszillationen der NMR-Signalamplitude niederschlägt, wenn die Dauer der Spinevolution im Niederfeld systematisch verändert wird, wobei der Transfer ins Nachweisfeld nicht-adiabatisch durchgeführt muss. Derartige Oszillationen konnten sowohl in CIDNP Experimenten als auch bei Relaxationsmessungen aufgezeigt werden.

Bei den DNP-Untersuchungen ging es hauptsächlich um die Überprüfung, inwieweit das elektronische Spinsystem durch gepulste Anregung und damit durch Ausnutzung kohärenter Spinbewegung effizienter aus dem thermischen Gleichgewicht getrieben werden kann als durch konstantes Pumpen. Ziel war unter es anderem, bei gleichem Polarisationsgrad die Erwärmung der Probe zu vermindern. Im Niederfeld sind die Bedingungen für solche Messungen wesentlich günstiger als im Hochfeld.

Eine besonders hohe Polarisation (PHIP) wurde mit Hilfe von Parawasserstoff erzielt, dem Singulett-Spinisomer von Wasserstoffgas, das sich bei tiefen Temperaturen anreichern lässt und zur Hydrierung von Styrol zu Ethylbenzol verwendet wurde. Der Einbau der beiden singulett-korrelierten H-Atome führt zu spektralen Polarisationsmustern, deren Änderung als Funktion des Magnetfeldes untersucht wurde. Insbesondere der Polarisationtransfer auf benachbarte Kerne ist von großem Interesse im Hinblick auf Kontrastmittel in der Kernspintomographie. Hier konnte gezeigt werden, dass solch ein Transfer besonders effektiv im Bereich von Level-Crossings ist. Numerische Simulationen konnten das gemessene Polarisationsmuster und seine Feldabhängigkeit mit hoher Genauigkeit reproduzieren.

Die Einsatzmöglichkeiten von Hyperpolarisation zur Analyse von chemischen Reaktionen wurden vor allem durch Kombination mehrer CIDNP-Techniken aufgezeigt. Untersuchungsobjekte waren Aminosäuren, Nukleotide und zyklische Ketone. Die umfangreichsten Studien betreffen kurzlebige Radikale der essentiellen Aminosäure Methionin

und verschiedener Peptide mit Methionin-Residuen, die bei Photoreaktionen mit Triplett-angeregten Farbstoffmolekülen entstehen. Dabei wurden sowohl Feldabhängigkeit als auch Zeitverlauf der dabei erzeugten Hyperpolarisation gemessen, um daraus Struktur der Radikale einerseits und Reaktionswege und -kinetik andererseits zu bestimmen. Die Ergebnisse zeigen unter anderem, dass in wässriger Lösung der pH-Wert das Verzweigungsverhältnis verschiedener Reaktionswege nicht nur über den Protonierungszustand der Ausgangssubstanz, sondern auch über die Reaktionsintermediate beeinflusst. Aufgrund dieser Kenntnis war es möglich vier verschiedene Methionin-Radikale nachzuweisen und mithilfe ihrer magnetischen Parameter (Hyperfeinkopplung, g-Faktor) zu charakterisieren. Bei den Peptiden konnten außerdem Effekte von Nachbargruppen oder der Einfluss von C und N Terminus gezeigt werden.

Insgesamt gesehen erwies sich die Variation der Magnetfeldstärke in Kombination mit hochauflösendem NMR-Nachweis als sehr vielseitige und aussagekräftige Methode, die sowohl für die optimale Generierung von Hyperpolarisation, für der Verlängerung ihrer Lebensdauer und beim Transfer auf gewünschte Spins eingesetzt werden, die aber auch bei der Analyse komplexer Reaktionen und der dabei auftretenden Zwischenprodukte wertvolle Informationen bringen kann.

Abstract

Nuclear magnetic resonance experiments on multi-spin systems using variation of the external magnetic field were performed with high spectral resolution. The main focus was investigating the behaviour of hyperpolarized nuclear spin states in the coupled spin systems in its dependence on the strength of the magnetic field in order to discriminate field dependent effects from others and to optimize the hyperpolarization (HP) yield. The experimental method of the field dependent measurements employs fast transfer of the spins between two field positions: the desired field at which the system is studied and the constant detection field. Extensive improvements of the field-cycling setup were introduced making the field variation faster and enhancing the spectral resolution. For this task, a novel material with compensated magnetic susceptibility was developed and a probehead with reduced metallic parts was constructed in order to suppress eddy currents and their magnetic field and, thus, preserve the detection field from disturbances. A new control unit of the experimental setup was devised allowing a better timing control of the experiments.

Thus, for the first time variable field measurements were obtained with high spectral resolution that allow distinguishing signals of individual nuclei in the molecules at a controllable time profile of field variation in a range between 100 μT and 7 T. All experiments were done on liquid state solutions, thus, the main interaction between the spins was scalar spin-spin coupling, which is not averaged in low viscosity liquids in contrast to dipolar spin-spin interaction. It was demonstrated that scalar coupling despite its small value has a high impact on the hyperpolarization experiments. At sufficiently low magnetic field the spins reach the regime of strong coupling where all hyperpolarization measurements as well as relaxation experiments are affected by the scalar interaction

In the nuclear magnetic relaxation dispersion (NMRD), i.e. in the dependence of the relaxation rate on the field strength, strong coupling in multi-spin systems was shown to lead to several distinct features that have to be taken into account in a quantitative analysis. For instance, strongly coupled spins tend to relax with a common rate even when at high field their relaxation is distinctly different. Also, pronounced peaks and dips were observed in the NMRD curves of systems with more than two nuclear spins 1/2 that were attributed to spin level anti-crossings. In addition, a site specific influence of paramagnetic additives in the solution on the NMRD of the solute was analysed. It was possible to separate this paramagnetic effect from the strong coupling effect.

Several methods of hyperpolarization were explored: Chemically Induced Dynamic Nuclear Polarization (CIDNP), Parahydrogen Induced Polarization (PHIP), and Dynamic Nuclear Polarization (DNP). Experiments were performed with the aim to manipulate hyperpolarization by control of spin coherences and to exploit the encoded information for analytical purposes. In all cases it was found that hyperpolarization is distributed among coupled spins when they are in the strong coupling regime. It was proven that the transfer has a coherent nature that manifests itself as quantum beats in the NMR signal amplitude upon changing the spin evolution time at the polarization field and subsequent non-adiabatic field variation to the high detection field. Such oscillations were observed both in CIDNP experiments and in relaxation measurements. Criteria for the polarization manipulation at variable field were derived and experimentally checked.

The DNP experiments were conducted with driving the electronic spins off equilibrium by applying a train of radio-frequency pulses in comparison with cw irradiation. The electron pumping was done at low field where the coupling factor is close to its theoretical maximum. Length, amplitude and repetition time of the pulses were optimized to achieve maximal DNP while keeping the average pumping power constant. For analyzing the data an adequate theoretical approach to pulsed DNP was developed. Optimal conditions for getting maximum signal enhancement at minimal microwave power and thus avoiding sample heating were studied on solute and solvent molecules.

Strong hyperpolarization was obtained in the hydrogenation reaction of styrene with the singlet spin isomer of hydrogen gas (parahydrogen) and studied at variable field. While for the protons originating from parahydrogen the high polarization was observed at all field amplitudes, in low field also polarization of the phenyl ring protons of the product was detected as a result of polarization transfer among strongly coupled spins. The highest transfer efficiency was seen at the field of spin level anti-crossing. The theoretical simulations reproduce the shape of the PHIP spectra in excellent agreement with the experimental data.

CIDNP techniques were applied to amino acids, nucleotides and cycloketones. The most extensive investigation was performed on radical intermediates of the essential amino acid methionine and of methionine containing peptides. Their reactions with photo-exited dye molecules were investigated by combining field dependent and time-resolved CIDNP that allowed revealing the radical structure and the reaction kinetics. It was found that in aqueous solution the pH influences the branching of the radical formation not only through the protonation state of the precursor but also through the reaction intermediates. Exploiting these results formation of four methionine radicals was observed. Simple methionine containing

dipeptides chosen to model the behaviour of methionine residues in proteins showed a behaviour similar to that of the free amino acid although they have several additional peculiarities. It was shown that the effects of neighbouring groups, of position at N vs C terminus, and of degenerate electron transfer have to be taken into account when studying proteins by CIDNP. The kinetic constants of the radical reaction as well as the nuclear relaxation times at the radical stage were determined from the CIDNP kinetics.

In summary, it was shown that field variation can be used for optimizing the generation of hyperpolarization, for preserving it from relaxation and for transferring it to target nuclei of interest. In addition, the hyperpolarization methods in combination with high spectral resolution were demonstrated to be versatile tools that allow extracting structural and dynamic information on diamagnetic molecules and on short-lived radical intermediates.

Abbreviations and symbols

ADC	Analog-to-digital converter
AMP	Adenosine monophosphate
AQS	9,10-anthraquinone-2-sulfonate
CBP	4-carboxybenzophenone
CIDNP	Chemically induced dynamic nuclear polarization
C-11	Cycloundecanone
DNP	Dynamic nuclear polarization
DP	2,2'-dipyridyl
E	Energy
EPR	Electron paramagnetic resonance
FID	Free induction decay
HFI	Hyperfine interaction
His	N-acetylhistidine
HP	Hyperpolarization
ISC	Intersystem crossing
J	Scalar spin-spin coupling
Met	Methionine
MRI	Magnetic resonance imaging
MTPA	3-methylthiopropylamine
NMet	N-acetylmethionine
NMR	Nuclear magnetic resonance
NMRD	Nuclear magnetic relaxation dispersion
P	Polarization
PHIP	Parahydrogen induced polarization
RF	Radio frequency
RP	Radical pair
SCRP	Spin correlated radical pair
T	Tesla
T_1	Longitudinal relaxation time
T_2	Transversal relaxation time
TR-CIDNP	Time-resolved CIDNP

Table of contents

Introduction

During the last decades nuclear magnetic resonance (NMR) spectroscopy has been established as standard analytical method in physics, material science, chemistry, medicine and the biosciences known for its high content of information. Magnetic resonance imaging (MRI) provides noninvasive spatial and functional information that is superior to any other imaging technique particular in the field of medical diagnostics. One major drawback is its comparatively low sensitivity resulting from the small energy difference between the involved spin states. Therefore, much effort has been directed to the improvement of detection sensitivity. The invention of pulse methods has drastically improved the sensitivity of NMR spectroscopy and MRI. Hardware developments such as magnets operating at fields of 23.5 Tesla and higher and cryoprobes with low detector noise temperature led to further improvements in sensitivity. However, these methods seem to have reached their limits. Another potential way of boosting the sensitivity of NMR is exploiting non-equilibrium spin polarization also called dynamic polarization or hyperpolarization. When optimized, this route is predicted to increase sensitivity of proton NMR by up to four orders of magnitude such that the routine single shot characterization of materials, even at picomole levels, will become possible.

Thus, the first aim of this work is to study the ways of optimization of the nuclear hyperpolarization in low viscosity solutions and their application. Hyperpolarization can be generated by several means. One of the ways is the Chemically Induced Dynamic Nuclear Polarization (CIDNP), which manifests itself in abnormal phases and amplitudes in the NMR signals of the diamagnetic products of spin-selective radical reactions.[1] Another technique that gives strong enhancements of the NMR lines is the Parahydrogen Induced Polarization (PHIP) caused by hydrogenation of molecules having a double or triple C-C bond by parahydrogen (i.e., H_2 molecules in their singlet spin state).[2] A more recent method is temporary association of a substrate and parahydrogen via a transition metal center in low magnetic field.[3] Several other methods of hyperpolarization include optical pumping[4-6] optical nuclear polarization[7,8] and transfer of polarization from the electronic spins by pumping electron transitions, dynamic nuclear polarization (DNP) (solid effect, thermal mixing, Overhauser effect)[9-11] or by cross-polarization between spin reservoirs by Hartmann-Hahn matching.[12,13]

Hyperpolarization is a transient phenomenon since spin polarization that is driven from equilibrium immediately starts to relax to its thermal equilibrium (spin lattice relaxation). Thus, the preservation of hyperpolarization is an important issue of the method. Moreover, slower relaxation allows to accumulate higher polarization levels since the formation process saturates

with the time constant of relaxation. The hyperpolarization generation includes also the polarization transfer to the nuclei of particular interest. It is, in many cases, the limiting stage of hyperpolarization that also has to compete with the relaxation. In this respect, the ability of using scalar spin-spin coupling is studied in order to establish an efficient way of polarization transfer.

The efficiency of polarization generation, of its transfer and of it relaxation is field dependent. For example, it is known that DNP in high field is less efficient than at low field making field variation studies of DNP relevant. The relaxation in low field, in many cases, is faster than in high field, however, in low field so-called long-lived spin states can occur that relax much slower than normal states.[14] Thus, the application of field variation techniques provides information on the optimal conditions of generating and preserving hyperpolarization.

Application of hyperpolarization is not limited to increase the sensitivity of NMR method. It has its own value as an analytical tool for studying physicochemical properties of molecular systems. CIDNP as hyperpolarization generated in the course of radical reactions is used to investigate radical reactions pathways and radical structures. Individual nuclei in the radicals are polarized according to their hyperfine interaction with the unpaired electron and, thus, to the spin density distribution. CIDNP is particular useful in investigations of short-lived radicals allowing to acquire information which is complementary to that obtainable by electron paramagnetic resonance (EPR). Together with high resolution NMR detection it allows atomic resolution, permits elucidation of the reaction mechanisms and a straightforward assignment of hyperfine coupling constants to the structure of reactive intermediates. Field dependent CIDNP measurements can provide additional magnetic resonance parameters (g-factor and electron exchange interaction) of the radicals. Time-resolved CIDNP allows investigation of such processes as paramagnetic nuclear relaxation for individual nuclei, intramolecular electron transfer and degenerate electron exchange. PHIP is used in the investigation of catalytic hydrogenation reactions, their intermediates and pathways.Despite its negative side of reducing the hyperpolarization nuclear spin relaxation, especially investigations of its field dependence known as nuclear magnetic relaxation dispersion provide valuable information on molecular mobility. Thus, the second task of this work is to study the ability of hyperpolarization techniques – field dependent and time-resolved – as analytical tools.

Since the hyperpolarization technique is still in its infancy, there are no commercially available setups for such hyperpolarization experiments. Modern high-resolution NMR spectrometers operate, for reasons of sensitivity and resolution, at a fixed magnetic field. Commercially available field-cycling setups do not provide sufficient spectral resolution. In order to study the influence of magnetic field dependent effects and to discriminate them against

field independent effects special equipment is needed. Such experimental aspects are discussed in a separate chapter.

The structure of the thesis is as follow: Chapter 1 provides the reader with some theoretical background, which will help in understanding the technique and observation described thereafter. First the hyperpolarization methods used here are introduced. Afterwards the polarization transfer by scalar spin-spin coupling is described.

The experimental technique is subject of Chapter 2. Here, experimental setups for the acquisition of field dependent and time-resolved HP spectra are depicted. As the centerpiece the field-cycling setup is described in detail because essential improvements were introduced during the PhD work. The modifications necessary for DNP measurements are shown at the end of the chapter.

In Chapter 3 the experiments concerning polarization transfer are described. The first part deals with the polarization transfer during CIDNP experiments in low magnetic field which allows precise time control. In the second part relaxation is shown to be influenced by the strong scalar coupling in the same way as hyperpolarization.

Topic of Chapters 4 and 5 are the PHIP and DNP experiments, respectively, with the aim to maximize the output of HP and re-distributing it over the entire molecule.

Application of hyperpolarization methods to the analysis of fast reactions and characterization of short-lived reaction intermediates is discussed in Chapter 6. Main examples are photo-CIDNP experiments on radical reactions of the amino acid methionine and related peptides.

The final Chapter 7 presents some conclusions and an outlook on future developments.

1. Hyperpolarization of nuclear spins

At thermal equilibrium the population, p, of the nuclear spin eigenstates is given by the Boltzmann factor, $p \propto \exp(-\Delta E/kT)$, with $\Delta E = \hbar\gamma B$, and varies at ambient conditions by less than 1.5×10^{-4} among all energy levels in diamagnetic molecules, even at the highest magnetic field presently used in NMR and for protons(stable isotope with the largest γ). Because of such a small polarization $P=(p_i-p_j)/(p_i+p_j)$ the sensitivity of NMR detection being proportional to P is low, thus limiting the application of NMR in many fields. For more than four decades numerous attempts are described in literature to increase the polarization by driving the spin system far off thermal equilibrium. These techniques were summarized as Dynamic Nuclear Polarization (DNP), but recently the term Hyperpolarization (HP) was introduced instead in order to make a better discrimination from microwave driven DNP methods. Here, several methods for generating HP are introduced; and their mechanisms are described; their dependence on the external magnetic field is discussed, in particular, the effects resulting from field variation are analyzed.

1.1 Chemically induced dynamic nuclear polarization

The term Chemically Induced Dynamic Nuclear Polarization (CIDNP)[1] is used for hyperpolarization observed in the NMR spectra of reaction products resulting from a radical reaction that often exhibit anomalous intensities and phases in their spectral lines. The polarization pattern arises from the spin evolution in transient radical pairs and is often used to characterize short-lived radical intermediates of chemical reactions. CIDNP is stored in the stable reaction products and during the time needed for nuclear spin-lattice relaxation, typically several seconds for protons, it can be considered as a finger print of the elusive radical species, which are often beyond the reach of EPR spectroscopy, despite the remarkable achievements in high-field EPR spectroscopy[15-17] during the last decades. Although only the diamagnetic reaction products are detected, the NMR lines of individual nuclei carry information on the paramagnetic stage encoded in the line intensities. Magnitude and phase differ characteristically from their value at thermal equilibrium, because spin polarization is formed in the radical strongly depending on the hyperfine coupling constant of the particular nuclei. CIDNP combining the analytical potential of high resolution NMR with high detection sensitivity and selectivity with respect to the hyperfine interaction constants provides information about the spin density distribution and the chemical structure of the short-lived intermediate radicals.[1]

Since its first observation by Bargon et al.,[18] CIDNP has been studied in detail and turned into a widely used tool for the investigation of chemical reactions with radical intermediates. The leading mechanisms of its formation are well understood and shall be reviewed only briefly. For more detailed information the reader is referred to various textbooks.[19-21]

Soon after the discovery of CIDNP it was proposed that the observed nuclear spin polarization is formed by the so called triplet mechanism. However, this model fails to explain many features of CIDNP and was superseded by the radical pair mechanism. Although the triplet mechanism can give nuclear polarization, it is usually much smaller than HP generated by the radical pair mechanism. Hence, the triplet mechanism will be described only briefly.

In the triplet mechanism electron spin polarization is generated in the photo excited triplet precursor. By an Overhauser type cross-relaxation process the initial electron polarization may be transferred to the nuclear spin system (see Chapter 1.2). The electron polarization arises from spin-selective intersystem crossing from excited singlet to triplet states governed by spin-orbit coupling rules. It depends on the molecular orientation in the external magnetic field and vanishes when the triplet molecule is rotating very rapidly. The next step is production of electron spin polarized radicals from the photoexited triplet precursor in course of the radical formation reaction. Population difference of the triplet sublevels may be transferred to the radical pair spin states resulting in Chemically Induced Dynamic Electron Polarization (CIDEP) if the radical pair producing reaction is faster than spin relaxation in the triplet state. It is followed by transfer of the electron spin polarization to the nuclear spins by cross-relaxation. finally the polarized radicals react with conservation of their polarization to diamagnetic products until longitudinal relaxation lead to thermalization of the polarization.

While the key processes of triplet mechanism is spin-selective polarization of the radicals the radical pair mechanism relies on spin-selective decay of a radical pair. This mechanism depends on the existence of a stage of interaction between two radicals in a solvent “cage”, when they constitute a radical pair (RP). The “cage” is a region of efficient reaction between two radicals forming a pair. In this region the radicals react only within the RP whereas the probability of their reaction with other radicals is negligible. While the two radicals constituting the RP diffuse with respect to each other, a reaction between them takes place only at their direct contact. The nuclear polarization is induced by singlet-triplet transitions occurring within the RP lifetime in the “cage” in combination with spin-selective product formation. While spin dynamics is different for low and high magnetic field the radical pair mechanism is basically the same. Since the formation of polarization in high field is particularly easy to visualize, the spin

sorting mechanism in high field will be discussed in more details. For the modifications at low field see Ref. 1

In Fig.1.1.1 the scheme of CIDNP formation in radical pair mechanism is shown. Although radical pairs can be formed in different ways here only laser induced photoreactions will be discussed. A liquid solution containing two types of molecules will be considered, a dye (D) and a quencher (Q). For simplicity the quencher molecule is assumed to have a single magnetic nucleus with spin 1/2 while the other molecule does not have any magnetic nuclei with HFI. Under light irradiation the dye molecule absorbs a photon and is excited into a higher singlet state. After internal conversion followed by inter-system crossing (ISC) due to spin-orbit interactions it goes into its lowest triplet state. The triplet formation in a molecule is usually fast (<1ns) compared to the laser pulse duration (5-15ns). The next step is quenching of the triplet excited dye by the quencher molecule. This process strongly depends on the nature of the reactants and proceeds usually via electron (e^-) or hydrogen atom ($H^\bullet$) transfer from Q to D or vice versa. Depending on the structure of starting molecule and the quenching mechanism the radicals formed can be charged or neutral. Another important factor influencing the quenching reaction is the solvent characteristics.

Since the total spin multiplicity does not change in the quenching process the primary "geminate pair" is generated in a well defined spin state (spin correlated radical pair, SCRP, denoted by an over bar). In the case considered the RP is born in its triplet state (Fig. 1.1.1). Subsequently the radical pair can react to give geminate diamagnetic products or the radical partners can leave the "cage" by diffusing apart. The probability that the components of such a separated geminate pair re-encounter is finite, but falls off with time, and in low-viscosity solvents it becomes negligible after ~10^{-7}s.

Let us assume that the radical pair is terminated by back e^- or ($H^\bullet$) transfer and can proceed only from a SCRP with the same multiplicity as the subsequent ground state which usually has singlet multiplicity. While caged there is little mixing of the spin states because of the large electronic exchange energy, i.e. the large singlet-triplet splitting in the spin correlated pair at close distance. In addition, at high magnetic field the energy levels of a triplet RP are split by Zeeman interaction into three sublevels: T_+, T_0, T_- (Fig. 1.1.1). The magnitude of this splitting equals $g\beta B$, where g is the electron g-factor, β is the Bohr magneton and B is the magnetic field strength. However, exchange interaction decreases exponentially with distance so that once the radicals separate J becomes negligible and the energy difference between the S and T_0 spin states is small. In this case, spin multiplicity can change under the influence of Zeeman and hyperfine

interaction (HFI). As a consequence of HFI, when the partner radicals in the spin-correlated RP re-encounter they have different degrees of electronic singlet and triplet character depending on their nuclear spin states. In contrast, in low magnetic field the Zeeman interaction is small and HFI can mix all triplet sublevels with singlet state.

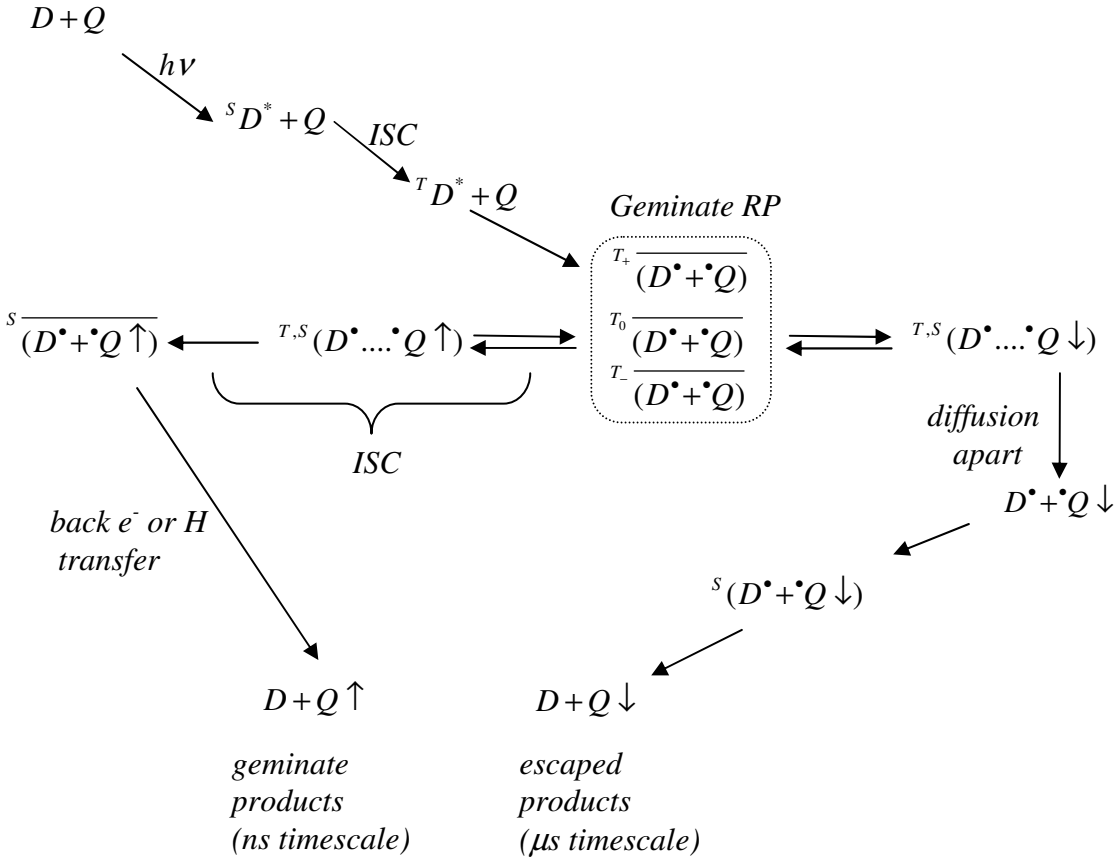

Figure 1.1.1. Radical pair mechanism of CIDNP formation in a low viscosity solution in high magnetic field. Here, SCRPs are denoted by a bar. For details see text.

Once radical are separated the electron spin state of RPs starts oscillates between triple and singlet multiplicity because of differences of their Larmor frequencies in the two radicals which depend on the electron g-factors of the two radicals and HFI. However, the lifetime of the RP is short compare to the oscillation frequency and ,thus, only the beginning of the oscillations are seen. Consequently, the rate of multiplicity mixing is proportional to difference in the Larmor precession frequencies which is different for nuclear spin states (α and β) of the radicals (Fig. 1.1.2). For a positive HFI constant and a g-factor higher for $^{\bullet}Q$ than for $^{\bullet}D$ the Larmor frequency is higher for the RP with the nuclear spin oriented along the field (α-projection). The rate of multiplicity mixing for RPs with α-projection is proportional to difference in g-factors and HFI constant, *A*, and equal to:

$$\Delta_{\alpha,\beta}\omega = \left| \frac{\beta \Delta g B}{\hbar} \pm \frac{1}{2} A \right| \qquad (1.1.1)$$

where, A is the HFI constant.

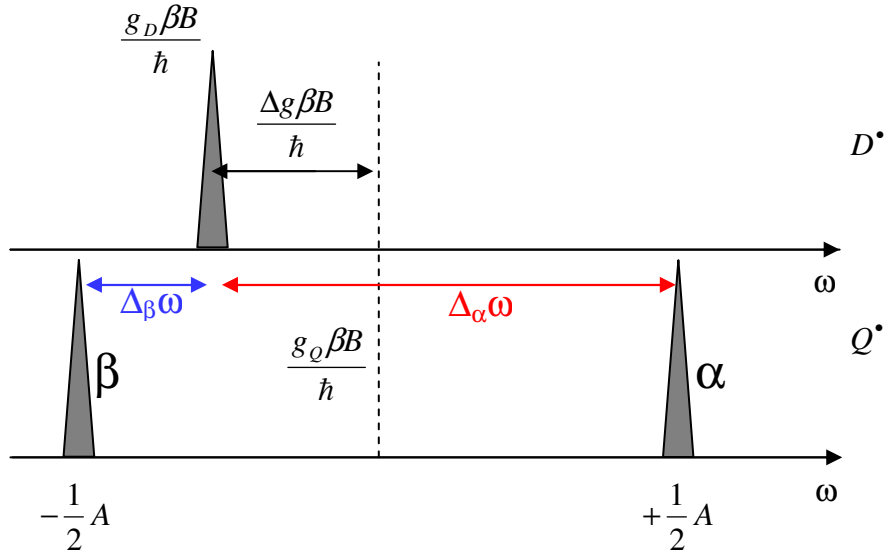

Figure 1.1.2. EPR spectrum of the radicals in a RP. A radical Q having a nuclear spin projection α has a higher dephasing rate than one with a β projection. Here, the HFI constant, A, is positive.

With the assumption that the reaction product formed at a re-encounter is a diamagnetic species in its singlet state the probability of formation is proportional to the singlet character of the spin correlated pair. Thus, the geminate products will be enriched in α nuclear spin states, $Q^{\uparrow}$, and depleted in β states, $Q^{\downarrow}$ (Fig. 1.1.1). This process termed "spin sorting" leads to nuclear spin polarization in the geminate products and to an equally large polarization of opposite sign in the remaining radicals. The spin-sorting process in typical organic radicals with hyperfine coupling constants of 15-60 MHz takes no more than 10 ns, and geminate product formation stops after 100 ns. The number of radicals that react in the geminate stage is a usually small, whereas most of them diffuse to bulk. Escaped radicals can re-encounter and form escape products with opposite to geminate polarization (Fig. 1.1.1).

The multiplicity mixing of the RP state and, hence, the efficiency of the sorting depends on the competition between hyperfine and difference in Zeeman interaction, $\left|g_1 - g_2\right|\beta B$, see Fig. 1.1.2; hence, the CIDNP effect varies with the external field. In return, this dependence on the magnetic field can be exploited for determining HFI couplings in the radicals as well as differences in their g-factors (see Chapter 1.2).While the high field part of the CIDNP depends on both the difference of g-factors and the hyperfine interactions of the radicals, the CIDNP at

low field is conditioned solely by the HFI. Although the CIDNP formation is in general a superposition of geminate polarization and polarization formed in bulk, the modeling used here is restricted to geminate polarization because there is so far no consistent theory worked out that describes electron and nuclear paramagnetic relaxation on the time scale of bulk reactions at low magnetic fields. The procedure employed here for simulation the field dependence of CIDNP has been developed by Adrian.[22]

The above described mechanism can give rise to two CIDNP effects: net and multiplet. The net effect occurs in the case of $\Delta g \neq 0$ as shown in Fig. 1.1.2. A simple analysis of CIDNP spectra can be obtained by empirical Kaptein's rules[23] which allow to predict the sign of the polarization (absorption or emission). For the net effect the sign determined by four decisive parameters, according to:

$$\Gamma_i = (\mu)(\varepsilon)(\Delta g)(\mathrm{A}_i) \qquad (1.1.2)$$

where μ denotes the initial electron multiplicity of the RP at its formation(+ for triplet, - for singlet), ε the type of reaction leading to the observed products (+ for cage product, - for escaped products), $\Delta g = g_1 - g_2$ the sign of difference in g-factors of the two radicals(g_1 is the g-factor of the radical with nucleus under observation), A_i the sign of the HFI constant. The sign product of these four parameters determines, whether the sign, Γ_i, of the polarization for nucleus *i* is absorption (+) or in emission (-).

If $\Delta g=0$ there can be no net polarization in any product but there can be a mixture of emissive and enhanced absorptive polarization – multiplet effect. This effect can form only in the RP with more than one nuclear spin and they are scalar coupled. In case of two nuclei, there is a difference in the rate of electron multiplicity mixing for parallel and anti-parallel mutual alignment of the two nuclear spins. For the multiplet effect there is the Kaptein's rules[23] as well. In this work no multiplet CIDNP effect will be evaluated and it will not be introduced here. However, the multiplet effect occurs in the course of PHIP that is described and presented in Chapters 1.3 and 4. It is important to note that multiplet effect can populates so-called long-lived spin states, in which polarization is stored for a much longer time than the longitudinal relaxation time. For a coupled two-spin 1/2 system the long-lived state is singlet state which may occur in low field.[14] In course of long CIDNP generation the long-lived states and consequently the multiplet CIDNP would acquire larger polarization than the net CIDNP. It should be taken into account when evaluating the steady state CIDNP in field dependent experiment.

CIDNP is a time-dependent effect. After the geminate stage the polarization formation in F-pairs (not shown in Fig. 1.1.1) continues until all radicals react to diamagnetic products.

According to spin sorting process described above the time evolution of CIDNP has the shape depicted in Fig. 1.1.3 After a fast rise of the geminate stage a slow decay of equal amplitude during escape reactions leads to compensation of CIDNP (black line). During the radical lifetime nuclear spin lattice relaxation under influence of the unpaired electron (paramagnetic nuclear relaxation) is operative reducing the polarization in the radicals. Electron spin relaxation times are of the order of 10^{-6} s, while nuclear spin relaxation in free radicals takes approximately 10^{-4} s. In contrast, the polarization in the diamagnetic reaction product relaxes at a much slower pace (diamagnetic relaxation). The paramagnetic relaxation, leads to non-compensated polarization of the products in the end of the radical reaction. (red line). F-pair polarization adds a slowly increasing contribution (blue line).

For the case of cyclic reactions the procedure of evaluating the CIDNP kinetics is described in Refs. 24,25 It is based on the set of differential equations suggested by Fischer.[26,27] The polarization of one of the products in cyclic reaction (Fig. 1.1.1) after the geminate stage is given by the following set of equations:

$$R(t) = \frac{R_0}{1 + k_t R_0 t} \tag{1.1.3}$$

$$\frac{dP(R)}{dt} = -k_t P(R) R - k_t \beta R^2 - \frac{P(R)}{T_1} \tag{1.1.4}$$

$$\frac{dP(Pr)}{dt} = k_t P(R) R + k_t \beta R^2 \tag{1.1.5}$$

Here, R_0 is the initial radical pair concentration, $R(t)$ the concentration of radicals in the cyclic reaction, $P(R)$ the polarization of the radicals, $P(Pr)$ the polarization of the diamagnetic products (which coincide with the initial species), k_t the rate constant of radical termination, and T_1 the paramagnetic nuclear relaxation time. Parameter β denotes the polarization per radical pair created in so-called F-pairs. It is related to the geminate polarization P^G via the quantity γ, which denotes the ratio of polarization created in F-pairs with respect to the geminate polarization: $\beta = \gamma P^G / R_0$.[27] For a triplet precursor and a purely random statistics $\gamma = 3$ is expected. In accordance with literature[26,27] $\gamma = 2.8$ was generally used.

In non-cyclic reactions the equations become more complex and must be derived according to the reaction scheme. In Chapter 6 the CIDNP kinetics for the radical reactions of biomolecules will be considered in details.

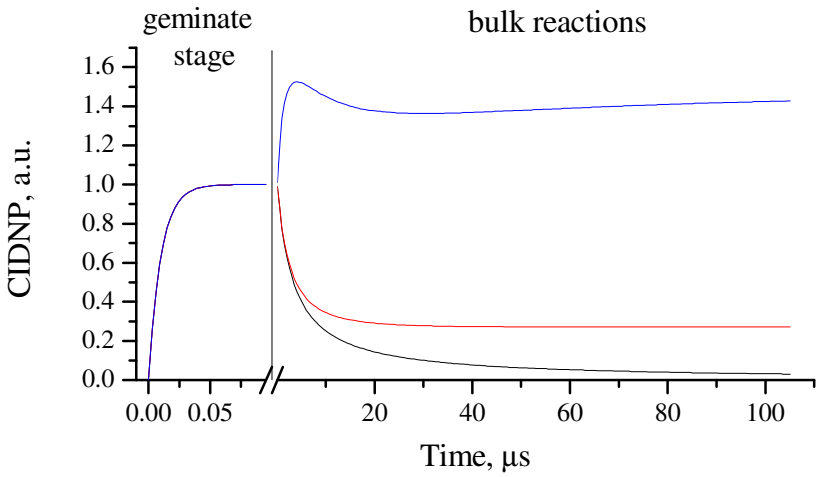

Figure 1.1.3. Kinetics of CIDNP (black line) taking into account nuclear relaxation in radicals (T_1=20 μs) (red line) and polarization generation in F-pairs (blue line). All kinetics start with fast formation of the geminate polarization.

As will be shown later in Chapter 1.4 observed polarization depends also on the spin evolution in the diamagnetic molecules which is a function of the magnetic field strength. One consequence of this evolution is polarization transfer among nuclei in the molecule.

The method of CIDNP can be combined with microwave irradiation and should be shortly mentioned here is stimulated nuclear polarization (SNP). It is based on EPR transitions pumping effect on singlet-triplet conversion of electrons in RP.[28,29] The microwave pumping (stimulation) causes selective for nuclear spins S-T conversions in RP that results in creation of the nuclear polarization in RP products at the same time as CIDNP. It leads to change in polarization intensity compare to CIDNP without stimulation. This method yields information about the structure of EPR spectrum of intermediate short-lived radicals in RP and about the pathway of the formation of the reaction products. Therefore, SNP is also called CIDNP-detected EPR spectroscopy.[29]

Microwave irradiation of a single radical without creating RP can also lead to HP. This is one of the oldest methods of HP generation called dynamic nuclear polarization (DNP).

1.2 Dynamic nuclear polarization

Dynamic nuclear polarization (DNP) is a term mainly used for a group of hyperpolarization techniques utilizing polarization transfer from an electronic spin reservoir to the nuclei. In this work only DNP via the Overhauser effect[10,30] in liquids is considered. In this case nuclear polarization originates from cross-relaxation processes involving unpaired

electronic and nuclear spins. For a complete transfer of spin order from electrons to the nuclei it is possible to obtain an enhancement as big as the ratio of gyromagnetic ratios of electron and nuclei: γ_e / γ_n ~660 for protons. The driving force of the transfer is the deviation of electronic polarization from thermal equilibrium induced by microwave driven resonant electron spin transitions, *S*. This concept, initially introduced by Overhauser is not limited to the case of electrons and nuclei. The Nuclear Overhauser Effect (NOE) with polarization transfer between spins of different nuclear species is widely used in NMR spectroscopy.

The Overhauser effect for two spins 1/2 (one is an electron spin and the other is a nuclear spin) is usually described using the four-level diagram shown in Fig. 1.2.1. The two spin species are coupled through dipolar or (and) scalar interaction. In an external magnetic field the spin-levels are split because of Zeeman interaction of the electron spin with the magnetic field. As molecular motion causes the spin-spin coupling to fluctuate it leads to relaxation processes in which both the electronic and nuclear spins flip simultaneously with relaxation rates W_0, W_2 for the zero and double quantum transition, respectively. Assuming that $W_0 >> W_2$, the flipping of an electron spin up is linked with the flip of a proton spin down. In thermal equilibrium, the same number of flips up and down of electron spin occurs, causing also the same number of down and up flips of the proton spin.

Irradiation at the resonance frequency of the electron spin transition *S* produces partial saturation by inducing more radiation transitions up than down. As a result another equilibrium of the system is reached by compensation of pumping and relaxation. In the new equilibrium the polarization of the nuclei spin levels is different from Boltzmann polarization. It is this deviation of the equilibrium population of the nuclear spins from Boltzmann polarization that is called dynamic nuclear polarization.

There are two aims of studying DNP in liquids containing free radicals. The first aim is to obtain information on the relative magnitude of scalar and dipolar interactions between unpaired electrons and nuclei that are responsible for the size of the relaxation rates W_i, on the time constants of molecular motion and electron spin exchange (Heisenberg spin exchange). The second aim is a more practical one. The application of DNP is based on the high polarization enhancement, ε, obtainable (of the order of 1000 for nuclei with a smaller γ_n than that of protons) that can be used to boost NMR sensitivity. DNP first observed at nuclei in metals having conduction electrons[30] has recently seen a renaissance after Ardenkjaer-Larsen et al.[31] reported enhancements higher than 10^4 by combining DNP with electron polarization at cryotemperatures. Numerous applications to NMR spectroscopy and imaging were published

recently.[32-37] Older reviews, with an accent on DNP as an analytical tool are Ref. 38,39. Recent studies in this field with the focus on local water dynamics were performed by S. Han et al.[40,41]

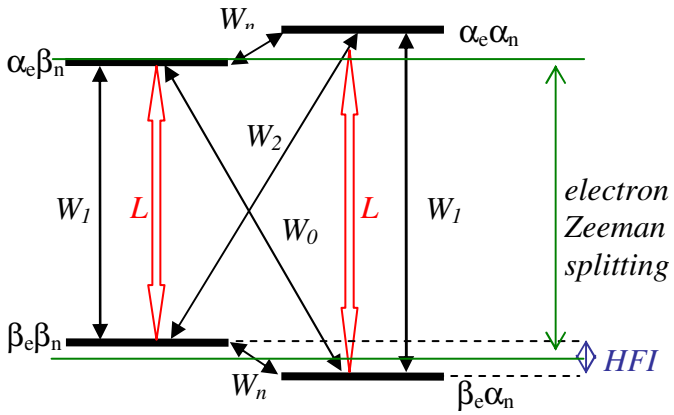

Figure 1.2.1. Four level energy diagram for coupled electron and nuclear spins. Here, α_e, β_e and α_n, β_n are electron and nuclear spin projections, respectively. W_1 and W_n describe single quantum relaxation of electron and nuclear spins respectively. Overhauser enhancements are obtained by exciting the electron transitions L, creating a non-equilibrium population of the electron spins. The cross-relaxation (W_0, W_2) transfer the polarization from the electron spins to the proton spins.

In liquid systems the DNP enhancement is usually described in terms of the leakage f, the EPR saturation s, and the coupling factor ξ [10] by

$$\varepsilon \equiv \frac{\langle I_z \rangle - I_0}{I_0} = \xi s f \frac{\gamma_e}{\gamma_n} \tag{1.2.1}$$

Here $\langle I_z \rangle$ and I_0 are the dynamic and the Boltzmann nuclear polarization, respectively, γ_e and γ_n are the gyromagnetic ratios of the electron and the nuclei. The coupling factor, ξ, depends on the relaxation mechanism involved and can take values in the range from –1 (pure scalar relaxation) to +0.5 (for pure dipolar):

$$\xi = \frac{W_2 - W_0}{W_0 + 2W_1 + W_2} \ . \tag{1.2.2}$$

The leakage factor, f, is defined as:

$$f = \frac{W_0 + 2W_1 + W_2}{W_0 + 2W_1 + W_2 + W^0} , \tag{1.2.3}$$

where W^0 takes into account those relaxation processes not involving the electronic spins S and not included in Fig. 1.2.1. The saturation factor, s, describes the saturation of the electronic levels by the pumping and is defined as:

$$s = \frac{S_0 - \langle S_z \rangle}{S_0}. \qquad (1.2.4)$$

Here S_0 and I_0 are the values of $\langle I_z \rangle$ and $\langle S_z \rangle$ in thermal equilibrium.

It is well-known that the DNP efficiency is strongly dependent on the external magnetic field B.[10] The main reason for this is the field dependence of the coupling factor ξ that in good approximation varies as the spectral density of the molecular motion at the EPR transition frequency and thus as $1/B^2$ even for low-viscosity liquids and moderate fields. Accordingly, maximal enhancements are expected at low fields. Even though the absolute polarization achievable is proportional to B and thus is small at low fields, nevertheless, low-field DNP studies are valuable, since it is relatively easy to achieve NMR enhancements of 100 or more. Sample heating by the EPR pump field is low; hence strong B_1 can be applied. DNP data obtained for EPR pumping at low fields also contribute to understanding the DNP mechanisms and with that knowledge to optimizing the experimental control parameters for achieving maximal NMR enhancement. Moreover, there are applications such as low-field imaging, non-invasive pH measurements,[42] oxymetry[43] or earth field NMR[44] where low fields are essential. Therefore, DNP is studied here at low field and combined with high resolution detection at high field. As for CIDNP, the effects of field variation are taken into account. However, continuous variation of the polarization field was not feasible, since the resolution condition for EPR pumping could only be met at a set of discrete frequency.

In Chapter 5 low-field pulsed ^{1}H DNP experiments in liquid samples of water and aqueous solutions of 3-furoic acid doped with stable nitroxide radicals will be considered. Previously it has been shown that for ^{1}H-DNP in water the enhancements are usually dominated by dipolar relaxation leading to negative enhancement with a maximum possible value of $|\varepsilon| = 330$.

1.3 Parahydrogen induced polarization

Any diatomic molecule that contains magnetically active centers exists in the gas phase in isomeric forms that differ in their nuclear spin configuration.[45] The dihydrogen molecule has two nuclear spin isomers: parahydrogen and orthohydrogen. Parahydrogen is an antisymmetric singlet spin state whereas orthohydrogen is a symmetric triplet spin configuration. They are different in the population of their rotation states. The difference in the populations of the rotation states results from the symmetrization postulate of quantum mechanics. The overall wavefunction of fermions has to be antisymmetric in exchange of the nuclei. Therefore,

symmetric rotation states with even J number are populated with antisymmetric spin configuration (parahydrogen) while antisymmetric rotation states are populated with orthohydrogen. In its Zeeman basis the spin wavefunction of dihydrogen can be written in following way:

$$\psi = \frac{1}{\sqrt{2}}(\alpha\beta - \beta\alpha) \qquad \text{parahydrogen} \qquad 1.3.1$$

$$\alpha\alpha\,,\ \psi = \frac{1}{\sqrt{2}}(\alpha\beta + \beta\alpha) \text{ and } \beta\beta \qquad \text{orthohydrogen}$$

Rotation states and, consequently, spin states have different energies. Their populations are therefore temperature dependent with lower temperatures favoring the parahydrogen. At high temperature the states are populated according to their degeneracy (25% parahydrogen and 75% of orthohydrogen). Already at cooling to the temperature of liquid nitrogen there are 51% of parahydrogen.[46,47] Normally, interconversion between the isomers is symmetry forbidden but the addition of a paramagnetic catalyst allows to overcome this selection rule. Hence, it is possible to enrich dihydrogen in its para-isomer and on removal of the catalyst enriched dihydrogen can be used at room temperature.

Since the total spin of parahydrogen is equal to zero it has no the Zeeman splitting and hence has no NMR signal. However, if the exact symmetry is broken while spin correlation is saved one can obtain NMR signals of two protons with high intensity. The HP which is possible in this case is order of unity that is by five orders of magnitude higher than normal Boltzmann polarization. Such HP resulting from experiments with parahydrogen is called parahydrogen induced polarization (PHIP).

The usual way of breaking the symmetry of parahydrogen is the hydrogenation reaction of unsaturated compounds (e.g. compounds with a double or triple bond) by parahydrogen or attachment it to a catalyst with formation of products where the protons are no longer magnetically equivalent. The PHIP phenomenon, however, only occurs if the two hydrogen atoms of parahydrogen are transferred jointly to the unsaturated bond of the substrate. The simultaneous transfer of the two parahydrogen atoms is crucial for the observation of PHIP signals since it makes sure that the original spin correlation, between these two nuclei is maintained throughout the whole hydrogenation cycle and also afterwards in the products. Such catalytic attachment of parahydrogen to styrene is investigated in Chapter 4. It is important to note that PHIP does not only produces strong non-thermal polarization but can also lead to the formation of so-called long-lived spin states, in which HP is stored for a much longer time than the longitudinal relaxation time.[14,48-51] An alternative way of creating PHIP based on reversible

complexation of the molecule under interest with parahydrogen, which do not require direct hydrogenation of molecules, has been proposed in a recent publication.[3]

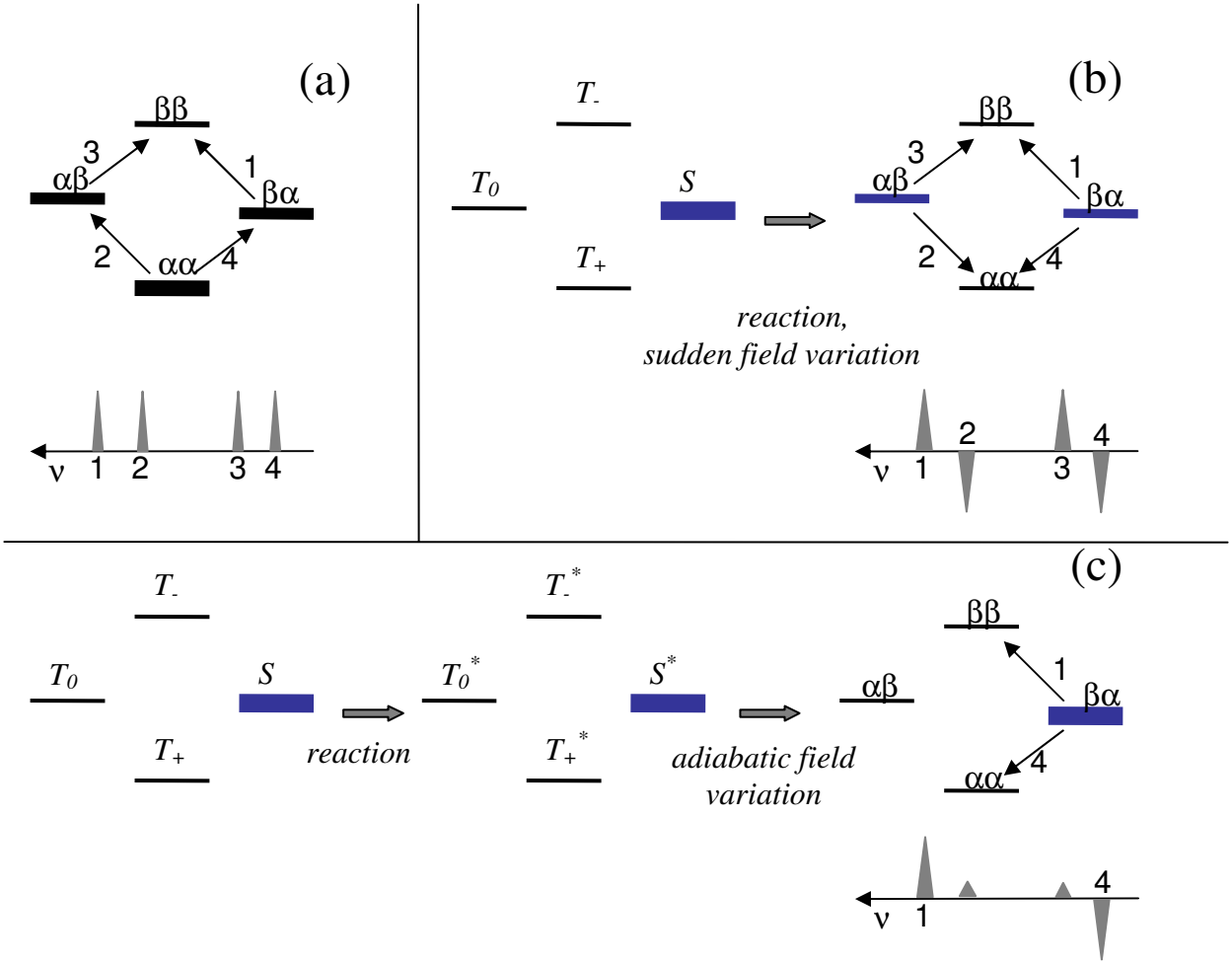

Figure 1.3.1. Populations and corresponding NMR spectra of AX system. (a) Thermal polarized NMR spectrum. Genesis of (b) PASADENA and (c) ALTADENA types of polarization.

In the literature there are two protocols of PHIP experiments described, which are referred to as ALTADENA (Adiabatic Longitudinal Transport After Dissociation Engenders Nuclear Alignment)[52] and PASADENA (Parahydrogen and Synthesis Allow Dramatically Enhanced Nuclear Alignment)[53] experiments. Both ALTADENA and PASADENA effects have been explained,[52,53] as described above, by equivalency removal for the pair of protons after chemical reaction and by their scalar spin-spin coupling. PASADENA experiments are performed at high field (Fig. 1.3.1b) inside the NMR magnet where the two polarized protons acquire only multiplet HP. The term multiplet polarization stands for non-equilibrium mutual orientation of the two spins. In the ALTADENA experiment (Fig. 1.3.1c) the parahydrogenation reaction is performed outside the NMR magnet, thus, non-thermal polarization is created, presumably, in the Earth magnetic field. The polarized sample is then transferred mechanically

into the NMR-spectrometer magnet where the ALTADENA spectrum is recorded. In the ALTADENA spectrum the two protons, which constituted the parahydrogen molecule prior to the reaction, acquire not only net polarization of equal amplitude but opposite sign but also multiplet polarization.

It is also known from a number of experiments that PHIP created at low magnetic field can be transferred to other nuclei in the molecule, most notably, to spin 1/2 hetero-nuclei (^{13}C, ^{15}N, ^{19}F).[54-59] PHIP transfer effects, too, can be explained (at least qualitatively, in many cases also quantitatively) by scalar spin-spin coupling of the protons coming from the parahydrogen molecule with the other nuclear spins. However, even though both ALTADENA and PASADENA phenomena are well understood there are still open problems left in the theoretical description of the PHIP phenomena. First, ALTADENA and PASADENA effects have been exhaustively described only for two-spin systems and only recently considered for three-spin systems,[60,61] whilst PHIP in higher-spin systems has not been analyzed quantitatively in a systematic way. Second, PHIP experiments are routinely run only with the reaction proceeding either at the Earth magnetic field or at the NMR-spectrometer field. However, in some cases it may be advantageous to use an intermediate field for HP preparation and its transfer to other spins. Third and finally, effects of sample transport between the reaction and observation field (or, alternatively, of field switching) on PHIP spectra have not been studied in detail so far. Such effects can be quite pronounced, especially when comparing very slow (adiabatic) and very fast (sudden) field switching.

As it will be shown in Chapter 1.4, in all cases considered, it is crucial whether the interacting spins are coupled weakly or strongly at the magnetic field where the spin system is polarized (i.e., the hydrogenation reaction is run). For the two-spin system the change in coupling conditions is the reason for the pronounced differences between the polarization pattern ALTADENA (strongly coupled spins at low preparation field) and PASADENA experiments (weakly coupled spins at high preparation field). Similarly, PHIP transfer effects in multi-spin systems are expected to be sensitive to the coupling regime. For instance, if at least one of the protons, which belonged to the parahydrogen molecule prior to the chemical reaction, is coupled strongly to other spins they can also acquire strong PHIP. In this context studying the influence of field variation on PHIP is of interest as it may allow one to optimize the HP amplitude and its transfer efficiency. Most notably, the re-distribution of polarization among the coupled spins is expected to proceed very efficiently in the vicinity of level anti-crossings.[62,63]

In Ref. 61 a general theoretical approach to the description of HP experiments at variable magnetic field strength was developed. Three-spin 1/2 systems were considered in detail and

numerical calculations for PHIP effects in the coupled three-spin system were performed. In another publication[64] the theoretical approach was extended to PHIP effects in multi-spin systems. Theoretical results obtained under this assumption will be compared to the experimental data in Chapter 4 in order understand the role of *J*-coupling in PHIP effects.

1.4 Hyperpolarization transfer among coupled spins

The evolution of spin observable is governed by distinctly different processes. One of them is relaxation, another is coherent polarization transfer. In case of CIDNP the polarization originally formed on nuclei having HFI at the radical stage can be transferred to other nuclei. This transfer can have positive and negative consequences depending on the aim of a particular investigation. The positive side is the possibility of distributing polarization from certain highly polarization source spins (which acquire HP directly) to other spins of interest. Enhanced NMR signals of such target nuclei can then be analyzed to provide structural and dynamic information on the molecular systems under study. In many cases this transfer step is the bottleneck of the HP experiment, in particular as the transfer time has to be fast in comparison with the relaxation time T_1. Optimization of polarization transfer to the desired target spin is therefore important for exploiting HP in chemical and biological applications. The other side is the use of HP (e.g., CIDNP and PHIP) for the determination of the pathways of chemical reactions and the properties of their intermediates becomes more complex. In this case HP transfer among the spins plays a negative role since after polarization re-distribution unraveling information on reaction pathways and intermediates is obscured and its analysis becomes problematic and ambiguous. Thus, understanding the mechanism and efficiency of HP transfer is a key problem in many experiments that exploit non-thermal spin polarization. In this chapter the theoretical approach to HP re-distribution among spins coupled by scalar spin-spin interactions developed by Ivanov et.al.[65] will be shortly described.

Following de Kanter and Kaptein,[66] the theory is based on HP re-distribution caused by scalar spin-spin coupling. Two spins are considered weakly coupled if the nuclear spin-spin interaction between them is much smaller than the difference in their Zeeman interaction with the external field. In other case they are considered strongly coupled. Thus, not the absolute, but only the relative strength of the coupling with respect to difference in Larmore frequency is important for fulfilling the strong coupling condition, which therefore depends on the external magnetic field. Even though the present theory will be applied here only to protons it is more general and also applicable to hetero-nuclei when the coupled spins have different gyromagnetic

ratios. For simplicity, detection only at high magnetic field where the spins are weakly coupled (in the case of two spins forming a so-called AX-system[67]) will be considered. This is by no means a principle limitation of the present theory, but it only makes the consideration simpler.

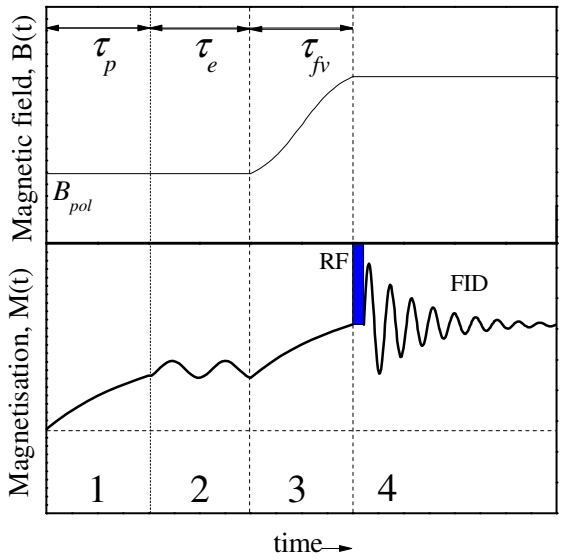

Figure 1.4.1. Timing scheme of a field-cycling experiment with HP. HP is created during time period τ_p (stage 1 – polarization) at magnetic field B_{pol}; it freely evolves at the polarization field during time period τ_e (stage 2 – evolution); then during time period τ_{fv} the polarized spins are subject to a magnetic field switch from B_{pol} to the detection field B_0 (stage 3 – field variation); here the polarized Fourier Transform NMR spectrum is recorded (stage 4 – detection).

When spins are coupled sufficiently strongly the eigen-states of the entire spin system are not characterized by the eigen-states of the individual spins, but represent their collective states. Therefore, the spin order is not represented by polarization of certain nuclei, but by a more complex distribution of population among all coupled spins.

Here the experimental protocol consisting out of four stages according to the Fig.1.4.1 will be considered: (1) HP is generated at the desired field B_{pol} during time τ_p (preparation stage); (2) after its preparation HP freely evolves at field B_{pol} during time τ_e (evolution stage) (3) the external magnetic field is switched from B_{pol} to the observation field B_0 during time τ_{fv} (field variation stage); (4) HP spectra are acquired by FT-NMR at $B = B_0$ (detection stage). Experimentally such a protocol is realized by using the mechanical field-cycling device described in Chapter 2.

In the simplest way, the effects of indirect polarization of the spins can be discussed for a system of two spins as the problem can be tackled analytically. The behavior of two nuclear spins-1/2, $\boldsymbol{I}_1$ and $\boldsymbol{I}_2$ where only one of the nuclei has initially non-thermal magnetization along z, parallel to external magnetic field, and the second is thermally polarized will be considered. This happens, for example, when during a radical reaction in which CIDNP is generated only one of the nuclei has considerable HFI in the radical and thus can be considered the origin of polarization.

As is typical for liquid samples the behavior of a system of K nuclear spins 1/2 in an external magnetic field B is described by the following Hamiltonian (in units of h):

$$\hat{H} = -\sum_{i=1}^{K} \nu_i \hat{I}_{iz} + \sum_{i<j}^{K} J_{ij} (\hat{\mathbf{I}}_i \cdot \hat{\mathbf{I}}_j), \tag{1.4.1}$$

where $\nu_i = (1-\sigma_i)\nu_0 = \gamma_{Ni} B(1-\sigma_i)/2\pi$ is the Larmor precession frequency of the i-th spin determined by its chemical shift σ_i (here γ_{Ni} is the nuclear gyromagnetic ratio of the i-th spin), and J_{ij} is the scalar spin-spin coupling of the i-th and j-th spins. Depending on the frequency off-set of the two spins at a field B_{pol}

$$\delta\nu_{pol} = \gamma_N B_{pol} (\sigma_1 - \sigma_2)/2\pi = \gamma_N B_{pol} \Delta\sigma / 2\pi, \tag{1.4.2}$$

the condition of either strong (when J is larger than or comparable to the difference in Zeeman interaction, $\delta\nu$), or weak coupling of spins ($J \ll \delta\nu_{\mathrm{pol}}$) is met for two spins.

HP can be prepared in several ways depending on the type of experiment. When the effects of CIDNP re-distribution due to the strong coupling among spins at the polarization field were first considered by de Kanter and Kaptein[66] to explain the low-field CIDNP spectra they assumed that the period τ_p during which CIDNP is formed by light irradiation is rather long in comparison with the reciprocal scalar coupling J between the interacting spins in the diamagnetic molecules, $\tau_p \gg 1/2\pi J$. Therefore, they neglected the role of any spin coherence (represented by off-diagonal elements of the respective spin density matrix) in the re-distribution of polarization among the spins. However, when using intensive laser irradiation it is possible to shorten τ_p to the limit that $\tau_p \leq 1/2\pi J$ and spin coherences can no longer be neglected. An experimental example for that will be shown in Chapter 3.

In the following all observables can be expressed via the spin density matrix of the spin system, which is given in the eigen-basis of Hamiltonian (1.4.1). Its elements at a given field B_{pol} are conditioned by the spin evolution in the precursor radical pair. Populations of eigen-states of the Hamiltonian are defined by the diagonal elements of the density matrix in its eigenbasis. Here will not be shown any details of calculating density matrix elements which is beyond the

scope of the present work. The spin eigen-states of the diamagnetic reaction product having two spins-1/2 written in the two-spin Zeeman basis[68]

$$\begin{aligned} |1\rangle &= |\alpha\alpha\rangle, \qquad |2\rangle = \cos\theta|\alpha\beta\rangle - \sin\theta|\beta\alpha\rangle, \\ |3\rangle &= \sin\theta|\alpha\beta\rangle + \cos\theta|\beta\alpha\rangle, \qquad |4\rangle = |\beta\beta\rangle, \end{aligned} \tag{1.4.3}$$

where the mixing angle θ of the states $|2\rangle$ and $|3\rangle$ depends on the coupling strength J and the quantity $\delta\nu_{\mathrm{pol}}$ as defined in eq. 1.4.2. At the polarization field it is given by

$$\tan 2\theta = \frac{J}{\delta\nu_{pol}}. \tag{1.4.4}$$

Let us assume that the populations are conditioned by only first nuclear and the diagonal elements are following: $p_{\alpha\alpha} = p_{\alpha\beta} = n_1$, $p_{\beta\alpha} = p_{\beta\beta} = n_2$. Already in the simple example of two coupled spins the HP patterns are substantially affected by the speed of field variation from B_{pol} to the field B_0 because $\delta\nu$ increases and the mixing angle θ decreases accordingly. For the sake of simplicity only a weakly coupled system (AX system) at the detection field and $J>0$ are considered, a situation facilitating the proper qualitative conclusions. In this situation the eigen-states at high field B_0 coincide with those of the Zeeman basis (1.4.3). Here, the two different limiting cases of purely adiabatic and purely non-adiabatic (sudden) transfer are discussed. In the first case (slow field variation) the eigen-states of the spin system keep their populations during the field variation. As a result the expectation values of the net magnetizations of HP of the two nuclei[65] become:

$$\langle I_{1z}\rangle = (1+\cos 2\theta)\frac{n_1 - n_2}{2}, \quad \langle I_{2z}\rangle = (1-\cos 2\theta)\frac{n_1 - n_2}{2}. \tag{1.4.5}$$

As is readily seen, both nuclei become polarized and the ratio of their HP signals,

$$\frac{\langle I_{2z}\rangle}{\langle I_{1z}\rangle} = \frac{1-\cos 2\theta}{1+\cos 2\theta}, \tag{1.4.6}$$

vanishes only when the mixing angle θ of the states $|2\rangle$ and $|3\rangle$ at the polarization field is zero, i.e., when the spins are coupled only weakly at B_{pol}.

In the limit of sudden transfer (abrupt field variation) the high-field state populations are correlated by the projection of the density matrix at the polarization field onto the high-field spin states. For two-spin system calculations gives the polarization ratio[65]

$$\frac{\langle I_{2z}\rangle}{\langle I_{1z}\rangle} = \frac{1-\cos^2 2\theta}{1+\cos^2 2\theta}, \tag{1.4.7}$$

which approaches zero only for a system of spins that are weakly coupled at B_{pol}.

Thus, at the two limits, because of strong coupling at the polarization field, the second nucleus (having no HFI in the radicals) takes a large part of CIDNP from the first nucleus. At intermediate speed of field variation a polarization transfer between the asymptotic curves is expected. It is important to emphasize that the condition of strong coupling of the nuclei is almost always fulfilled at low magnetic field. Indeed, even when assuming $\Delta\sigma$=3 ppm (which is fairly big for two protons), and J as small as 0.1 Hz (not resolvable by NMR because of field inhomogeneities) one obtains strong coupling of the two spins at fields B_{pol} below 1 mT. Thus, even in such cases indirect polarization of the nuclei, which are not polarized at the weak coupling, is expected. However, this prediction is in contradiction with the experimental observations, because at low-field polarization is not found distributed over the whole molecule except for some special cases discussed below in the light of the present study. Thus, the strong coupling condition at B_{pol} alone does not provide an adequate CIDNP transfer criterion. Moreover, in the situation considered above CIDNP is counter-intuitively re-distributed in the molecule "instantaneously", that is, immediately after the diamagnetic molecule is formed. Since any interaction, even if it is switched on instantaneously, needs a finite time to affect the observables, this concept cannot apply to fast field variation experiments.

The inconsistency of infinitely fast polarization transfer has a simple reason. In the foregoing analysis, to obtain the state populations at the detection field, it was tacitly assumed that the spin density matrix at the polarization field does not have any elements except for diagonal ones. However, this is not always true because, in general, at B_{pol} the spin eigen-states in the radicals (in CIDNP experiments) do not coincide exactly with those in the reaction products.[62,69-71] This inevitably leads to the formation of off-diagonal elements of density matrix, which represent coherences between the states $|2\rangle$ and $|3\rangle$ that are defined in equation (1.4.3). Once formed the coherences start oscillating at a frequency equal to the difference in energy of the states $|2\rangle$ and $|3\rangle$:

$$\frac{\Delta E_{23}}{h} = \nu_{23} = \sqrt{J^2 + \delta\nu_{pol}{}^2}\,, \tag{1.4.8}$$

i.e.,
$$\rho_{23}(t) = \rho_{23}(0)\exp(2\pi i\nu_{23}t). \tag{1.4.9}$$

where ρ_{23} is the off-diagonal element of the density matrix. If the polarization time τ_p is large enough ($\nu_{23}\tau_p$>>1) the coherences will be completely washed out. However, if this condition is not met, the dephasing will incomplete. The following evolution will depend on the way of field variation. The consequences of coherence formation and the effects of field variation on the re-distribution of polarization will be considered for the adiabatic and sudden cases.

In case of adiabatic field variation the coupled states $|2\rangle$ and $|3\rangle$ (1.4.3) have enough time to adjust themselves to the variable magnetic field so that the populations of the eigen-states remain unchanged, whereas the coherences oscillate with the frequency $\nu_{23}(t)$ that gradually changes with time as the external magnetic field varies. No mixing between phases and populations occurs in this case, hence the coherences formed at field B_{pol} do not affect the net polarizations at detection field B_0.

In case of sudden field variation at high field projection of the density matrix at the polarization field onto the high-field spin states has to take into account diagonal and off-diagonal terms. If it is then assumed that during polarization and/or evolution time at B_{pol} the coherence between the coupled levels $|2\rangle$ and $|3\rangle$ does not undergo any changes one immediately obtains that:

$$\langle I_{1z}\rangle = n_1 - n_2, \quad \langle I_{2z}\rangle = 0 \tag{1.4.10}$$

Hence, no indirect polarization of the second nucleus occurs. If, however, coherence formed due to the spin evolution in the radicals undergoes some changes at the polarization field (e.g., due to finite polarization or evolution times) the second nucleus acquires HP.

Altogether, this allows to conclude that HP transfer to the second nucleus proceeds efficiently in the following cases: (a) adiabatic sample transfer; (b) non-adiabatic sample transfer accompanied by evolution of coherences during the time τ_e or their decay during the finite polarization time τ_p; (c) intermediate situation when the transfer is not completely adiabatic and the spin coherence has enough time to evolve at $B=B_{pol}$. Certainly, strong coupling of the two nuclei at the polarization field is always a prerequisite for the HP transfer. The various situations discussed are fulfilled depending on the timing scheme of the experiment. Indeed, to meet condition (a) it is necessary that $J\tau_{fv}\geq 1$ (rough estimate for the time of adiabatic transfer[65]); for conditions (b) and (c) it is necessary that $J\tau_p\geq 1$ and/or $J\tau_e\geq 1$. Therefore, to transfer HP it is necessary that the τ_p, τ_e, and τ_{fv} times are not much smaller than the inverse of J, i.e., the timing of the experiments introduces limits for the re-distribution of polarization between the coupled nuclei. Hence, the modified criterion for indirect polarization is as follows:

$$J\geq\delta\nu_{\text{pol}} \quad \text{and} \quad J\tau_p, J\tau_e, J\tau_{fv}\geq 1 \tag{1.4.11}$$

Accordingly, the re-distribution time can be roughly estimated as J^{-1}. Even though in this more extended model polarization is no longer transferred "instantaneously", the HP re-distribution time of J^{-1} is still considerably shorter than the longitudinal relaxation times T_1, whereas the latter are usually shorter than the cross-relaxation times T_{CR}. Therefore, the mechanism discussed above provides faster polarization transfer than cross-relaxation does.

In Chapter 3.1 in Fig. 3.1.2 and 3.1.3 the experimental results of how indirect polarization of the second nucleus builds up as a function of the irradiation and waiting times. In the first experiment it is assumed that the polarization time is short ($\nu_{23}\tau_p$ <<1). The dependence of ratio of the individual net magnetizations and the total net CIDNP on the evolution time is following:

$$\frac{\langle I_{1z}\rangle}{\langle I_z\rangle} = 1-\sin^2 2\theta\cdot\frac{1-\cos(2\pi\nu_{23}\tau_e)}{2}$$
$$\frac{\langle I_{2z}\rangle}{\langle I_z\rangle} = \sin^2 2\theta\cdot\frac{1-\cos(2\pi\nu_{23}\tau_e)}{2}. \qquad (1.4.12)$$

As it is seen, both polarizations oscillate between their limiting values, (1-sin^{2}2θ) and 1 for $\langle I_{1z}\rangle$ and 0 and sin^{2}2θ for $\langle I_{2z}\rangle$. After a quarter of a period ($2\pi\nu_{23}\tau_e$=π/2) polarization is already distributed efficiently among the spins. Here, for simplicity dephasing of the coherence is neglected, which may lead to damping of the beats.

In the second experiment , τ_e=0 is taken and the polarization time is varied passing from very short ($\nu_{23}\tau_p$<<1) to very long ($\nu_{23}\tau_p$>>1) times τ_p. Continuous HP formation from 0 to τ_p results in washing out this coherence, which vanishes at large $\nu_{23}\tau_p$:

$$\frac{\langle I_{1z}\rangle}{\langle I_z\rangle} = 1-\frac{\sin^2 2\theta}{2}\cdot\left[1-\frac{\sin(2\pi\nu_{23}\tau_p)}{2\pi\nu_{23}\tau_p}\right]$$
$$\frac{\langle I_{2z}\rangle}{\langle I_z\rangle} = \frac{\sin^2 2\theta}{2}\cdot\left[1-\frac{\sin(2\pi\nu_{23}\tau_p)}{2\pi\nu_{23}\tau_p}\right]. \qquad (1.4.13)$$

Again, HP $\langle I_{2z}\rangle$ fully builds up only if the time of the experiment (τ_p in this case) is long enough as compared to the reciprocal coupling strength J^{-1}.

The theoretical description of coherent polarization transfer in a system with three coupled spins 1/2 was developed in Ref. 61. In a system with three and more spins 1/2 level anti-crossings may occur between spin levels with the same I_z (in case of three spins, three levels -1/2 and 1/2). It will lead to features in various field dependent measurements. At the field of level anti-crossing some of mixing coefficients undergo abrupt change.

The theoretical formalism shown is applicable not only CIDNP experiments but as well to PHIP and relaxation experiments. The theoretical formalism for description of PHIP experiments developed in Refs. 61,64 is closely related to the formalism shown above for polarization transfer. So far, no relaxation processes in diamagnetic molecules was taking in account, however, the HP disappear with the relaxation. Many effects are also seen in relaxation

experiment in coupled multi-spin systems at variable field. It will be the topic of the next Chapter 1.5.

1.5 Nuclear magnetic relaxation dispersion in scalar coupled systems

In the context of hyperpolarization spin-lattice relaxation is usually considered a detrimental process as it leads to thermalization and re-establishment of the small Boltzmann polarization. Thus any quantitative analysis of hyperpolarization, especially in field dependent measurements has to take into account relaxation processes. Moreover, any approach that is conducive to reducing the influence of relaxation will promote application of HP. Since all relaxation experiments involve in one way or another spin states off thermal equilibrium the treatment of relaxation resembles that of hyperpolarization. One of the common effects is polarization transfer among coupled spins as discussed in Chapter 1.4.

Investigations of nuclear spin relaxation, especially, of its field dependence known as nuclear magnetic relaxation dispersion (NMRD) provide valuable information on the characteristic times of molecular mobility.[72] Accordingly, field-cycling relaxometry[72] developed for measurements of spin relaxation dispersion is a powerful tool for probing the intra-molecular mobility of molecular crystals, polymers, proteins, DNA and other biologically important macromolecules.[72-81] In particular, the correlation times of stochastic motion, which is the cause of spin relaxation, can be determined. For example, in the simplest case of a spin relaxing due to fluctuations of the local magnetic field its longitudinal relaxation rate, R_1, is given by the equation:[82]

$$R_1 = \frac{1}{T_1} = (\Delta B)^2 \frac{\tau_C}{1+(\omega\tau_C)^2} \qquad (1.5.1)$$

Here, τ_C is the correlation time of the stochastic molecular motion, and $\omega=2\pi\nu$ with ν being the Larmor precession frequency of the spin proportional to external magnetic field $\omega=\gamma B_0$; ΔB is the fluctuating part of the magnetic field. Relaxation rates can depend on the external magnetic field because of either field-dependent ΔB or because of the denominator in equation (1.5.1). In the present treatment the first factor will not be discussed, i.e., fluctuating fields that depend on the external magnetic field, as they can be caused, for instance, by modulation of the chemical shift anisotropy, which is, however, small for protons that are the main focus of the present study. As far as the second factor is concerned, reflecting the spectral density of the fluctuation and its dependence on the strength of the external magnetic field, different relaxation regimes have to be considered. At low magnetic field so that $\omega\tau_C << 1$ (fast motional regime) R_1 does not depend on

ω, while at high magnetic field $\omega\tau_C >> 1$ (slow motional regime) R_1 is proportional to $1/\omega^2$. Thus, a characteristic change of the relaxation rate takes place at $\omega\tau_C \sim 1$ (passing from the fast to the slow motional regime) where R_1 drops down. Thus, from the inflection point of the relaxation relaxation dispersion the correlation time, τ_C, that characterizes the molecular motion can be found experimentally.

The two above-mentioned factors (magnetic field dependent ΔB and transition from fast to slow motional regime) are usually considered the only ones that cause a dependence of R_1 on the magnetic field. However, in real systems there are always intra-molecular interactions among the relaxing spins. Their effects on the NMRD were left out of consideration in literature since for elucidating them a site-specific study of relaxation is required. In the overwhelming majority of NMRD experiments only relaxation of spin magnetization integrated over the whole molecule is studied but not relaxation of individual spins. Because the data are not site-specific they require application of decomposition algorithms and presumptive guessing for interpretation of the collective magnetization recovery/decay data to provide information on the molecular mobility. In solids with their broad NMR lines a slowly fluctuating dipolar coupling among protons leads to efficient spin diffusion equilibrating their polarization. As long as spectra are highly resolved this mechanism is inefficient, hence lines relax with different rates. Nevertheless, coupling among the spins affects the rates, and it is the purpose of this study to demonstrate and interpret particular features in scalar coupled multispin systems.

The theory of re-distribution of non-thermal polarization among scalar coupled spins at variable external magnetic field presented in Chapter 1.4 gives one an idea how intra-molecular spin-spin couplings may affect the relaxation behavior of the coupled spins at low fields. The result was that re-distribution processes proceed very efficiently at low fields where the spins are strongly coupled. As a consequence of this strong coupling the eigen-states of the spin system are collective states of spins. Polarization transfer was found to be a coherent process, since its kinetics exhibits pronounced quantum beats. In addition, characteristic features were seen in the field dependence of the transfer efficiency with their positions coinciding with those of nuclear spin level anti-crossings.[62] Thus, it is clear that strong coupling among the spins (which always takes place when one goes to low magnetic fields) significantly affects the spin evolution of molecules including spin relaxation. Therefore, one may expect similar features in the relaxation dispersion curves.

As has been stressed before, for investigating the influence of strong coupling on spin relaxation at low magnetic fields it is necessary to obtain site-specific data. Thus, one has to

resolve signals from all individual spins in the NMR spectra detected at the observation field. This has to be combined with the possibility of investigating relaxation at an external magnetic field of variable strength. Therefore, high-resolution NMR in connection with fast field-cycling is required to obtain site-specific NMRD data.[83] First high resolution NMRD experiments utilizing the fringe field of superconducting magnet of commercial NMR spectrometer have been performed recently,[73,78,84,85] however, the lower limit of the field range was only 0.1 T.

The theoretical approach to describe high resolution NMRD experiments was developed by Ivanonv et.al.[86] Similar to the considerations in Chapter 1.4 the relaxation in a system of N nuclear spins 1/2 at arbitrary magnetic field B_0 is treated. The dynamic properties of such a system are given by the time-independent Hamiltonian (1.4.1). Relaxation effects are caused by the random fluctuation of the time-dependent part of the total Hamiltonian. A few simple relaxation mechanisms corresponding to fluctuation of different interactions involving nuclear spins are reviewed.

The experimental results obtained from several spin systems of increasing complexity and their simulations based on the theoretical formalism developed in Ref. 86 are described in Chapter 3.2.

2. Experimental setup

Since modern NMR spectrometers operate, for reasons of sensitivity and resolution, at a fixed magnetic field, it is difficult or impossible to use them for studying the influence of magnetic field dependent interactions and to discriminate these against field independent parameters (such as hyperfine, exchange, scalar or dipolar interaction). It is not feasible to have separate NMR spectrometer for each magnetic field. Therefore, special equipment is needed. A well-established technique is to cycle between two fields, i.e. one allows the spins to evolve at a variable field level and then changes to a fixed level for detection.

Because all commercially available high resolution NMR spectrometers are optimized for routine measurements at constant field, it was necessary to construct a home built spectrometer that is optimized for field-cycling experiments. The spectrometer is based on a 7 T superconducting magnet. The hardware and software components are optimized for field-cycling by means of shuttling the NMR probe. The quality of field dependent spectroscopy, relaxation and hyperpolarization measurements is conditioned by the technical specifications of the NMR spectrometer. Therefore, considerable efforts were directed to improving the performance of the NMR spectrometer.

2.1 Spectrometer control unit: DAMARIS

In the beginning of my PhD work the home built NMR spectrometer was controlled by a rather old computer system in combination with a pulse generator and an analog-to-digital converter (ADC). The design dated back to the late 1980s. The real time computer (a VMX system) was running on the now obsolete OS9 operating system. This design had several disadvantages. First, the obsolete hardware and software could not be upgraded as no new versions were sold and used anymore. Second, the old pulse generator had a limited number of channels not enough to control all devices from one source. Instead, the controlling was split into two parts: a slow branch with millisecond time resolution and a fast branch with sub-microsecond resolution. Moreover, the control unit of the field-cycling was programmed by a program located at a second computer separate from the rest of the spectrometer. The same difficulties are expected when using commercial spectrometers that are not optimized for field-cycling measurements. This arrangement did not allow for performing elaborate time sensitive experiments with complex pulse sequences. Last, but not least, the ADC had a dynamic range of only 11 bits and an internal memory of only 8192 data points. Since the spectrometer was originally constructed for solid state NMR measurements, where NMR lines are broad, the ADC

parameters had been sufficient. In contrast, the requirements for liquid state measurements include long acquisition times to allow high spectral resolution together with rather short sampling intervals corresponding to the necessary wide spectral range. As a result, acquisition of much larger sets of data points is necessary requiring an ADC with bigger memory.

Taking into account all necessary demands part of my experimental tasks was the implementation of an updated NMR spectrometer control. As the controlling computer a PC based variant was chosen. The specifications of modern IBM based personal computers allow using them in real time systems suitable for NMR spectrometers. On the other hand, their price is affordable and their standardization is high enough that they can be easily upgraded in the foreseeable future. The same assessment holds for suitable pulse generators and ADCs. Considering the NMR software it had to be optimized for the field dependent measurements, a task that is hard to fulfill with commercially available software. As a consequence, the software had to be self-written or based on open source software with modifications for field-cycling demands.

The most promising solution turned out to be developing the spectrometer control in cooperation with the Institute for Condensed Matter Physics of the Technical University Darmstadt in frame of the existing open source project **DA**rmstadt **MA**gnetic **R**esonance **I**nstrument **S**oftware (DAMARIS) with extensions according to field-cycling requirements. DAMARIS is a project for developing a framework for NMR spectrometer control. Information on this project can be found in the internet on the project website[87] and in Ref. 88.

The hardware used in this project is based on a standard personal computer, pulse control cards and ADC cards. The computer uses a common operating systems (here, Debian Linux) which provides access to the NMR specific hardware via the vendors' drivers. The drivers are controlled by a hardware bundled software, the so-called "back end" program that organizes the components' interactions with the magnetic resonance spectrometer components.

The user interface is organized through the hardware independent program so called "front end". The "front end" controls the "back end". The same "front end" can be used on all DAMARIS machines having, in general, a different "back end". Information is exchanged via a file system. The "front end" writes command files (jobs) on the hard disk. The files are taken and executed by the "back end". The result of "back end" operations (e.g., the digitized Free Induction Decay, FID) is written into the same folder and fed to the "front end" for further processing. In this way it is easily possible to replay experiments or analyze results on a single scan level. The time required for file write and read operations depends on the file size (usually, the FID produces the biggest file) and is sufficiently short that files can be stored during the

waiting time of the actual magnetic resonance experiment before the next acquisition starts. When the FID size does not exceed 16384 the delay time is not noticeable by spectrometer user.

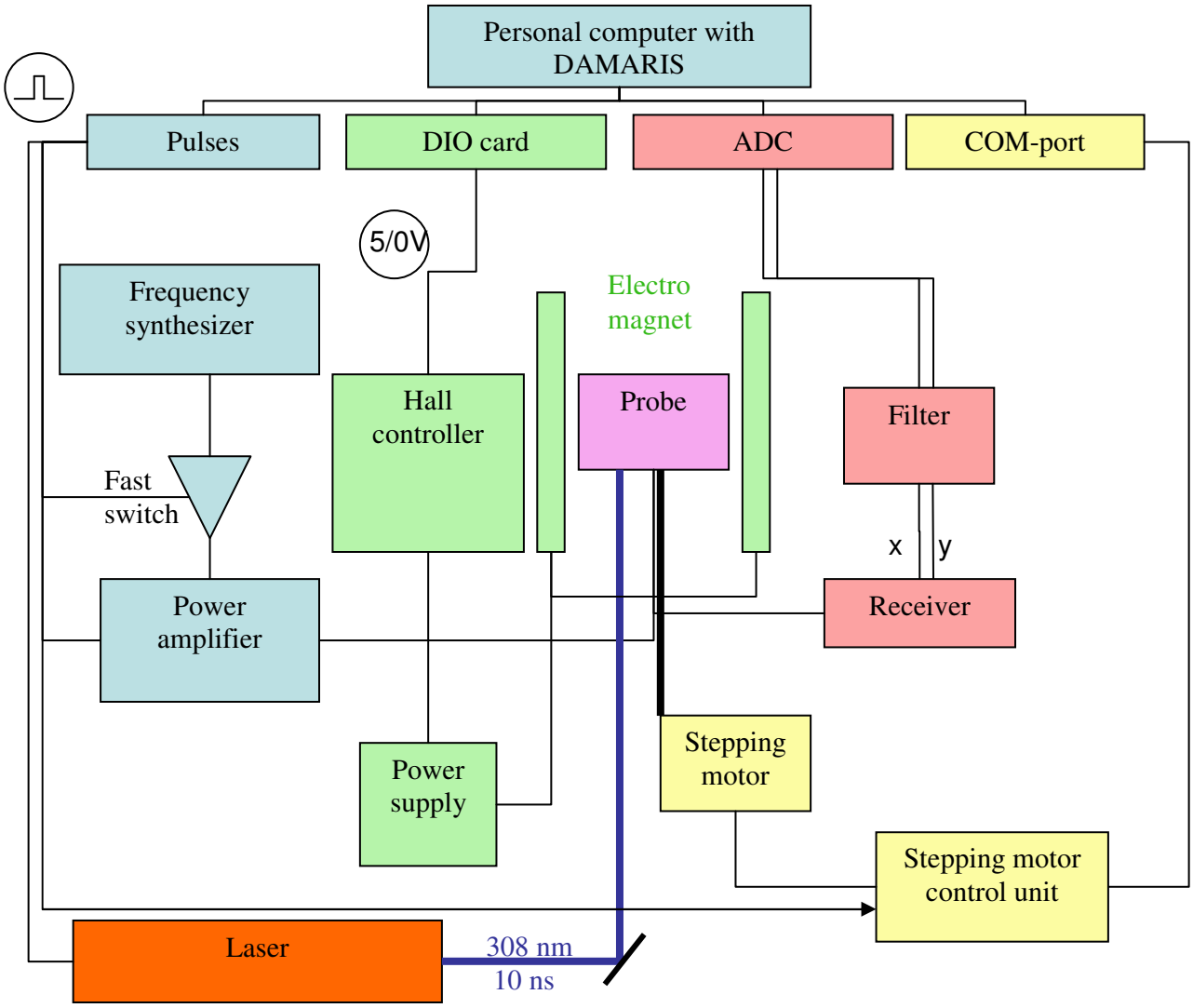

Figure 2.1.1. Block diagram of setup for field-cycling measurements based on DAMARIS.

The modularized approach requires from a user only to know how to program experimental scripts in one of the "front end" versions. The "back end" can be modified when hardware is upgraded. Moreover, the "front end" is written in a language that allows for easy transfer of the program code from one operating system to another. So far, "back ends" are available for Windows and Linux. Presently two types of "front ends" are available: a LabView (National Instruments) based "front end" and a "front end" solely dependent on free software based on the programming language Python and the GIMP (GNU Image Manipulation Program) toolkit GTK+. A "front end" of the second kind was chosen for use in the field-cycling experiments.

The “front end” provides the spectrometer user with two scripts which control the experimental procedure (Experimental script) and the data processing (Result script) separately. To monitor the spectrometer while the measurement is conducted, plots of the recorded datasets can be displayed and saved online. The experimental script programs the experimental sequence. The script pulse sequence of TTL pulses with is generated by the pulse card is translated by the “front end” to the job file. The job file is fed to the “back end” and the “back end” programs pulse sequence and trigger the pulse card to execute the pulse sequence. The pulse card triggers the ADC by a TTL pulse to acquire FID which is then stored as a result file. The result file is taken by the “front end” and processed by the result script. Since the scripts are based on the language Python they offer all features of a full programming language. Fast Fourier Transformation, baseline correction, spectral phasing and other processing tasks are possible. The processed data can be saved in files of different formats for further evaluation. The number of possible processing functions depends only on the Python modules used and the programming skills of the spectrometer user.

The present standard setup for DAMARIS works with a PulseBlaster 24Bit (SpinCore, Gainsville, FL) pulse card and a MI4021 (Spectrum GmbH, Grosshansdorf, Germany) ADC card.

Originally, DAMARIS was developed for experiments in Darmstadt without field-cycling options. To control additional devices which are necessary for field-cycling a digital input/output (DIO) card was implemented (National Instruments PCI-DIO-96). It provides slow TTL pulses for setting the low pass filter and constant TTL levels for setting the low field controller based on a Hall controller (B-H 11C, Bruker). The parameters of stepping motor control unit (Stepping motor ZSH 57-107 and Phytron stepping motor control unit IPP 172-140, Phytron) are set via a standard COM-port. The extension of the “front end” for controlling the required functions of the new hardware was done by Sebastian John. The modules controlling the DIO card and the stepping motor were written in the same Python language and implemented in the “front end”. Thus, the modified “front end” allows controlling all the hardware parts of the field-cycling setup from one experimental script.

In Fig. 2.1.1 a block diagram of the field-cycling setup is shown. The color coding used here is to simplify the description of the scheme. The units in light blue correspond to generation of RF-pulses for NMR excitation that are provided to the probehead (violet) while pink colour applies to units for acquisition of the FID in digital form. The DIO card sets the bandwidth of the analog filter and controls the electromagnet used in low field measurements (green colour). The laser (orange) for optical excitation is triggered from the pulse card. The pre-programmed stepping motor (yellow colour) is triggered by a TTL pulse from the pulse card. The pulse card

synchronizes the whole measurement by controlling TTL pulses. The precision of the synchronization is limited only by the clock of the pulse card whose precision is specified as 10 ns. For comparison, the specifications of the old control system, CXP, and the new DAMARIS are listed in Table 2.1.1.

Table 2.1.1. Comparison of parameters of old and new NMR spectrometer.

Spectrometer control unit	CXP	DAMARIS
ADC Memory size	16 kS	8 MS
Max ADC sampling rate	1 MHz	20 MHz
ADC dynamic range	11 bit	14 bit
Shortest pulse interval/resolution of pulse card	100/100 ns	80/10 ns

The large size of memory allows using oversampling to increase the dynamic range of the ADC.[89,90] Oversampling simply means that the analog signal is sampled at a frequency that is higher than required for the specified frequency bandwidth. Increase of the dynamic range of the ADC as the result of oversampling is equivalent to the reduction of quantization noise which appears due to digitizing process. Apart from the reduction of quantization noise, oversampling has other benefits. As the spectral width is increased, oversampling allows higher cutoff frequencies for the analog low-pass filters (Filter in Fig. 2.1.1). Consequently, a reduced or even negligible attenuation of the frequencies of interest can be achieved. Moreover, the higher cutoff frequency reduces the ringing time of the analog filter and thus transient signals resulting from the high excitation RF-pulse and provides better linearity of the phase response. The ringing leads to distortions of the first data points in the FID. Together with nonlinear phase response it introduces baseline artifacts in the spectra after Fourier transformation of the FID.[91]

The oversampling requires a large amount of disk space that is not practical for FIDs storage. In order to optimize data storage, oversampled FIDs are usually reduced to normal size FIDs before being stored (decimation procedure). In order to prevent falling noise into the spectral range of interest digital filtering should be applied to the FID. Because of the substantial calculations necessary, a special processor is usually required since there is only limited time available for the conversion during data acquisition. In commercial spectrometers dedicated digital signal hardware processors for digital filtering on NMR raw data are used.[92]. So far only infinite impulse response and finite impulse response digital filters are widely used. They are known to produce artifacts: linear phase response and unit impulse response[92] (for example in

the beginning of FID. DAMARIS so far allows only postprocessing of the data. Although the postprocessing is not as fast as hardware digital filtering it allows application of different digital filtering algorithms that do not have abovementioned problems.

Here a fairly simple digital filter with sinc coefficients was used.[90] A rather large number of coefficients was used (300 periods of sinc function) resulting in a sharp cutoff in the frequency domain without visible effects of truncation.[90] Because of the symmetric filter coefficients with their maximum at the center the filter does not introduce artifacts of phase and unit impulse responses.[92] The digital filtering is combined with decimation for reducing the size of FID data. Here the oversampling factor 4 was usually used.

2.2 Field-cycling part

In this subchapter, the part of the setup responsible for the field-cycling is described. Fig. 2.2.1 shows, in generalized fashion, a field-cycling scheme. The cycle consists of three periods, separated by field switching periods, which may be associated, respectively, with preparation, evolution, and detection. As was already mentioned, for the investigation of field dependent nuclear spin effects field-cycling NMR is generally superior to performing the whole NMR experiment at the variable field. The reason is that the signal can always be detected at the maximum instrumentally available magnetic field. This is beneficial for the signal-to-noise ratio and the spectral resolution. In most NMR experiments, the signal is picked up by a magnetic coil, in accordance with Faraday's Law: $|\mathrm{E}| \sim \frac{d\Phi}{dt} \sim \omega M_z$, where E is the measured voltage associated with the rate of change of the magnetic flux Φ, ω is the Larmor frequency and M_z is the magnetization to be detected. Since both terms ω and M_z increase with the field strength (when the Zeeman interaction is dominant, both are nearly proportional to the applied field), the measurement at the highest magnetic field gives substantial gain in sensitivity. Working at a single detection field results in a single spectrometer frequency that makes the resonance circuitry of the probehead simple.

Since the first of such field-cycling experiments was performed by Ramsey and Pound[93] a variety of alternative solutions have been developed and optimized for different purposes; for a review see Refs. 72,94-96 In general, there are two ways of switching the field: electromagnets with fast current switching[97-100] and sample transport between two fields by flow[101,102] or shuttling devices.[83,103,104] The requirements for the particular field-cycling technique of choice are determined by factors such as characteristic time constant of the spin evolution, necessary spectral resolution and desired field range. In the frame of the present investigations the subject

of interest is the field dependence of non-thermal spin polarization of diamagnetic molecule in low viscosity liquids.

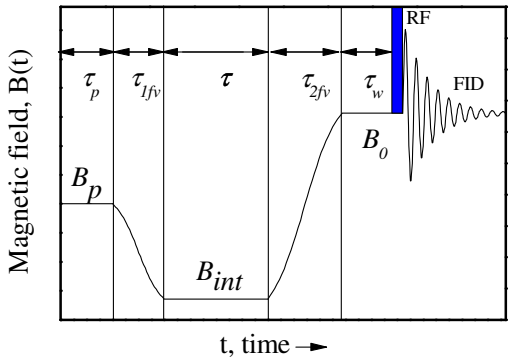

Figure 2.2.1. Typical time scheme of the field-cycling experiment. The cycle consists of a preparation period at field B_p with the duration τ_p, of a switching period to evolution field B_{int} lasting for the time τ_{1fv} and of a delay time τ at this field followed by switching to detection field B_0 during time τ_{2fv} and detection by applying an RF-pulse and recording the FID. Before detection is a short waiting time τ_w inserted allowing the magnetic field to settle after the disturbing field variation.

Essential requirements for the field-cycling setup are the following: first, spectral resolution has to be high enough to observe all relevant spectral features (couplings, chemical shifts, etc.), just as in ordinary liquid-state NMR experiments. High spectral resolution is essential for measuring the complex polarization pattern of multi-component spectra. Due to the interplay among several field dependent and field independent interaction terms, the polarization pattern changes in a complex way when going from zero magnetic field to high field. Therefore, it is important to have a wide range from the small local fields up to several Tesla accessible. The required standards for field switching times correspond to the nuclear relaxation time T_1 with typical values of a couple hundred milliseconds (for small proteins) or slower (for smaller molecules) to conserve a detectable amount of nuclear polarization created during evolution period. The spin system can be transferred in an adiabatic or sudden way depending on the transfer speed and parameters of the spin system. Controlling the time profile of the field switch provides additional information on spin system parameters. An additional requirement for CIDNP measurements is constant light irradiation, which should not be affected by field variation.

In part, these requirements are well solved by different techniques of field-cycling, but there was no solution fulfilling all required specifications. In electromagnets with fast current switching the field homogeneity is far from being acceptable; also with flow-systems or pneumatic sample transfer spectral resolution is insufficient since sample spinning at detection is not feasible. In addition, there are problems with light irradiation; also the timing of field variation could not be controlled with the necessary accuracy. A setup meeting all basic requirements described above had been developed and built in our laboratory.[105,106] However, many improvements concerning cycling speed, spectral resolution and reliability were desirable. Therefore substantial technical alterations were introduced. Below, the description of the setup in its present state is given.

The main idea is mechanical transfer of the sample container together with the whole NMR probe between the position of maximum field of the spectrometer cryomagnetic and a second, variable position in the fringe field of that magnet. This design combines the advantages of a standard NMR setup with a wide range of magnetic field: the highest field (7 T) is reached at the detection position while the use of an auxiliary electromagnet for compensating the fringe field sets the lower limit to a few μT. In contrast to a flow system the transfer of the whole probe allows sample rotation for spinning out field inhomogeneities and thus improve spectral resolution; also, sample temperature is much easier to control. In contrast to both flow system and pneumatically shuttling the sample, the mechanical transfer of the whole probe can be done in a digitally controlled manner along the full transfer path.

General description

The mechanical transfer is based on the stepping motor driven transfer of the whole NMR probe (shuttling) along the bore axis of the 7 T cryomagnet of the spectrometer down to an electromagnet located in the stray field. The scheme of field-cycling setup is shown in Fig. 2.2.2. A real photo of the setup is shown in Fig. 2.2.3. The shuttling system allows positioning the probe at any desired position along the transfer path. In this way it is possible to utilize the stray field of the cryomagnet and to measure HP experiments in the full field range up to 7 T. The achievable field resolution is limited by the field gradient across the sample volume of about 10mm in height. For calibration purposes the stray field has been measured accurately with a Hall probe field meter. At the maximum gradient of about 55 T/m (see Fig. 2.2.2 for the contour of the gradient) the resolution is 350 mT with a step size of 5mT. At fields below 0.1 T the field variation with resolution of 0.03 mT is done by control of the electric current through the

electromagnet. Integrated into the NMR-probe is a spinner system for slow sample rotation (0-150 Hz). The rotor runs continuously keeping sufficient stability during the transfer cycle. Light irradiation can be done at any probe position employing a flexible liquid light guide outside the probe. This way has the advantage of constant irradiation conditions across the full field range.

Auxiliary magnetic system

Below the NMR magnet at a position where the stray field is around 50 mT the auxiliary magnetic system is installed. The z-axis of the electromagnet coincides with that of the super-conducting solenoid. Therefore, depending on direction of magnetic field of the electromagnet one can compensate the stray field to values below Earth field or increase the field up to 100 mT at the center of the electromagnet. A previous electromagnet with a Helmholtz structure of coils[105] was replaced by a solenoid with additional shim coils. The new system provides a more homogeneous magnetic field B_{pol} especially in radial directions (dB/dx and dB/dy). The residual field gradient of the stray field along z is compensated by three incorporated coils reducing the field variation over the sample volume to less than 1 µT. For compensating the small, but perturbing stray field of the electromagnet at the observation position in the NMR magnet a compensation coil is placed between the cryomagnet and the electromagnet, electrically in series with the latter. The geometry and position of the coil are optimized for suppressing offset and linear gradient during detection. As result the residual shift is less than 2 Hz for the whole range of current settings at the electromagnet while no broadening is discernible.

The electrical current is fed to the magnet from a power supply that is controlled by a Bruker field controller using a Hall sensor placed at a bottom plate of the electromagnet. The control parameters are set by DAMARIS.

In order to prevent heating of the electromagnet and compensation coil they are water cooled. The temperature stability turned out to be crucial for stability of the auxiliary magnetic field. For a field stability of 1 µT a stable and uniform temperature with a stability better than ±1 °C is necessary. This is achieved by placing the electromagnet in a silicon oil bath (not shown in Fig. 2.2.3) internally stabilized by a heat exchanger in combination with an external thermostat.

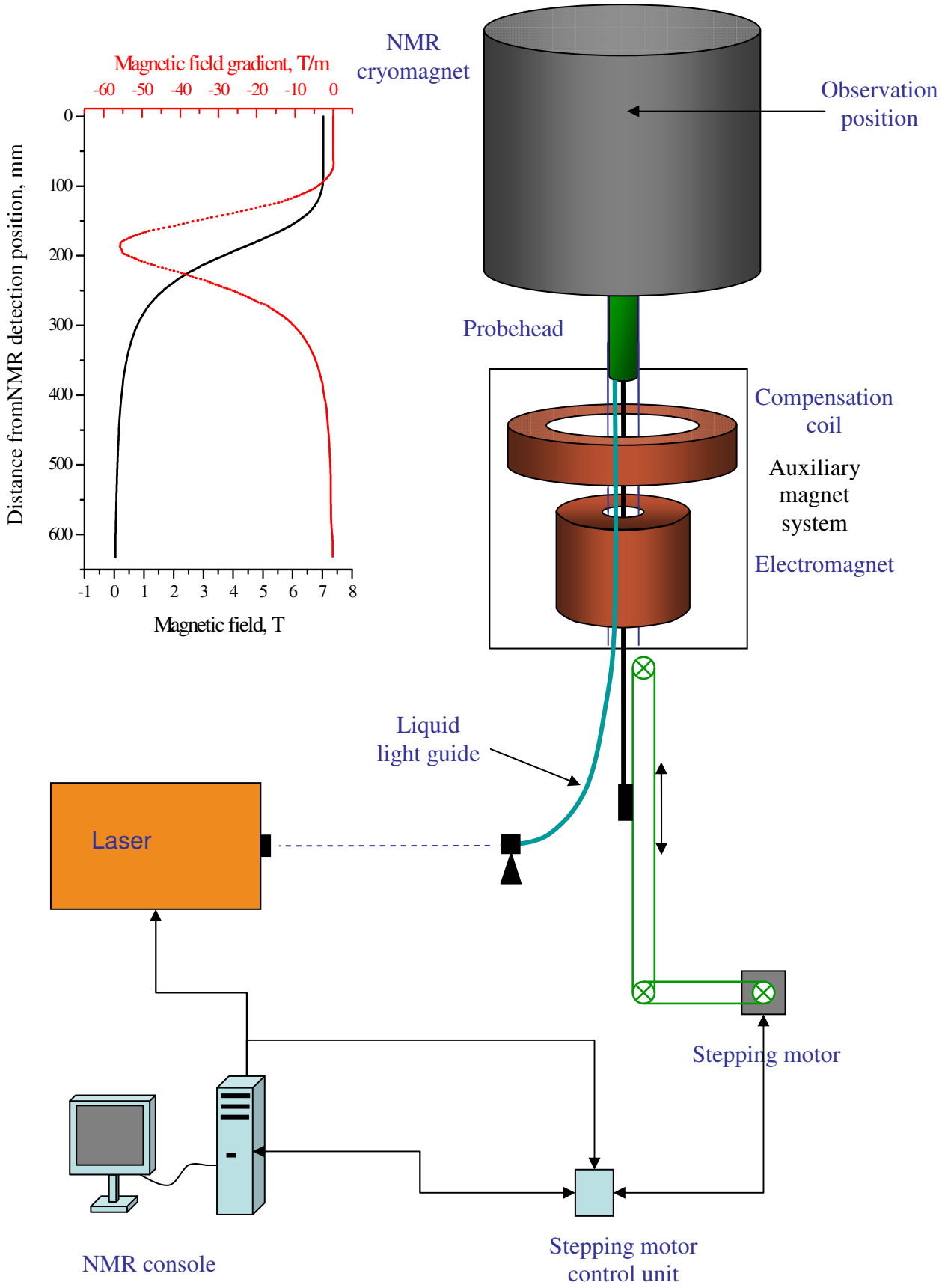

Figure 2.2.2. Scheme of the field-cycling setup with mechanical probe transfer. Insert: magnetic field strength and gradient profile along the transfer path.

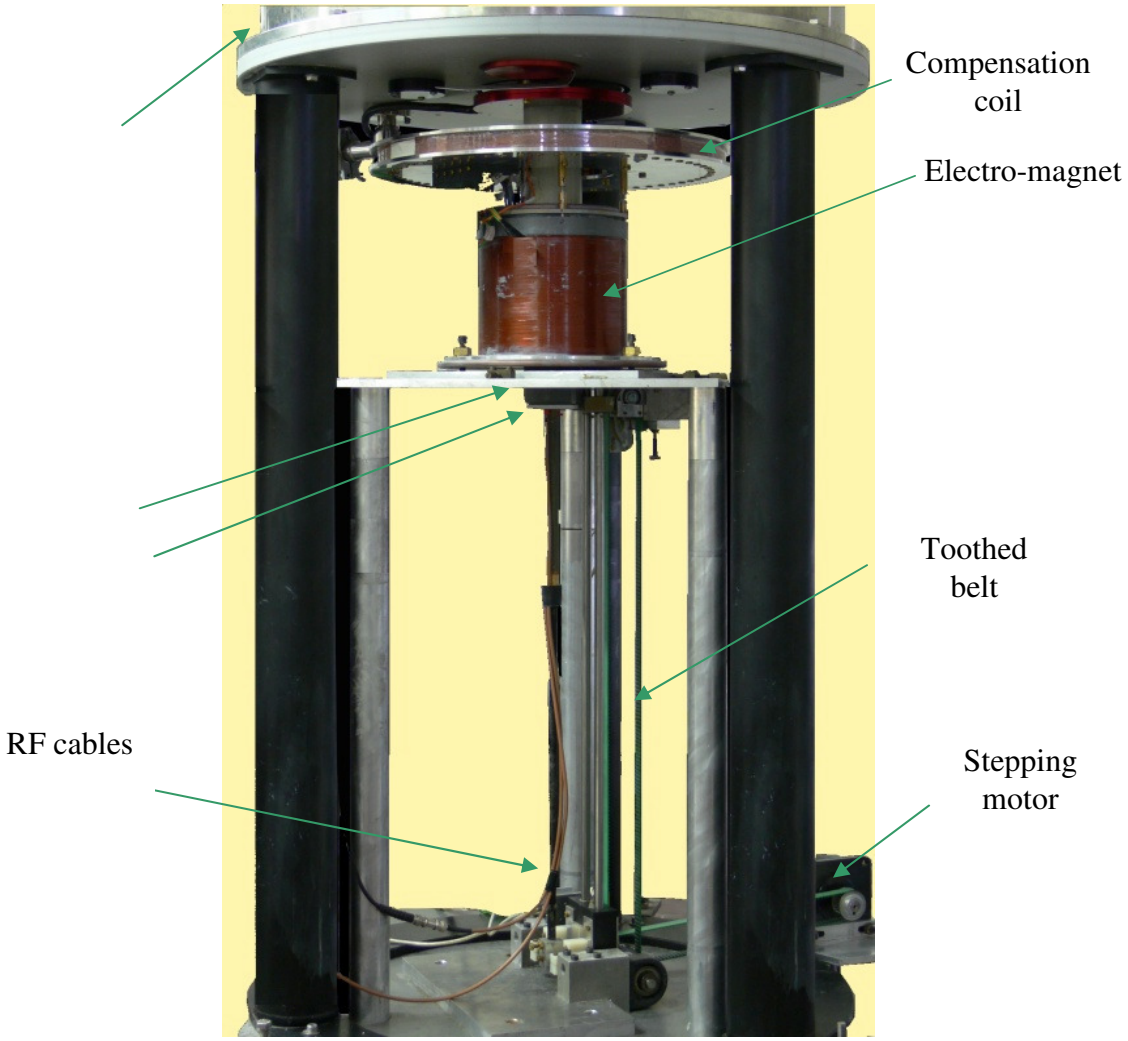

Figure 2.2.3. Photo of the field-cycling setup.

Mechanical shuttling system

The shuttling device consists of a stepping motor, a programmable controller and a transmission system. The probehead is connected via a carbon fiber stick and a slide-rail to a toothed belt which is moved by the stepping motor. Accuracy and reproducibility of the positioning determined by the resolution of the stepping motor and the ratio of gearing are better than 0.1mm. With the distance between the two centers of electro- and cryomagnet being 620 mm and the transferable mass around 0.3 kg the shortest transfer-time is below 0.3 s. For routine use the shuttling unit is controlled by a separate micro-processor. It calculates the motion profile from input parameters (acceleration, velocity and distance) and makes motion possible that has linear acceleration and deceleration and constant velocity. For synchronization purposes the preprogrammed motion is initiated by a trigger pulse from DAMARIS. In principle, a more

versatile shuttling profile can be achieved by direct controlling each step of the stepping motor by the DAMARIS pulse card.

Light irradiation

An essential part of photo-CIDNP experiments is light irradiation of the sample to induce the primary photo-excitation. As the source of light an eximer XeCl laser working at 308 nm is used with a maximal pulse repetition rate of 50 Hz. The individual laser pulses are triggered by DAMARIS. Constant irradiation conditions are very important for measurements of photoreactions. The CIDNP effects strongly depend on the light intensity used for radical pair generation. In order not to obscure field dependent effects the irradiation must be uniform for all probehead positions. This requirement is fulfilled by using a flexible liquid light guide which provides constant light output independent on the position. The commercially available light guide (LUMATEC, S.250) was modified by removing its metallic parts to reduce eddy currents during probe shuttling. The liquid light guide is fixed to the bottom of the probehead where the light is transferred to a cylindrical quartz light guide. The top of it is polished under 45° (Fig. 2.2.4). The resulting surface reflects the light to irradiate the sample from the side. The irradiation pathway through the sample is 4mm (for 5 mm diameter sample tubes). The concentration of light absorption molecules in the solution was adjusted to get an optical density not higher than 0.5.

Probehead

For field-cycling experiments a commercial NMR probehead is not suitable, thus, requiring developing a special probehead. Here only the probehead used for ^{1}H and ^{19}F measurements is described. It was developed in close cooperation with Matthias Seurig.[107] The probehead is a single channel probehead with a resonance circuit tunable between 300 MHz (^{1}H) and 282 MHz (^{19}F) at 7 T. For a description of the probehead used for DNP experiments see Chapter 2.4.

The scheme of the probehead is shown in Fig. 2.2.4. For the reasons that will be discussed below it is necessary to reduce, as much as possible, the formation of eddy currents caused by shuttling of the probehead in the inhomogeneous stray field. To prevent eddy currents in the conducting parts the probehead is built with the minimum possible amount of metallic parts. For this reason, plastic material was used whenever possible. The outer cover was made out of carbon fiber-reinforced plastic that is mechanically strong and light in weight. In addition

it contains graphite additives making its conductivity high enough for electromagnetic shielding of the internal circuit but not high enough for inducing considerable eddy currents. The bottom parts of the probehead are plated with thin copper layer having cuts in radial directions to prevent eddy currents.

The rotation system used is a standard design used in liquid state NMR measurements. The rotation is driven by air flow below the rotor containing the sample tube.

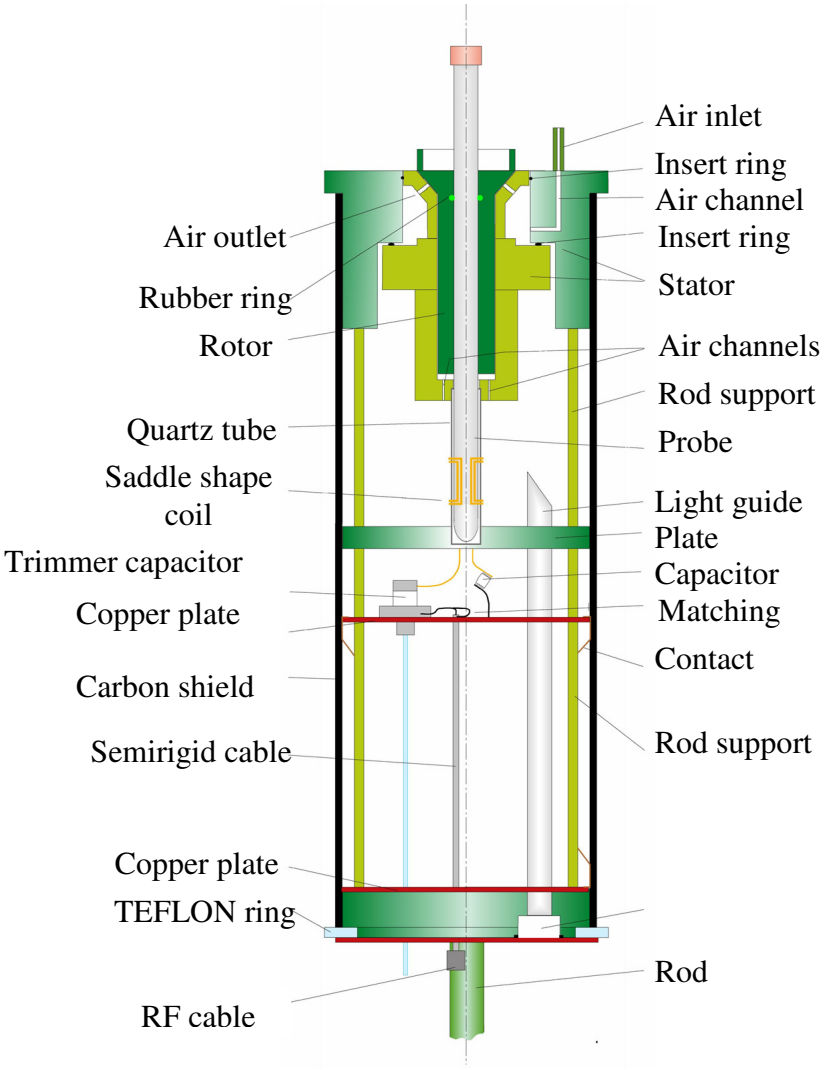

Figure 2.2.4. Scheme of the ^{1}H and ^{19}F field-cycling probehead.

Influence of magnetic susceptibility

The motion of the diamagnetic probehead in the strayfield of the NMR cryomagnet affects the field-cycling measurements. In Fig. 2.2.5 the spectra of acetone measured using different waiting time (τ_w) at B_0 (the protocol shown in Fig. 2.2.1) are shown. As it is seen in Fig.

2.2.5 (upper part) the motion of the probehead induces a field drift during the acquisition of the FID which manifests itself as wiggles on the left side of the NMR line and the shift of the line position over 65 Hz. In order to reduce the waiting time required for an undistorted line shape a new probehead with reduced diamagnetic susceptibility was constructed. In Fig. 2.2.5 the position of the line directly corresponds to the magnetic field in the sample during the acquisition. As is seen the new probehead with reduced diamagnetism produces only a small residual line shift proving that the magnetic susceptibility is the origin of the line distortion.

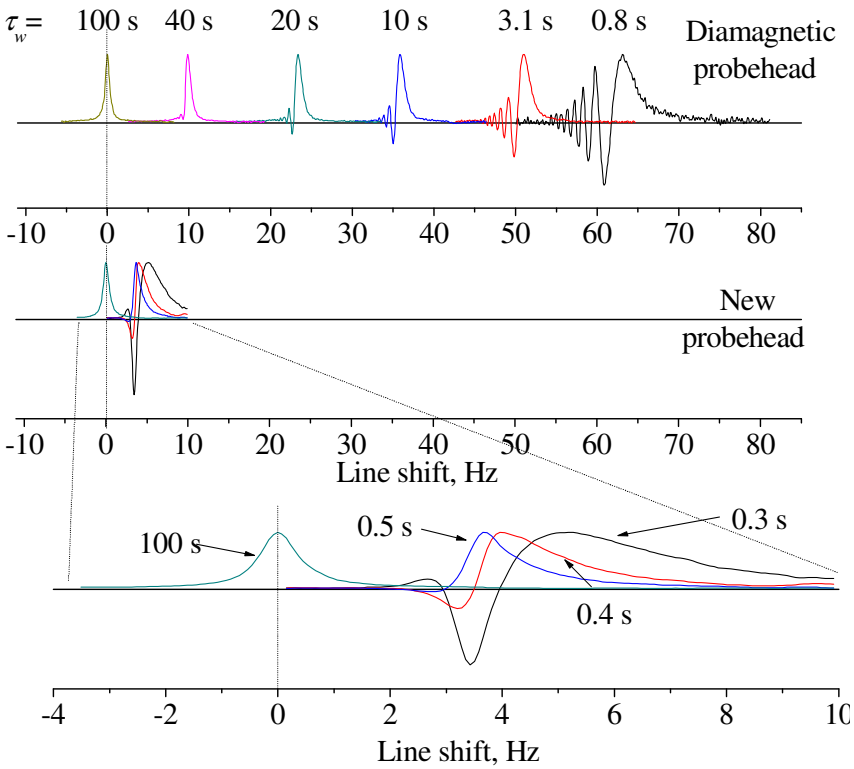

Figure 2.2.5. ^{1}H NMR spectra as function of the waiting time at 7 T (τ_w) after shuttling from the lowest position. Comparison of the old diamagnetic and the new probehead with compensated susceptibility.

The new probehead was produced using self-made compensated plastic material. As was expected and confirmed by the measurements diamagnetic and paramagnetic materials affect the magnetic field in opposite ways and consequently the line shift. Hence, it is possible to mix a paramagnetic with a diamagnetic compound to achieve a material with reduced effect on the field. A two component epoxide resin which is diamagnetic and a paramagnetic filler were chosen to make the desired material. The two components of the epoxide resin are liquid in the beginning making it easy to mix them homogeneously with filler powder. After solidification the

material was used to substitute the probehead parts which were originally made out of diamagnetic material.

To study the influence of magnetic susceptibility one needs to perform very sensitive measurements. The tiny influence of diamagnetism on NMR experiments is probably better observed by the NMR method itself. Here, the ability of a ^{2}H field-lock system to monitor the magnetic field amplitude was used. One can conclude from the correction voltage on z_0 shim coil how magnetic field changes. It was found that old diamagnetic probehead considerably changes the magnetic field when it is placed in the superconducting magnet near the lock resonance coil. Paramagnetic salts placed at the same place change the field in opposite direction.

To find the proper ratio of diamagnetic and paramagnetic compounds the following experiment was conducted. The new material was produced with a different content of filler. Cylinder-shape pieces of this material were placed in the superconducting magnet. The position of the pieces was varied along the bore axis and the correction voltage of the lock was monitored (Fig. 2.2.6). Size of the pieces was the same for all samples (diameter equal to the diameter of the magnet bore 64 mm and height 20 mm). The maximal effect is observed within the height of the pieces but a remarkable effect is still seen ~30 mm apart. The maximal correction voltage depends linearly on the amount of the filler. From the dependence of the correction voltage on the concentration of the paramagnetic filler the proper ratio for compensated material was found.

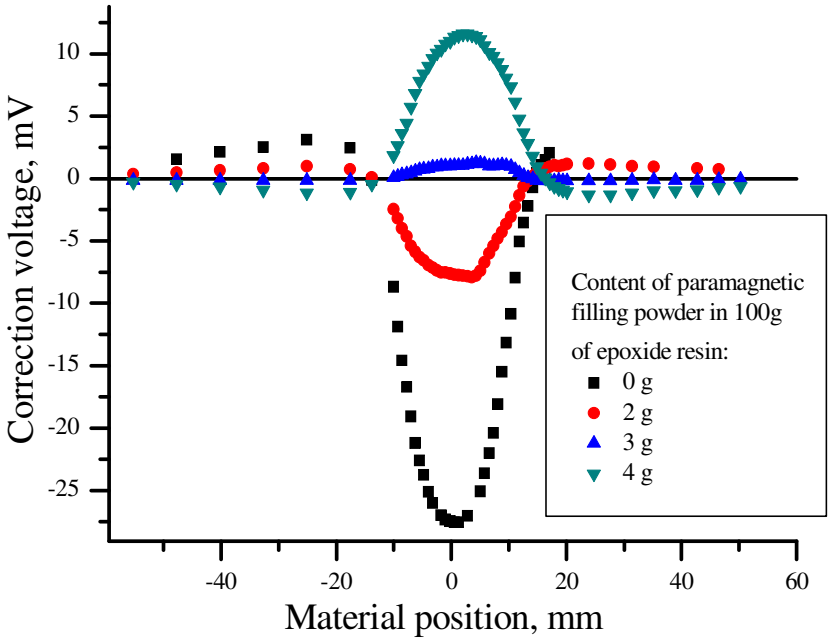

Figure 2.2.6. Dependence of the lock correction voltage on the position of the material in superconducting magnet.

After such a compensation of magnetic susceptibility effects, the residual line shift was attributed to eddy currents in the metallic parts of the probehead.

Reduction of eddy currents

The new probehead built out of zero susceptibility material has much less influence on the magnetic field. However, there were still metallic parts, which are responsible for the fast component in the field drift of the old probehead (see Fig. 2.2.8). The large field drift due to diamagnetism was masking other causes of field change. After the diamagnetism was compensated the residual drift was investigated more closely. The major part was attributed to effects of eddy currents in metal parts of the probehead.

Therefore a further probehead improvement was to remove unnecessary metallic parts. In addition, the copper plates playing the role of electromagnetic shielding of the probehead circuitry were cut in radial directions and the pieces were connected only in one point near the shield of the cable. This modification prevents the flow of eddy current in a big loop, hence the currents produce less magnetic field. However, for reasons of shielding, these plates can not be removed completely.

The previously installed semirigid RF-cable was substituted by one long piece of flexible cable. The semirigid cable has a solid outer conductor with good conductivity perfect for the formation of eddy currents. Also, the metallic connector at the front end of the flexible liquid light guide was replaced by a plastic one.

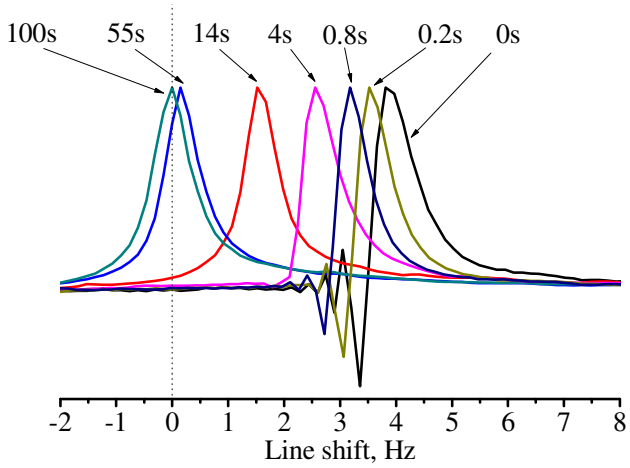

Figure 2.2.7. Line shift obtained for the probehead having less amount of metallic parts as a function of τ_w (τ_{tr2}=376 ms).

After the described modifications were introduced additional test measurements were performed. The shapes of the singlet line of acetone in $CDCl_3$ at variable delay after shuttling from lowest position are presented in Fig. 2.2.7. Compared to the previous probehead with metallic parts (Fig. 2.2.5) the line wiggles became much smaller and narrower as a result of reduction of fast component in the field drift. The slower drift component of the line (3 Hz) is the same as before removing the metal parts. It is reasonable to assume that this effect is due to residual diamagnetism the effect of which can be mathematically corrected.

Mathematical correction of FID

The dependence of the line shift on the waiting time for the old and new probeheads is shown in Fig. 2.2.8. The old probehead has at least a biexponential decay dependence of the field drift with at least two components having different time constant. One is related to diamagnetism and the other are to eddy currents in the metallic parts.

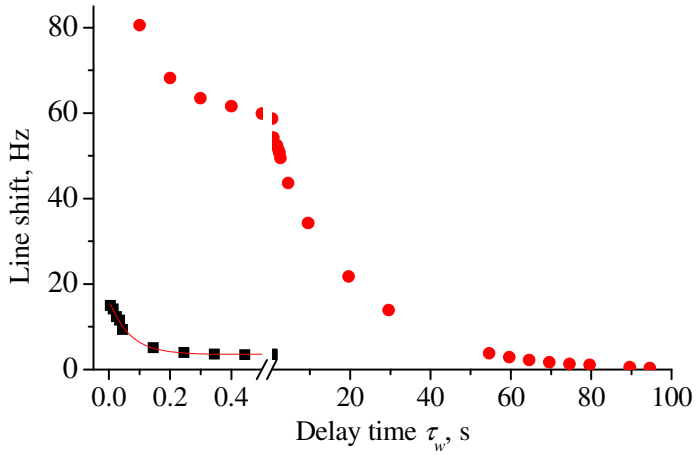

Figure 2.2.8. Line shift dependence on waiting time τ_w. Old diamagnetic probehead (•) with biexponential decay and new probehead (■) with monoexponential decay. The solid red curve is a monoexponential fit to the decay of the new probehead with τ_{decay}=67 ms.

The influence of field drift can be further reduced mathematically by correcting the FID after it is recorded and stored in the computer. The procedure of correction is fully described in Ref. 106 One can assume that resonance frequency, ω, variation is described by a multiexponential decay. If one considers the decay to be the superposition of three exponential functions than equation for ω is the following:

$$\omega(t) = \omega_0 + \Delta\omega_1 e^{-k_1 t} + \Delta\omega_2 e^{-k_2 t} + \Delta\omega_3 e^{-k_3 t}, \qquad (2.2.1)$$

where ω_0 is the resonance frequency without disturbance, $\Delta\omega_i$ is the frequency shift, and k_i is exponential decay of the frequency shift. Under these assumptions the FID is affected by the field drift in the following way:

$$FID_{drift}(t) = e^{-t/T_2} e^{(\omega_0 + \Delta\omega_1 e^{-k_1 t} + \Delta\omega_2 e^{-k_2 t} + \Delta\omega_3 e^{-k_3 t})it}, \quad (2.2.2)$$

where T_2 is transversal relaxation time.

In the program for evaluation the spectra the following function for correction of FID was implemented:

$$f_{cor}(t) = e^{-(\Delta\omega_1 e^{-k_1 t} + \Delta\omega_2 e^{-k_2 t} + \Delta\omega_3 e^{-k_3 t})it} \quad (2.2.3)$$

Three pairs of $\Delta\omega_i$ and k_i parameters were used whose values were varied manually until the line acquires Lorentzian shape. These parameters may change for spectra taken after shuttling from different position in the stray field because they have different waiting time at 7 T. After the probehead modification only monoexponential decay left that significantly simplified procedure of data evaluation.

Summary

In the Table 2.2.1 the specifications of the old and new modified probeheads are summarized. The new one has the following advantages. The first is its light weight because less material was used and the temperature chamber was not yet mounted. The lightness allowed higher possible acceleration/ deceleration and speed. All together it led to the shorter transfer time (290 ms). The second advantage is due to the strongly reduced susceptibility and metal content of the probehead transfer time and minimal total delay was shortened to 290 ms and 30 ms respectively.

Table 2.2.1. Specification of the new and old probeheads.

Probehead	New	Old
Mass, g	370	630
Acceleration, m/s^2	45.2	22.6
Deceleration, m/s^2	-45.2	-22.6
Speed, m/s	2.7	2.2
Transfer time for the full distance, ms	290	400
Minimum total delay τ_w, ms	30	400

Before modification of the probehead the field drift resulting from its diamagnetism and eddy currents was much higher than the line width (65 Hz). The large drift

caused the problem that every spectrum obtained at different fields had to be mathematically corrected individually to obtain good line shape. After reducing the magnetic susceptibility and eddy currents in the probehead the field drift was strongly decreased (<5 Hz). As result, only one set of the correction parameters is necessary for spectra measured at all fields. In this case the line has Lorentzian shape with line broadening of 1 Hz line. It is usually sufficient for the most experiments. One can still uses three set of the correction parameters without line broadening to obtain higher resolution which is limited only by shimming.

2.3 High field time-resolved CIDNP setup

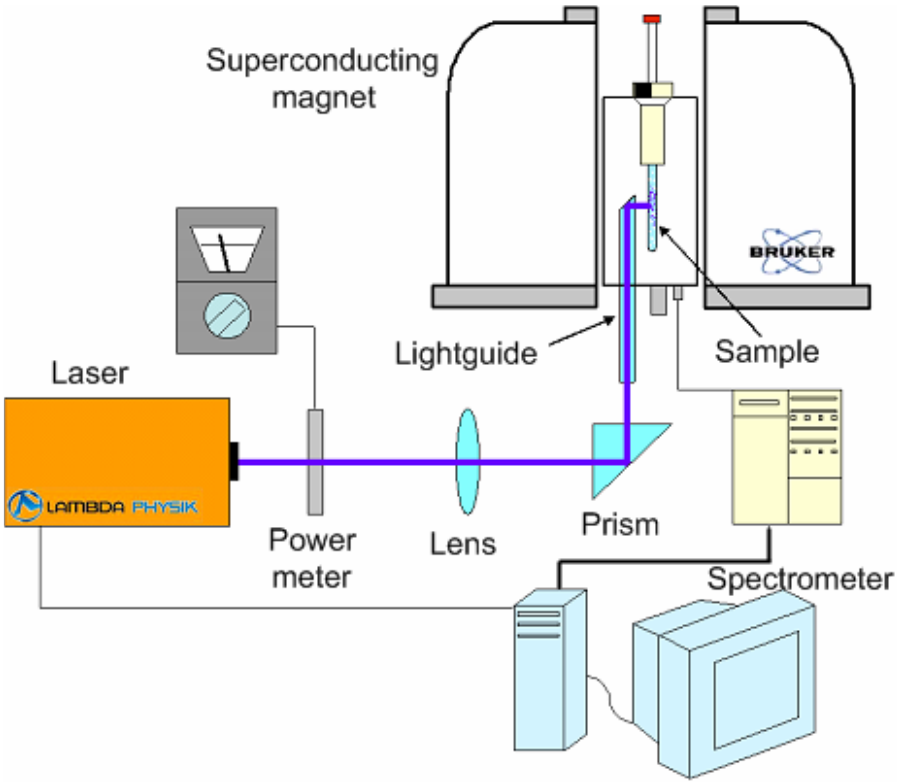

Figure 2.3.1. Scheme of the time-resolved CIDNP setup with side irradiation.

The time-resolved CIDNP (TR-CIDNP) measurements presented here were performed in Novosibirsk at the International Tomography Center. In Fig. 2.3.1. the TR-CIDNP setup is shown. It consists out of NMR spectrometer DRX 200MHz (Bruker) and eximer laser COMPEX Lambda Physik (λ=308 nm) similar to the one used in the field-cycling setup. A commercially available probehead was modified for light irradiation of the sample from the side. The light of the laser is focused on the end of a lightguide inserted in the probehead by an optical system of a quartz lens and a prism. The lightguide is a 5 mm diameter cylindrical quartz rod with the upper

end cut under 45°. This surface acts as a mirror to deflect the light by 90°, as it is done in the prism. The convex surface of the quartz rod acts as a cylindrical lens. After reflection on upper surface the light beam is concentrated to achieve the optimal irradiation conditions of the sample.

The general principles of the time-resolved CIDNP method have been described in Chapter 1. The time sequence of the measurements is shown in Fig. 2.3.2. The sample in the NMR spectrometer is irradiated by the laser. Before applying the laser pulse it is advantageous[108] to remove any equilibrium polarization or residual CIDNP from the preceding sequence by a train of homonuclear saturation pulses provided by the instrument's decoupler (Waltz 16 sequence). This presaturation takes a few milliseconds and has the advantage that only pure CIDNP signals appear in the final spectrum. Shortly after the laser pulse is fired to initiate the radical pair reaction, and during an appropriate and variable delay, τ, the light induced reactions evolve. Then an RF-pulse is applied to measure the magnetization of the diamagnetic polarized products formed during τ. For increasing the time resolution usually the duration of the pulse is much smaller than the duration for a $\pi/2$ flip angle although signal intensity is sacrificed. The FID is acquired in the normal way and the experiment is repeated to obtain the desired signal-to-noise ratio. A kinetic profile of the appearance of the polarized products is obtained by varying τ.

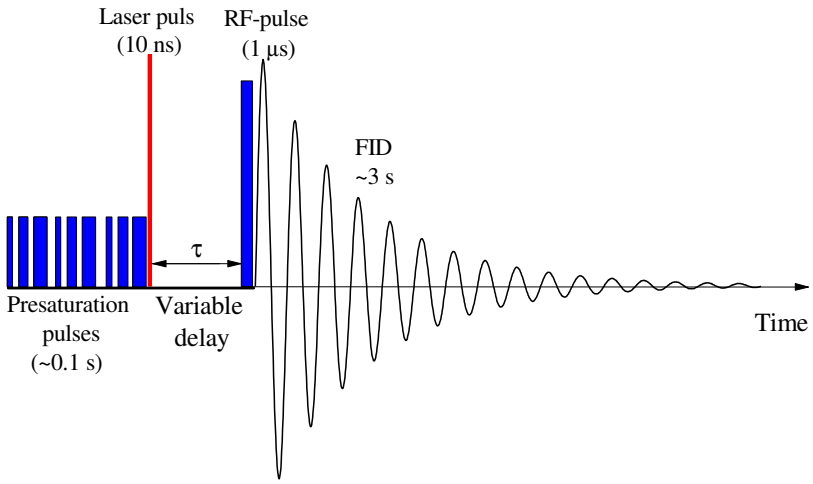

Figure 2.3.2. Pulse diagram of the TR-CIDNP experiment. The time axis has a non-linear scale.

This experiment monitors only the rates of formation of the final diamagnetic products. The paramagnetic intermediates cannot be seen as their spectral lines are much wider and shifted out of the excitation range. A "snapshot" picture of the reaction is taken at the time τ, giving one the polarization of the products at that particular time. Any products formed after the RF-pulse are not seen because their magnetization remains parallel to the main applied field B_z and does

not induce any voltage in the probe coil. The nuclei in the free radicals are not excited by the RF-pulse because their resonance frequencies are shifted by the HFI as compared to diamagnetic molecules.

The time resolution of the experiment depends on both the excitation and probing pulse widths. Here, the laser pulse is short (~10ns) and the limit is determined by the length of the RF-pulse. Usually an RF-pulse of 1 μs was used; the rise time of the RF-pulse was about 50 ns.

2.4 DNP setup

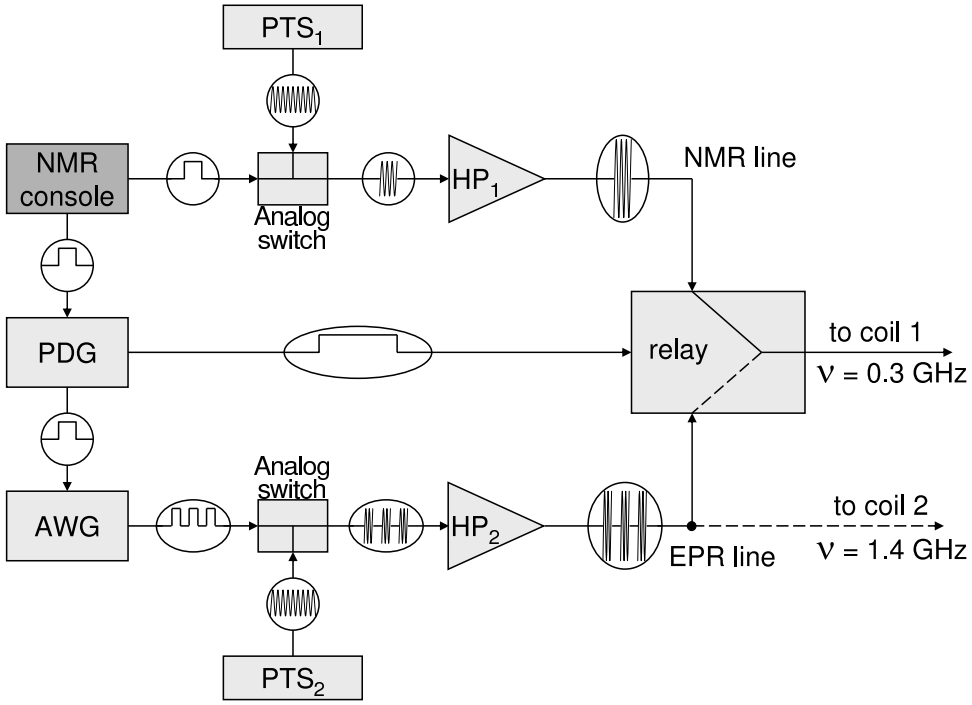

Figure 2.4.1. Block diagram of the DNP setup.

For the low-field DNP experiments (see Chapter 5) several modifications of the field-cycling spectrometer are necessary. Since DNP is a double resonance technique with electron and nuclear spin transition, the corresponding resonance conditions have to be fulfilled. There are possibilities to pump electronic transition at the same magnetic field as NMR detection or use two different fields for them utilizing field-cycling method. Here the DNP electron pumping was performed at two magnetic fields (10.2 mT and 50 mT) while NMR detection was done at 7 T. In the first case of 10.2 mT the electron resonance frequency is the same as resonance frequency of proton detection (300 MHz). So the same as described previously in Chapter 2.2 probehead is

used with minor modifications. In second case, the probehead is equipped with two resonance circuits utilizing two coils: one for NMR detection at 300 MHz and another for electron pumping at 1.4 GHz (Fig. 2.4.2).

Fig. 2.4.1 shows the block diagram of the hardware used to perform EPR pumping and combine it with field-cycling NMR. Since the basic design applies to both the 300 MHz and 1.4 GHz setups the 300 MHz variant will be described first and as a supplement will be added the few changes for 1.4 GHz. From the NMR console (DAMARIS) TTL pulses were send to the frequency generator PTS_1, which created the input pulses with carrier frequency of 300 MHz for the high-power amplifier HP_1 (Class AB amplifier, KALMUS, 500 W Pulse, 150 W CW). The output signal of HP_1 was used for the RF-pulse in NMR detection. In addition, from the NMR console gating TTL pulses were sent to the Pulse Delay Generator (PDG, Stanford Model DG535). Two channels of PDG were used. From the first channel a long TTL pulse was obtained to operate a relay. It allowed to switch between the two power sources used for 300 MHz NMR detection (signal created by HP_1) at 7 T and for EPR pumping performed at $B=B_{pol}$ at a frequency ν_{irr} (signal created by HP_2, see text below). From the second channel of PDG a trigger pulse was sent to the input of the arbitrary waveform generator (AWG) (AWG2021, Sony Tektronix). At the output of AWG one obtains a train of pulses. They gate the frequency generator PTS_2 operating at a carrier frequency of ν_{irr} and driving the high-power amplifier HP_2 (Class A broadband linear amplifier, Electronic Navigation Industries Inc. (ENI) Model 5100L), whose output signal was used to perform the EPR pumping at the frequency ν_{irr}. The field-cycling (i.e., the mechanical transport of the NMR probe) was computer controlled in such a way that during the EPR pumping the sample was at magnetic field B_{pol}. At the end of the EPR pumping cycle the relay was switched from power amplifier HP_2 to HP_1 and synchronously the sample transferred to the detection field of 7 Tesla (corresponding to the 300 MHz NMR frequency of protons). Finally the RF-pulse created by HP_1 was applied and the high-resolution NMR spectrum was recorded. Since pumping of the EPR transitions is done near the frequency of the NMR detection the standard ^1H probehead for field-cycling could be used with slight modifications taking care of the fast electronic spin evolution. The main change is higher damping of the tank circuit to the extent that rise and fall time of the RF-pulses is around 10 ns.

For the pumping at 1.4 GHz a new probehead was designed consisting of a concentric two-coil arrangement shown in Fig. 2.4.2a. The inner saddle shape coil is part of a 300 MHz resonance circuit for NMR detection (RF-coil) with its B_1 field orthogonal to that of the outer coil that is used for EPR pumping at 1.4 GHz. A simplified scheme of the mw resonance circuit

is shown in Fig. 2.4.2b. The ground of the feeding line is decoupled from the coil by a small capacitor for reducing the influence of this coil on the RF circuit characteristics. Because of the smaller filling factor of the outer coil with respect to the inner one and the lower output level of the 1.4 GHz MW amplifier (40 W TWT, Hughes) the maximum B_1 achievable at 1.4 GHz is by a factor of about 8 smaller than at 300 MHz.

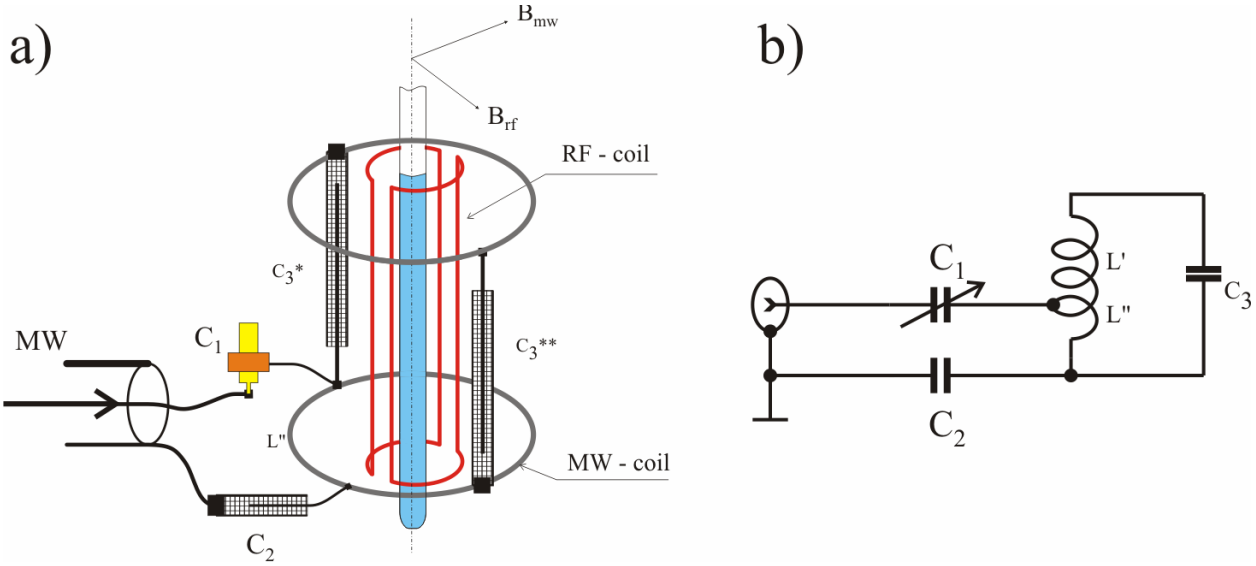

Figure 2.4.2. 300MHz/1.4GHz double resonance circuit: (a) schematic view of the two-coil arrangement, (b) equivalent circuit diagram of 1.4GHz coil.

The MW frequency of 1.4 MHz is a result of following factors. On one hand the size of the MW-coil should be as small as possible to increase the factor of conversion "power - a field". On the other hand the upper limit of frequency is defined by the dimensions of the MW-coil which should be larger than the RF-coil of the NMR contour. The compromise solution of this results in diameter of 10 mm for the MW-coil whereas the RF-coil has diameter of 6 mm. The MW-coil has a degenerate saddle geometry.[109] Applied to the MW contour power is almost 40 W, so it was impossible to use in this circuit nor the conventional surface mounted capacitors nor more powerful high voltage capacitors - the latter are too large compared with the coil size. Instead, as the c_2, c_3^* and c_3^{**} capacitors short pieces of Teflon-insulated coax cable with out diameter 1 mm were used (it is known, that 50 Ohm cable has self-capacitance approximately 1 pF per cm).

3. Polarization transfer in scalar coupled multi spin systems

In field-cycling experiments the magnetic field can be set so low that scalar coupled spins become strongly coupled (eq. 1.4.11), and polarization transfer can take place. Although this effect is more pronounced in hyperpolarized (HP) systems it also influences relaxation experiments. HP transfer is very useful in increasing the sensitivity of nuclei which can not be directly polarized but acquire their high polarization from other nuclei. Channeling polarization to desired target nuclei may become a tool for enhancing the notoriously low sensitivity of NMR spectroscopy. It can be utilized, for instance, in field-cycling NMR studies of biopolymers to re-distribute polarization of specific subsets of the nuclear spin system (directly polarized by CIDNP, PHIP, DNP or other dynamic nuclear polarization techniques) over the molecule.

On other hand, the polarization transfer phenomenon has the negative effect that application of HP for determination of the pathways of chemical reactions and the properties of their intermediates becomes complicated because the process of re-distribution scrambles the information. In field-cycling measurements[72] of relaxation dispersion the strong scalar coupling among relaxing spins was not considered so far. However, the polarization transfer is of coherent nature and the time of efficient polarization re-distribution is expected to be faster than that of the stochastic relaxation processes. Thus, it is very important to understand the mechanism and efficiency of polarization transfer in scalar coupled systems.

The polarization transfer effect does not depend on the particular way of HP generation, it is a general feature of all non-thermal polarizations in field-cycling experiments. Here, the polarization transfer will be considered for the cases of CIDNP and relaxation experiments. CIDNP is chosen because the polarization formation can be well controlled allowing time-resolved measurements of the polarization transfer. Time resolution permits confirmation of the coherent nature of the polarization transfer in strongly coupled spin systems.

In the context of PHIP and DNP experiments polarization transfer will be discussed separately in Chapters 4 and 5.

3.1 Photo-CIDNP transfer in adenosine monophosphate, N-acetylhistidine and cycloundecanone

Polarization generated in CIDNP experiments can be strongly affected by polarization transfer processes leading to drastic changes of the polarization pattern. Hence, it is important to take into account the polarization transfer before applying magnetic field variation techniques to quantitative analysis of the magnetic resonance parameters of radicals studied in photo-CIDNP (Chapter 6).

In this chapter three model systems are studied to check the theory of polarization transfer described in Chapter 1.4. The first system is the molecule adenosine monophosphate (AMP) having only two coupled protons with spin 1/2 in its purine base. This example can be directly compared to the theory. Since polarized systems of only two spins 1/2 are rarely met in practice it is important to demonstrate that analogous polarization transfer effects manifest themselves also in more general situations. To demonstrate this the second system a more complex system, the molecule N-acetylhistidine (His), with five coupled spins 1/2 is chosen. In a third system it is investigated whether the polarization transfer is also effective in multi-spin systems where the target and the source spins of polarization are coupled not directly but through a network of scalar couplings between intermediate spins. This is important for channeling polarization to certain target spins that cannot be polarized directly. In order to study such a long-range polarization transfer the cyclic ketone cycloundecanone $C_{11}H_{20}O$ with its long methylene chain containing twenty protons is used.

Experimental part

The experiments were performed at the field-cycling setup described in Chapter 2 according time scheme shown in Fig. 1.4.1. During τ_p (stage 1) the sample is irradiated by laser pulses with a repetition rate 50 Hz and energy of up to 150 mJ/pulse. Typical time of field variation, τ_{fv}, of the sample transfer to the detection field (stage 3) is 290 ms. The detection of the spectra (stage 4) is done by Fourier transform of the free induction decay recorded after a 90° RF excitation pulse. CIDNP spectra are the differences of spectra taken with and without light irradiation under otherwise identical conditions.

All samples were purged with pure nitrogen gas and sealed in a standard 5 mm Pyrex NMR tube. In order to avoid vortex formation and sample shaking during the transfer, a Teflon plug was inserted into the tube on top of the liquid. AMP, His, cycloundecanone $C_{11}H_{20}O$ (C-11), and the solvents D_2O , DCl, NaOD and $CDCl_3$ were used as received from Sigma-Aldrich. The

dye molecule used, 2,2´-dipyridyl-d_8 (DP), was kindly provided by Herbert Zimmermann (MPI, Heidelberg). The structures of AMP and DP in D_2O at the pH values chosen are shown in Fig. 3.1.1. In the experiments the following samples were used: 5 mM of AMP and 0.7 mM of DP in D_2O at pH=5.0, 100 mM of N-acetylhistidine and 5 mM of DP in D_2O at pH=5.5 and 27 mM of C-11 in $CDCl_3$. The pH value of the aqueous solutions was adjusted by adding small amounts of DCl or NaOD.

Photo-CIDNP transfer in AMP

Basic features of polarization transfer at low magnetic field are observable at the simple system consisting of two coupled spin 1/2 where only one of the spins is initially polarized in a radical reaction while the second one acquires polarization during spin evolution. CIDNP experiments are particular suitable for time-resolved studies because the time of the polarization generation is short comparable to the transfer processes and can be well controlled. As a model AMP molecule was chosen where two coupled protons are present, at the H2 and H8 positions of the purine base, while all other protons of the ribose phosphate moiety are only weakly coupled. Considerable polarization is acquired during the reversible electron transfer reaction between photoexcited DP in the triplet state and AMP:

$$DP + AMP \xrightarrow{h\nu, ISC} {}^{T}DP + AMP \rightarrow {}^{T}\overline{(DP^{\bullet -}...AMP^{\bullet +})} \xleftrightarrow{ISC} {}^{S}\overline{(DP^{\bullet -}...AMP^{\bullet +})} \rightarrow DP + AMP^{*} \qquad (3.1.1)$$

In the course of each reaction cycle polarized AMP molecules (polarization is denoted by the asterisk) are formed due to the nuclear-spin selective intersystem crossing (ISC) in the radical pair stage. Only H8 has considerable HFI in the radical $AMP^{\bullet +}$ and thus acquire CIDNP as a result of the radical reaction while all other protons can obtain polarization only by means of polarization transfer. Using time-resolved CIDNP at high field one can derive the HFI constants from the geminate polarization.[110]

As follows from the intensities of CIDNP at high magnetic field (spectrum 2 in Fig. 3.1.2c) in the radical stage the HFI constant of the H8 proton is much larger than that of the H2 proton. Hence, these two spins constitute a two-spin 1/2 model system with only one proton having strong directly formed polarization and thus are appropriate for studying the CIDNP transfer effects. The fact that at low magnetic fields their CIDNP intensities are close to each other with a ratio being almost constant (not shown here) indicates that HP transfer tends to equalize the polarization of both spins.

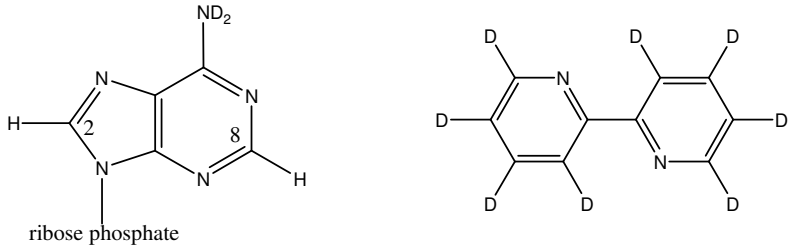

AMP DP

Figure 3.1.1. Structures of the adenosine monophosphate (AMP) and dipyridyl-d_8 (DP) molecules in D_2O.

The case of two coupled spins was considered theoretically in Chapter 1.4 and its analytical solution was derived. Polarization transfer requires that scalar coupling in the regime of strong coupling is present. As a check one-dimensional high resolution NMR experiments (line-width of 0.2 Hz for the single line of water, HDO) were performed the lines of the H2 and H8 signals were 0.4 and 0.7 Hz broad, respectively, and their shapes noticeably differ from a Lorentzian. This line-width is attributed to non-resolved smaller couplings with protons of the ribose moiety and deuterium atoms of the amide group. Only at the top of the H2 and H8 lines some structure (two maxima with a distance of around 0.15 Hz) is seen; simulation allows estimating the coupling to be about 0.3 Hz. Additional homo-nuclear ^{1}H COSY experiments at 9.4 T exhibit cross peaks showing the presence of scalar coupling between H2 and H8 and residual couplings of H8 to the H1' proton of ribose. To show existence of polarization transfer and to demonstrate the coherent nature of the transfer additional measurements with varying the parameters in the timing scheme of the experiments were done. In order to make sure that the condition of strong coupling (1.4.11) is met the experiments were done at the magnetic field of 1 mT where $\delta\nu_{pol}$ is less than 0.01 Hz.

In the first set of experiments, keeping the irradiation time short (that the coherences are not averaged out because of finite τ_p) the evolution time at field B_{pol} , τ_e, was varied (Fig. 3.1.2a). At small values of τ_e the CIDNP of H8 is much stronger than that of H2, however, at longer τ_e the polarization of H2 grows and after one second it is even higher than that of H8. Both polarizations, $\langle I_z^{H2}\rangle/\langle I_z\rangle$ and $\langle I_z^{H8}\rangle/\langle I_z\rangle$, are oscillating around the level of one half of the total polarization $\langle I_z\rangle$ according to (1.4.12). Even though these oscilations have faded after 2.5 s due to relaxation one oscillation period still can be resolved allowing to obtain the oscillating frequency, ν_b, which is about 0.3 Hz. From this result the coupling between H2 and H8 protons is estimated to be 0.3 Hz because at 1 mT $\nu_b >> \delta\nu_{pol}$, with the result that can be obtained from

(1.4.8), $\nu_b \approx J$. The oscillations due to coupling of the two protons with the ribose moiety should have a frequency similar to the coupling value which is around 0.1 Hz. These slow oscillations can not be seen because the damping is too fast. Thus AMP can be considered a system of two coupled spin system.

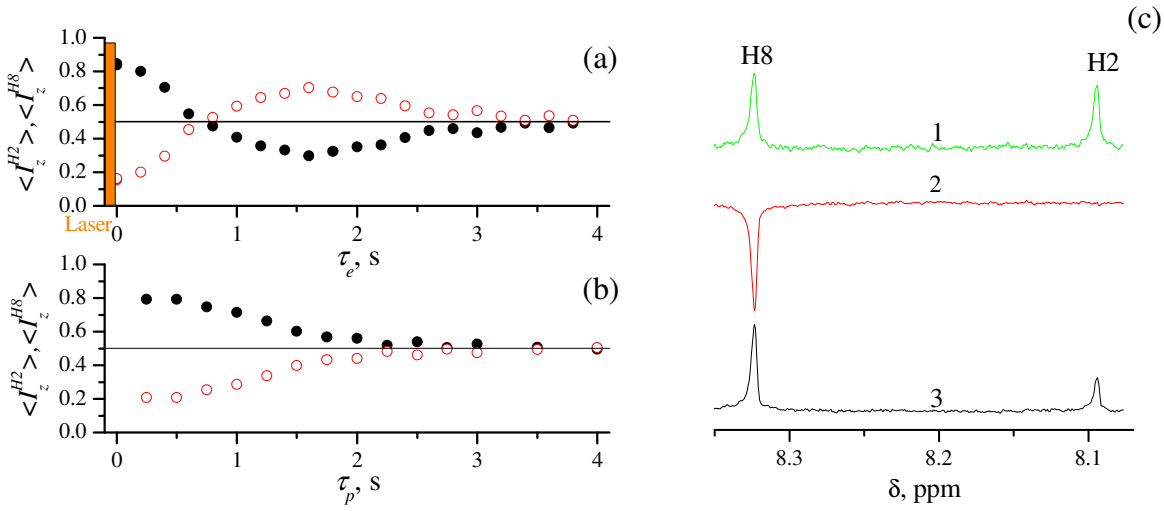

Figure 3.1.2. Kinetics of CIDNP transfer between the H2 and H8 protons of AMP as a function of (a) evolution time τ_e at the polarization field recorded with τ_p=0.2 s, (b) irradiation time τ_p recorded with τ_e=0 and (c) ^{1}H NMR spectra of AMP at 7 T (spectrum 1), CIDNP spectra of AMP at B_{pol}=7 T (spectrum 2) and at B_{pol}=1 mT (spectrum 3) recorded with τ_p=0.2 s, τ_e=0, τ_{tr2}=0.3 s, and an excitation flip angle of 90°. Full black circles refer to the source spin of polarization (H8-proton) and open red circles to the target spin (H2-proton. The CIDNP amplitudes of the spins shown here are normalized by dividing them by the total polarization $\langle I_z \rangle$.

In the second set of measurements τ_e=0 was taken and CIDNP was recorded as a function of the polarization time τ_p (Fig. 3.1.2b). In order to keep the total number of photons constant that are absorbed by the sample the laser repetition rate was varied so that the number of laser flashes was the same for all τ_p values. As in the previous case, when the time of the experiment is short (small τ_p) the CIDNP of H8 is much higher than that of H2. With longer τ_p the polarization of the H8-proton decreases and the polarization of the H2-proton increases, and after τ_p=2 s their CIDNP signals have the same intensities (complete CIDNP re-distribution). This is in accordance with the value of J obtained in the previous experiment.

Both experimental dependences in Fig. 3.1.2 agree with the theoretical predictions (1.4.12) and (1.4.13) made in Chapter 1.4. As is clearly seen, at short times of the experiment the H2-proton is only slightly polarized, but gains polarization from the H8-proton when the

evolution and the polarization times are long enough. The observation of oscillations in the experiment with variable τ_e allows to conclude that the CIDNP transfer proceeds coherently due to strong coupling of the spins at low magnetic fields. It is important to note that for such a small J the field variation from 1 mT to 7 T proceeds non-adiabatically. In these experiments it was not possible to reach the regime of adiabatic field variation because the longitudinal relaxation times (about 2 seconds at low magnetic field) of the spins set a limit.

In case one wants to prevent the polarization re-distribution in strongly coupled spin system ($J \geq \delta\nu$, e.g. in low field), one has to make sure that the second condition of the polarization transfer criterion (1.4.11) is not met. The times of polarization formation (τ_p), evolution ($\tau_{e)}$ and field variation (τ_{fv}) should be sufficiently shorter than $1/J$. Here short τ_{fv} means non-adiabatic field variation for the spin system.

Photo-CIDNP transfer in N-acetylhistidine

A more complex illustration of polarization transfer at low magnetic field is the spin system of N-acetylhistidine (His) with five coupled spins. During the CIDNP experiment four spins are originally polarized and polarization transfer among them is considered. The radical reaction proceeds after quenching of photoexcited DP in the triplet state by His, during which the His protons (H2, H4 and β-CH_2) acquire considerable polarization. The field of 0.8 mT was used as polarization field. At this field all protons except for those of the CH_3-group are strongly coupled.

In Fig. 3.1.3 the CIDNP was recorded as a function of the evolution time after 0.1 s laser irradiation. After laser irradiation, only the protons H2, H4 and β-CH_2 acquire strong CIDNP. Only the protons H2 and H4 are shown because they exhibit the most pronounced oscillating of line intensity as result of the polarization transfer. In contrast to the polarization in the two-spin system, the polarization oscillations of the H2 and H4 protons have more than one oscillating frequency component because of more than one scalar coupling. No analytical solution for this system can be obtained. However, the CIDNP kinetics of both spins can be described by the following equation with three common frequencies:

$$\begin{aligned} < I_z^i > = & < I_1^i > (\cos(2\pi f_1 \tau)) e^{-\tau / T_2^1} + < I_2^i > (\cos(2\pi f_1 \tau)) e^{-\tau / T_2^2} + \\ & < I_3^i > (\cos(2\pi f_1 \tau)) e^{-\tau / T_2^3} + < I_{tot} > e^{-\tau / T_1} + < I_{off}^i > \end{aligned} \qquad (3.1.2)$$

where τ is the evolution time at the polarization field, T_1 is the longitudinal relaxation time of the total polarization and T_2^i is the relaxation times of the coherences, f_1, f_2, f_3 are the frequencies of

the oscillating components, $< I_1^i >, < I_2^i >, < I_3^i >$ are the amplitudes corresponding to the three frequencies, $< I_{tot} >$ is the total polarization and $< I_{off} >$ is an offset.

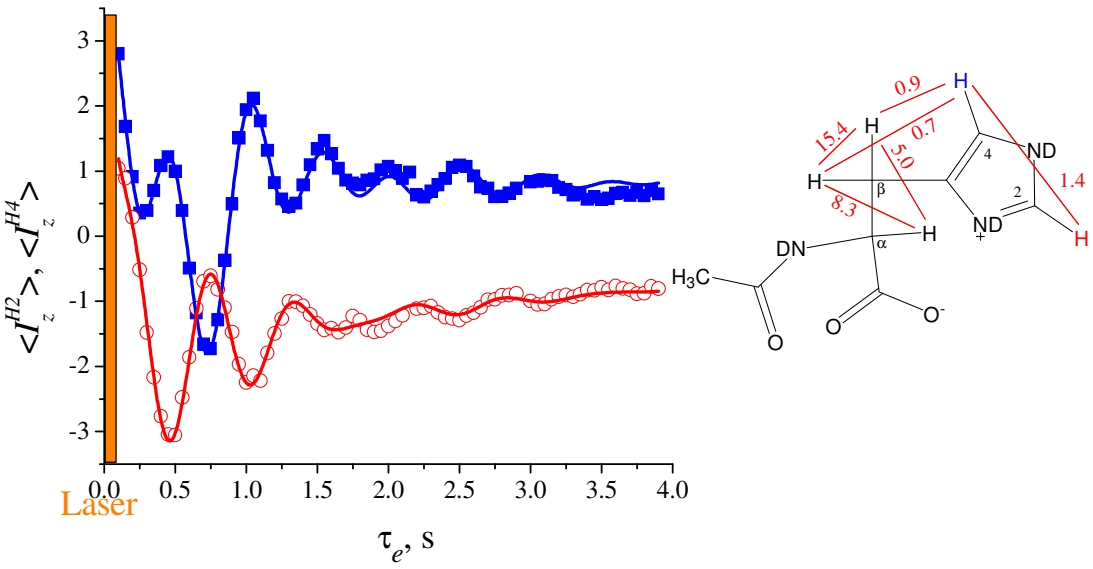

Figure 3.1.3. Kinetics of CIDNP transfer between the H4 (■) and H2 (○) protons of N-acetylhistidine as a function of evolution time τ_e at the polarization field B_{pol} of 0.8 mT recorded with τ_p=0.1 s and simulations by (3.1.2) (solid line of corresponding color) (left), and structure of N-acetylhistidine in D_2O with spin-spin couplings in Hz (right). The CIDNP amplitudes of the spins shown here are normalized to $< I_z^{H2} >$ at zero delay.

The best fit was obtained with the following frequencies: f_1=1.40 Hz, f_2=0.73 Hz and f_3=1.97 Hz that should correspond to coherence frequencies. The frequencies of coherences depend on the difference in energy of the spin states between which the polarization is transferred. In low field where $\delta\nu$ is much smaller than scalar couplings only the couplings should determine the difference in energy between spin levels with the same I_z and thus the frequencies. Two of the oscillating frequencies (1.40 Hz and 0.73 Hz) coincide with spin-spin couplings of the His spin system whereas the third is not. The third frequency, which does not correspond to any scalar coupling, can be combination of the all scalar couplings in the molecule. There can be different reasons for observing only three frequencies. The slow frequencies are damped by short T_2 (all T_2^i are below 1 s and thus is smaller than T_1) and therefore are not seen. The criteria to observe the coherences with the fast frequencies may not be fulfilled because of the insufficiently fast field variation which is in order of 0.3 s. Thus, the frequencies higher than 3 Hz are not seen.

The results show that the coherent polarization transfer occurs also in complex spin systems. It can be used for optimal hyperpolarization manipulation. On the other hand, the observed polarization is significantly different from the polarization produced in course of radical reaction that should be taken into account. For example the polarization of H2 proton even changes the sign.

Long-range polarization transfer in cycloundecanone

Typical CIDNP spectra of the ketone $C_{11}H_{20}O$ (C-11) taken at different fields are shown in Fig. 3.1.5. Here polarization is formed[19] in the highly reversible photoreaction of α-cleavage (Norrish type I photolysis) (Fig. 3.1.4). As a result, after each reaction cycle polarized molecules of the starting compound C-11 are formed. In C-11, the α-CH_2-protons and the β-CH_2-protons of the alkyl moiety of the biradical have the strongest HFI,[112] consequently, they acquire the strongest CIDNP at high magnetic fields. For the other protons (in γ-, δ-, and ε-positions of the cyclic ketone) being far from either radical center the HFI is very small (less than 0.1 mT)[112] and therefore their polarization is negligible at B_{pol}=7 T (see spectrum 2 in Fig. 3.1.5). At B_{pol}=30 mT (spectrum 3) and 2 mT (spectrum 4), however, the observed CIDNP pattern is qualitatively different showing polarization distributed evenly among all the protons. Hence its intensity pattern is no longer consistent with the HFI of the corresponding nuclei. Since it is known from the high-field spectra that only the α-CH_2 and β-CH_2-protons are polarized directly, the polarization of the protons in the γ-, δ-, and ε-positions was attributed to indirectly formed CIDNP due to transfer from the α-CH_2- and β-CH_2-protons.

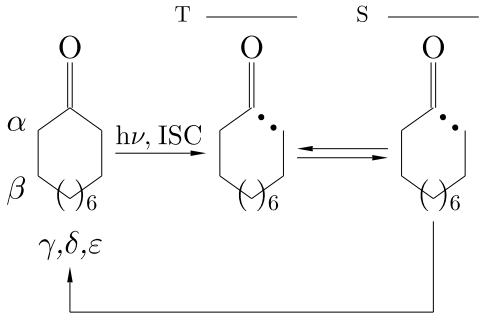

Figure 3.1.4. Scheme of Norrish type I photolysis of cycloundecanone (C-11).

In the case under study the transfer is long-range, e.g., the protons in the β- and ε-positions are separated by five chemical bonds and the scalar spin-spin coupling between them is

very weak so that it does not fulfill the criterion (1.4.11) with respect to the timing of polarization transfer. As before, the cross-relaxation processes between these protons are very inefficient.[113] However, the mechanism of polarization transfer due to the strong coupling of spins is still operative for the following reason. Each group of protons (those in α-, β-, γ-, δ-, ε-position) is strongly coupled to their nearest neighbors (e.g., the α-CH_2-protons to the β-CH_2-protons, the β-CH_2-protons to the γ-CH_2-protons and so on) at low fields. As a result, all the spins are strongly coupled indirectly via the network of the intervening protons. For instance, since the α-CH_2-protons are strongly coupled to the β-CH_2-protons their individual spin states are entangled and the β-CH_2-protons do not interact with the γ-CH_2-protons individually, but together with the α-CH_2-protons. More generally, the eigen-states of the entire spin-system are not the states of the individual protons in the α-, β-, γ-, δ-, or ε-position, but are the entangled combination of all of them. As a consequence, by polarizing the states of the α-CH_2 and β-CH_2-protons in the course of the chemical reaction one produces non-equilibrium population of the states of the *entire* spin system and all the protons exhibit significant CIDNP at the detection field. With the spin-spin coupling constants and the chemical shifts taken from the spectra it is estimated that the condition of strong coupling between the protons of neighboring CH_2-groups (vicinal protons) holds for fields lower than 0.25 T (the couplings between the vicinal protons in the aliphatic chain are typically about 7 Hz and the maximal Δσ value is about 0.7 ppm). At the same time, the vicinal spin-spin coupling constants ensure efficient CIDNP transfer within the timing scheme chosen guaranteeing that a generalized criterion analog to (1.4.11) is fulfilled.

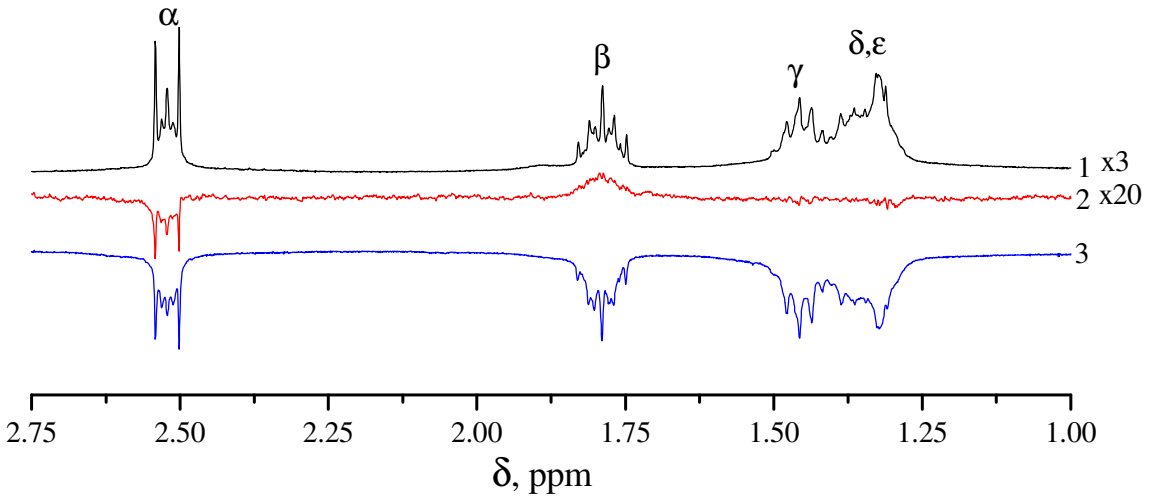

Figure 3.1.5. ^{1}H NMR spectrum of cycloundecanone (C-11) at 7 T (spectrum 1) and photo-CIDNP spectra of C-11 at B_{pol}=7 T (spectrum 2), 30 mT (spectrum 3) and 2 mT (spectrum 4). Experimental conditions: τ_p=1 s, τ_{fv}=0.3 s, all spectra were recorded with a 90° RF-pulse flip angle.

Summary and conclusions

Taking the CIDNP formed in photo-reactions of adenosine monophosphate, N-acetylhistidine and cycloundecanone as examples it was demonstrated that CIDNP at low magnetic fields is strongly affected by scalar coupling of the nuclear spins in the diamagnetic reaction products, leading to a re-distribution of polarization. Indirect polarization of nuclei that have no HFI in the radical stage and therefore are not polarizable at high magnetic field was observed. In a straightforward way the result can be generalized for all dynamic spin polarization phenomena of liquid samples.

On the other hand, the condition of strong coupling alone does not assure efficient polarization transfer. As follows from the theoretical prediction of Chapter 1.4 the timing scheme (the duration of the irradiation, τ_p, of waiting ,τ_e, and field variation, τ_{fv}) of the field-cycling experiment plays a very important role in the low-field CIDNP patterns and the efficiency of polarization re-distribution. On the example of CIDNP of AMP and His the criterion of polarization transfer (eq. 1.4.11) was verified. It is important to emphasize that the polarization transfer due to strong coupling of spins as a coherent process is more efficient than the slower cross-relaxation as a stochastic process. While for the two-spin system an analytical treatment of the kinetics and the comparison with the experimental data was feasible (see eqs. (1.4.12) and (1.4.13)), the CIDNP transfer effects were also observed and qualitatively discussed for more complex spins systems. As is demonstrated on the example of the cyclic ketone the CIDNP transfer can proceed over a long distance without direct coupling. In general, in low-field polarization experiments one can expect long-distance polarization transfer between remote nuclei if they are linked by a network of strongly coupled spins. If, however, the chain of strong interactions is broken (for instance, by introducing a link interacting only weakly with its neighbors) the long-range polarization transfer will no longer occur.

Polarization re-distribution among coupled spins plays a negative role when CIDNP is applied as analytical tool for the investigation radical reactions. In order to get reliable information on initially polarized nuclei one has perform polarization and field variation with minimal time to prevent polarization transfer. In the limit of infinitively short polarization period and sudden field variation no indirect polarization of the other originally non-polarized nuclei occurs (1.4.10). In case of finite time of polarization period and field variation one may try to extrapolate the value of the polarization at time zero from the CIDNP kinetics.

3.2 Relaxation experiments with scalar coupled spin systems

A quantitative study of HP is not complete without the investigation of relaxation effects. Once spin polarization is driven from equilibrium it starts to relax to its thermal equilibrium, therefore the evolution of the spin system is affected by relaxation processes. On the other hand, the analysis of relaxation as it is often used for the characterization of molecular motion is influenced by the preparation of the initial spin order. Moreover, the measurement of relaxation dispersion will depend on how the field variation is performed. In multi-spin systems couplings in the range from the weak to the strong coupling limit are have to be considered.

In the present study the effects of spin-spin couplings, which can be weak or strong depending on the external field strength, on the longitudinal relaxation dispersion of the five systems of increased complexity, from two to five interacting spins 1/2 is explored with the aim to verify the validity of the general theory and its results. These molecules have well-defined NMR properties of the spin system. A general theoretical approach to the longitudinal spin relaxation at arbitrary field strength based on the Redfield theory[82] was described in Chapter 1.5. Site-specific Nuclear Magnetic Relaxation Dispersion (NMRD) of the chosen molecules was studied experimentally by using the fast field-cycling setup described in Chapter 2. Field variation in the range of 100 μT - 7 T enables changing from weak to strong coupling of the spin system upon decreasing of the magnetic field. All the molecules under study are small and have correlation times of their tumbling motion about 100 ps.[114] Thus, in the whole magnetic field range available the condition of fast molecular motion is fulfilled and no influence of the molecular motion on the relaxation dispersion is expected in the conventional model of spin relaxation(1.5.1), i.e. NMRD curve is expected to be flat. Therefore, the site-specific NMRD study will allow elucidating the role of intra-molecular spin-spin interactions and exploring new features of relaxation at low magnetic fields, which is important for the interpretation and correct analysis of relaxation dispersion curves. This knowledge can be applied to molecules having lower mobility and, therefore, showing motional effects in relaxation e.g. to large biomolecules.

Experimental part

5-imidazolecarboxylic acid (ICA), aspartic acid (Asp), N-acetylhistidine (His) and glass distilled deuterated water were received from Sigma-Aldrich. The solution of His was prepared by dissolution of the compound in the NMR-tube without pH adjustment (pH=5.25) and any purification. The other two compounds were found to contain a significant amount of paramagnetic additives, which have a field dependent influence on the relaxation rate in the

solution (*vide infra*). These additives are ions of paramagnetic metals, which can be removed prior to the measurements. The procedures of purification of the aqueous solution were performed as described in Refs. 115,116. All tubes, plugs, caps and glassware were soaked overnight in an solution of alkaline ethylenediaminetetraacetic acid, rinsed thoroughly with Millipore water and dried. After dissolving the compound in D_2O and adjusting the pH value by addition of a small amount of DCl or NaOD the solution was extracted five times with a 0.05% solution of dithizone in carbon tetrachloride. Then it was freeze-dried and again dissolved in glass distilled D_2O that does not change the pH value but reduces the residual abundance of water protons in the sample. The last step was necessary as a large amount of protonated water can give a line in the NMR spectra that strongly overlap with other proton signals. For some relaxation measurements the sample of ICA was not completely purified in order to ensure different relaxation times of the two protons in high field. All samples were sealed in a standard 5 mm Pyrex NMR tube. In order to avoid vortex formation and sample shaking during the transfer, a Teflon plug was inserted into the tube on top of the liquid.

NMRD experiments were carried out according to the protocol depicted in Fig. 3.2.1. The timing scheme of the experiment consists of 5 consecutive stages. At first, the spin system is relaxed to thermal equilibrium during a sufficiently long time, τ_R (far exceeding the relaxation times of the spin system), at the magnetic field B_R and acquires longitudinal Boltzmann spin magnetization at this field (stage 1). Then, during time τ_{1fv} the magnetic field is rapidly switched from B_0 to the field B_{int} of intermediate strength (stage 2). This is the end of the preparation period. At this point the spin system starts to relax to a new equilibrium during the variable time interval τ (stage 3). As the equilibrium magnetization is proportional to the external magnetic field and $B_R \neq B_{int}$, there is longitudinal relaxation taking place during stage 3. At the end of this stage the magnetic field is rapidly switched again during time τ_{2fv} from B_{int} to the observation field B_0 of the NMR spectrometer (stage 4), where the Fourier Transform NMR spectrum is detected (stage 5). At this field the spins are only weakly coupled and therefore can be studied individually. To obtain the relaxation kinetics the intensity of the NMR signal of individual spectral lines was studied as function of the variable time interval τ. The relaxation time, T_1, of the longitudinal relaxation was extracted from such a kinetics by a mono exponential fit (in the case of non-exponential relaxation kinetics this fit gives an apparent relaxation time); finally, the dependence of the extracted T_1 relaxation times on the magnetic field B_{int} is the NMRD curve.

The choice of magnetic field B_R is conditioned by optimization of the signal-to-noise ratio. In the high temperature approximation (valid at ambient temperature) the equilibrium

magnetization at a certain field is proportional to this field, thus, the change in magnetization during relaxation is proportional to $(B_R - B_{\text{int}})$. In the experiments the variation of spin magnetization during relaxation at $B=B_{int}$ was maximized. For this reason, for $B_{\text{int}} < B_0/2$ it is optimal to take $B_R=B_0$ (experiment with magnetization decay at the intermediate field), while for $B_{\text{int}} > B_0/2$ we used $B_R=0$ (magnetization recovery at the field B_{int}). At fields B_{int} close to $B_0/2$ the relaxation times measured were checked whether they coincide for the two choices of B_R. Field variation times τ_{1fv} and τ_{2fv} were taken short (the longest field variation time was 290 ms), $\tau_{1\,fv}, \tau_{2\,fv} << T_1$, so that practically no spin relaxation was taking place during field switching (the shortest T_1 in the experiment was 1.55 s). However, once $\tau_{2\text{fv}}$ is longer than or comparable to the reciprocal of the spin-spin interactions, $1/J_{ij}$, there is re-distribution of the polarization formed at $t=\tau_R+\tau_{1\text{fv}}+\tau$ among coupled spins during field variation. Such effects affect the observed spin polarizations. Since in the experiments there are different spin systems studied with different ratios of $\tau_{2\text{fv}}$ and $1/J_{ij}$, the effects of polarization were taken into account using the real $B(t)$ time profile of field variation were considered.

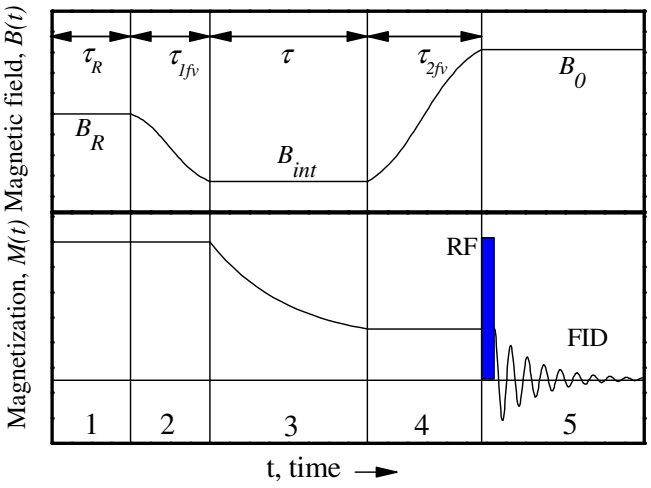

Figure 3.2.1. Experimental protocol of NMRD experiments.

Coherent polarization transfer during relaxation in two-spin system

The aim of experiments described in this chapter is to demonstrate the existence and to quantify the influence of coherent polarization transfer in relaxation processes. Here a simple model of two-spin 1/2 systems, 5-imidazolecarboxylic acid (ICA), was studied. Its ^{1}H NMR spectrum shown in Fig. 3.2.2 contains two doublets. The relaxation times for ICA in the solution prepared from the commercial available compounds are equal to 13 s for H2 and 4 s for H4. These relaxation times depend on the concentration of the additives (*vide infra*).

For the measurements of coherent polarization transfer the first stage of the experimental protocol (Fig. 3.2.1) was slightly modified to make the polarization of the two protons different at $t=\tau_R+\tau_{1fv}$. To the fully relaxed sample at B_R=7 T a non-selective, inverting π-pulse was applied followed by a waiting time to let the magnetization of the protons evolve with their different T_1 and thus acquire a different polarization before field variation (stage 2). The delay time after the π-pulse was chosen to obtain either almost zero total polarization of the two protons or a negative total polarization.

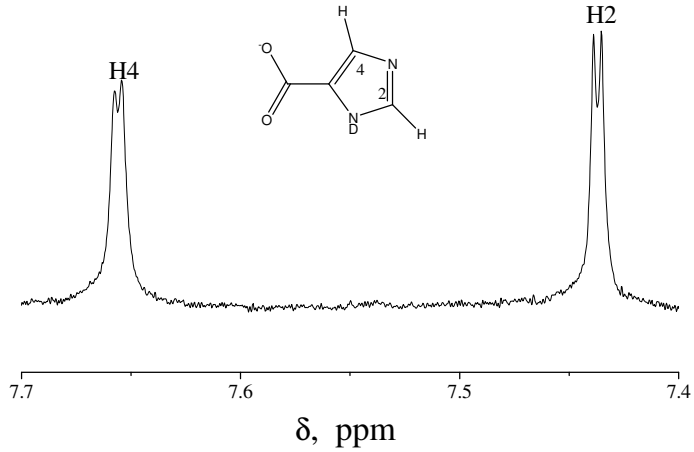

Figure 3.2.2. NMR spectrum and chemical structure of 5-imidazolecarboxylic acid in D_2O pH=11.

The high field relaxation times T_1^i of the two protons H2 and H4 of ICA after its purification from paramagnetic additives in deoxygenated solution of purified D_2O are equal to 55 s for both protons. In order to get different T_1^i value for the two protons in the molecule and thus a more pronounced difference in polarization during preparation period the aqueous solution was prepared without removal of paramagnetic additives. Metal ions can bind specifically to certain parts of a molecule and shorten the relaxation of one spin more efficiently than that of the other. This is the case for ICA (for structure see Fig. 3.2.2) where one of two nitrogen atoms and the carboxyl group have lone electron pairs coordinating with heavy metal ions. However, this coordination is weak and the resident time of the ion in the molecule is short as compared to the NMR time, therefore spin-spin couplings between the ion and protons under study are averaged and not seen in the ^{1}H NMR spectrum; thus they are not included in the simulation discussed below.

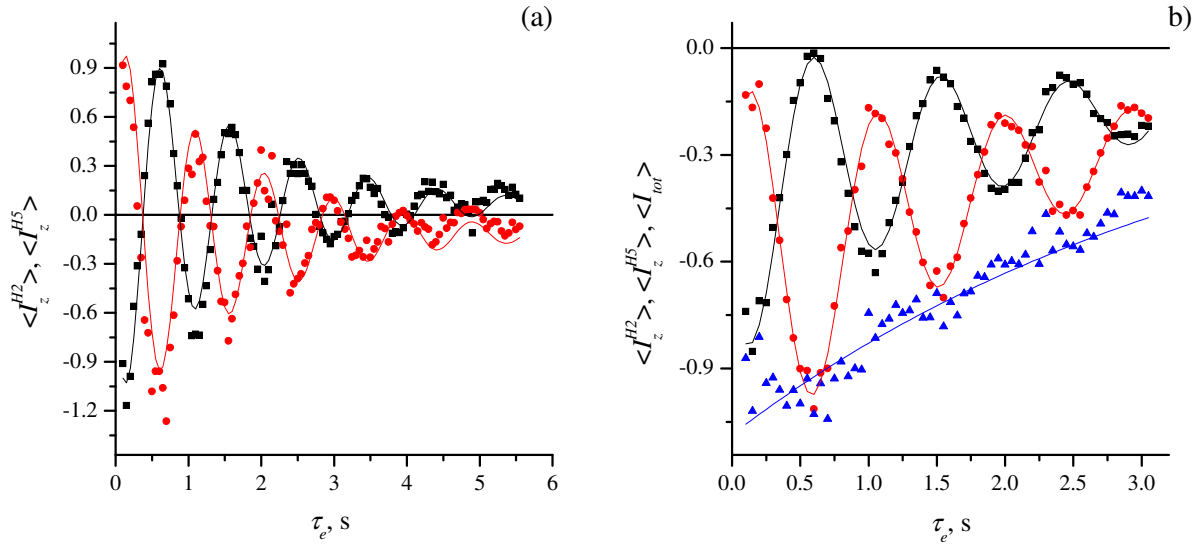

Figure 3.2.3. Relaxation kinetics of 5-imidazolecarboxylic acid at pH=11.9 at B_{int}=10 mT with different starting polarization: a) almost zero total polarization, b) negative total polarization. ■-, ●- and ▲- are polarizations of H2, H4 and their sum, respectively. Simulations shown by solid lines are described in the text. The polarization amplitudes of the spins shown here are normalized to the polarization maximum of H4.

The relaxation kinetics of the two-spin system of ICA is shown in Fig. 3.2.3. After non-adiabatic field variation from B_R to B_{int}=10 mT coherences are produced. The coherences start to oscillate in the strongly-coupled two-spin system. At this point the situation resembles the CIDNP evolution in the two-spin system of AMP described in the previous chapter. The only significant difference is the total polarization of the two protons. Here, the total polarization was produced to be zero. The oscillation frequency, ν, is defined by spin-spin coupling at low field (eq. (1.4.8), $\nu \approx J$). The relaxation kinetics with zero total starting polarization was simulated using an equation similar to (3.1.2) for the detected polarization, $< I_z^i >$:

$$< I_z^i >=< I_0^i > (\cos(2\pi(\tau-\varphi)J))e^{-\tau/T_2} + < I_{off}^i >, \qquad (3.2.1)$$

where τ is evolution time at B_{int}, φ is a phase factor, T_2 is the relaxation time of the coherences, $< I_0^i >$ is the starting polarization and $< I_{off}^i >$ is an offset. The phase shift, φ, occurs because of evolution during the finite time of the field variation. The result of the fitting procedure is shown in Fig. 3.2.3 by the solid lines. The derived constant of the spin-spin coupling J=1.05 Hz coincides with the value (1.0 Hz) obtained from simulation of the ^{1}H NMR spectrum (Fig. 3.2.2). From the fit also the relaxation time T_2=1.77 s was obtained.

From the relaxation kinetics with negative total starting polarization, $< I_{tot} >$, its longitudinal relaxation time T_1 can be obtained using following equation:

$$< I_z^i >=< I_0^i > (\cos(2\pi(\tau-\varphi)J))e^{-t/T_2} + < I_{tot} > e^{-\tau/T_1} + < I_{off}^i > \quad (3.2.2)$$

Knowing T_2 from previous experiment the longitudinal relaxation time T_1=3.7 s was obtained.

The oscillatory behavior proves the coherent nature of polarization transfer during relaxation experiments at low field. Non-adiabatic field variation is necessary for creating non-diagonal elements in the density matrix and, thus, for coherent polarization transfer. In case of the adiabatic sample transfer no oscillatory polarization transfer is expected. However, as a consequence of strong coupling the eigen-states of the spin system are collective states of spins. Thus, it is clear that strong coupling between the spins significantly affects the relaxation processes of molecules. In order to demonstrate the consequence the nuclear molecular relaxation dispersion of several molecules was investigated and described in the following subchapters.

Relaxation dispersion of two-spin 1/2 system

The Nuclear Magnetic Relaxation Dispersion (NMRD) of ICA in D_2O was measured to check the theoretical predictions for two-spin 1/2 systems described in Ref. 86. In order to obtain different relaxation times of two protons the solution was not purified. As a small molecule in a low-viscosity solvent, ICA is expected to have a relaxation dispersion that is independent of the magnetic field. However, the experimental results shown in Fig. 3.2.4 represent a stepwise behavior of the T_1 dispersion. The two protons relaxing with individual T_1 at high magnetic field tend to relax with a common longitudinal relaxation time at low field. The NMRD curve of the H4 proton does not stay flat. Below 0.5 T the T_1 of H4 increases coming closer to T_1 of H2. The NMRD curves of both protons were simulated using the NMR parameters obtained from simulation of the spectrum shown in Fig. 3.2.2. The individual T_1^i times were taken from the relaxation measurements at 7 T (13.3 s and 4.0 s for H2 and H4, respectively).

While the simulation base on scalar coupling reproduces the position in the field where both protons start to relax with a common rate it deviates in the values of T_1 times. In the field range, where spins are strongly coupled, they are expected to relax with the average rate. In this case the average is T_1=6.2 s. In the experiment the common T_1 at 0.1 mT is found to be 4 s. The reason for the deviation is an additional field dependent relaxation mechanism. As was shown in the previous subchapter paramagnetic additives in the solution act as a source of relaxation. The

relaxation rate of typical paramagnetic metal ions depends on the magnetic field. Moreover, such a dispersion should be seen within the field range of the experiment.[73]

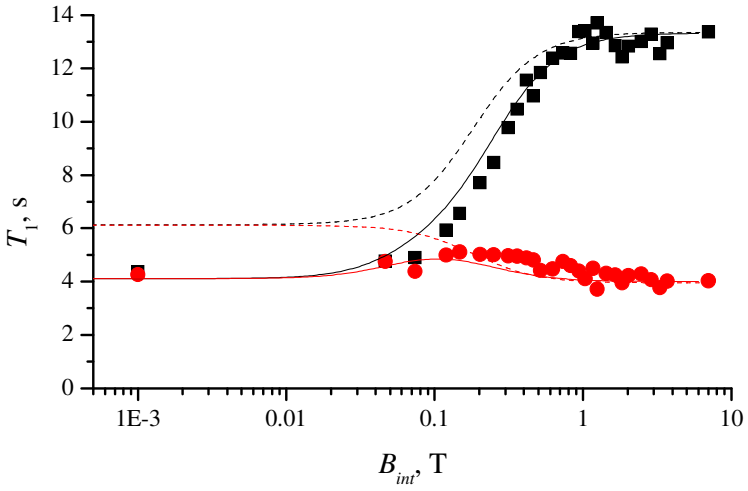

Figure 3.2.4. NMRD of 5-imidazolecarboxylic acid: experimental data (■-H2, ●-H4) and simulation (line of corresponding color). Dashed lines are simulations taking into account only scalar spin-spin interaction. Solid lines are simulations which considering both scalar interaction and paramagnetic influences on the NMRD. NMR parameters: J=1.05 Hz, Δσ=0.23 ppm. In the simulations sudden field variation was considered. Paramagnetic influence was taken into account with following correlation times: τ_c=29 ps (H2) and τ_c=115 ps (H4).

Both field dependent effects can be modeled in the following way. Before taking into account strong coupling of the spins the relaxation rate, T_1^i, is defined by intrinsic relaxation of the diamagnetic molecule and additional relaxation from paramagnetic ions:

$$R_1^i = \frac{1}{T_1^i} = R_0^i + R_{para}^i . \qquad (3.2.3)$$

Here R_0^i is intrinsic relaxation rate of the molecule and R_{para}^i is relaxation rate due to paramagnetic additives. The kind of paramagnetic additives and its partial concentrations were not known therefore a simple model describing its field dependence was chosen (1.5.1) with τ_c representing the residence time of the metal ion on the ICA molecule.

Simulations with different correlation times, τ_c, were performed and the best simulation is shown in Fig. 3.2.4. A good agreement between experimental data and simulation was obtained using different correlation times for the two protons: τ_c=29 ps (H2) and τ_c=115 ps (H4). The simulation is surprisingly good considering the oversimplified model of paramagnetic influence on the relaxation rate in the complex.[73,114]

The effect of paramagnetic additives on the relaxation is often used as a source of structural, thermodynamic, and dynamic information, for example in metalloproteins.[117] The site-specific relaxation dispersion measurement introduced here have therefore immediate relevance to such investigations.

To suppress the effect of paramagnetic additives all other relaxation experiments were performed with purified solutions.

Relaxation dispersion of three-spin 1/2 system

With an increasing number of spins in a coupled system the complexity of the system grows. The theoretical calculations predict that a three-spin 1/2 system can already have one level anti-crossing in the field dependence with resulting features in the NMRD (Chapter 1.4). It will be shown that the occurrence of the level anti-crossing depends on the relative signs of the spin-spin couplings. In this chapter two compounds, aspartic acid and 3-furoic acid, were used to demonstrate this behavior.

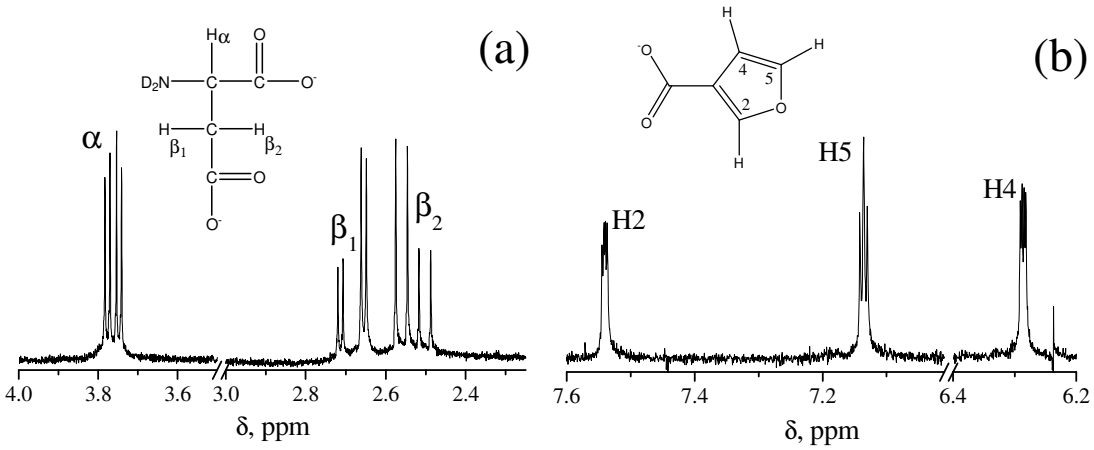

Figure 3.2.5. NMR spectra and chemical structures of (a) aspartic acid at pH=8.9 0.1M and (b) 3-furoic acid at pH=8.2 0.05M in D_2O.

The NMR spectra and structure of the compounds are shown in Fig. 3.2.5. Aspartic acid is a relatively simple amino acid containing one proton in its α-position (α-CH) and two protons in its β-position (β-CH_2). A three-spin system of this kind is part of many other amino acids, hence the results obtained by its investigation can be used in other amino acid studies.

The relaxation dispersion of aspartic acid is shown in Fig. 3.2.6. The α-CH proton relaxing at high magnetic field with long individual T_1^i of 7.1 s and two β-CH_2 relaxing with short T_1^i of 1.6 s tend to relax with a common relaxation time at low field. However, the T_1

values of them do not coincide as it was in the case of the two-spin system but stay separate although the condition of strong coupling is completely fulfilled (1.4.11). In addition, around 0.5 T a dip appears in the relaxation dispersion of α-CH. The position of the dip corresponds to a spin level anti-crossing in the three-spin system. Simulations for both, sudden and adiabatic field variation are shown in Fig. 3.2.6. In the simulations the NMR parameters obtained from Fig. 3.2.5a were used. Both simulations reproduce the position of the steep stepwise growth of the relaxation time at 0.4 T, but only the sudden field variation predicts the dip in the α proton relaxation dispersion. Moreover, the adiabatic field variation results in a common T_1 at low field whereas the sudden field variation predicts that the T_1's stay apart in agreement with the experimental observations. Therefore, the one can draw the conclusion that the field variation was non-adiabatic, close to the sudden limit.

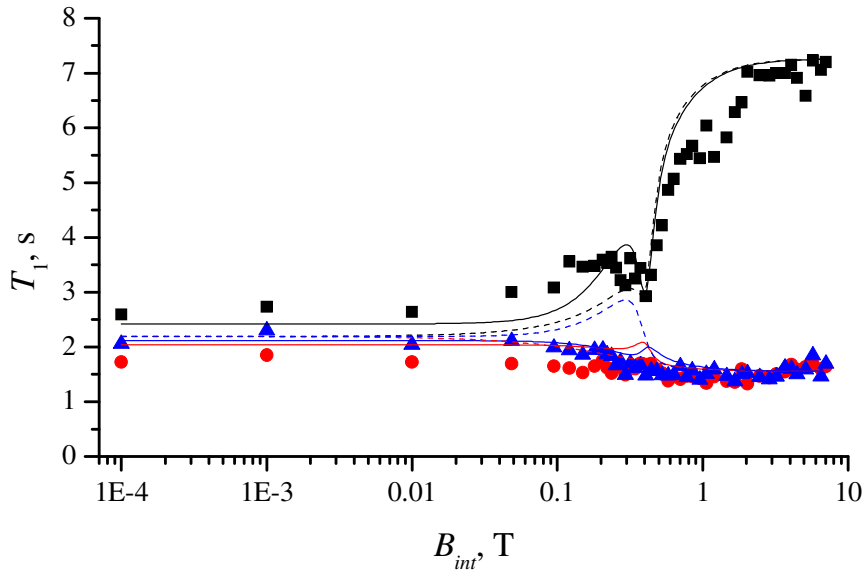

Figure 3.2.6. Relaxation time dispersion of aspartic acid protons: experimental data (■ - α proton, ● - β_1 proton, ▲ - β_2 proton) and simulation (line with corresponding color). Solid lines represent simulation with sudden field variation whereas the dashed lines represent adiabatic field variation. For the simulation NMR parameters obtained from the spectrum and $\mathcal{T}_1^i$ obtained from the high-field measurements were used: α-CH-proton δ=3.76 ppm $\mathcal{T}_1^\alpha$ =7.1 s, β_1-CH_2-proton δ=2.7 ppm $\mathcal{T}_1^{\beta_1}$ =1.55 s, β_2-CH_2-proton δ=2.53 ppm $\mathcal{T}_1^{\beta_2}$ =1.55s, $J_{\alpha\beta1}$=3.80 Hz, $J_{\alpha\beta2}$=8.93 Hz, $J_{\beta1\beta2}$=-17.3 Hz.

The NMRD of 3-furoic acid has a shape different from that of aspartic acid (Fig. 3.2.7). No sharp dip or peak are observed. In contrast to aspartic acid, in 3-furoic acid H5 is closer to H2 in the spectrum than H4 and their NMRD curves approach to each other at a higher than that

magnetic field where H4 is influenced. At lower field H4 becomes also strongly coupled and its T_1 grows. At field below 0.02 T T_1 of H4 is longer than that of H5. A similar behavior is observed for aspartic acid where T_1 of the β_2-CH_2-proton is closer to that of the α-CH-proton although the chemical shift difference is larger than that of β_1-CH_2-proton. In addition, because of different chemical shifts and scalar coupling the onset of strong coupling is at different field.

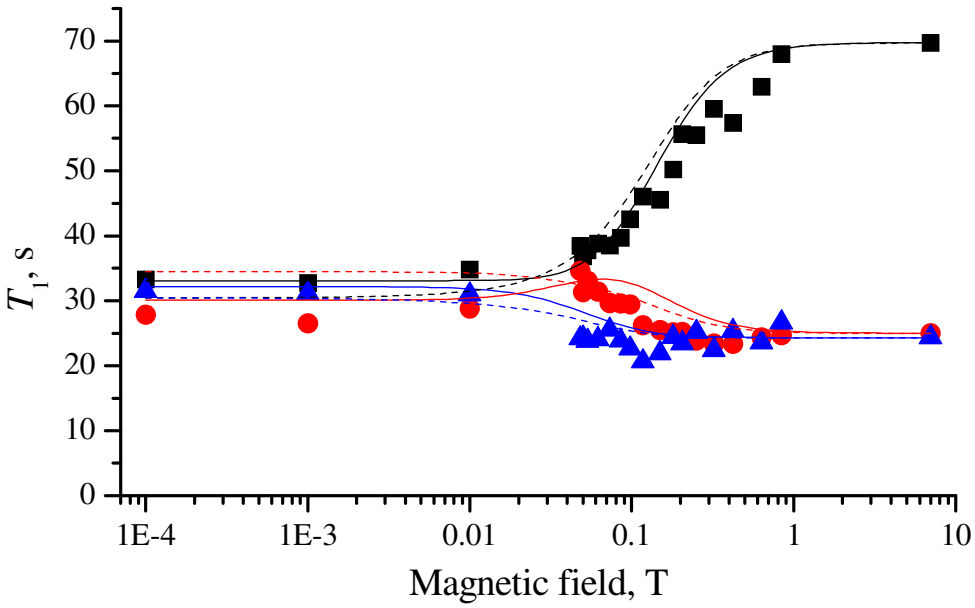

Figure 3.2.7. Relaxation time dispersion of 3-furoic acid protons: experimental data (■ - H2 proton, ▲ - H4 proton, ● - H5 proton) and simulation (line with corresponding color). Solid lines represent a simulation with sudden field variation while dashed lines represent adiabatic field variation. For the simulation NMR parameters obtained from the spectrum were used: H2 proton δ=7.54 ppm T_1=69.7 s, H4 proton δ=6.29 ppm T_1=24.3 s, H5 proton δ=7.14 ppm T_1=25.0s, J_{H2H4}=0.86 Hz, J_{H2H5}=1.58 Hz, J_{H4H5}=1.90 Hz.

The relaxation dispersion of a three-spin 1/2 system strongly depends on the relative signs of the spin-spin couplings. Only the simulation assuming spin-spin couplings with the same sign reproduces the change of the T_1 order ($T_1^{H2} > T_1^{H4} > T_1^{H5}$) in the relaxation dispersion at 0.02 T. Other sign combinations do not show this feature. As for aspartic acid the assumption of sudden field variation leads to a simulation that reproduces well the experimental data. The simulation under assumption of adiabatic transfer results in a wrong order of T_1 at low field. When, however, this experiment is performed with slow field variation (τ_{fv1} and τ_{fv2} equal to 2.5 s) the order of T_1 at 0.1 mT changes and agree with the simulation for adiabatic field variation.

Relaxation dispersion of two-proton and two-fluorine system

In this chapter a system having two protons and two fluorine nuclei will be studied in its relaxation dispersion behavior. It is a simple model of hetero-nuclear systems. The difference in Larmor frequencies of the coupled hetero-nuclear spins is large in comparison with the chemical shift scale of only protons. Only in very low fields the strong coupling limit among hetero-nuclei is reached. For protons and fluorines it happens around 3 μT. In the experiments only fields above 0.1 mT were used, thus no coherent polarization transfer between hetero-nuclei due to scalar coupling is expected. Thus, the proton and the fluorine spin subensembles can be considered independently.

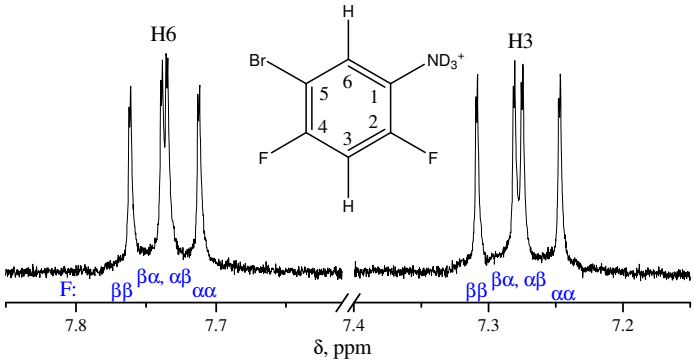

Figure 3.2.8. ^{1}H NMR spectrum of 5-bromo-2,4-difluoroaniline in D_2O. Blue symbols describe spin subensembles of the two fluorines.

Table 3.2.1. NMR parameters of 5-bromo-2,4-difluoroaniline.

	H3	H6	F2	F4
δ(ppm)	7.28	7.74	-	-
J (Hz)				
H3	-	0.35	10.1	8.4
H6	0.35	-	8.0	6.8
F2	10.1	8.0	-	8.2
F4	8.4	6.8	8.2	-

The structure and NMR spectrum of 5-bromo-2,4-difluoroaniline is shown in Fig. 3.2.8. One of the features of this system is small spin-spin coupling between the protons (0.35 Hz) and large coupling among all other nuclei (>8 Hz). If one considers only the proton spectrum the signals are split in four subensembles with different spin projections of the two fluorines. These subensembles can be conveniently written in the two-spin Zeeman basis as: αα, αβ, βα and ββ in high field and αα, $½^{-1/2}$(αβ+βα),$½^{-1/2}$(αβ-βα) and ββ in low field, where α and β represent the spin projections of the two fluorines. While the αα and ββ subensembles stay undisturbed in

the whole field range, the subensembles with αβ and βα spin projection are mixed in the field range where fluorines are strongly coupled. Thus, in further considerations, the proton subensemble is divided into three subensembles according to the fluorine spin projections: (1) αα, (2) αβ, βα and (3) ββ.

The experiment show that the different subensembles of the two protons relax differently. The proton relaxation dispersions of individual subensembles and the inverse of the average relaxation rate, T_1^{av}, $\frac{1}{T_1^{av}} = \frac{1}{N}\sum_i^N \frac{1}{T_1^i}$ of all protons of 5-bromo-2,4-difluoroaniline are shown in Fig. 3.2.9. The averaged relaxation rate of the protons is independent of the field strength except for fields higher than 1 T, where relaxation of different lines in the multiplet of the H3 proton has different T_1. The high-field increase of T_1^{av} can be explained by dipole-dipole interaction between protons and fluorine. The multiplet effect is seen only for the H3 proton which is much closer to its fluorine neighbors than for H6 and a similar multiplet effect is observed for fluorines. It is known that the dipole-dipole interaction is distance dependent in contrast to polarization transfer due to the scalar spin-spin couplings which are similar for the both protons. The influence of dipole-dipole interaction is beyond the scope of this work and, thus, is not considered here.

The flat NMRD of the average relaxation time T_1^{av} below 1 T proves that no polarization transfer among protons and fluorines occurs due to scalar coupling as it was assumed in the beginning of the chapter. The field dependent effects below 1 T are solely due to polarization transfer between the proton spins of the system. In contrast to what was seen in the previous two subchapters only the βα, αβ subensemble relaxes with the same T_1 below 0.1 mT while the other T_1s stay apart. In addition, the ββ subensembles of H6 and H3 relax with the same T_1 at 99 mT but are different at other fields. The αα subensembles of H6 and H3 relax with individual T_1s all over the measured field range. Such a behavior is observed only in a hetero-nuclear system and, in the first approximation, can be explained in the following way. Although the fluorines do not participate in coherent polarization transfer they affect the criterium of strong coupling between protons by shifting the proton resonance frequencies by scalar interaction. At 99 mT the different chemical shifts of the two protons and their scalar couplings with the fluorines lead to the coincidence of the Larmor frequency of the protons. Thus they became strongly coupled at this field and relax with the same T_1. The strong coupling can be seen in inserts of Fig. 3.2.9 where the simulated spectrum at 99 mT is shown. Only the lines of the ββ subensemble collapse into one line. However, going to lower field results again in different Larmor frequencies and, thus,

to individual T_1s of the protons (see insert for 30 mT). In contrast, the lines of the αα subensembles of the two protons never come close, and the minimal distance between them at minimal field of 0.1 mT is still 1.95 Hz. Taking into account the proton-proton scalar coupling of 0.35 Hz the strong coupling case does not apply to them at any observed fields. The resonance frequencies of the βα, αβ subensembles of H6 and H3 stay close to each other below 0.01 T and the subensembles relax with the same T_1s.

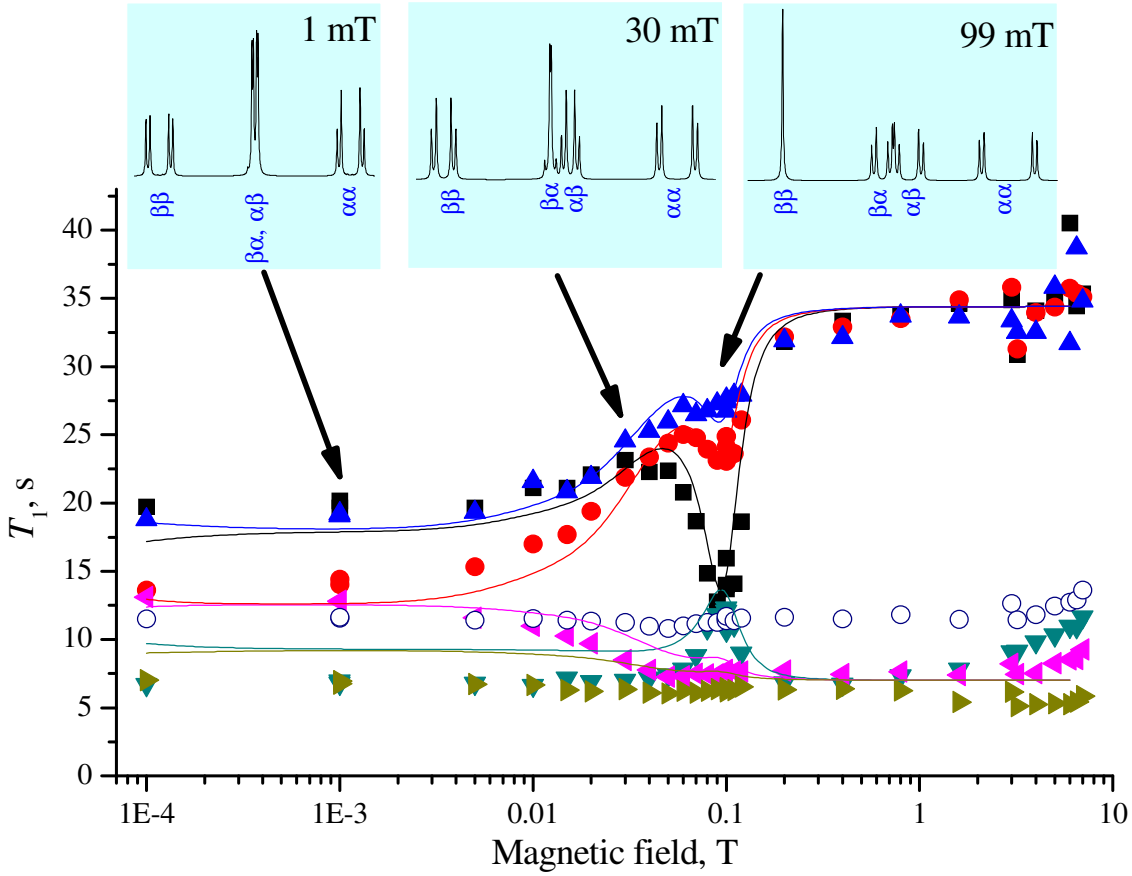

Figure 3.2.9. Relaxation time dispersion of 5-bromo-2,4-difluoroaniline protons: experimental data (■-H6 proton, ββ subensemble, ●-H6 proton, βα, αβ subensemble, ▲-H6 proton, αα subensemble, ▼-H3 proton, ββ subensemble, ◀-H3 proton, βα, αβ subensemble, ▶-H3 proton, αα subensemble, and ○- inverse average relaxation rate, T_1^{av}) and simulations (lines with corresponding color). Inserts above: simulated NMR spectra at three fields (0.1 Hz linewidth).

In the previous simplified description it was assumed that the subensembles do not interconvert between each other. However, during their relaxation the fluorines change spin projection. One of the consequences is seen in the relaxation dispersion of the protons. Although the level-crossing effect at 99 mT is most pronounced for the ββ subensemble other ensembles also tend to relax with common T_1s at this field. This effect is larger for the βα, αβ subensemble

because it needs to change only one of the fluorine spin projection. For the αα subensemble the change of the both fluoric spin projections is necessary that is much less probable, thus a smaller effect is seen in their relaxation curves. Indeed, the simulation in Fig. 3.2.9 shows that at B_{pol}<0.1 T the αα and ββ subensembles tend to relax with common T_1 value but do not reach their limit. In the simulation the T_1 34 s and 7 s were used for H6 and H2 respectively. The T_1 of both fluorines was taken 12 s. The faster the relaxation of the fluorines is assumed the closer the T_1s of the αα and ββ subensembles approach each other. The simulation reproduces very good the position of the features in the relaxation dispersion although the values of the T_1's do not perfectly coincide. This deviation can be attributed to the fact that the fluorine relaxation is more complex than it was considered. In the simulation spin relaxation only due to fluctuations of the local magnetic field was taken into account however for fluorine nuclei it is known that other relaxation mechanisms such as chemical shift anisotropy can play a significant role.

Relaxation dispersion of N-acetylhistidine (five coupled spins 1/2)

In this subchapter the relaxation of one of the amino acids, N-acetylhistidine (His), will be considered while in Chapter 3.1 the CIDNP kinetics of His was described.

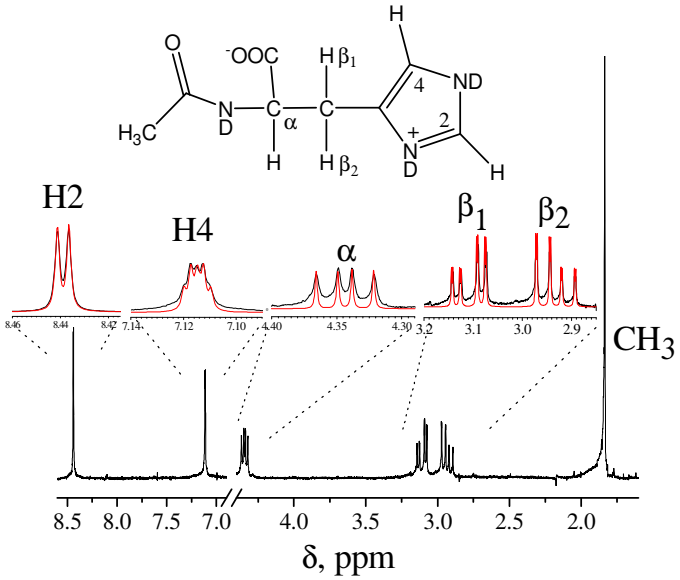

Figure 3.2.10. ^{1}H NMR spectrum (300 MHz) and simulation of the N-acetylhistidine. The simulation parameters are collected in Table 3.2.2. The structure shown applies to N-acetylhistidine in solution of D_2O at pH=5.25.

The ^{1}H NMR spectrum obtained at 7 T and its simulation are shown in Fig. 3.2.10. At 7 T the two β-CH_2-protons (two multiplets at 3 ppm) are strongly coupled, while the H2 and H4 protons of the imidazole moiety are weakly coupled to each other (J=1.4 Hz). The α-CH-proton is weakly coupled to both β-CH_2-protons. Close inspection allowed to reveal additional small splitting due to the coupling between H4 and the two β-CH_2-protons (0.9 and 0.7 Hz). The NMR parameters – chemical shifts and scalar spin-spin interactions of protons derived from the ^{1}H NMR spectrum (Fig. 3.2.10.) are collected in Table 3.2.2. The methyl protons of the acetyl group are not coupled to any of the other five protons of the amino acid within the accuracy limit determined by the linewidth (0.3Hz).

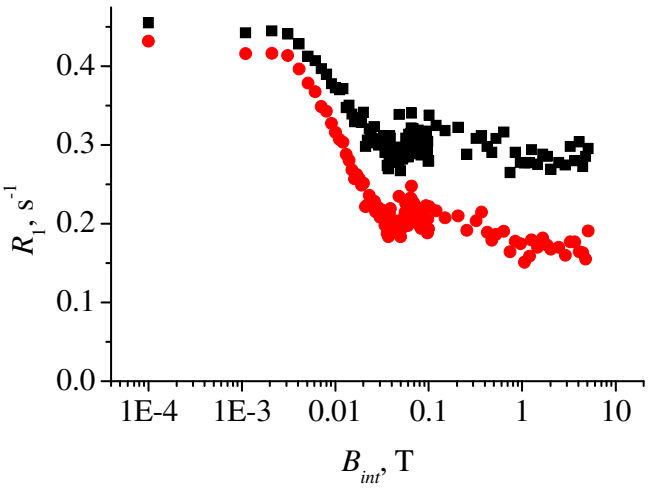

Figure 3.2.11. Relaxation dispersion of the sum of all protons (■) in the ^{1}H NMR spectrum of His and all protons of His but without CH_3-protons (●).

To stress the importance of high resolution detection for the relaxation dispersion the experimental data for each individual proton of the amino acid are compared with the NMRD of the effective R_1 integrated over all protons of His and with the NMRD of the effective R_1 integrated over all coupled protons of His but without the CH_3-group protons (Fig. 3.2.11). In this way one can model the experimental data obtainable from conventional field-cycling experiments where only the common spin relaxation of all protons in the whole sample is studied.[118,119] The signal of residual protonated water (HDO) in D_2O was not included into consideration because its content strongly depends on sample preparation, hence the results presented here can not be directly compared with literature data. Although the relaxation kinetics of a sum of several protons is in general not mono-exponential one can get from a mono-exponential fit an estimate of how fast the relaxation proceeds. Surprisingly, the relaxation dispersions in Fig. 3.2.11 have a stepwise shape and the stepwise variation of the relaxation rate

looks similar to one that caused by the change of the molecular motion regime. In Refs[118,119] the presence of a stepwise feature in NMRD was considered solid evidence for supporting a de-convolution algorithm developed for the analysis of the relaxation dispersion in proteins. However, in the case under study the molecule always stays in the fast motional regime and, thus, supposedly has a flat NMRD. Having obtained these two relaxation dispersions with different position of their inflection point, it is reasonable to conclude that de-convolution algorithms will give unsatisfactory results. Thus, the stepwise feature in the NMRD has an origin different from crossing from fast to slow motional regime upon increase of magnetic field, because in standard relaxation theory model no dependence of R_1 on B_{int}< 7 T is expected for a small molecule with correlation times of that are below 100 ps. A similar case of apparent low field spin-lattice relaxation dispersion that cannot be attributed to the collective molecular dynamics of protons was reported recently for a liquid crystal, however, no exhaustive explanation was given for its origin.[120]

The study of NMRD at high resolution instead of the unresolved NMRD of all protons in the sample allows one to rationalize the origin of the unexpected feature (Fig. 3.2.11). Accordingly, in this chapter the relaxation data of all protons that are well-resolved in the NMR spectrum of His were analyzed.

Table 3.2.2. NMR parameters of N-acetylhistidine protons obtained from simulation shown in Fig. 3.2.10 and T_1^i.

	β_1	β_2	α	H2	H4	CH_3
δ/ppm T_1^i/s	3.15 0.75	2.98 0.75	4.38 4.4	8.48 24.4	7.16 11.1	1.88 2.0
J/Hz						
β_1	-	-15.4	5.0	0	-0.9	0
β_2	-15.4	-	8.3	0	-0.7	0
α	5.0	8.3	-	0	0	0
H2	0	0	0	-	1.4	0
H4	-0.9	-0.7	0	1.4	-	0
CH_3	0	0	0	0	0	-

The three protons of the CH_3-group have an effective relaxation time of 2.0 s which does not depend on the external magnetic field in the range between 0.1 mT and 7 T (Fig. 3.2.12). Again, this is completely consistent with the conventional model of longitudinal relaxation since the condition of fast motion is fulfilled in the whole field range studied. Whereas for the CH_3 protons being decoupled from all other protons no changes are observed in the relaxation rate, for the other five protons the situation is qualitatively different. A strong dependence of the

individual T_1 relaxation times on B_{int} is found. These features are attributed to effects of strong coupling of the five-spin system at low field.

At the observation field of 7 T the five protons, which are coupled, have very different T_1-relaxation times (Table 3.2.2). As the magnetic field decreases, individual spins, which have strongly different T_1 times at high magnetic field, tend to relax with a common longitudinal relaxation time. The average relaxation rate would correspond to T_1=1.65 s. At the lowest field of 0.1 mT the common T_1 for H2 and H4 is 3.6 s, while for three aliphatic protons of the peptide backbone T_1=1.6 s is obtained. As the Larmor frequency decreases with decreasing magnetic field, the α-CH-proton, H2 and H4 protons having the longest T_1 relax faster whilst T_1 of the two β-CH_2-protons increases.

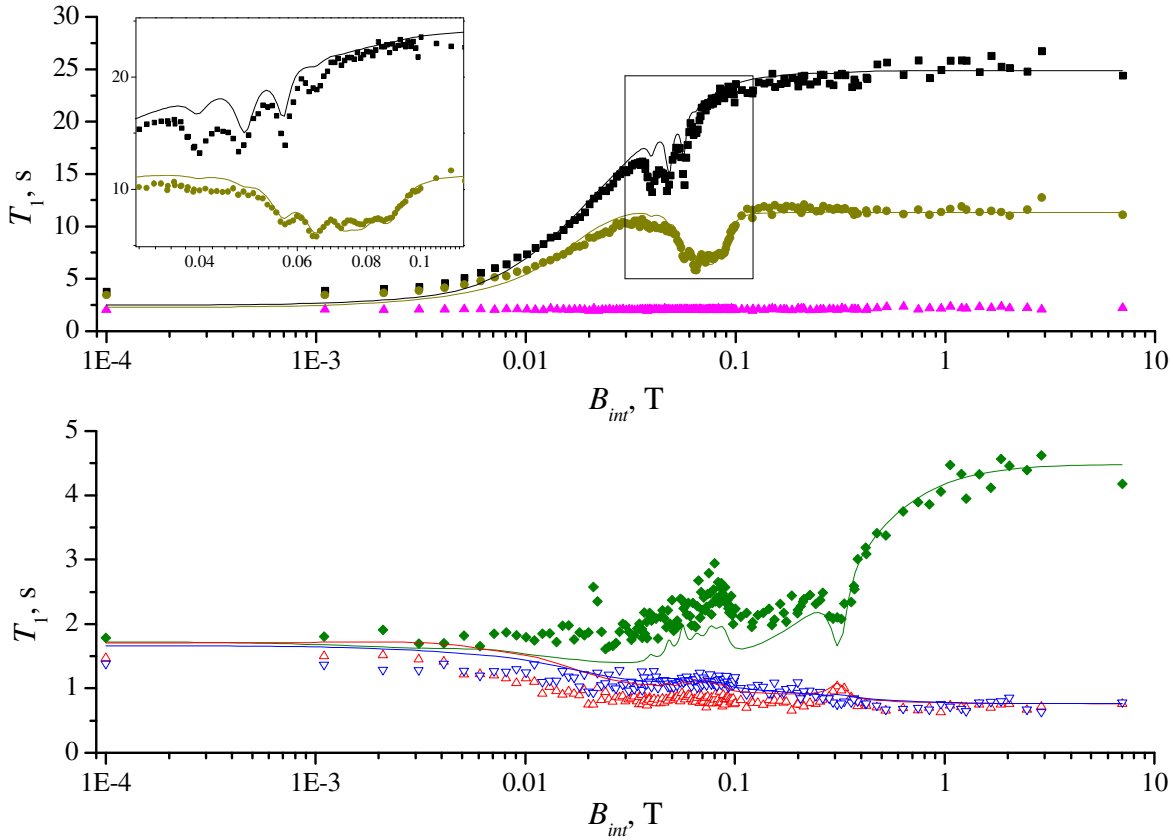

Figure 3.2.12. Relaxation time dispersion of His protons: experimental data (■ - H2, ● - H4, ◆ - α-CH-proton, △ - β_1-CH2-proton, ▽ - β_2-CH2-proton and ▲ - CH_3-protons) and simulation (line with corresponding color).

At the detection field only the β-CH_2-protons are coupled strongly and form a so-called AB-system, while all other protons are coupled only weakly. As the field decrease the spins subsequently become strongly coupled. First the α-CH and the two β-CH_2-protons form a strongly coupled three-spin 1/2 system upon lowering the field. This three-spin configuration

resembles the case of aspartic acid. As a result, while the α-CH-proton starts relaxing faster at B_{int}<1 T, the relaxation of the β-CH_2-protons, on the contrary, becomes slower. At about B_{int}=0.3 T a pronounced feature is seen, which shows up as a peak for the β-CH_2-protons and as a dip on the NMRD curve of α proton. This feature is due to the level anti-crossing in the three-spin system. In tryptophan,[62] which has nearly the same NMR parameters for the three-spin system consisting of the α-CH-proton and β-CH2-protons, the position of the anti-crossing almost coincides with that for His.

At magnetic fields below 0.1 T, not only the three spins are strongly coupled, but the entire five-spin system. Even though the H2 proton has no direct coupling to the α-CH and β-CH_2-protons it is strongly coupled with them indirectly via the H4 proton. Indeed, once the H2 proton is strongly coupled to both the H4 proton and the three-proton system the eigen-states of the entire five-spin system are collective spin states of all protons. As a consequence, all five spins become strongly coupled. Therefore at low field the aromatic protons start relaxing much faster, while the collective relaxation of the three-spin system slows down. These changes in relaxivity are very well pronounced: for instance, the relaxation of the H2 proton becomes about 6 times faster as compared to high field.

The changes in relaxation time at B_{int}<0.1 T are non-monotonous. For example, T_1 of the aromatic protons goes down passing through a sequence of peaks and dips. At magnetic fields from 40 mT to 100 mT there are well-pronounced broad dips with fine structure (Fig. 3.2.12). All the dips correspond to spin level anti-crossings in the entire five-spin system. Numerical calculations support this. For simulating the relaxation data the theoretical approach described in Chapter 1.5 and Ref. 86 was used. The NMR parameters of the five-spin system were taken from simulation of the NMR spectrum of His, and the times T_1^i of independently relaxing spins were taken from relaxation measurements at 7 T (Table 3.2.2). It should be mentioned that a small amount of paramagnetic additives is still present in the solution under study because the T_1 values are shorter than those obtained in Ref. 121. However, their influence decreases with decreasing T_1. Because the NMR is limited in spectral resolution while the simulation strongly depends on the value of NMR parameters, a slight adjustment of the parameters was done to fit all peaks and dips in the NMRD. The adjustment, however, did not exceed 0.1 Hz which is within linewidth of the NMR spectrum (about 0.3 Hz). In contrast to the previous simulation of NMRD curves in this chapter, the simulation of His is not limited to sudden or adiabatic field variation but it takes into account the real field variation with time. The simulation with the real field profile allows to obtain a much better agreement with the experimental data. The simulation

(Fig. 3.2.12) well reproduces both the width and position of the peaks and their fine structure. These features in NMRD of the aromatic protons are accompanied by their counter-parts in the relaxation dispersion of the faster relaxing α-CH and β-CH_2-protons. The latter are less pronounced because for protons that relax faster the signal-to-noise ratio was considerably worse. Features, which are due to the level crossings of the five-spin system show up not only in the site-specific NMRD, but also in the common T_1 field dependence of all protons of His (Fig. 3.2.11). The shape of simulated NMRD curves strongly depends on the relative signs of spin-spin couplings. After comparison of the calculations with experimental data only one set of the couplings constants was left (Table 3.2.2).

It is important to emphasize that in the study of His that was hyperpolarized at variable field by CIDNP also sharp features in the polarization of the H2 and H4 protons were found.[106,122,123] Since they appear at the same fields, where peak/dips show up in the NMRD (Fig. 3.2.13) they are attributed to level crossings. This allows one to conclude that these structures in the polarization curves results from peculiarities of the spin evolution of His in its diamagnetic ground site. Both phenomena, relaxation and CIDNP, depend on the coherent spin evolution at B_{int}.

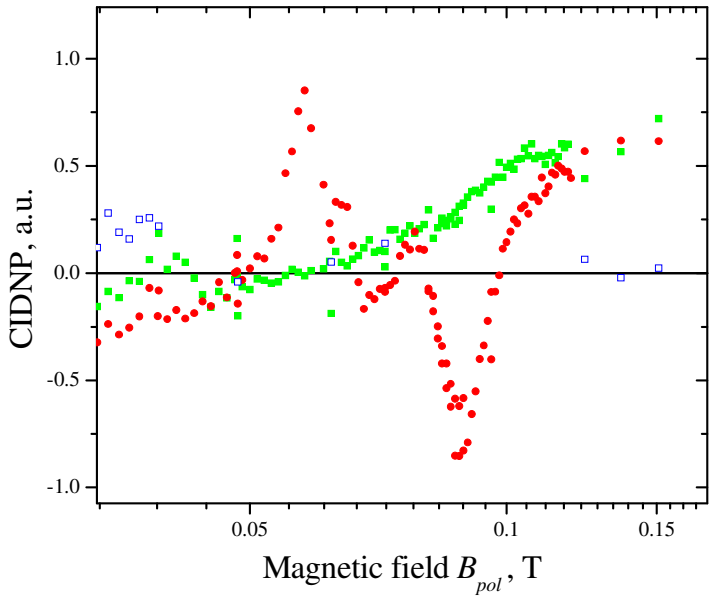

Figure 3.2.13. CIDNP field dependence of net polarization of ■ - H2, ● - H4 and □ - β protons. Data from Ref. 106.

Knowledge of the site-specific relaxation in the His molecule at low field allows one to interpret the NMRD of the sum of all His protons (Fig. 3.2.11). The stepwise change in R_1 at $B_{int} \approx 10^{-2}$ T as well as the feature at 0.1 T are conditioned solely by strong intra-molecular

couplings of spins and have nothing to do with change of the motional regime. While the individual curves differ strongly in relaxivity, R_1^i, and its variation with field, the magnetization integrated over all lines tends to overestimate the fast components as the contributions are weighted proportional to the R_1^i. Decomposition algorithms turn out to give unsatisfactory results, because they are based on the assumption that all the features in relaxation dispersion are due to changing from fast to slow motion regime, which is not the case for the small His molecule. Instead, upon lowering the field the onset of strong coupling between pairs of spins is reflected by the convergence of the respective dispersion curves.

Summary and conclusions

In this chapter it was shown that scalar spin-spin couplings places an important role in the field-cycling relaxation experiments of diamagnetic molecules. The obtained results completely prove the validity of the theoretical treatment described in Chapter 1.4 and Ref. 86 based on the Redfield theory. In low-viscosity solution of small molecules where the flat NMRD is expected the changes in the relaxation rates of individual spins are due to their strong coupling, which forces spins to relax with common T_1. Positions of sharp features at intermediate magnetic fields coincide with those of the avoided crossings of the nuclear spin levels. The polarization transfer has a coherent nature and, thus, from Chapter 1.4 and example in Chapter 3.1 one can establish conditions, under which strong coupling affects the NMRD curves. Strong coupling cannot influence the low-field relaxation if the relation $\jmath_{ij}\mathcal{T}_1^i << 1$ is fulfilled. Coherences result in oscillatory components in the relaxation kinetics that has been seen in example of 5-imidazolecarboxylic acid. Same behavior was seen in Ref. 111 with example of AMP.

The influence of scalar coupling on the NMRD of protons is of more general nature and is expected to be seen in the NMRD of various systems with coupled spins. Understanding and simulating the relaxation dispersion curves is a prerequisite for their use in differentiating between various field-dependent relaxation mechanisms and analyzing intra-molecular dynamics and mobility of molecules, in particular, of biologically relevant compounds. The present site-specific study of relaxation shows that strong coupling of spins is an important factor, which has to be taken into account in the interpretation of relaxation dispersion curves. For instance, when this factor is ignored a decrease of the relaxation rates with the decreasing field can be erroneously attributed to mechanisms that give magnetic field dependent relaxation rates, e.g., by chemical shift anisotropy.

4. Parahydrogen induced polarization in the hydrogenation reaction of styrene

In this chapter experimental results of parahydrogen induced polarization (PHIP) formed after catalytic parahydrogenation of styrene will be presented. This system is characterized by a high intensity of HP.[57] It is for the first time that the PHIP experiment is performed at variable magnetic field strength (in a range of 0-7 Tesla) in a controlled way and that the experimental results for PHIP of a multi-spin system are modeled quantitatively. The predictions of the theoretical approach described in Chapter 1.3 will be compared with the experimental data. In the course of the chemical reaction parahydrogen is attached to the double C-C bond of the styrene molecule yielding a polarized ethylbenzene molecule. In the experiments proton polarization of ethylbenzene and styrene has been studied. The structure of the molecules under investigation and the reaction scheme are shown in Fig. 4.1. In the ethylbenzene molecule the five protons belonging to the CH_2 and CH_3 groups acquire strong PHIP throughout the whole accessible field range. At low magnetic field the aromatic protons of ethylbenzene also get polarized. In addition, PHIP of ethylbenzene molecules forming a complex with the catalyst is observed in the experiments and at some conditions PHIP of the starting material, too (i.e., styrene molecules, see below for details).

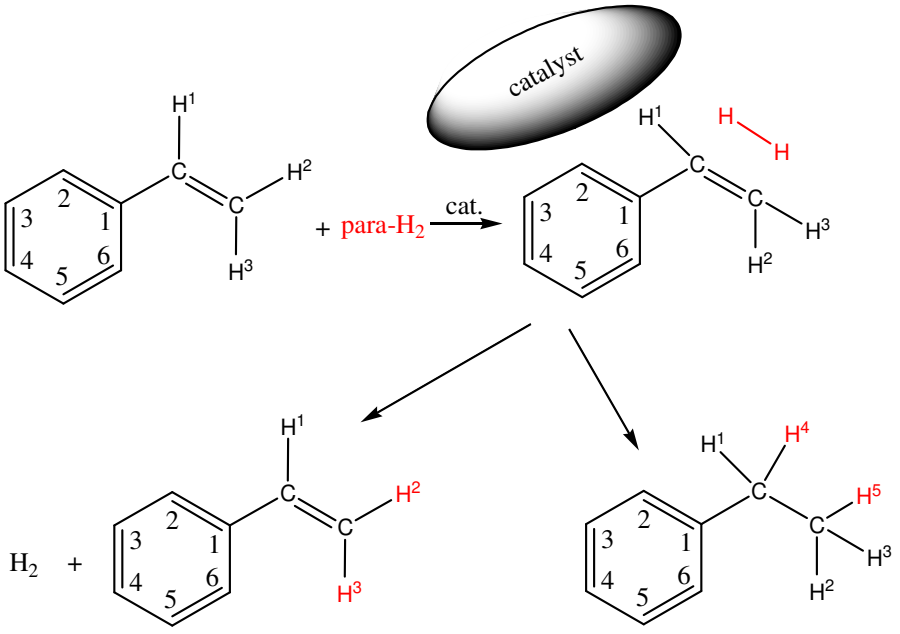

Figure 4.1. Reaction between styrene and parahydrogen and structure of styrene and ethylbenzene.

Experimental part

All chemicals used in this study (styrene, acetone-d_6, the precatalyst of the hydrogenation reaction ([1,4-Bis(diphenylphosphino)butane](1,5-cyclooctadiene)rhodium(I) BF_4^-) were obtained from Aldrich and used without any further purification. Parahydrogen was prepared in a metal vessel (Fig. 4.2) under pressure and directly used from it. The vessel contains charcoal as conversion catalyst, which was set under vacuum for two hours to activate its surface before use. The part of the vessel containing charcoal was submerged in liquid nitrogen, and then dihydrogen gas was added at a pressure of 3 bar. Under these conditions (77 K), a mixture of 51% parahydrogen and 49% orthohydrogen is generated[46] and was used after approximately 3 hours. Such a content of parahydrogen is about a factor of two higher than that found at thermal equilibrium at ambient conditions.

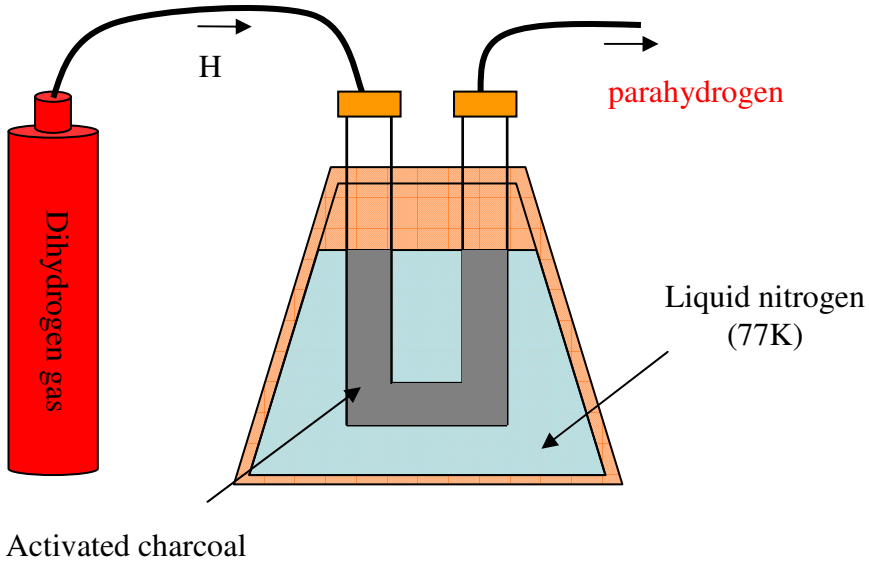

Figure 4.2. Scheme of the parahydrogen generation setup.

The measurements at variable magnetic field were done using the field-cycling setup described in Chapter 2.2. The timing scheme of the experiment is shown in Fig. 4.3. The hydrogenation reaction was performed inside the NMR sample tube. The solution for the hydrogenation reaction contained 96 mM of styrene and 2.8 mM of the precatalyst dissolved in acetone-d_6 and was purged with dry N_2 gas for 10 min to remove dissolved oxygen. To start the reaction parahydrogen gas was bubbled through a plastic capillary into the solution at 1 bar at room temperature for 30 s (τ_b) outside the NMR spectrometer. Then the capillary was removed, and the sample was placed into the NMR probe. Under these conditions dissolved parahydrogen continued to react with styrene for approximately 5 min. Thus, in the sample solution containing

styrene and parahydrogen the hydrogenation reaction, which gave rise to PHIP, was going on throughout the whole measurement cycle.

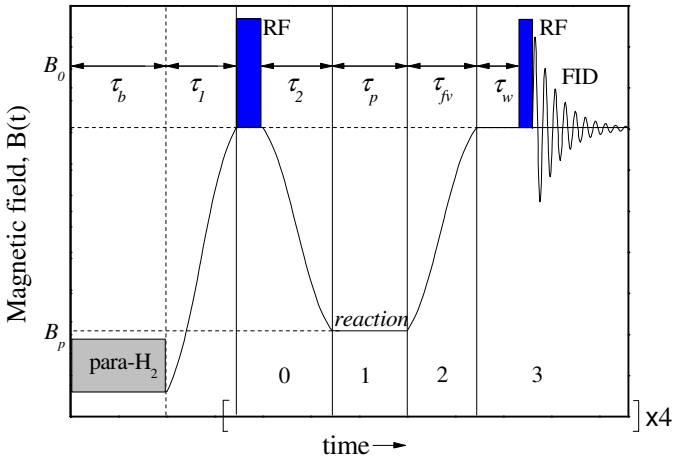

Figure 4.3. Timing scheme of the PHIP experiment at variable field. Parahydrogen (*para*-H_2) is blown through the solution during τ_b~30 s. Transfer times are $\tau_1 = \tau_2$ =300 ms, waiting time τ_w was varied from 30 to 140 ms while the sum of τ_{fv} and τ_w was kept constant and equal to 320 ms. The reaction time at field B_p was τ_p = 30 s. Stages 0,1,2,3 were repeated four times for each polarization field B_p.

After the sample had been placed inside the NMR probehead it was transferred to the observation field B_0 = 7 T during time τ_1. Then a $\pi/2$ RF-pulse was applied to destroy all polarization created prior to the measurement cycle. The efficiency of this method of polarization removal was tested on a thermally polarized sample showing that the remaining signal intensity was below the noise level. Then, during a period of duration τ_2, the probehead was transferred to the field B_p (application of the RF-pulse and transfer to B_p constitute **stage 0**) where the reaction with dissolved parahydrogen continued for τ_p=30 s (**stage 1**). Subsequently the sample was transferred back (transfer time τ_{fv}, **stage 2**) to the observation field B_0 where after a short delay τ_w a $\pi/4$ (45±2°) detection pulse was applied and the free induction decay (FID) was recorded (**stage 3**). After recording the FID (~10 s) the measurement cycle was repeated three times more from **stage 0** to **stage 3**. Thus, in the experiment four PHIP spectra for each magnetic field were obtained. They were identical except for the total intensity of the multiplets. For the analysis only the first spectrum was taken while the other three were used as control

measurements. All three field variation times τ_1, τ_2 and τ_{fv} slightly depend on B_p but were always shorter than 300 ms; the waiting time was 30 ms < τ_w < 140 ms; the sum of τ_{fv} + τ_w = 320 ms was kept constant. At B_p<1 T the contributions of the Boltzmann polarization were negligible. To obtain the PHIP spectra the experiments were repeated in the same manner as described above with and without addition of parahydrogen. The PHIP spectrum was calculated as the difference of the two spectra. Here, the rise of ethylbenzene intensity in the equilibrium NMR spectrum due to the hydrogenation reaction during one measurement cycle was negligible and was not taken into account. Although the experimental protocol described does not exactly coincide with that considered in the theoretical section (Chapter 1.3) the difference between the two protocols is only marginal. In experiments **stage 0**, which precedes the PHIP preparation, was performed to destroy the background signals coming from thermal polarization. Thus, this **stage** was needed to compare directly the experimental data with the theoretical results, which are dealing with non-thermal polarization only. Waiting times at high field, also not explicitly included in the theoretical treatment, are so short that they do not affect the PHIP pattern and only improve the spectral resolution. The three stages responsible for the formation of the PHIP pattern were the same in the theoretical consideration and in the experiment.

Table 4.1. NMR parameters (chemical shifts and J-couplings) of ethylbenzene;[124] equivalent protons are grouped; spins I_1 and I_2 (coming from para-H_2) belong to the CH_2 and CH_3-groups.

Proton and chemical shift	CH_3	CH_2	H2,H6	H3,H5	H4
CH_3, δ=1.201 ppm	–	7.6 Hz	0	0	0
CH_2, δ=2.625 ppm		–	–0.6 Hz	0.3 Hz	–0.5 Hz
H2,H6, δ=7.207 ppm			–	7.7	1.3 Hz
H3,H5, δ= 7.265 ppm				–	7.4 Hz
H4, δ=7.155 ppm					–

Table 4.2. NMR parameters (chemical shifts and J-couplings) of the aliphatic part of styrene.

Proton and chemical shift	H^3	H^2	H^1
H^3, δ_1=5.231 ppm	–	J_{12}=1.0 Hz	J_{13}=10.9 Hz
H^2, δ_2=5.809 ppm		–	J_{23}=17.7 Hz
H^1, δ_3=6.760 ppm			–

Results and discussion

In the course of the hydrogenation of styrene ethylbenzene molecules are produced. Their thermal NMR spectrum at 7 Tesla and four PHIP spectra obtained for different polarization fields are shown in Fig. 4.4. At all magnetic fields in the range 0.1 mT – 7 T strong PHIP of the CH_2 and CH_3-protons is seen. As B_p grows the spectrum gradually changes from the ALTADENA-like pattern (net polarization of the two groups having opposite sign) to the PASADENA-like pattern (only multiplet HP is seen in the spectra). In addition, at fields below 0.2 T the aromatic protons of ethylbenzene acquire some non-thermal polarization. Their HP is identified to result from polarization transfer from the CH_2-protons, which is possible because of their J-couplings with the H2,H6-protons. Although this coupling does not reveal itself in a resolved splitting of the NMR lines belonging to the CH_2-protons, these lines are inhomogeneously broadened. Scalar coupling between the CH_2-protons and the aromatic protons of approximately 0.6 Hz (see Table 4.1)[124] is responsible for this broadening.

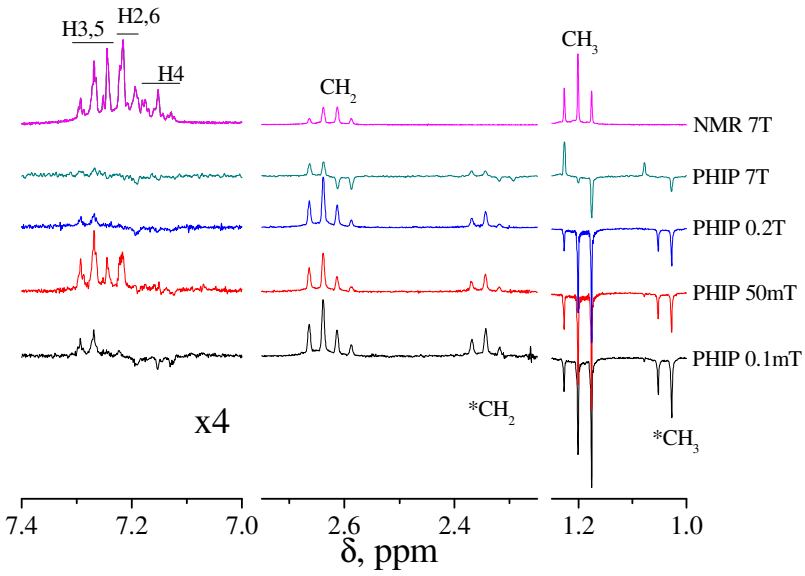

Figure 4.4. ^{1}H NMR at 7 T and PHIP spectra at different polarization fields B_p. Aromatic parts of the spectra are multiplied by 4, flip angle was $\varphi = \pi/4$. Asterisks denote the signals of the ethylbenzene molecules bound to the catalyst.

A comparison of the measured and calculated PHIP spectra of the CH_2 and CH_3-protons is shown in Fig. 4.5. In the calculations the treatment developed in Chapter 1.3 was applied. It should be mentioned that the calculated PHIP spectra of the CH_2 and CH_3-protons are (as was checked by calculation) only slightly affected by the aromatic protons. This is because of the

small coupling between the CH_2-protons and the aromatic protons. For this reason the spectra of the aliphatic protons were calculated under neglect of any coupling between the CH_2-protons and the ring protons of ethylbenzene. Thus, consideration was restricted to only five protons belonging to two groups of two and three magnetically equivalent nuclei. Spin-spin interactions and chemical shifts of the protons were taken from Table 4.1. The hydrogen is attached to styrene in such a way that one of the atoms constituting the para-H_2 molecule belongs to the CH_2-group and the other one to the CH_3-group of ethylbenzene. It is assumed that the preparation time at any field was sufficiently long for neglecting the coherences between the spin eigen-states. To consider the effects of field variation the real time profiles $B(t)$ during the field switch from B_p to B_0 was taken. It is important to note that despite the rather short switching time, τ_{fv}<300 ms, the field variation was almost adiabatic due to the relatively high spin-spin coupling between the CH_2 and CH_3-protons of 7.61 Hz (see below).

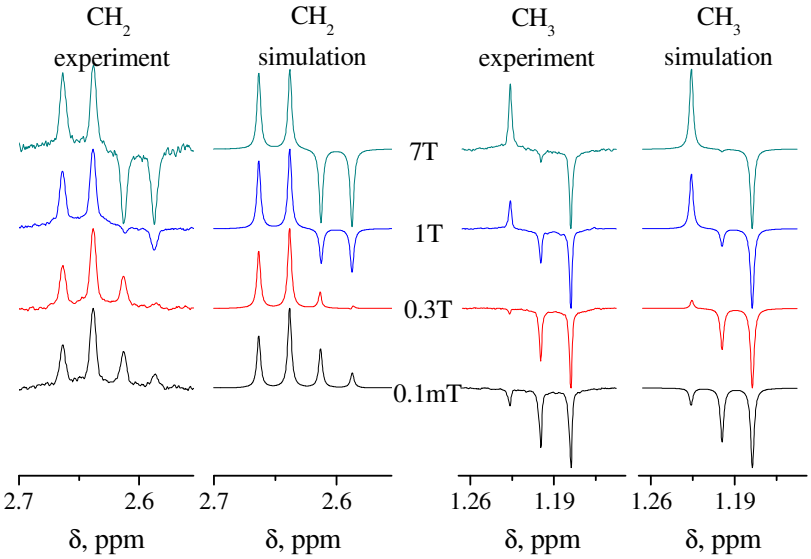

Figure 4.5. PHIP spectra of the CH_2 and CH_3-groups of ethylbenzene at different fields B_p: data on the left and simulations on the right. NMR parameters of ethylbenzene are shown in Table 4.1, flip angle was $\varphi = \pi/4$.

In the whole range of magnetic fields the agreement between theory and experiment is almost perfect. Not only the values of the net PHIP are reproduced by the calculation but also the shape of the multiplets of both groups of protons (see Fig. 4.5). In the experimental PHIP spectra the transition from the ALTADENA-type of pattern to the PASADENA-type pattern occurs around a B_p of 1 T.

In the experimental PHIP spectra (Fig. 4.4) there are extra lines seen resembling those of the CH_2 and CH_3-groups of ethylbenzene but shifted to higher fields. As has been shown in Ref. 125 they originate from ethylbenzene molecules produced by hydrogenation on the catalyst and still forming a complex with the catalyst through their arene ring. Ethylbenzene bound to the catalyst has slightly different NMR parameters as compared to the free molecule in solution (Fig. 4.6). The field dependences of PHIP of free (Fig. 4.5) and complexed (Fig. 4.6) ethylbenzenes, although similar to each other, exhibit noticeable differences. Again, the agreement between the experimental data and simulation (Fig. 4.6) is very good in the whole range of fields B_p.

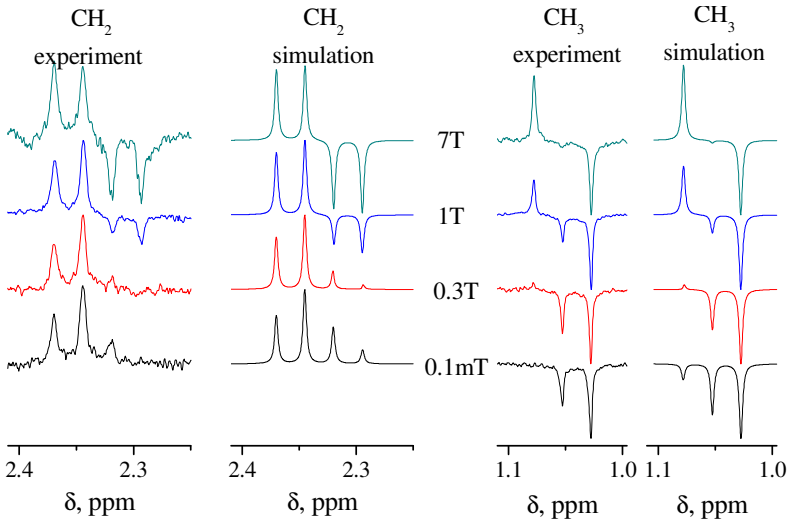

Figure 4.6. PHIP spectra of the aliphatic protons of ethylbenzene forming a complex with the catalyst at different B_p: data on the left and simulations on the right. NMR parameters of ethylbenzene bound to the catalyst used in simulation: $\delta(CH_3)$=1.053, $\delta(CH_2)$=2.332, J=7.55Hz, flip angle was $\varphi = \pi/4$.

In addition, PHIP of the aromatic protons of the free ethylbenzene has been modeled assuming that it results from transfer of HP from the CH_2 and CH_3-protons due to strong coupling of the entire spin system at low fields. In this field range even the small spin-spin interaction of 0.6 Hz is sufficient for establishing strong coupling of spins; hence, PHIP transfer to the aromatic protons becomes operative. Since in the experiments long preparation times of 30 s were used ($\tau_p >> 1/J$), considerable re-distribution of polarization took place. To model PHIP of the aromatic protons the entire coupled ten-spin system was taken into account with spin-spin interactions and chemical shifts listed in Table 4.1. The calculated and experimental PHIP spectra of the aromatic protons of ethylbenzene are shown in Fig. 4.7. The agreement between theory and experiment at all three B_p values used is surprisingly good even despite the rather small PHIP amplitude of the aromatic protons as compared to that of the CH_2 and CH_3-

protons. Based on all these results it is justified to concluded that spin-spin interaction is indeed the leading factor governing HP re-distribution among protons at low fields whereas cross-relaxation as a major mechanism of polarization transfer is ruled out. PHIP of the aromatic protons is very small at zero B_p and, obviously, decreases to zero at high polarization fields as the coupling between the aromatic and aliphatic protons becomes weak. Thus, by adjusting the field B_p to 50 mT it was possible to get maximal PHIP of the aromatic protons. In general, the variation of B_p value can be very useful in PHIP experiments as it allows one to optimize the HP amplitude for selected nuclei.

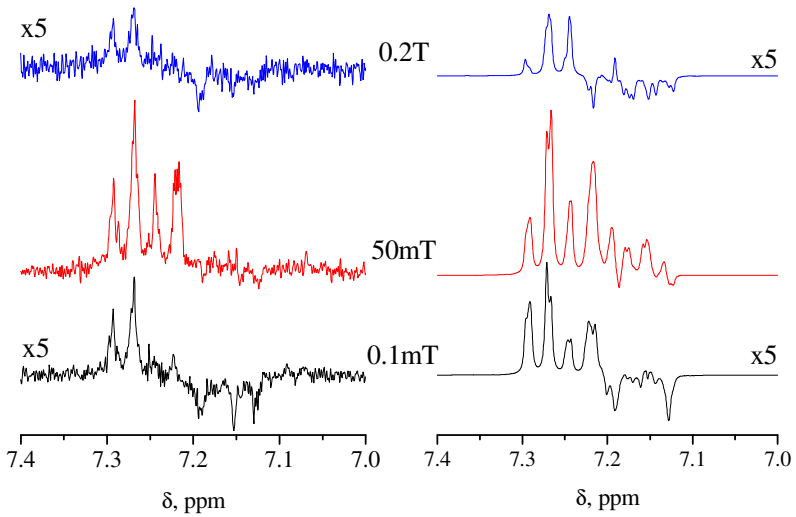

Figure 4.7. PHIP effects for the aromatic protons of ethylbenzene at $B_p \leq 0.2$ T, experimental data (left) and simulation (right). NMR parameters for simulations have been taken from Table 4.1, flip angle was $\varphi = \pi/4$. Experimental spectra are scaled to calculation.

As long as the solution of styrene and catalyst was fresh PHIP effects were seen only for ethylbenzene, which is the product of hydrogenation reaction. However, after several reaction cycles also non-equilibrium polarization of styrene appeared (Fig. 4.8). Previously, such polarization effects on styrene have been assigned[126,127] to proton exchange between parahydrogen and styrene. This reaction becomes possible because in the course of hydrogenation the catalyst slowly changes its properties and partly gets exhausted. As a consequence, dihydrogen exchange instead of hydrogenation proceeds resulting in the production of polarized styrene. Thus, in the course of the reaction protons of styrene in geminal positions (H^2, H^3) are replaced by parahydrogen and a polarized three-spin system is formed. To model the PHIP effects of styrene the NMR parameters for the three-spin system[126] were used,

which are presented in Table 4.2. In this simulation HP exchange between the H^1, H^2, H^3-protons on the one hand and the ring protons on the other hand was completely neglected. To measure the rather weak PHIP spectra of styrene the experimental protocol was slightly modified. No RF-pulse was applied to destroy polarization that was generated in the fringe field of the magnet. Therefore the polarization field was not well defined and the styrene polarization was generated across a field range from 0.05 to 50 mT. Numerical calculation predicted that the shape of the styrene PHIP pattern was field independent in this range. Therefore the experimental PHIP spectra of styrene were compared to the simulation performed for the polarization field of 0.1 mT. At B_p=0.1 mT there was a very good agreement between theory and experiment as can bee seen from Fig. 4.8. The experimental PHIP spectra of styrene can be modeled only with the assignment given in Table 4.2 (spins 1 and 2, which belong to the protons in the H^2 and H^3 positions, originate from the para-H_2 molecule), which clearly indicates that in the course of the chemical reactions the geminal and not the vicinal protons are replaced by the para-H_2 molecule.

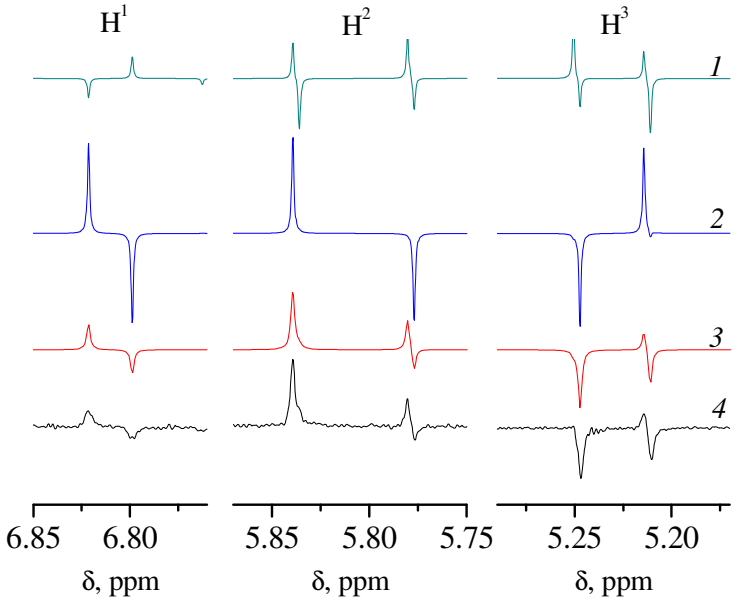

Figure 4.8. PHIP effects as found for styrene molecule in old solution at B_p=0.1 mT: experimental spectra (bottom trace 4) and simulation for sudden (1), adiabatic (2) and real (3) profiles of field variation. NMR parameters used for simulation are given in Table 4.2, H^2 and H^3 protons are originating from the parahydrogen molecule. Experimental spectrum is normalized to simulation curve 3, flip angle was $\varphi = \pi/4$.

To obtain good agreement between the calculated and measured spectra it is not sufficient to restrict consideration to the two limiting cases of adiabatic and sudden field switching as both

of them are in poor agreement with the experimental PHIP pattern (Fig. 4.8, spectra 1 and 2). Thus, for the protons of styrene field switching is neither adiabatic nor sudden. At the same time the calculation performed with the real $B(t)$ profile represents a case from the intermediate regime of field variation. Only this calculation is in perfect agreement with the experimental data.

To consider in more detail the effects of the field variation on the ethylbenzene the calculated PHIP spectra taking into account real time profiles $B(t)$ during the field switch from B_p to B_0 were compared with the PHIP spectra assuming a very slow linear field variation with τ_{fv}>10 s. The difference between such PHIP spectra is minimal indicating that for the ethylbenzene the field variation was almost purely adiabatic. Only when the time of the linear field variation was shorter than 1 s the difference between the spectra calculated with linear and those with the real $B(t)$ profile became pronounced. Such a field switching time is longer than the τ_{fv} value in the experiments, however, in the real $B(t)$ profile at $t \approx 0$ the speed, dB/dt, tends to be zero in contrast to the case of linear switching. Thus, the low-field part (where the spins are strongly coupled) is passed with a speed, which is considerably lower than the average one and the adiabaticity condition is fulfilled at shorter τ_{fv}=0.3 s time as compared to the case of linear field variation ($dB/dt = (B_0 - B_p)/\tau_{fv}$ =const). This consideration and example of the styrene polarization vividly demonstrate the necessity of considering the real profile $B(t)$ in modeling the PHIP data.

Summary and conclusions

In the present chapter the theoretical approach described in Chapter 1.3 was applied to PHIP in multi-spin systems. Non-thermal polarization prepared at arbitrary magnetic fields B_p was considered taking into account the effects of field switching on the PHIP pattern. In the simulation scalar coupling of spins and Zeeman interaction as the only factors for PHIP formation and re-distribution in the molecule were considered. Even though effects of spin coherence in PHIP distribution among the strongly coupled spins was not considered it has to be mentioned that PHIP re-distribution effects are of coherent nature. In principle, reaction leading to PHIP can be initiated photochemically;[128-130] hence, the timing of HP preparation can be performed in a controllable way with short polarization period τ_p. In this case a pronounced coherent (oscillatory) contribution to the transfer kinetics is expected as observed in analogous photo-CIDNP experiments (Chapter 3.1). By exploiting the coherences one can achieve particularly selective transfer of HP to the target spins of choice.

So far, PHIP experiments were restricted to zero (ALTADENA experiment) or high (PASADENA experiment) polarization field B_p. In the present work this limitation was overcome and PHIP spectra of ethylbenzene for B_p between 0.1 mT and 7 T were measured. In all cases studied the theory developed here was found to describe very well the experimental spectra. Very good agreement has been found between the experimental data and calculations for the aliphatic (CH_2 and CH_3) protons of both, the free ethylbenzene molecule and that bound to the catalyst. In addition, PHIP of the aromatic protons has been observed at $B_p \leq 0.2$ T and modeled theoretically. Moreover, PHIP effects were observed and simulated for the starting compound, styrene, when the catalyst becomes exhausted.

The very good agreement between theoretical calculations and experimental data allows to conclude that the formalism described in Chapter 1.3 is very precise. Thus, the theory developed here can serve as a valuable tool for modeling and predicting PHIP effects in multi-spin systems. In the present consideration it has been taken for granted that scalar spin-spin interactions are the key factor, which governs PHIP formation and its subsequent re-distribution. This assumption has been thoroughly confirmed by comparison of theory and experiment. Inasmuch as the strong J-coupling leads to efficient re-distribution of the original HP in the molecule it may cause polarization of nuclei, which cannot acquire HP directly in the course of chemical reactions. Such a polarization (which can be observed, for instance, for the aromatic protons in ethylbenzene) should not be erroneously assigned to formation in the course of parahydrogenation. Thus, analysis of the effects of spin-spin interactions on PHIP is necessary to avoid misinterpretation of the reaction pathways. In general, PHIP re-distribution has both positive and negative consequences. A negative feature of polarization transfer is that it complicates determination of the position in the molecule, to which non-thermally polarized dihydrogen is attached. A positive effect of PHIP transfer is that it allows one to enhance considerably the NMR signals of certain nuclei.

The achievements in measuring for the first time the field dependence of PHIP and in performing PHIP preparation at variable magnetic field open new attractive experimental possibilities. For instance, by adjusting the field one can optimize PHIP transfer to particular target nuclei of choice to enhance their NMR signals. Particularly strong and selective PHIP transfer in the vicinity of anti-crossings of the nuclear spin levels is expected. Such level crossings can be found at well-determined magnetic fields, which are given by the NMR parameters of the spin system. Furthermore, variation of B_p at fields below 0.1 mT may allow one to transfer PHIP to hetero-nuclei (^{13}C, ^{15}N, ^{19}F, etc.) in an optimal and controllable way as at such low fields strong coupling between protons and hetero-nuclei is expected.[56]

For preservating the hyperpolarization from relaxation the so called long-lived spin states can be particularly useful, especially in case of PHIP. They relax much slower than allowed by the usual relaxation time mechanisms since the are insensitive to dipolar fluctuating fields. In addition, the slow relaxation has the second advantage that efficient generation of hyperpolarization can be extended for a longer time because the saturation time constant is given by the relaxation time. For two coupled spins in singlet state the prolongation of their relaxation is the highest although other spin states may also have long relaxation. By PHIP method one can selectively populate such states of the multi-spin system. This may cause relaxation of other spin orders except for the longitudinal one.[50,60,131]

5. Dynamic nuclear polarization

The field of dynamic nuclear polarization has been investigated for more than four decades, nevertheless new techniques and experimental methods have been introduced in recent years or are under development.[132] The main objective of the present study is to use field-cycling for maximizing HP generation in DNP experiments and to develop procedures of HP transfer to target nuclei in a molecule under study. One way to achieve this goal is to increase the enhancement factor, ε, in eq. (1.2.1) by performing experiments at low field where the DNP coupling constant, ξ, is the highest. In addition, HP transfer is usually more efficient at low field (see Chapter 3). Following this line a number of new DNP experiments were performed at 10 and 50 mT, which will be discussed in this chapter. They take advantage of the field-cycling setup described in Chapter 2. The setup makes resolving DNP effects for individual spins possible and, thus, utilizing the signal enhancement in NMR spectroscopy more efficiently. The speed of field variation is sufficiently high for allowing the DNP enhancement detection before nuclear spin relaxation destroys the HP.

Another new feature is the use of pulsed pumping of electron spin transitions with the aim to get maximum efficiency out of a minimal deposit of microwave power which is necessary to avoid sample heating. Except for a few studies[133-134] in all the previous DNP investigations pumping was performed in cw-mode. DNP experiments in the cw-mode have the disadvantage that a relatively high power of continuous pumping is needed to keep the EPR transitions at a high level of saturation all the time. In many cases heating of the sample is the limiting factor for the maximum enhancement achievable, particularly for pumping at frequencies in the microwave range. Turning the pumping on for only short periods of time can potentially remedy the situation and lead to the same value of the DNP effect with much smaller power input. As has been proposed in Refs. 133-134 excitation of the EPR transitions by a train of pulses allows one to reduce the pumping power needed to acquire maximal enhancement. In pulsed experiments a strong pumping B_1 field is switched on only for a short period of time, but sufficient to considerably take the electronic spins off their equilibrium. For $\gamma_e B_1 >> 1/T_1, 1/T_2, 1/T_e$ coherent spin motion can invert electron spin population. Between pulses is a long period of free evolution of the electronic spins, letting them relax back toward thermal equilibrium. During the relaxation process of the electron spins, they give part of their non-thermal polarization to the nuclear spins via cross-relaxation. Thus, considering the power deposition there is a trade-off between the increased B_1 amplitude of the EPR pumping field (necessary to let the electronic spins rotate coherently) and the reduced duty-cycle of the pulse sequence with respect to the cw

DNP experiment. Varying the flip angle, φ, of the electronic spin magnetization as is easily done by changing the pulse amplitude or duration allows one to manipulate the DNP efficiency. Thus, the pulse length, amplitude and repetition time were systematically varied to achieve maximal DNP while keeping the average pumping power constant. To analyze the obtained data an adequate theoretical approach to pulsed DNP was developed that is presented in the theoretical part of this chapter.

The present work is focused on ^{1}H DNP experiments in liquid samples of water and aqueous solutions at room temperature doped with stable nitroxide radicals. Previously it has been shown that for ^{1}H-DNP in water the enhancements are usually dominated by dipolar relaxation leading to negative enhancement with a maximum possible value of $|\varepsilon|_{\min} = 330$. The experiments were performed with EPR pumping at two different transitions frequencies at (300 MHz and at 1.4 GHz.) and corresponding fields.

For optimal pumping all spin packages in the sample would have to be inverted. However, hyperfine interaction leads usually to a spectral width too large to be excited non-selectively. For rectangular MW-pulses a rough estimation leads to an excited bandwidth of $\Delta\omega \approx \gamma_e B_1$. Broadband excitation by using shaped pulses or complex sequences as it is often done in NMR[135,136] is not yet technically feasible for EPR systems. The nitroxide radicals used are known to have an EPR spectrum consisting of three sharp lines (~1.2 mT HFI constant on nitrogen) that allows for excitation of only one of the lines without effecting the other lines. The highest B_1 amplitude of the setup was 0.9 mT. Therefore only one third of the electron spins (one half for ^{15}N-labelled nitroxides) is affected and can lead to DNP. On the other hand, B_1 was significantly larger than the unresolved splitting by ^{1}H hyperfine interaction (inhomogeneous line broadening), thus the excitation is non-selective for one line. No gain is expected for using deuterium labeled nitroxides.

Experimental part

The experimental protocol of pulsed DNP with field-cycling is depicted in Fig. 5.1. Subplot (a) shows the timing scheme of the field-cycling experiment, while subplot (b) presents the pulse sequence used.

The DNP experiments were done at the field-cycling setup with the modifications described in Chapter 2.4. The measurement consists of three consecutive stages. At first (**stage 1**), irradiation of the EPR transitions of a stable radical is performed at low field B_{pol} during time $\tau_{irr} \geq 5\, T_1^n$. This guarantees saturation of the DNP effect for the nuclear spins. For technical reasons pumping of the EPR transitions has been performed only at two different frequencies:

300 MHz and 1.4 GHz. The polarization field B_{pol} was set that at ν_{irr} it was on resonance with one of the electronic spin transitions. For finding this resonance the polarization field was varied around 10 mT (ν_{irr} =300 MHz); and around 49 mT (ν_{irr} =1.4 GHz). After performing irradiation at low field the magnetic field was rapidly changed from B_{pol} to the detection field B_0 (**stage 2**). The total time, τ_{fv}, of field variation was 0.27 s. The experiments were performed under following timing conditions. The free radical concentration was chosen that the T_1 relaxation times of all protons became significantly shorter, at the same time the ratio τ_{fv}/T_1^n was always less than 1/3. Thus, $\tau_{fv} < \frac{1}{3}T_1^n$ and polarization losses during the field variation stage are less than 30 %. Then, after the sample arrives at the observation field B_0 the RF-pulse for FID detection was applied and the Fourier transform NMR spectrum was recorded with high spectral resolution (**stage 3**).

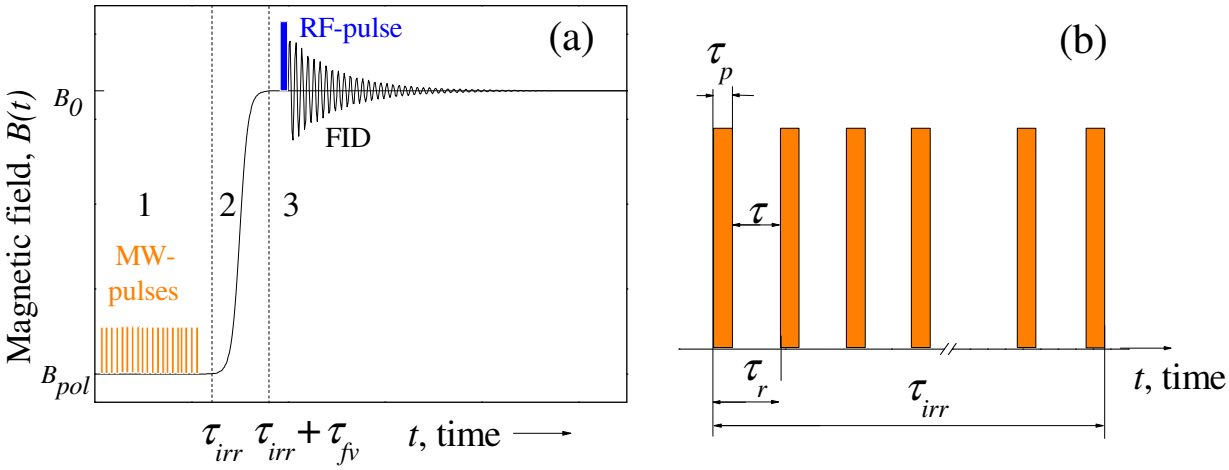

Figure 5.1. Experimental protocol (a) and pulsing scheme (b) as described in the text.

The pulse sequence of EPR pumping, which was used to produce the DNP effects, is shown in Fig. 5.1 (b). A periodic train of rectangular pulses was applied. The duration of each pulse, τ_p, was varied from 5 ns up to 25 μs allowing one to change the flip angle, φ, of the electronic magnetization over several periods. Assuming that the high field approximation is sufficiently precise at the low B_{pol} standard Bloch equations were used, i.e., a flip angle $\varphi = \gamma_e B_1 \tau_p$ where B_1 is the amplitude of the co-rotating field component. The RF-pulse shape

was checked via a pickup antenna positioned near the RF coil and monitored by a digital oscilloscope. For 300 MHz B_1 of the pumping was calibrated by measuring the length of a π/2 pulse for protons at B_0=7 T. In all cases, relatively short times τ_p were used in order to minimize effects by the electronic longitudinal and transverse relaxation times, T_1^e and T_2^e respectively. For the pulse repetition time the term τ_r was used, while the duty cycle, DC, is defined by the ratio of τ_p and τ_r: DC= $\frac{\tau_p}{\tau_r}\times 100\%$. It was varied in the range 1% ≤DC≤50%. Finally, $\tau = (\tau_r - \tau_p)$ is the time delay between subsequent pulses.

DNP effects were studied for aqueous solutions doped with small molecules of stable nitroxide radicals 4-hydroxy-2,2,6,6-tetramethylpiperidine 1-oxyl (TEMPOL). Here, experimental data were obtained for the following samples: 1 mM ^{15}N TEMPOL (perdeuterated) and 90 mM 3-furoic acid in D_2O; 0.2 mM ^{15}N TEMPOL (perdeuterated) and 90 mM 3-furoic acid in D_2O; 1 mM ^{14}N TEMPOL in H_2O.

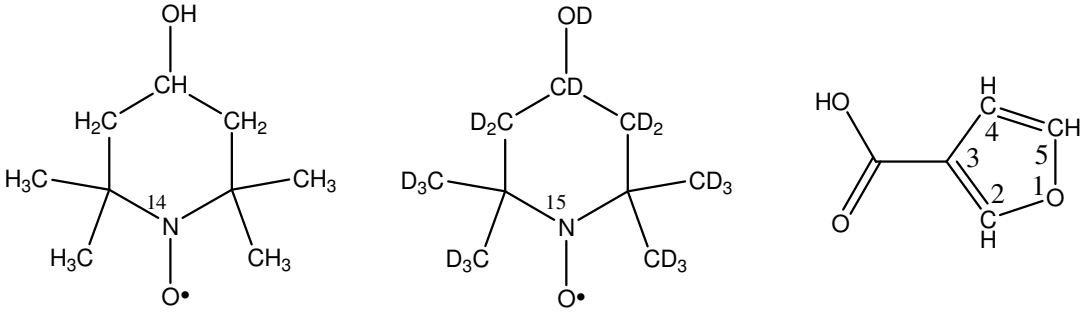

^{14}N TEMPOL ^{15}N TEMPOL 3-furoic acid

Figure 5.2. Structures of the compounds used.

The chemical structures of the compounds used are depicted in Fig. 5.2. All samples were purged with pure nitrogen gas (the sample with 0.2 mM 0.2 mM ^{15}N TEMPOL was degassed via a freeze/pump/thaw cycle) to remove O_2 and sealed in a standard 5 mm Pyrex NMR tube. In order to avoid vortex formation and sample shaking during the transfer, a Teflon plug was inserted into the tube on top of the liquid. D_2O (99.9%) as solvent was used as received from Deutero GmbH (Germany). H_2O was de-ionized without any extra treatment. ^{14}N TEMPOL (97%) was received from Aldrich. The isotopically labeled ^{15}N TEMPOL compound was synthesized by Herbert Zimmermann (MPI, Heidelberg) according to Rozantsev.[137] First TEMPONE–^{15}N-perdeuterated was prepared in modified procedures out of acetone-d_6/h_6 and $^{15}ND_3$ in order to use the isotopes in an economically efficient process. The labeled TEMPONE radical was subsequently reduced to the corresponding TEMPOL radical by sodium borodeuteride in EtOD/D_2O. The nitroxide was

checked by mass spectroscopy as well as TLC and were found to be 98% deuterated, ^{15}N=98 %; the chemical purity was better than 99%.

Theoretical description of the pulsed DNP experiment

The calculation of how the nuclear polarization is accumulated in the pulsed DNP experiments follows the approach proposed by Ivanov et al.[138] Each pulse selectively rotates the electronic magnetization by an angle φ, while the nuclear spin is not affected by the pulse. Between two subsequent pulses the electronic spin polarization vector, **S**, relaxes during time $\tau = (\tau_r - \tau_p)$ toward its equilibrium value, $\mathbf{S}_0$. At thermal equilibrium the longitudinal component, S_0, is non-zero and proportional to the external magnetic field B_{pol}, while the transverse component is zero. As long as $\mathbf{S} \neq \mathbf{S}_0$ electron-nuclear cross-relaxation takes place. It is caused by the random fluctuation of the electron-nuclear dipole-dipole interaction and leads to transfer of spin polarization from the electronic to nuclear spin reservoir; as a consequence, NMR enhancement is produced. The vector **P** which has three components describes the state of the spin system:

$$\mathbf{P} = \begin{pmatrix} S_z \\ S_\perp \\ I_z \end{pmatrix}, \qquad \mathbf{P}(t=0) = \mathbf{P}_0 = \begin{pmatrix} S_0 \\ 0 \\ 0 \end{pmatrix}. \tag{5.1}$$

Here S_z and $S_\perp$ denote the longitudinal and transverse components of the electronic spin polarization, I_z stands for the longitudinal nuclear spin polarization. In the definition of $\mathbf{P}_0$ it is assumed that the equilibrium value of the nuclear polarization is much smaller than S_0. The sequence of vectors $\{\mathbf{P}_0, \mathbf{P}_1, \ldots, \mathbf{P}_n, \ldots\}$ describes the state of the spin system under action of the periodic sequence of pulses. Here $\mathbf{P}_n$ is the value of the **P** vector just before the application of the (n+1)-th pulse, $\mathbf{P}_0$ is the initial state of the spin system as introduced in eq. (5.1). Under the action of a short ($\tau_p << T_1^e, T_2^e$) pulse $\mathbf{P}_n$ changes to $\mathbf{P}_n'$:

$$\mathbf{P}_n' = \begin{pmatrix} \cos\varphi & -\sin\varphi & 0 \\ \sin\varphi & \cos\varphi & 0 \\ 0 & 0 & 1 \end{pmatrix} \mathbf{P}_n \Rightarrow \begin{cases} (S_z)_n' = \cos\varphi (S_z)_n - \sin\varphi (S_\perp)_n; \\ (S_\perp)_n' = \sin\varphi (S_z)_n + \cos\varphi (S_\perp); \\ (I_z)_n' = (I_z)_n. \end{cases} \tag{5.2}$$

Hereafter a prime is used to denote the polarization value right after action of the pulse. Between two subsequent pulses the evolution obeys the following equations:[139]

$$\begin{cases} \dfrac{dS_z}{dt} = -\dfrac{S_z - S_0}{T_1^e}; \\ \dfrac{dS_\perp}{dt} = -\dfrac{S_\perp}{T_2^e}; \\ \dfrac{dI_z}{dt} = -\sigma s_{\max}(S_z - S_0). \end{cases} \tag{5.3}$$

Here for simplicity it is assumed that $T_1^e = T_2^e = T_e$. The validity of this simplification is discussed below in comparison with the results. Also, the paramagnetic nuclear relaxation of the radical is neglected, which is known to lead to saturation transfer to the off-resonance EPR hyperfine components.[140] In eq. (5.3) σ describes the efficiency of the electron-nuclear cross-relaxation. σ is the difference between the zero-quantum and double quantum relaxation rates and can be positive or negative depending on the type and the correlation times of molecular motion. Here, intermolecular dipole-dipole interaction is assumed to be the relevant term. In aqueous solution at room temperature (short correlation times in the extreme motional narrowing regime) σ is expected to be negative. In this equation the longitudinal nuclear relaxation of the diamagnetic molecules is neglected because its characteristic time, T_1^n, is much longer than the repetition time τ_r. T_1^n will be incorporated in the final equations for I_z (see below).

Finally, s_{max} in eq. (5.3) is introduced by analogy with the saturation factor of the EPR in the cw-pumping case. This analogy will be clearly seen from the expressions for ε, which will be derived below. The quantity s_{max} is equal to the statistical weight of the EPR lines, which are excited by the pulse. In the cw-pumping case s_{max} defines the upper limit of the saturation factor s, which is usually smaller than s_{max} because of incomplete saturation of the resonant EPR line. Here, it is always assumed that in pulsed experiments the pumping pulse flips only certain components in the EPR spectrum of the radical, while the other components are completely off the resonant condition and thus are not excited. Thus it will be only differentiate between the resonant EPR lines (excitation is characterized by a certain φ value) and off-resonant lines (which do not experience any effect of the pumping pulse).

The solution of the equations (5.3) for $t = \tau \equiv (\tau_r - \tau_p)$ is as follows:

$$\begin{cases} S_z(\tau) = (S_z)_{n+1} = ((S_z)_n' - S_0)\,u + S_0; \\ S_\perp(\tau) = (S_\perp)_{n+1} = (S_\perp)_n'\,u; \\ I_z(\tau) = (I_z)_{n+1} = (I_z)_n + \sigma s_{\max} T_1^e ((S_z)_n' - S_0)(u-1). \end{cases} \tag{5.4}$$

Here $u = \exp(-\tau / T_e)$ is introduced. The set of equations (5.4) for the sequence of spin polarization components, $\mathbf{P}_n$, can be solved by using the recently developed[141,142] formalism of calculating the response of spin systems to periodic pulse sequences. However, as n grows the first two vector components of the polarization vectors, S_z and $S_\perp$, rapidly (roughly speaking, as a geometric series with the common ratio $u<1$) converge to their stationary (n-independent) values S_z^{st} and $S_\perp^{st}$, respectively. This treatment resembles that for the optimum flip angle in FT-NMR[143,144]. These stationary values, which can be found from equations

$$S_z^{st} = \left(\left(S_z^{st}\right)' - S_0\right) u + S_0; \qquad S_\perp^{st} = \left(S_\perp^{st}\right)' u, \tag{5.5}$$

are as follows:

$$S_z^{st} = \frac{1 - u(\cos\varphi + 1) + u^2 \cos\varphi}{1 - 2u\cos\varphi + u^2} S_0, \qquad S_\perp^{st} = \frac{u \sin\varphi}{1 - 2u\cos\varphi + u^2} S_0. \tag{5.6}$$

Using these values of electronic polarization the DNP effect can be calculated. As follows from eq. (5.4) after each pulse and free evolution period the following value is added to the nuclear spin polarization:

$$\delta I_z = \sigma s_{\max} T_1^e \left(\left(S_z^{st}\right)' - S_0\right)(u-1) = \sigma s_{\max} T_e \frac{(1-\cos\varphi)(1-u^2)}{1 - 2u\cos\varphi + u^2} S_0. \tag{5.7}$$

Per time unit the following amount of nuclear polarization is added to I_z due to the DNP effect:

$$W = \frac{\delta I_z}{\tau_r} = \frac{\sigma s_{\max} T_e}{\tau_r} \cdot \frac{(1-\cos\varphi)(1-u^2)}{1 - 2u\cos\varphi + u^2} S_0. \tag{5.8}$$

This allows one to write down an equation, which describes the evolution of the nuclear spin polarization with nuclear spin relaxation included:

$$\frac{dI_z}{dt} = W - \frac{I_z}{T_1^n}, \qquad I_z(t=\infty) = W T_1^n. \tag{5.9}$$

Thus, for $\tau_{irr} >> T_1$ the DNP enhancement, ε, is equal to

$$\varepsilon = \frac{W T_1^n}{I_0} = \frac{\sigma s_{\max} T_e T_1^n}{\tau_r} \cdot \frac{(1-\cos\varphi)(1-u^2)}{1 - 2u\cos\varphi + u^2} \cdot \frac{\gamma_e}{\gamma_n}. \tag{5.10}$$

If one assumes $\tau_p << \tau_r$ (i.e. $\tau_r \approx \tau$) and introduces the notation $x = \tau / T_e$ one arrives at

$$\varepsilon = \xi f s_{\max} \frac{1}{x} \cdot \frac{(1-\cos\varphi)(1-e^{-2x})}{1 - 2e^{-x}\cos\varphi + e^{-2x}} \cdot \frac{\gamma_e}{\gamma_n} = \xi f s_{\max} \cdot \frac{\gamma_e}{\gamma_n} F(x,\varphi). \tag{5.11}$$

Here, following, e.g., Hausser and Stehlik[10] the product of σ and T_1^n is denoted as ξf with ξ being the coupling parameter and f being the leakage factor. For $\varphi=\pi$ and $\varphi=\pi/2$ simpler expressions can be obtained

$$\varepsilon\big|_{\varphi=\pi/2} = \xi f s_{\max} \frac{1}{x} \cdot \frac{1-e^{-2x}}{1+e^{-2x}} \cdot \frac{\gamma_e}{\gamma_n} = \xi f s_{\max} \frac{\tanh(x)}{x} \cdot \frac{\gamma_e}{\gamma_n} = \xi f s_{\max} \cdot \frac{\gamma_e}{\gamma_n} F(x, \varphi = \pi/2),$$
$$\varepsilon\big|_{\varphi=\pi} = \xi f s_{\max} \frac{2}{x} \cdot \frac{1-e^{-x}}{1+e^{-x}} \cdot \frac{\gamma_e}{\gamma_n} = \xi f s_{\max} \frac{\tanh(x/2)}{x/2} \cdot \frac{\gamma_e}{\gamma_n} = \xi f s_{\max} \cdot \frac{\gamma_e}{\gamma_n} F(x, \varphi = \pi). \quad (5.12)$$

Thus, in the simplest cases of $\pi/2$-pulses and π-pulses used the DNP effect is determined by only one parameter, $x = \tau / T_e$. For any flip angle used at small x (i.e., very high repetition rate as compared to the relaxation rate) the DNP is equal to $\xi f s_{\max} \cdot \frac{\gamma_e}{\gamma_n}$. This result can be easily understood: after a large number of pulses the polarization component S_z reaches its stationary value, which is approximately $\frac{x}{2} S_0 \to 0$. Then the situation is qualitatively equivalent to the cw DNP: the rate of polarization transfer leading to the DNP effect is time-independent and equal to $W_{cw} = \sigma s_{\max} S_0$, which is exactly the same expression (if $s=s_{max}$) as in the cw-experiment. At large x values the electronic spins have enough time between the two subsequent pulses to relax to equilibrium. In the case of π-pulses one gets the result, that prior to the pulse $S_z=S_0$ and just after the π-pulse $S_z= -S_0$. The DNP tends to reach $\xi f s_{\max} \cdot \frac{\gamma_e}{\gamma_n} \cdot \frac{2}{x}$ with the coefficient 2 explained by the fact that during each pulse the electronic longitudinal polarization varies by $2S_0$. Thus, using π-pulses the efficiency of polarization transfer from electrons to nuclei increases per each cycle by a factor of 2 with respect to $\pi/2$-pulse irradiation. However, as x becomes larger, the rate of polarization transfer to the nuclear spins, W, and, consequently, the DNP efficiency decrease. This is because for $x>>1$ the polarization transfer efficiency becomes independent of x and tends to approach $2\sigma s_{\max} T_e S_0$ (see eq. (5.7) at $u \to 0$ and $\varphi = \pi$), whereas the repetition rate, $1/\tau_r$, is proportional to $1/x$. If $\pi/2$-pulses are used at $x>>1$ one obtains that ε tends to become $\xi f s_{\max} \cdot \frac{\gamma_e}{\gamma_n} \cdot \frac{1}{x}$, i.e. by a factor of 2 smaller than for $\varphi = \pi$. This is because the variation in S_z per each cycle is S_0 but not $2S_0$ as at application of π-pulses. For large $x>>1$ the flip angle dependence of ε has the universal form:

$$\varepsilon = \xi f s_{\max} \frac{1-\cos\varphi}{x} \cdot \frac{\gamma_e}{\gamma_n}. \quad (5.13)$$

Theoretical predictions for the DNP efficiency are shown in Fig. 5.3. At fixed x (Fig. 5.3a) ε is strongly dependent on the flip angle: for $\varphi = 2\pi, 4\pi, 6\pi, \ldots$, obviously, no DNP effect can be observed because the electronic spins are at thermal equilibrium at any instant of time. At

$\varphi = \pi, 3\pi, 5\pi, \ldots$ pronounced maxima in the flip angle dependence of ε are expected. The dependence on φ changes in shape for different x values taken; namely, for small x the sine-like behavior is somewhat distorted. As follows from eqs. (5.11) and (5.13) only at rather large x the DNP flip angle dependence is proportional to $(1-\cos\varphi)$. If the φ value is fixed and x is varied (Fig. 5.3b), the DNP efficiency monotonously decreases with x. At any φ (in Fig. 5.3b the two values $\varphi = \pi, \pi/2$ are considered) ε tends to reach $\xi f s_{\max} \cdot \frac{\gamma_e}{\gamma_n}$ at $x \to 0$, whereas at large x the DNP effect decreases as $1/x$. The coefficient of the asymptote $x \to \infty$ is flip angle dependent as follows from eq. (5.13). For π-pulses this coefficient is two times larger than for $\pi/2$-pulses (Fig. 5.3b).

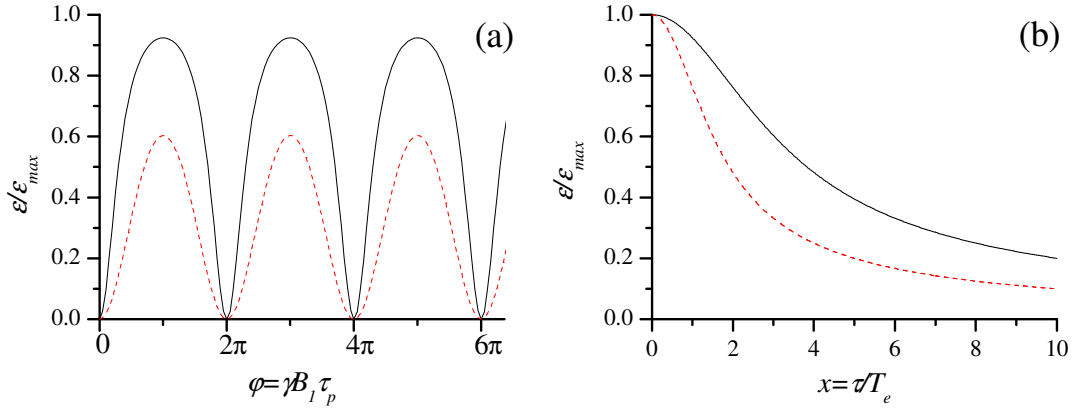

Figure 5.3. Theoretical dependence of DNP enhancement on (a) magnetization flip angle φ and (b) parameter x. For subplot (a) x is equal to 1 (solid black line) and 3 (dashed red line); for subplot (b) flip angle is π (solid black line) and $\pi/2$ (dashed red line). DNP enhancement ε is normalized to $\varepsilon_{\max} = \xi f s_{\max} \gamma_e / \gamma_n$.

Discussing Fig. 5.3b it is important to note that for $\varphi = \pi$ even for x=1 (i.e., τ=T_e) the enhancement is only slightly different from ε_{max}, while for $\varphi = \pi/2$ using τ=T_e one would loose about 20 % of maximal enhancement. Even for x=2 (i.e., τ=2T_e) at $\varphi = \pi$ one would reach the enhancement of almost 80 % of ε_{max}, which demonstrates the advantage of using π pulses. Using x=1 also guarantees high enhancement at relatively small duty cycle. Indeed, $\tau_p = \pi / \gamma_e B_1 << T_e$, thus obtaining $\mathrm{DC} = \pi / \gamma_e B_1 T_e << 1$. At the same time, the pumping power, P_0, during the pulse should be almost the same as in the cw experiment: in both cases B_1 should be taken so that $\gamma_e B_1 T_e >> 1$. This condition guarantees both, a high degree of EPR saturation (in the cw case)

and $\tau_p << T_e$ (in pulsed experiments). Thus, the theoretical approach predicts substantially lower total pumping power for pulsed experiments with nearly the same enhancement.

The present treatment has certain limitations. First, it has been assumed that the pulse length τ_p fulfils the condition $\tau_p << T_1^e, T_2^e$ allowing neglecting electronic spin relaxation effects during the pulse. Second, T_1^e and T_2^e were taken equal, which may not be the case for higher magnetic fields or in the presence of spin exchange.

So far, in the treatment the effects of the nuclear spin relaxation during field variation were omitted. Spin relaxation tends to reduce the obtained DNP enhancement; therefore, it is necessary that $\tau_{fv} / \langle T_1^n \rangle << 1$ where $\langle T_1^n \rangle$ is the average nuclear T_1-relaxation time during the field switching (here it is assumed that, in general, T_1 is field-dependent). Since at a first glance the addition of stable radicals shortens T_1^n it seems advantageous to perform DNP experiments on samples with low radical concentration. However, an increase of the nitroxide concentration, c_R, leads also to an increase of the electron-nuclear cross-relaxation rate, σ. In terms of eq. (5.2) this is described by the leakage factor f representing the contribution of the radical-induced relaxation rate, R_1^{rad}, to the total nuclear T_1-relaxation rate, $R_1^n = 1/T_1^n$,[10] and thus strongly depending on c_R:

$$f = \frac{R_1^{rad}}{R_1^n} \equiv \frac{R_1^{rad}}{R_1^{rad} + R_1^0}. \tag{5.14}$$

Here R_1^0 is the longitudinal relaxation rate in the absence of free radicals. At low radical concentrations $R_1^{rad} << R_1^0$ and $f \to 0$ while at large c_R the leakage factor saturates: $f \to 1$.[145] Thus, one should adjust c_R so that the f value is close to 1 while keeping the concentration low enough so that $\tau_{fv} / \langle T_1^n \rangle << 1$.

DNP spectra

Experiments have been performed with EPR pumping at 300 MHz and 1.4 GHz for solution of 1 mM ^{15}N TEMPOL and 90 mM 3-furoic acid in D_2O; at 300 MHz for solution of 1 mM ^{14}N TEMPOL in H_2O; and at 1.4 GHz for 0.2 mM ^{15}N TEMPOL and 90 mM 3-furoic acid in D_2O. From the experiments performed on Samples 1 and 2 it is seen that DNP is observed not only for the residual protons of the solvent but also for the 3-furoic acid molecules. Comparison of the results for solutions with 1 mM and 0.2 mM of ^{15}N TEMPOL will demonstrate the influence of the electronic and nuclear relaxation. Using sample with ^{14}N TEMPOL in

protonated water, which contained only the radicals and solvent H_2O molecules the possibility of enhancing the NMR signals of solvent protons in high concentration was considered. Fig. 5.3a presents the NMR spectra of different solutions in the presence and in the absence of DNP.

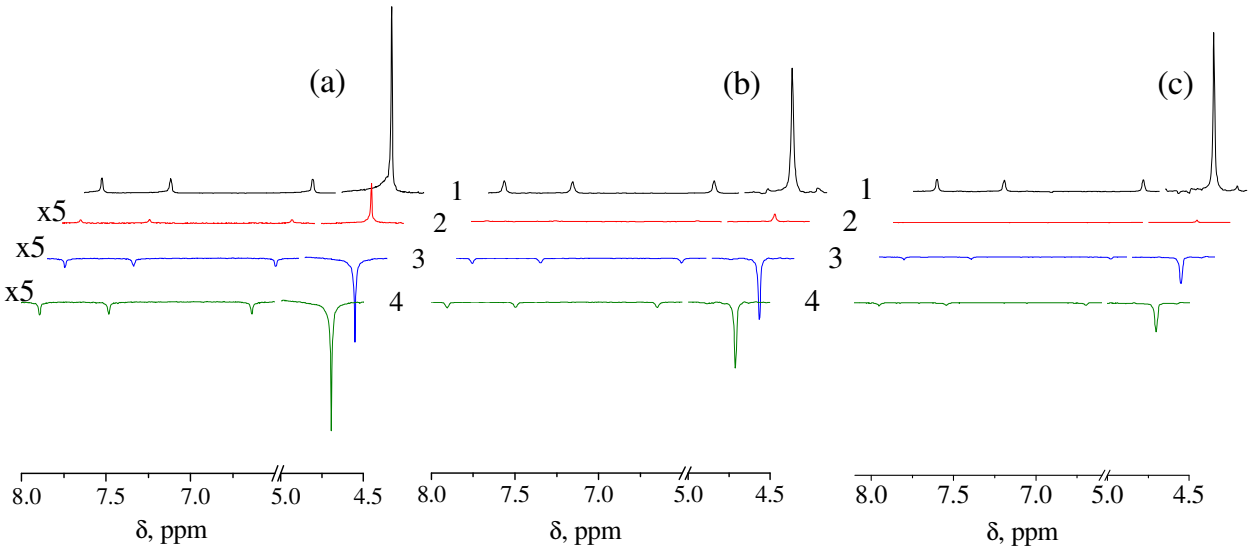

Figure 5.3. NMR spectra of 1 mM ^{15}N TEMPOL and 90 mM 3-furoic acid in D_2O (a,b) and 0.2 mM ^{15}N TEMPOL and 90 mM 3-furoic acid in D_2O (c). Spectrum 1 is the NMR spectrum corresponding to thermal equilibrium at 7 T, spectra 2 and 3 are the spectra obtained after sample transport from field B_{pol} with $\tau_{fv} = 0.27$ s, without and with pumping, respectively. Spectrum 4 is the difference of spectra 3 and 2. Subplot (a) B_{pol} = 9.3 mT, $\tau_p = 25$ ns, τ_{irr} = 5 s, 10 % duty cycle and total power 10 W. Subplot (b). B_{pol} = 48.6 mT, $\tau_p = 125$ ns, $\tau_{irr} = 5$ s, 10 % duty cycle and average power 4 W. Subplot (c). B_{pol} = 48.6 mT, $\tau_p = 125$ ns, $\tau_{irr} = 15$ s, 10% duty cycle and average power 4 W. The spectra scaled to the intensity of 3-furoic acid. The concentration of a residual protons of water and, thus, intensity of HDO signal, varies because of preparation procedure.

Fig. 5.3a shows the NMR spectra of the solution of 1 mM ^{15}N TEMPOL and 90 mM 3-furoic acid in D_2O recorded at 7 T (corresponding to a ^{1}H Larmor frequency of 300 MHz) at Boltzmann equilibrium conditions (spectrum **1**) and those obtained after fast field variation using the protocol shown in Fig. 5.1a (spectra **2, 3** and **4**). Spectrum 2 was obtained when the spin system is equilibrated at low field (9.3 mT or 49 mT), while spectrum 3 was recorded using EPR pumping at the same low field and spectrum 4 being the difference of spectrum 3 and 2 represents the DNP effect. In spectrum 2 the line intensity is conditioned by re-polarization of

the nuclear spins during field variation because of longitudinal relaxation. Since thermal spin polarization is proportional to the magnetic field and $B_{pol} \approx B_0/660$, very low line intensity in spectrum 2 is expected as long as spin relaxation effects during the shuttling to high field can be neglected. Indeed the line intensity in spectrum 2 is considerably lower than in spectrum 1, however, it is above the noise level even at the highest switching speed. In spectrum 4 all lines are emissive according to the negative sign of coupling parameter ξ for aqueous solutions at room temperature. Under these conditions the maximal enhancement achievable at ν_{irr}=300 MHz is ε= –165 at $B=B_{pol}$=10 mT (ξ= –0.5 and selective excitation of one of the two ^{15}N hyperfine components). Thus, if maximal enhancement is reached at $B=B_{pol}$ and relaxation effects during field switch are negligible spectrum 4 will have exactly a quarter of the intensity of spectrum 1 and opposite phase (inversion of the NMR by DNP effect). Considering that the leakage factor at experimental conditions is $f \cong 1$ the actually achieved enhancement ε= –85 shows that relaxation losses during field switching and imperfect saturation lead to a reduction of 50%. The first factor can be reduced by using a lower radical concentration, since the relaxation times T_1^n are known to be strongly dependent on the concentration of the stable radicals.[145] Thus, comparing c_R=1 mM and 0.2 mM one can estimate the influence of relaxation. In Fig. 5.3b the DNP effects observed for the solution but with pumping at 1.4 GHz and 1 mM concentration of the free radical corresponding to B_{pol}=48.6 mT are shown. Here, spectra 2, 3 and 4, have the same scaling as the Boltzmann NMR spectrum at 7 T corresponding to the gain in DNP which is expected because the electron spin polarization is higher by a factor of 14/3.

Fig. 5.3c shows the NMR spectra of the solution of 0.2 mM ^{15}N TEMPOL and 90 mM 3-furoic acid in D_2O. Because of the lower radical concentration and the improved removal of dissolved O_2 by an additional freeze/pump/thaw procedure the line intensity in spectrum 2 where it is conditioned merely by spin relaxation during the field variation stage has decreased. At the same time because of lower free radical concentration the DNP enhancement (spectrum 4) also has decreased. The enhancement achieved at cw irradiation is ε= –125 without taking into account the losses caused by the field-cycling. For the quantification of these losses it was necessary to consider in detail the nuclear longitudinal relaxation in the course of field variation (Fig. 5.1a, **stage 2**). The relaxation effects were modeled numerically and the nuclear polarization, M, was calculated from a Bloch equation with field dependent relaxation and equilibrium polarization:

$$\frac{dM}{dt} = -R_1^n(B)(M - M_0(B)). \tag{5.15}$$

Here $M_0(B)$ is the equilibrium polarization at the magnetic field B, which is proportional to B, while $R_1^n(B)$ is the field-dependent rate of the longitudinal nuclear spin relaxation. The maximal value of M_0 defined as M_{max} corresponds to the equilibrium polarization at the detection field of 7 T. To solve this equation the real profiles $B(t)$ of field variation during **stage 2** and the $R_1^n(B)$ relaxation dispersion curves have been taken. The relaxation dispersion has been measured individually for all spin positions in the molecules (Fig. 5.4b). The $R_1^n(B)$ curves were fitted by the Redfield-type functions

$$R_1^n = R_a + \frac{R_b}{1+\alpha B^2} \tag{5.16}$$

to interpolate the relaxation dispersion in the whole field range. The polarization, M_{fin}, was calculated at the end of field variation period as a function of the initial polarization, $M_{in}=M(t=0)$ at the beginning of **stage 2**. In the absence of EPR pumping at $B=B_{pol}$ during **stage 1** polarization M_{in} was taken zero, while in the presence of pumping it may take different values according to the enhancements achieved. The dependence of M_{fin} on M_{in} is linear (because eq. (5.15) is a simple linear differential equation); its slope was determined by numerical calculation using the data shown in Fig. 5.4(a,b). To confirm the consistency of this approach the calculated M_{fin}/M_{max} value for $M_{in}=0$ (absence of pumping at low field) and the experimental one were compared. Good agreement between theory and experiment allowed to apply this procedure to obtain M_{in} in the presence of DNP effects. In this way it was found that for the protons of HDO in the solution of 1 mM ^{15}N TEMPOL and 90 mM 3-furoic acid in D_2O M_{in} in the presence of pulsed pumping at 300 MHz was $-0.25M_{max}$. As a result, the enhancement reached at $B=B_{pol}$ is equal to $660\times(-0.25)= -165$. For the other protons in this sample the enhancements were as follows: $\varepsilon_{H2}= -170$, $\varepsilon_{H5}= -160$, $\varepsilon_{H4}= -160$, with 5% error margin. For solution of 1 mM ^{14}N TEMPOL in H_2O $\varepsilon_{H_2O} = -135$ was obtained, which is noticeably higher than $1/3\times\xi\times\gamma_e/\gamma_n = -110$ (limiting ε value for selective excitation of one ^{14}N hyperfine component). This value of ε_{H_2O} can be explained by partial excitation of all three hyperfine components during the EPR pumping as a result of ^{14}N relaxation[146] and Heisenberg spin exchange.[147]

For the second pumping frequency of 1.4 GHz a different approach to calculate the ε value was used because the line intensity in spectrum 2 (Fig. 5.3b,c) is too small to be compared with both M_{max} and the line intensity in the DNP spectrum. Therefore, in the presence of pumping M_{fin} was compared with M_{max} taking into account the polarization losses during field variation by eq. (5.15). The calculation gave a slightly higher enhancement $\varepsilon = -69$ than that

($\varepsilon = -65$) obtained by straightforward comparison of the line intensity in spectra 1 and 4 in Fig. 5.3c.

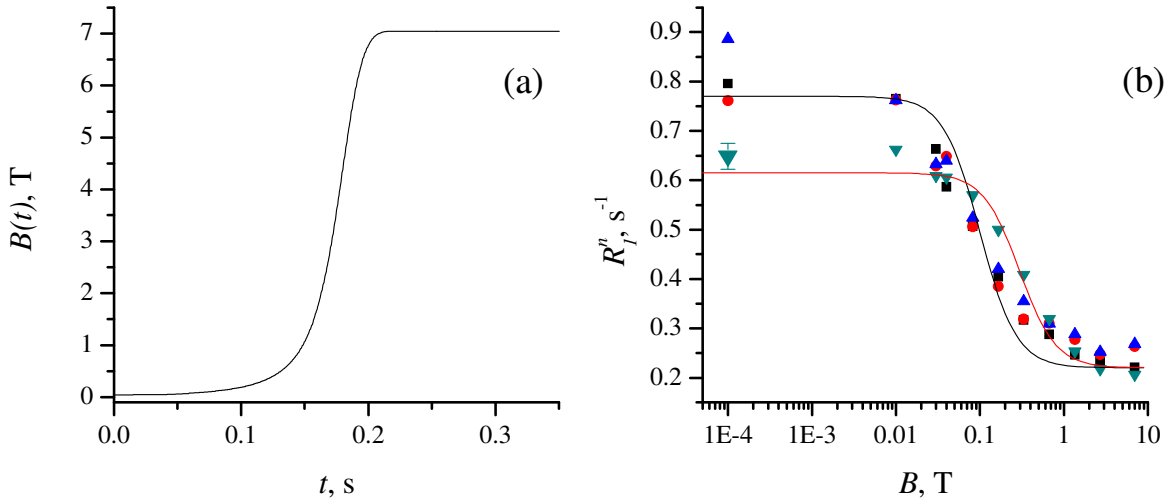

Figure 5.4. Time profile of the magnetic field, *B(t),* during **stage 2** of experimental protocol (a) and relaxation time T_1^n field dependence for the ■-H2 proton, ●-H4 proton, ▲-H5 proton of 3-furoic acid ▼-HDO proton (Sample 1) (b). Solid lines in subplot (b) represent the fit of the relaxation dispersion by the function given in eq. (5.16). Parameters of simulation: black line - α=100 T^{-2} and red line - α=11.5 T^{-2}.

Having established the procedure to determine the DNP enhancements from now on the results will be presented in units of ε instead of NMR intensity units. This is advantageous because the actual enhancement values give a better insight into the problem under study and also because the ε units are free from effects of field variation on the observed signals.

DNP effect as resonance phenomenon

The NMR enhancements obtained are strongly dependent on the exact value of the polarization field B_{pol} because the DNP effect depends on the efficiency of EPR saturation (in the cw-experiment) or nutation of the electronic spins during the excitation pulses (in the pulsed experiment). Thus, DNP should be seen only as long as the pumping frequency, ν_{irr}, is on resonance with one of the EPR transitions in the nitroxide. Thus, stepwise varying the magnetic field B_{pol} at constant pumping frequency changes the resonance conditions for the EPR transitions, and in this way a DNP-detected EPR spectrum of the stable radical can be obtained.

As examples in Fig. 5.5 such EPR spectra of ^{14}N TEMPOL and ^{15}N TEMPOL observed via DNP for the solution of 1 mM ^{14}N TEMPOL in H_2O and the solution of 1 mM ^{15}N TEMPOL and 90 mM 3-furoic acid in D_2O, respectively, are shown. As it is expected, the EPR spectrum of ^{14}N TEMPOL is a triplet, while that of ^{15}N TEMPOL is a doublet. On increasing the amplitude, B_1, of the excitation field, the lines in the DNP detected EPR spectrum become broader (see Fig. 5.5b) and eventually collapse (not shown).

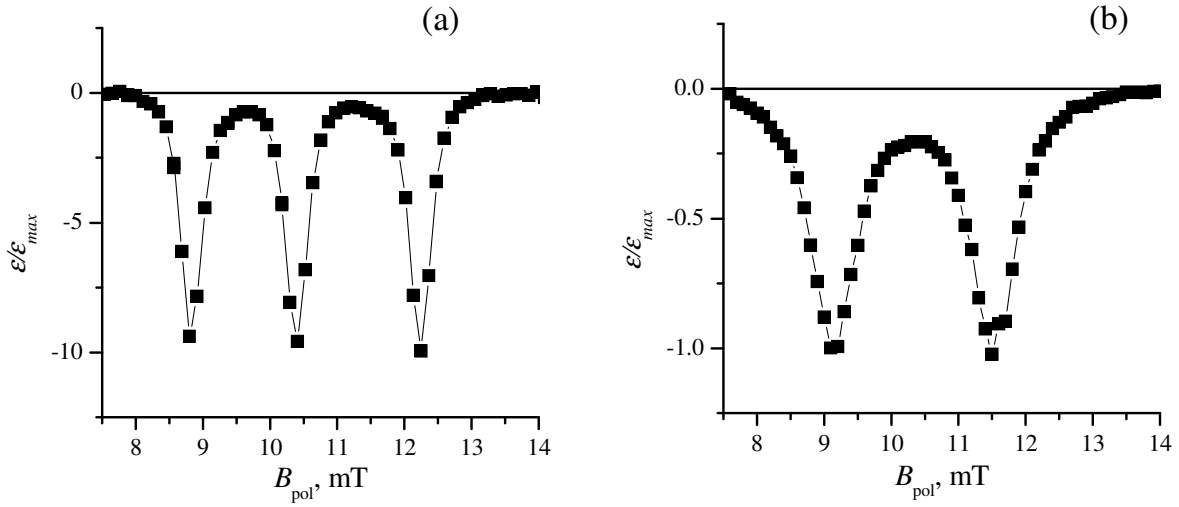

Figure 5.5. DNP detected EPR spectra of ^{14}N (a) and ^{15}N (b) TEMPOL of HDO proton. Spectrum (a) was recorded for Sample 3, spectrum (b) was recorded for Sample 1. Experimental parameters: cw irradiation at 1 W (a) and 4 W (b), τ_{fv}=0.27 s, τ_{irr}=5 s.

Exploiting coherent spin motion for optimizing DNP efficiency

In pulsed DNP experiments pumping is applied only for short periods of time, consequently, power consumption can be optimized by applying short strong pumping pulses at particular instants of time. If the spin motion caused by the EPR pumping pulses is faster than the electronic spin relaxation (the case considered in the present work) DNP relies on driving the electronic spin system away from equilibrium by coherent motion of the spins, i.e. by nutational motion of the electronic spin polarization in the rotating frame about the B_1-field. Coherent effects can only be observed when the B_1-field is sufficiently strong $\frac{2\pi}{\gamma_e T_e} << B_1$ ($\tau_p << T_e$), and homogeneous (flip angle, φ, is the same for all spins in the sample). Thus, by varying the pulse length τ_p being proportional to the nutation angle φ one should see characteristic oscillations in the DNP effect as they are predicted by eq. (5.11). An indication of such an oscillatory component in the efficiency of pulsed DNP was presumably observed in Ref. 134. However, this component was not very well pronounced (see Fig. 4 of Ref. 134) probably because of the

relatively small B_1 values available. Exploiting the specifications of the field-cycling setup the oscillatory component of the DNP effect is analyzed. The coherent evolution of the electronic spins is utilized for optimizing the DNP efficiency, which is, in general, a rather complicated function of pulse length, duty cycle and applied power.

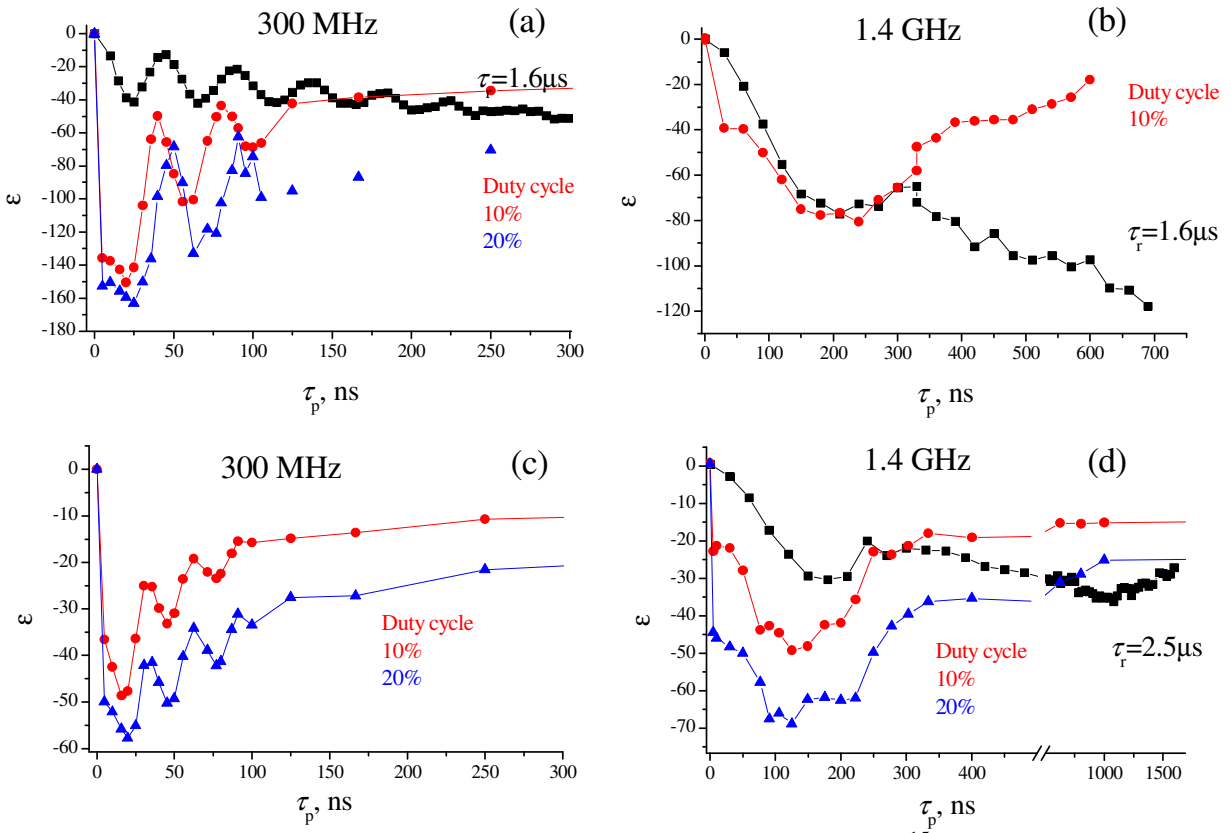

Figure 5.6. DNP of HDO and H_2O protons: (a) the solution of 1 mM ^{15}N TEMPOL and 90 mM 3-furoic acid in D_2O, P_0=100 W, ν=300 MHz at B_{pol}=9.3 mT, dependence on the pulse length τ_p with fixed τ_r=1.6 μs (black) and with fixed DC (10% red and 20% blue); (b) the solution of 1 mM ^{15}N TEMPOL and 90 mM 3-furoic acid in D_2O, P_0=40 W ν=1.4 GHz at B_{pol}=48.6 mT dependence on the pulse length τ_p with fixed τ_r=1.6 μs (black) and with fixed duty cycle (10% red); (c) the solution of 1 mM ^{14}N TEMPOL in H_2O, P_0=100 W, ν=300 MHz at B_{pol}=9.3 mT, dependence on the pulse length τ_p with fixed DC (10% red and 20% blue); (d) the solution of 0.2 mM ^{15}N TEMPOL and 90 mM 3-furoic acid in D_2O, ν=1.4 GHz at B_{pol}=48.6 mT dependence on the pulse length τ_p with fixed τ_r=2.5 μs (black) and with fixed duty cycle (10% red and 20% blue).

Fig. 5.6 (black curves) shows the dependence of the DNP effect at different ν_{irr} and of different samples as a function of the pulse length τ_p. In this experiment the repetition time τ_r was kept constant. An oscillating variation of the dynamic polarization and on top of it a slow, monotonous increase can be seen. The period of oscillation equals exactly $2\pi/(\gamma_e B_1)$ as described by eq. (5.11), whereas the additional increase results from electron-nuclear cross-relaxation during the pulse. For the case of 1.4 GHz excitation the period of oscillation is much longer because of low energy and smaller efficiency of the resonance circuitry. The highest B_1 amplitude available was only 0.11 mT corresponding to a full nutation period of 320 ns, a time of the order of T_e. For the clearly visible damping of the oscillations, three different reasons are obvious: the first is dephasing of the coherent spin motion because of B_1 inhomogeneities. The contribution of B_1 inhomogeneities was checked only for 300 MHz excitation by measuring the ^{1}H NMR nutation at 7 T. The nutation amplitude is reduced by a factor of 2 after 5 periods. This corresponds only to about 30% of the damping seen in Fig. 5.6a. Second, it is assumed that in the pulsed experiments one is dealing with selective pulses, which excite only one component of the EPR spectrum of the nitroxide radical. As already mentioned, this expectation may not be completely true, and the other components of the EPR spectrum may be partly excited by the pulses, but with different φ values in the effective rotating B field. This will also cause φ inhomogeneities resulting in damping of the oscillations for 300 MHz excitation. For 1.4 GHz excitation it is less pronounced because of considerably smaller B_1 field. Last, but not least, around a duration of 200 ns τ_p becomes comparable to T_2^e [147] meaning that the present theory is no longer applicable at such pulse lengths. Because of long nutation period at 1.4 GHz excitation, the oscillations are strongly damped and hard to see. For the solution with 0.2 mM ^{15}N TEMPOL the oscillation of DNP is seen better than for the solution of 1 mM ^{15}N TEMPOL because of the longer T_2^e.

In a second set of measurements Fig. 5.6 (red and blue curves) the duty cycle was kept constant while τ_p was varied. As a consequence, the flip angle, φ, was varied simultaneously with the repetition time τ_r because the pulse length is directly proportional to both quantities: $\tau_p = \tau_r \times \mathrm{DC}/100\%$ and $\tau_p = \varphi/\gamma_e B_1$. Again, all curves measured exhibit damped oscillations with several extrema corresponding to flip angles $\varphi = \pi, 3\pi, 5\pi, \ldots$ (maximal negative DNP effect) and $\varphi = 2\pi, 4\pi, 6\pi, \ldots$ (minimal negative DNP effect) as expected from eq. (5.11). For pumping at 1.4 GHz the oscillations are strongly damped and hard to see. Nevertheless, the DNP enhancement shows a distinct optimum for pumping at constant total power.

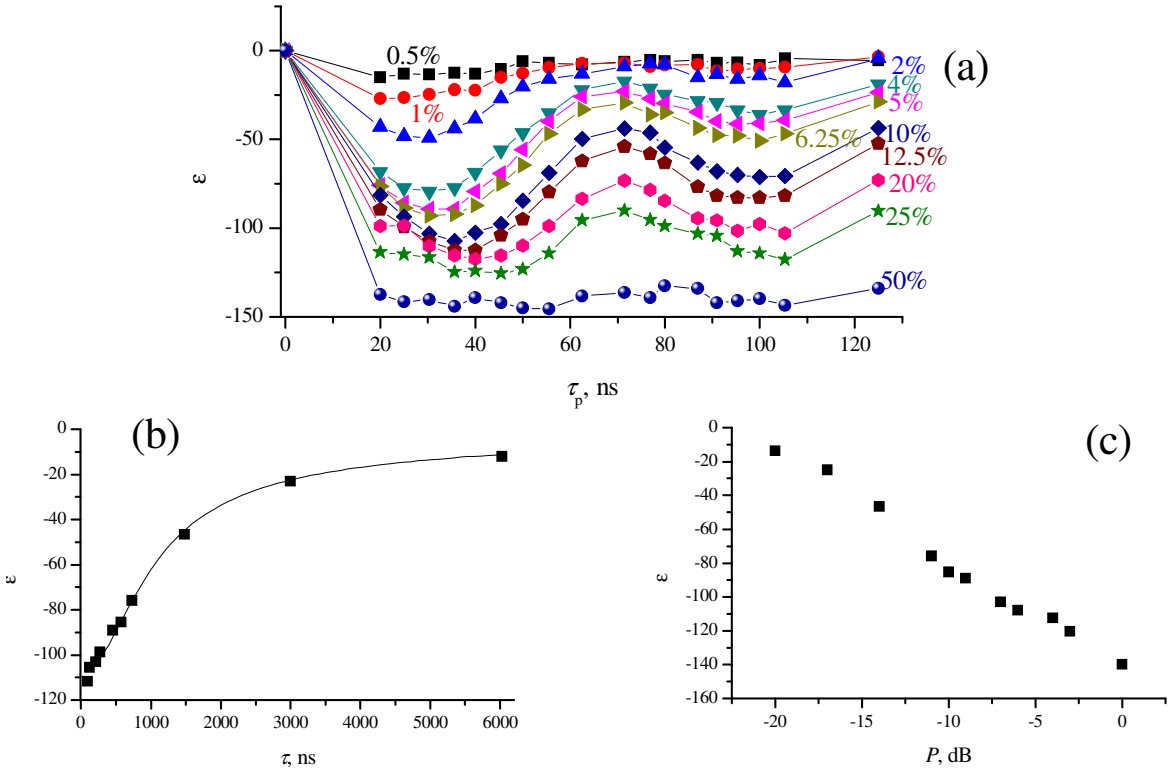

Figure 5.7. Optimization of the pulse sequence for gaining higher DNP enhancements ε for the solution of 1 mM ^{14}N TEMPOL in H_2O at constant P_0=100 W for different duty cycles: (a) dependence of ε on τ_p; (b) dependence of ε at fixed magnetization flip angle $\varphi = \pi$ (25 ns) on delay $\tau = \tau_r - \tau_p$; and (c) dependence of ε at fixed magnetization flip angle $\varphi = \pi$ (25 ns) on total power P. In subplot (b) the solid line shows the best fit with function from eq. (5.12) at $\varphi = \pi$.

Thus, once the B_1 amplitude allows getting π-pulses of a duration τ_p comparable to T_e and the B_1 homogeneity over the sample volume is high enough, pronounced effects of the pulse length on the DNP effect are observable. It becomes clear that optimization of the pulse sequence is crucial for achieving highest possible enhancements. To gain a better insight into the optimization problem the parameters of the pulse sequence (flip angle, duty cycle, repetition time) were varied more systematically. The results of the optimization are shown in Fig. 5.7. The study was performed at a constant EPR pumping power, P_0, during the pulse. Each individual curve shown in Fig. 5.7a corresponds to a different, but constant duty cycle while τ_p was varied. Hence, the six curves shown differ in the total power, P=P_0×DC/100%. Fig. 5.7a thus represents the DNP effect at different total pumping power as the function of the pulse length τ_p. All the dependences shown have an oscillatory component (flip angle dependence of ε) with the first

maximum (maximal negative enhancement) corresponding to $\varphi = \pi$. As follows from Fig. 5.7a for different power levels strongly different DNP amplitudes are obtained. If at fixed $\varphi = \pi$ the duty cycle is increased at constant power P_0 one has to decrease the delay $\tau = \tau_r - \tau_p$, i.e., the x value. Thus, the amplitudes of the first maximum can be plotted versus the delay τ, i.e., versus x, as it is done in Fig. 5.7b. When the resulting variation of ε as a function of x is analyzed by means of eq. (5.12), the T_e value can be obtained. The best fit (solid line in Fig. 5.7b) gives T_e=320 ns. In the fitting procedure the first point in the function $\varepsilon(x)$ was not taken into account because it corresponds to DC=50%, i.e. to values comparable with τ_p and τ_r, whereas in the theoretical treatment it is always assumed $\tau_p << \tau_r$. Thus, eq. (5.12) does not apply to this case. The fit in Fig. 5.7b is almost perfect showing even that at small x the effect turns to a constant level as expected for $\tanh(\frac{x}{2})/\frac{x}{2}$ (see eq. (5.11)). The residuum is smaller than the experimental error margin and is seen only in the logarithmic plot.

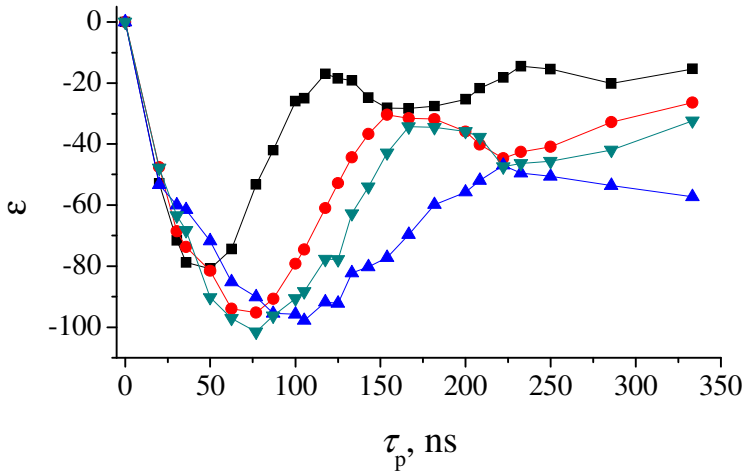

Figure 5.8. Optimization of P_0 for gaining higher DNP enhancements ε at constant total applied power of 3.2 W for different duty cycles (■-5 % P_0=64 W; ●-10 % P_0=32 W; ▼-12.5 %; P_0=25.6 W; ▲-20 % P_0=16 W). Solution of 1 mM ^{14}N TEMPOL in H_2O.

Also, the dependence of the enhancement on the total power, P, which is shown in Fig. 5.7c, was studied. For each value of DC at a fixed P_0 value the maximal enhancement, which corresponds to $\varphi = \pi$, was determined by systematic variation of the pulse length. On a logarithmic P scale this dependence was found to be almost linear. There is no simple explanation for such a linearity because the enhancement in a complicated way depends on the duty cycle, the ratio of τ_r and T_e and the flip angle φ. As can be seen from Fig. 5.7c at –10 dB (only 10 % of the maximal applied power P) the ε value achieves more than one half of the

maximal enhancement whereas at –5 dB (32 % of the maximal power) the achieved ε value is about –120. These results demonstrate the advantages of performing DNP experiments in the pulsed mode with relatively low duty cycle: proper matching $\varphi = \pi$ of the electronic magnetization flip angle allows one achieving negative NMR enhancements of the order of 100 with approximately 20 % of the maximal applied power.

Variation of P_0 at fixed total power allows to further optimize the enhancement/applied power ratio. At Fig. 5.8 the dependence of ε on τ_p at different P_0 is shown. For each individual curve the maximal enhancement is obtained at τ_p corresponding to $\varphi = \pi$ which depends on P_0. It can be seen that at the same total power there is an optimum for getting the highest enhancement. At this particular total power τ_p with the highest ε is much longer than the shortest τ_p obtainable at the setup. The optimum τ_p on the electronic relaxation times and, thus, on the concentration of the free radical. Hence, knowing the total power which can be applied to a sample without considerable heating one has to optimize P_0 in order to get maximum enhancement.

While heating of the sample was not observed at 300 MHz excitation a remarkable line broadening was obtained during 1.4 GHz excitation. After 15 s of 10 % DC at P_0=40 W the temperature of the sample increases by 0.3 degree corresponding to 0.9Hz of line. The enhancement at $\varphi = \pi$ was 50 (Fig. 5.6d). At the same conditions but 20 % DC the increase of the temperature was already 2.3 degree with enhancement of 70. Thus, there is a trade of between the enhancement and the heating of the sample.

Summary and conclusions

In this chapter pulsed DNP experiments are described where the EPR pumping was performed at low magnetic fields and NMR spectra were detected under high-resolution conditions at 7 T. First, two different fields were used for EPR pumping. In principle, it is possible to vary the magnetic field in a broad range from 0.1 mT to 7 T in a controllable way. Thus, using double frequency NMR probes with one frequency (300 MHz) for observation and a second variable frequency ν_{irr} it would be possible to extend the EPR pumping to the corresponding field $B_{pol}=2\pi\nu_{irr}/\gamma_e$.

The mechanism and efficiency of pulsed DNP were considered in detail. At pulse duration τ_p corresponding to flip angles of odd multiples of π the DNP efficiency goes through pronounced maxima. A strategy for optimal conditions for pulsed DNP at 300 MHz was experimentally established from the experimental study of ε as a function of pumping power,

pulse length and duty cycle. The spin-lattice relaxation time for TEMPOL was obtained (T_e=320 ns at 11.8 mT) by analyzing the DNP dependence on the delay between the pulses. A theoretical model has been developed for describing the polarization transfer from the electron to the nuclear spins by pulsed RF irradiation. For better description of the results, the theoretical model has to be extended to include both T_1 and T_2 relaxations of the electron.

The methods of calculation of the enhancement factor, ε, was developed. It requires to know the full profile of relaxation rate dependence on the magnetic field. Thus, it allows to present results in units of ε. At ν_{irr}=300 MHz for H_2O, for the residual protons of the solvent (HDO) and the diamagnetic solute molecules large negative DNP enhancements were obtained. They all were close to the theoretical limit of –165 (ξ=0.5, f=1 and s_{max}=1/2 for ^{15}N-labelled TEMPOL). The determined ε values are –135 (HDO) and between –155 and –175 (protons of 3-furoic acid). For pure H_2O the ε value of –135 is even higher than the limit of –110 (corresponding to s_{max}=1/3 for ^{14}N-labelled TEMPOL), which is presumably due to partial excitation of the off-resonant components in the EPR spectrum of the nitroxide. For the second pumping frequency, ν_{irr}=1.4 GHz, the achieved enhancement was ε= –150 at cw pumping of 17 W. In the pulsed mode the enhancement $\varepsilon\approx$–80 was noticeably smaller being equal to approximately one half of the upper theoretical limit of -165, because of (a) relaxation during the RF-pulse, since with the MW-amplifier available the shortest π pulse length is close to the electronic relaxation time and (b) the low repetition rate as a consequence of long τ_p. Nevertheless, at both pumping frequencies strong NMR enhancements were achieved, which are of the order of one hundred. To get a high enhancement it is necessary to excite all component in the EPR spectrum of the free radical. For this the B_1 field should be as big as the EPR spectral width. It requires more powerful MW-amplifiers used for pumping the electron transitions. Increase of the B_1 field will result in very short π pulse, τ_p, that, accordingly, would desire high damping of the excitation circuitry and, again, more powerful MW-amplifier. On the other hand one can use longer pulse duration τ_p corresponding to flip angles of odd multiples of π higher than one without damping the circuitry. It can be solution if heating is low enough, homogeneity of the B_1 field is high and τ_p is still shorter than electronic relaxation. Another way of the exciting all component of EPR spectrum is applying more complex pulse schemes similar to NMR excitation pulses.

The obtained results demonstrate that at low magnetic fields B_{pol} strong polarization enhancements ε close to the upper theoretical limit can be reached by DNP in both cw and pulsed modes and be combined with high resolution NMR spectroscopy at high observation

field. Performing the DNP experiments in the pulsed mode one can substantially reduce the power losses. While in cw DNP experiments it is necessary to keep continuously a high degree of EPR saturation in pulsed experiments it is advantageous to flip the electronic magnetization by 180 degrees by a short, strong RF-pulse keeping a rather long delay ($\tau \approx T_1^e$) between the subsequent pulses. This experimental protocol allows one to get close to the maximum achievable ε value at small duty cycle and, consequently, low power deposition. Thus, utilization of the coherent electronic spin motion in DNP experiments may find its useful applications. The study also suggests that the advantages of the pulsed DNP experiments will remain valid at magnetic fields higher than those studied here. Even though at high fields the maximum achievable enhancement goes down (as the coupling factor ξ decreases with increasing field) one can still rely on coherent motion of the electronic spins and tailor the pulse sequence for approaching ε_{max} at relatively low pumping power.

The results of DNP experiment on 3-furoic acid showed almost equal polarization on all protons of the molecule. It can be consequence of the polarization transfer among coupled at low field proton spins. For the HP re-distribution generation of DNP in low-field is superior compare to high field DNP experiments.

6. Application of CIDNP to biomolecules (amino acids and peptides)

CIDNP is a hyperpolarization generated in the radical reactions, as was described in Chapter 1.1, and, thus, it is used to investigate radical reactions pathways and radical structure. Individual atoms in the radicals are polarized according spin density distribution that together with NMR technique detection allowing atomic resolution permits elucidation of the reaction mechanisms and the structure of reactive intermediates. The polarization pattern is detected by pulsed NMR method that leads to submicrosecond time resolution. With this time resolution investigation of such processes as paramagnetic nuclear relaxation for individual nuclei is possible that gives information on intramolecular mobility of polarized parts of the radicals. In addition, CIDNP is one of the few methods that is sensitive to intramolecular electron transfer and degenerate electron exchange. For more details see Chapter 1.1.

A particular application of CIDNP is the probing of protein structure[148-150] and folding.[102,151,152] For such protein studies, CIDNP is created by reactions involving reversible electron or hydrogen atom transfer between a photo-excited dye molecule and CIDNP-active amino acid residues. The polarization of the CIDNP-active residues in the protein depends on their accessibility for the probing dye molecule. The assumption underlying the photo-CIDNP technique is that only residues accessible to dye molecule acquire high polarization. Therefore, one can analyze CIDNP of the protein in order to obtain the accessibilities of residues on the protein surface.

The ability of the CIDNP method to elucidate the radical structure and radical reaction pathways was applied here to methionine and methionine containing dipeptide radicals. The sulfur-containing amino acids methionine functions in many basic and essential processes of life. Methionine is a nutritionally important amino acid and the precursor of several metabolites that regulate plant growth and responses to the environment. Methionine, among the 20 amino acid residues normally found in proteins, is the one that is most readily oxidized via electron transfer from its sulfur atom. Oxidation of methionyl residues in proteins plays an important role during pathological conditions and biological aging.[153] It is associated with long term harmful biological consequences as Alzheimer's disease[154] or *in vivo* irreversible protein damage.[155]

For some time it was believed that among the 20 common amino acids only three (histidine, tyrosine, and tryptophan) are sufficiently CIDNP-active, that is, acquire substantial CIDNP when exposed to excited dye molecules. However, more recent experiments performed on methionine with flavin mononucleotide used as a dye revealed that methionine is also CIDNP-active.[156,157] The intensity of methionine CIDNP, however, is increased when

4-carboxybenzophenone is used as the dye.[158] While the CIDNP kinetics and field dependences of histidine, tyrosine and tryptophan have been studied in detail, there is still insufficient knowledge concerning the CIDNP of methionine. The previous CIDNP investigations on methionine radicals employed only steady state version of CIDNP at one field[158,159] or field dependence but only in neutral solution[157] while a local pH in peptides can be different from neutral. It was shown for three above mentioned amino acids that the steady state results can be not sufficient for understanding the pathways and the kinetics of the their reaction. In particular, it was shown for histidine, tyrosine, and tryptophan[160,161] that the reaction of degenerate electron exchange between radicals of the amino acid and the diamagnetic species leads to efficient transfer of nuclear polarization from the radical to the diamagnetic molecule and strongly affects the CIDNP kinetics leading to the fast decay of polarization. For all three amino acids studied so far the exchange was found to be important in the regime of pH when the structure of the intermediate radical and the resulting diamagnetic molecule differs only by an electron. CIDNP of methionine as a part of peptide for the first time was observed in Ref. 162 however no so far systematic investigation of methionine residue radical was performed.

In this context the present investigation is aimed at studies of the photochemical reactions of methionine, its analogues and methionine containing peptides (Met-Gly and Gly-Met) with several dyes 4-carboxybenzophenone (and its analogues) and 9,10-anthraquinone-2-sulfonic acid, by analyzing the dependence of the observed CIDNP on the external magnetic field and the CIDNP kinetics. The photoexited dye molecules are models of electron acceptor. The dipeptides Gly-Met and Met-Gly have been chosen for this investigation since they represent the simplest combinations of two residues for which the peculiarities of CIDNP formation and oxidation reaction were revealed. Gly does not have any functional group that may have its own properties. It will be shown that in these photoreactions new types of radicals are formed which were not observed before. Here a particular advantage of CIDNP to detect short lived radical intermediates which can not be detected by EPR or optical methods was used.

Experimental part

The experimental setup used for CIDNP at variable magnetic field and TR-CIDNP has been described in detail in Chapter 2.2 and 2.3 respectively. L-Methionine (Met) (98%), N-acetyl-l-methionine (NMet) (98%), 3-(methylthio)propylamine (MTPA) (97%), 4-carboxybenzophenone (CBP) (99%), 3-carboxybenzophenone (99%), 3,3′,4,4′-benzophenone-tetracarboxylic acid (99%), DCl (99%), NaOD (99%) and D_2O (99.9%) were used as received from Sigma-Aldrich. 9,10-Anthraquinone-2-sulfonate sodium salt (AQS) (97%, Sigma-Aldrich)

was recrystallized from ethanol/H_2O before use. The dipeptides, Gly-Met and Met-Gly, were purchased from Bachem (99%). Concentrations were 1.2 mM for CBP, 0.7 mM for AQS, 3 mM for Met, 3 mM for MTPA, unless otherwise stated. The pH of the NMR samples was adjusted by addition of DCl or NaOD. No correction was made for the deuterium isotope effect on the pH.[163] All samples were purged with pure nitrogen gas and sealed in standard 5 mm Pyrex NMR tubes.

Field dependent CIDNP measurements have been carried out according to the protocol described in Chapter 2.2 and shown in Fig. 2.2.1. During the first stage the sample is located at the lowest position and at lowest possible magnetic field, B_p, to get the smallest thermal polarization. Then it is transferred to the variable field, B_{int}, and irradiated (typically for 0.5 s) by a XeCl excimer laser at 308 nm with a repetition rate of 50 Hz and an energy of up to 30 mJ/pulse (after liquid lightguide). After irradiation the sample is transferred to detection field, B_0, where the FID is recorded. The reactions between a dye molecule and an amino acid are not completely cyclic. The solutions become exhausted after prolonged photolysis, and the observed enhancements are certainly not linear in the number of transients accumulated. This so-called depletion was mathematically corrected. For this the sets of the measurements at various fields were divided by a set of measurements obtained at a single field with maximal polarization. The depletion was kept below 30%.

The CIDNP kinetics was measured according to the experimental protocol described in Chapter 2.3. To avoid the problem of sample depletion, one sample was used to acquire two or four scans for each τ-value. The number of points in a single CIDNP time dependence (8-13) was chosen to provide less than 30% depletion during irradiation of one sample. Depending on the CIDNP enhancement factor, 8 to 32 samples were used to complete one full CIDNP time evolution with an appropriate signal to noise ratio, so that every data point in the CIDNP kinetics represents 32 to 64 signal accumulations. In all kinetic measurements, an RF-pulse of 1 μs duration was used for detection. The timing corresponds to the center of the RF-pulse (i.e., 0.5 μs for $\tau = 0$) on all CIDNP plots.

6.1 Methionine, N-acetylmethionine and 3-(methylthio)propylamine

The dominant mechanism for the quenching of aromatic triplets by sulfur containing amino acids and methionine (Met) containing peptides is electron transfer.[164-166] The carboxyl group of CBP and sulphonic group of AQS are deprotonated in the pH range used in present research (pH 6…13). Met and MTPA has a pK_a of 9.27 and 10.5, respectively, (in H_2O) for its amino group, therefore Met exists either in its protonated form as NH_3^+ at a pH below this value

or otherwise as NH_2 with a lone electron pair. The result of the quenching reaction is the formation of a spin correlated radical pair consisting of an amino acid cation radical and the radical anion of the dye molecule. The quenching rate constant of triplet CBP has been measured as $k_q=2.6 \times 10^9 M^{-1}s^{-1}$.[164,165] Two pH-dependent structures of methionine radicals (S-N cyclic and "open form" S-centered) were detected using transient optical absorption[165-172] and magnetic resonance spectroscopy[157,173-176] showing that the high reactivity of the methionine residue is associated with the presence of the sulfur atom. Another competitive reducing quenching mechanism that can be operative at basic conditions for methionine is electron transfer from the nonbonding electron pair at the nitrogen to triplet excited photosensitizers leading to the formation of the N-centered aminium cation radical. The N-centered radicals are one of the main species involved in the oxidative damage of proteins. Up to now, due to the lack of a chromophore group in the N-centered radicals these radicals were not detected by transient optical absorption. On the other hand the N-centered radical is too short-lived to be detected by the EPR method. In case of CIDNP method, back electron transfer from the anion radical of the dye to the cation radical of the amino acid leads to nuclear spin polarization of both, the amino acid and dye, due to the hyperfine interaction with the unpaired electrons. Here only polarization of Met, N-acetylmethionine (NMet) and 3-methylthiopropylamine (MTPA) will be considered.

The N-acetylmethionine was taken as prototype of Met residues present in proteins where one of the peptide bonds is modeled by the amide bond with the acetyl group. Its amino group is acetylated consequently the lone electron pair on nitrogen atom of NMet is in interaction with the carbonyl group. This is the same reason why the amino group of N-acetylmethionine (NMet) is not protonated in the pH range used here and retains its structure throughout. It models a small peptide with one peptide bond of between N-terminus Met residue and the neighboring amino acid residue. Hence, the results presented here can be used for optimizing the conditions in analogous experiments on peptides.

In the course of the oxidation reaction, the Met is known to undergo decarboxylation reaction,[170,177] which significantly complicates the analysis of the radical intermediates (*vide infra*). In order to get dipper understanding of the reaction pathway the MTPA molecule was studied as a model of Met without carboxylic group.

Several types of CIDNP methods were combined to get full information on the radical structure and radical reaction pathway of methionine and its analogs.

CIDNP spectra

The NMR signals of the nuclei that exhibit polarization generated in the course of the reversible photoreaction have the same chemical shifts as in the non-polarized starting material and thus can be easily differentiated from polarization formed in competing reactions. Using CIDNP allows to establish the complete oxidation mechanism of Met with an unambiguous identification of the structure of the radicals involved and the determination of the reaction pathways. The polarization observed within about a microsecond after the creation of the radicals arises solely from recombination of geminate radical pairs and is free of confounding effects from side processes such as nuclear spin-lattice relaxation in the radicals, degenerate electron exchange, radical recombination, or polarization generated in random encounter pairs (F-pairs). As a rule, the geminate polarization of nuclei in the recombination products is simply proportional to the corresponding hyperfine couplings in the radicals.[178] The CIDNP technique for probing the structure of various radical species of the Met residue is particularly suitable because the radicals so formed have essentially different distributions of their spin density (*vide infra*).

Met has a pK_a of 9.27 and 4.2 (in H_2O) for its amino and carboxylic group, respectively. Therefore, Met exists either in its protonated form as NH_3^+ at a pH below 9.27 or otherwise as NH_2 with a lone electron pair. In neutral solution methionine exists in a zwitter-ionic form with a positive charge on the protonated nitrogen atom thus only lone electron pairs on S atom is available. In the CIDNP spectrum in Fig. 6.1.1 left taken with no delay after the laser pulse the nuclear polarization of only the protons in γ and δ positions of the amino acid is found. The absolute intensity of all signals that belong to methionine is much lower in the spectrum taken at 100 μs after the laser pulse than that formed in the geminate recombination as shown in the spectrum taken with zero delay. Form polarization of the protons in γ and δ positions a conclusion that radical center is located on S atom of Met can be made. This indicates the formation of "open form" radical (radical **V**).

For Met in basic solution, the situation is distinctly different. Here, across the entire magnetic field range polarization was detected not only for the δ and γ protons of Met but also for the α proton. This observation is in full accordance with that by Goez et al.[158] Such a polarization is feasible only for a radical with sufficient spin density at the α position. A likely candidate for such a species is the cation radical of Met with a five-membered ring and a three-electron bond between S and N atoms as shown in Fig. 6.1.1 right (radical **II**) and originally suggested by Hiller et al.[180] to explain the results obtained from pulse radiolysis experiments.

Polarization of the α, γ and δ protons in the absence of β proton polarization is an indication for the existence of the cyclic structure of the involved radical of Met. The formation of this cyclic structure arises from intramolecular reaction of a positively charged radical center at the sulfur atom with the partly negatively charged nitrogen atom, which has a lone electron pair at this pH.

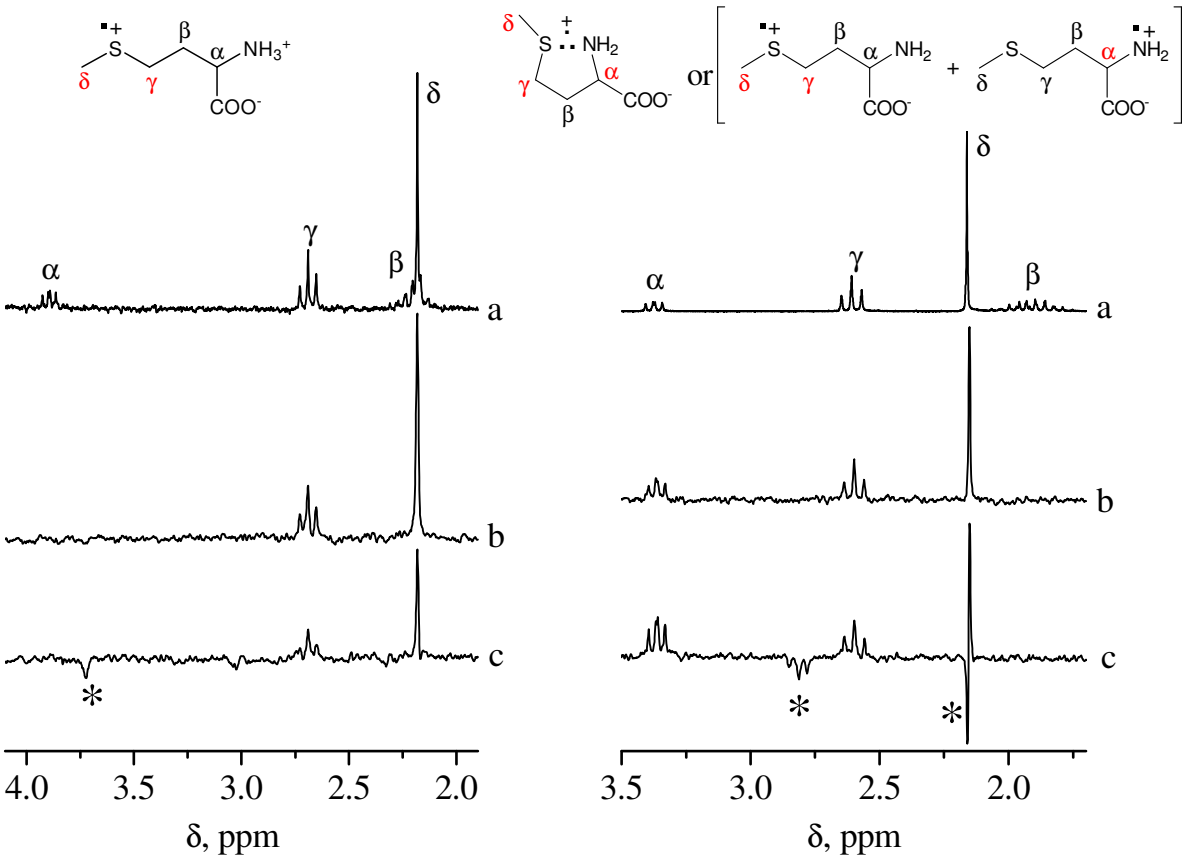

Figure 6.1.1. ^{1}H NMR spectrum of Met at pH 6.7 (left) and pH 13.3 (right) (a). ^{1}H CIDNP spectra obtained at pH 6.7 (left) and pH 13.3 (right) in the photoreaction of Met and CBP immediately after the laser pulse (b), and with a delay of 100 μs after the laser pulse (c). The NMR spectrum is scaled independently while the two CIDNP spectra have the same scaling within the same pH. Asterisks denote the signals of side products.

The geminate polarization (obtained at τ=0) contains signal contributions only from reactants formed in the reversible electron transfer reaction. In the CIDNP spectrum taken 100 μs after the laser pulse at pH 13.3 additional emissive lines of side products are present. These emissive signals were assigned in Ref. 179 to γ (triplet, 2.8 ppm) and δ (singlet, 2.2 ppm) protons from the CH_2 and CH_3 groups bonded to the sulfur atom of the aldehyde O=CH-CH_2-CH_2-S-CH_3. Since the α-aminoalkyl radical ($H_2N-\dot{C}H-CH_2-CH_2-S-CH_3$) is formed as the result of decarboxylation of the methionine cation radical **II** escaped from

geminate recombination, the polarization of protons in γ and δ positions is emissive in accordance with spin-sorting S-T_0 mechanism of polarization formation in high magnetic field.[23] After hydrogen atom abstraction from the α-aminoalkyl radicals by CBP in the ground state, this negative polarization is inherited by the HN=CH-CH_2-CH_2-S-CH_3. This thioimine is the main product of side reactions of α-aminoalkyl radicals with CBP, and it is converted to the aldehyde O=CH-CH_2-CH_2-S-CH_3 via fast reaction with water.[179]

In Fig. 6.1.1 at pH 13.3, in the spectrum taken with a delay of 100 μs after the laser pulse the intensity of the α-proton of methionine is much larger than that in the geminate spectrum, while the growing of the intensity of the γ protons is not detected. This observation is not in accordance with the data obtained in Ref. 158, where the measurements were made at pH below 12.2 under the steady-state irradiation conditions. Moreover, it contradicts the key assumption made in Ref. 158 that polarization of methionine is formed solely at the geminate stage of the reaction, and allows to suggest that in strong basic solution the polarization of the α and γ protons does not exclusively originate from the same radicals.

In the cyclic form of the radical **II** with a three electron two center bond between sulfur and nitrogen, all protons in the γ, δ and α positions of methionine are polarized, while in the "open form" of radical **V** only the protons in the γ and δ positions are polarized. However, the polarization pattern of Met in basic solution can be, in principle, result of two parallel reaction pathways with two different radical pairs were involved in the triplet quenching process. In this case the first reaction occurs with electron transfer from the sulfur atom of the amino acid with the formation of an S-centered radical, whereas the second one proceeds from the lone pair on the nitrogen with the formation of an aminium radical,[181] as it is shown in Fig. 6.1.1. As evidence for the formation of the cyclic radical structure the ratio of polarization level of the protons in the α and γ-position of methionine and its variation with the pH were taken by Goez and Rozwadowski,[158] but a similar pH dependence is expected also for the relative contribution to polarization by the corresponding protons of the two "open formed" radicals. Moreover, time-resolved CIDNP measurements performed here on the kinetics of this reaction at different pH show that the assumption[158] of CIDNP creation exclusively at the geminate stage is unsustainable and that the pH dependence of the stationary CIDNP signal is not at all given by the interconversion of different radicals of methionine at the geminate stage.

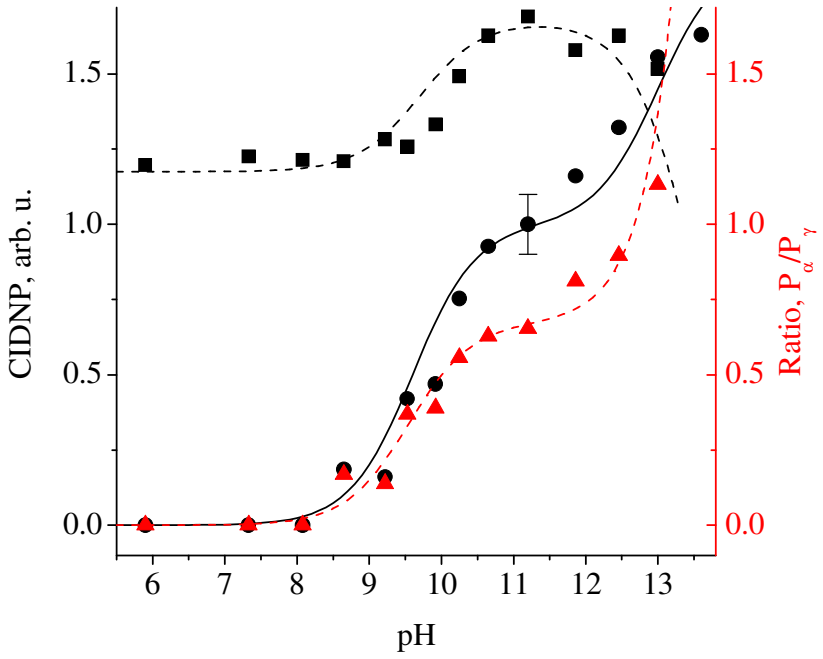

Figure 6.1.2. pH dependence of ^{1}H CIDNP obtained in photoreactions of Met and CBP immediately after the laser pulse for the α proton of Met (black circles), for the γ protons of Met (black squares), and for the CIDNP ratio of α and γ protons (red triangle). The solid line shows simulation according to eq. (6.1.3) with p_1=0, p_2=1.9, pK_b=1. The dashed lines do not represent the simulation, because the experimental data for the γ protons, in contrast to MTPA, are distorted by the overlapping of the side-product signal in the spectrum.

The pH dependence of CIDNP detected immediately after the laser pulse for the α and γ protons of Met in the photoreaction with CBP is shown in Fig. 6.1.2. In full accordance with previous results,[158] at pH below pK_a of Met (9.6 in D_2O), polarization is observed for the γ and δ protons only, whereas at pH above pK_a the α proton is also polarized. To allow quantitative comparison with the data reported by Goez[158] the pH dependence of P_α/P_γ (geminate polarization ratio of α and γ protons) of Met is shown in Fig. 6.1.2 by red triangle. This dependence differs significantly from the corresponding curve found in Fig. 3 of Ref. 158. First, inflection point at pH 9.6 is in accordance with pK_a value of the diamagnetic molecule, while in Ref. 158 the pH dependence showed a remarkable deviation from the titration curve of the chemical shift of the polarized protons. Thus, the excellent agreement as it was stated[158] for the pH dependence of the ratio (P_α/P_γ) obtained from the analysis of stationary CIDNP patterns and compared with data calculated by modifying standard radical pair theory by taking into account the interconversion of radicals in the geminate stage has still to be substantiated. Second, at pH above 11.5 an

increase of α proton CIDNP and a slight decrease of polarization of the γ protons is detected, altogether leading to an increase of the ratio of polarizations in disagreement with to Ref. 158.

In contrast to Ref. 158 the pH dependence of CIDNP was also measured at higher pH values where an additional step of the pH dependence is seen. In the full pH range three distinct regions are seen indicating that, at least, three different radicals are responsible for the formation of CIDNP.

As it was said above, the intensities of CIDNP in geminate spectra reflect the electron spin density distribution within the radical. Intensities at four different pHs corresponding to different pH ranges with various radicals are summarized in Table 6.1.1. They are scaled with respect to the polarization of the δ protons. At pH below pK_a the CBP molecule is not soluble; thus, in order to obtain the CIDNP spectra at acid conditions another dye molecule, 2,2'-dipyridyl (DP), was used. Although at pH 3.25 the Met carboxylic group is protonated the geminate intensities at acidic and neutral conditions are the same indicating formation of a similar S-centered radical. Thus, the conclusion can be drawn that only the protonation state of the amino group influence the radical formation reaction. At pH 11.2 the ratio between δ and γ protons is different. It case that CIDNP in basic solution is formed in S-centered and N-centered radicals the ratio would be the same as at pH 6.7. Thus, the existence of the cyclic radical with polarization on α, δ and γ protons is more probable.

Table 6.1.1. Line intensities of geminate CIDNP spectra at different pH.

	Met +DP pH 3.25	Met + CBP pH 6.7	Met + CBP pH 11.2	Met + CBP pH 13.3
δ protons	1.00	1.00	1.00	1.00
γ protons	0.54	0.53	0.62	0.98
α proton		-	0.45	1.53

It should be mentioned that DP reacts with Met only at pH below the pK_a of the DP (4.3). It allows using DP as a selective dye for tyrosine, tryptophan and histidine amino acids at neutral and basic conditions.

CIDNP field dependence

A possible way to discriminate the occurrence of one cyclic or two "open form" intermediates is to determine the g-factor of the radicals so formed. The most direct way for measuring the g-factor is EPR, but because of their high reactivity and, consequently, low concentration the cation radicals of methionine is difficult to detect in aqueous solution. An

alternative way to obtain the desired information on the g-factors of the participating radicals and on the reaction pathway is to utilize the dependence of CIDNP on the external magnetic field described in Chapter 1.1. Standard CIDNP theory relates the maxima of polarization at high magnetic field B_0 to the difference in g-factor $\Delta g = (g_q - g_d)$, where g_q and g_d stand for the g-factor of the quencher radical and of the dye radical, respectively. Since the g-factor of the S-centered radical of structure (Fig. 6.1.1 left) is expected to be considerably larger than that of the aminium radical (Fig. 6.1.1 right), the maxima of CIDNP of these radicals are expected to appear at different field strength of B_0 so that they can be distinguished in the field dependences of the methionine protons. Alternatively, if only the cyclic radical is involved, one common field of maximum polarization for all protons of methionine is expected with its location determined by the g-factors of the cyclic cation radical and the radical of the dye.

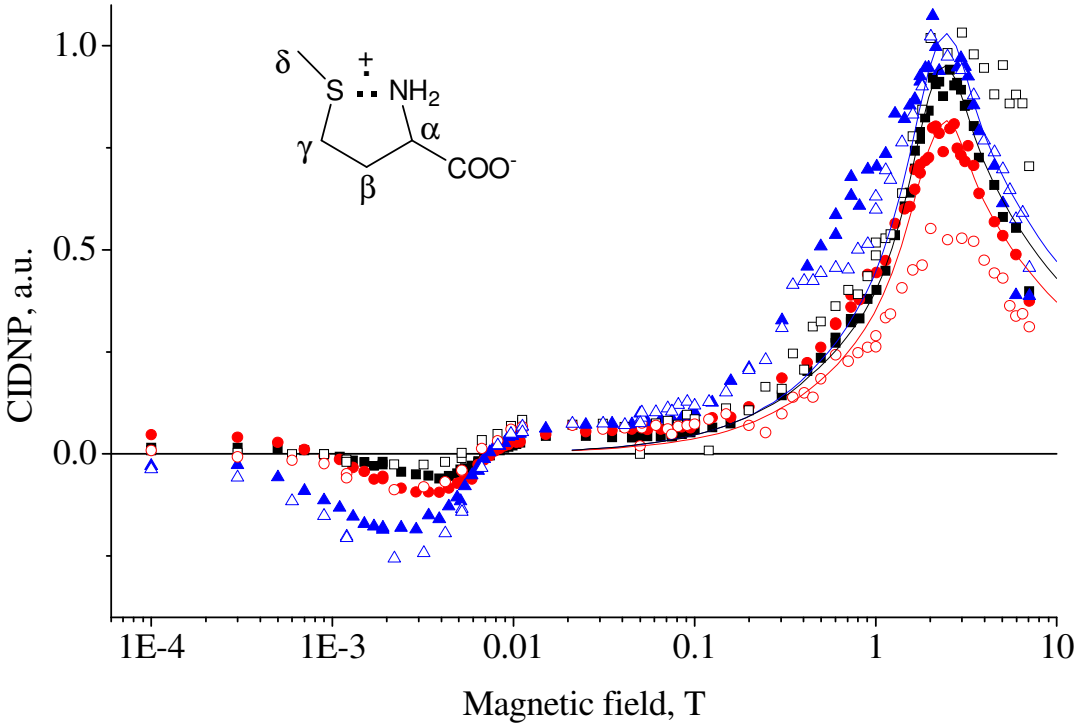

Figure 6.1.3. Field dependence of ■- α, ●- γ and ▲- δ protons of methionine with photoexited CBP at pH 11.5 and of □- α, ○- γ and △- δ protons at pH 13.2. Polarization of α proton is normalized to one. Lines with correspondent color are the simulated CIDNP. Simulation parameters for the cyclic radical (**II**): g=2.0064, A_α=1.0 mT , A_γ=0.8 mT, A_δ=0.7 mT and A_N=2.0 mT.

From Fig. 6.1.3, where the field dependences of the α, γ and δ protons of methionine at pH 11.5 and 13.2 are shown in the range between 0.1 mT and 7 T it is evident that only a single

polarization maximum appears. No other CIDNP maxima were detected at high magnetic field; hence it can be excluded that any other cyclic radical with a two-center three-electron bond either between sulfur and oxygen or between sulfur and nitrogen is formed for the Met, in agreement with Ref. 170.

Only field dependence of δ protons shows shoulders at low and high fields. The polarization of the α, γ and δ protons of the same sign gives additional evidence for a bond between S and N in the cation radical. These facts prove the formation of cyclic cation radical **II**.

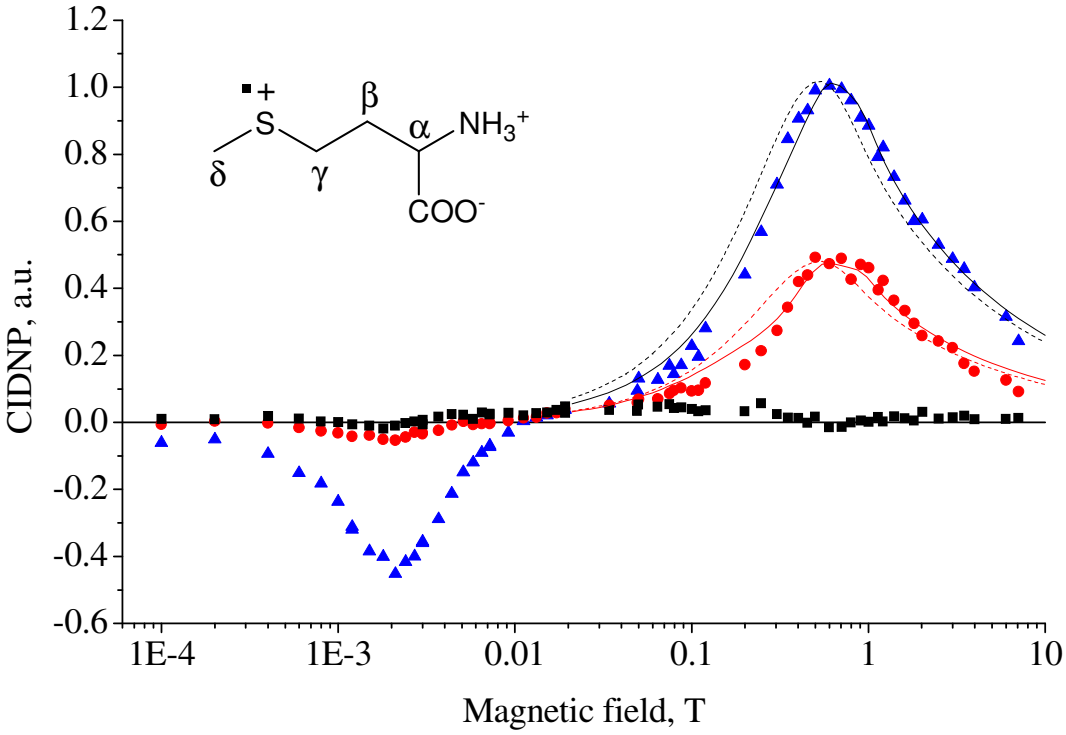

Figure 6.1.4. Field dependence of ■- α, ●- γ and ▲- δ protons of methionine at pH 6.0 in reaction with photoexited CBP. Lines with correspondent color are the simulated CIDNP of methionine in neutral solution assuming monomeric "open form" radical (simulation parameters: g=2.01012, A_γ=1.03 mT, A_δ=1.32 mT) while dashed lines are the simulations assuming dimeric radical with parameters from Ref. 173 (g=2.01012, A_γ=0.566 mT, A_δ=0.712 mT). Polarizations of protons are normalized to the maximum polarization of δ protons.

For quantitative evaluation of the CIDNP field dependences the simulation approach described in Chapter 1.1 was used. Keeping in mind the limitations of the CIDNP method (Chapte 1.1) the HFI constants and the g-factor of the cyclic radical of Met in basic solution were optimized to get the best simulation of the high field part of the CIDNP field dependence at pH 11.5. The best simulation is shown by the solid line in Fig. 6.1.3. Because bulk reactions and

relaxation influence different proton groups differently the intensity of the simulations were normalized for each proton group individually. Since CIDNP depends on the difference Δg between the radical pair partners, the g-factor of one radical species can only be determined with reference to the magnetic resonance parameters of its partner. In the present case, there is the problem that the g-factor and HFI constants of the CBP radical are unavailable from the literature. However, Säuberlich et al.[182,183] measured the g-factors of both benzophenone (2.0033) and of 3,3′,4,4′-benzophenone-tetracarboxylic acid (2.0035). It is reasonable to assume that the magnetic-resonance parameters of the radicals benzophenone and CBP do not differ much and values g_{CBP} = 2.0033, A(4H,o) = 0.29 mT, A(4H,m) = 0.11 mT, A(1H,p) = 0.35 mT[183] were taken. As g-factor of the cyclic cation radical g = 2.0064 was obtained, which is significantly smaller than the typical g-value of S-centered organic radicals (2.0100) indicating that part of the spin density is located at the nitrogen atom.

The field dependences of δ protons of Met at pH 11.5 and 13.2 show shoulders on the low field (0.7 T) side while γ protons are without it. This feature can be explained by a contribution from of the "open form" radical to polarization of the δ protons. The position of the shoulder in magnetic field (0.7 T) coincides with field dependence of the "open form" radicals (Fig. 6.1.4) and (Fig. 6.1.5)**.** The shoulder is more pronounced for the δ protons as their polarization in "open form" radical is higher than the polarization of the γ protons. At higher pH value the α proton has a shoulder at high field indicating the existence of other N-centered radical with smaller g-factors.

In the case of Met in neutral solution the formation of the cyclic cation radical is impossible due to the lack of the lone electron pair at nitrogen atom because of the protonation of the amino group. The CIDNP field dependence (Fig. 6.1.4) shows only one common maximum position in high field for both γ and δ protons, whereas the α proton is not polarized in high field. The maximum of high field polarization is shifted to lower fields compared to Met in basic solution showing that the radical of Met in neutral solution has a larger g-factor. Thus in neutral solution the existence of the "open form" Met radical is expected. This type of radical is more often investigated that the other types of Met radicals, however, only the magnetic resonance parameters for a dimer sulfur radical cation are available[173] for ambient temperature and aqueous solution. It was found that simulations with the parameters of the dimer do not coincide with the experimental data. At the same time the simulation fits well if one uses the parameters of the monomer cation radical **V** which were recalculated from the dimer parameters. The g-factor was taken the same as for the dimer while HFI constants were obtained by duplication of the

corresponding dimer constants because all spin density is located only on one molecule. After only a slight adjustment of the HFI coupling constants to fit the high field part of the field dependence in the simulation the curves shown in Fig. 6.1.4 with the parameters given in the legend were obtained. The HFI constants coincide with those obtained from Ref. 173 within the linewidth of the EPR spectra in the reference.

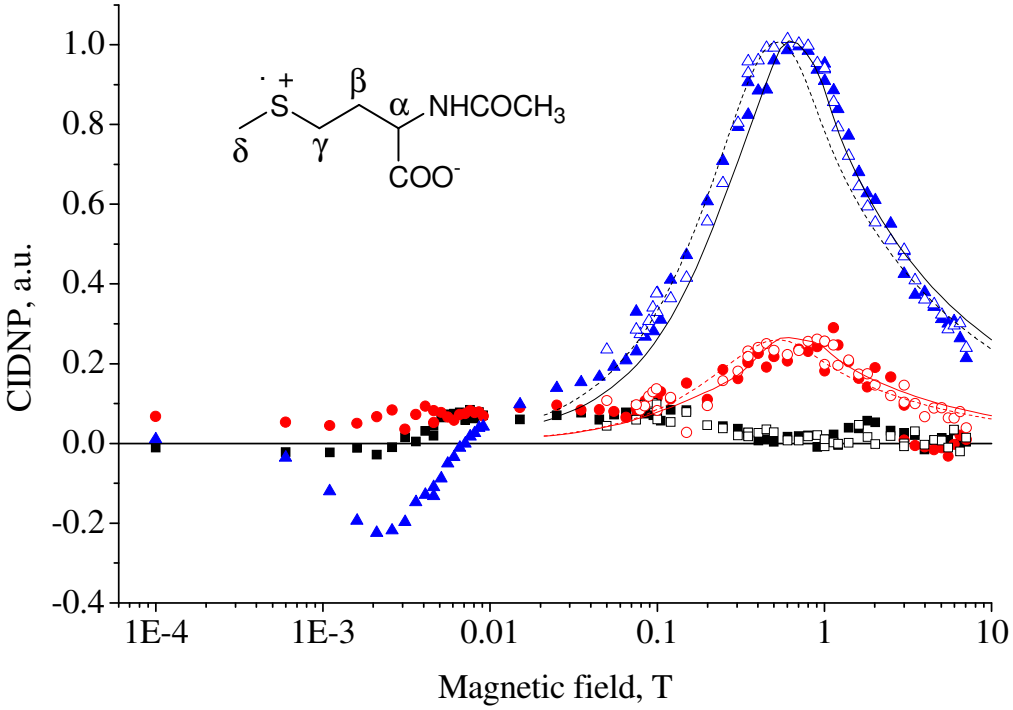

Figure 6.1.5. Field dependence of ■- α, ●- γ and ▲- δ protons of N-acetylmethionine at pH 6.4 and □- α, ○- γ and △- δ protons at pH 11.3 in reaction with photoexited CBP. Lines with corresponding color are the simulated CIDNP. Simulation parameters were taken the same as for Met in neutral solution: g=2.01012, A_γ=1.03 mT, A_δ=1.32 mT. Dashed lines are the simulations assuming dimeric radical with parameters from Ref. 173 (g=2.01012, A_γ=0.605 mT, A_δ=0.692 mT). Polarizations of protons are normalized to the maximum polarization of δ protons.

In intermediate field (10 mT < B_{pol} < 100 mT) the polarization of the α proton is observed while the β protons are not polarized. Because the α proton is not polarized at high field its low field polarization is purely originating from polarization transfer from the γ protons due to strong coupling in the intermediate field. Polarization transfer is a complicated process and can lead to the fact that the low field part of the simulation does not reflect the intensity and shape of the experimental data. Unfortunately the influence of degenerate electron exchange (6.1.1) of the

Met radical on CIDNP at low field is not yet described by theory. Hence, the low field part was not included in the CIDNP simulations.

In case of NMet in neutral and basic solution the lone pair of the nitrogen interacts with the π-orbital of the carbonyl group and thus cannot be used for the formation of a bond between the S and N atoms. This is the same reason why acetylated amino groups can not be protonated in aqueous solution. The similarity of the CIDNP field dependence of NMet with that of Met in neutral solution (Fig. 6.1.5) indicates the formation of an S-centered radical similar to the "open form" radical of Met (Fig. 6.1.4). Moreover, the shape of the field dependences and, hence, the structure of the radical does not depend on pH because the diamagnetic precursor does not change with pH. Thus, the amide bond which models the peptide bond in proteins prevents the formation of the cyclic Met radical. Hence, in methionine containing peptides the Met residue is expected to form only the "open form" S-centered radical.

Another model molecule is the MTPA which is similar to Met molecule in structure except for the missing carboxyl group. In order to use MTPA as a model of Met in kinetic CIDNP studies one has to be sure that it forms the similar radical. To check it the field dependent CIDNP study of MTPA was performed. It was found out that MTPA reacts with photoexited benzophenone type dyes only in basic solution. The field dependence of the reaction of MTPA with photoexited 3-carboxybenzophenone at pH 12.4 is shown in Fig. 6.1.6. The dye molecule is different from that used in case of Met but it is very close in properties to CBP. The magnetic resonance parameters of the radical of 3-carboxybenzophenone are assumed here to be identical with those of CBP. In high field only the α, γ, δ protons are polarized whereas the β protons are not polarized and the position of the high field maximum is very close to that of Met indicating formation of the cyclic radical.

In contrast to Met the MTPA β protons are polarized in low field. The intensity found for the polarization of the β protons is comparable to the polarization of α and γ protons, and the field dependences have the same position of the low field extremum (3.5 mT) while the low field extremum of δ protons polarization has a different position (2.5 mT). These facts indicate that polarization transfer occurs from the γ and the α protons to the β protons due to strong scalar coupling among them in low field whereas the δ protons are decoupled at any field. The polarization of the β protons observed in MTPA in contrast to Met can only be explained by a different configuration of their spin systems. The Met molecule has five coupled protons in configuration of two of non-equivalent β protons, two equivalent γ protons and a single α proton whereas MTPA has three CH_2-groups each with a pair of chemically equivalent protons.

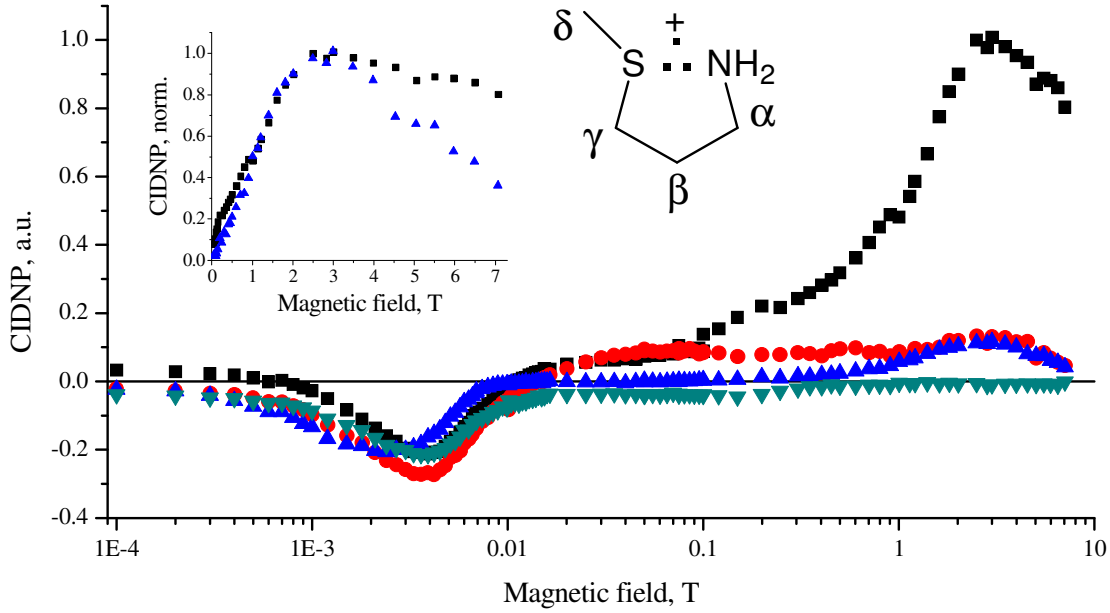

Figure 6.1.6. Field dependence of ■- α, ▼- β, ●- γ and ▲- δ protons of MTPA in the reaction with photoexited 3-carboxybenzophenone at pH 12.4. Polarizations of protons are normalized to the maximum polarization of α protons. Insert: field dependence of α and δ protons normalized to unity.

The field dependence of the α proton polarization in high field has a shoulder at the high field wing (see insert in Fig .6.1.6), which is not seen for other protons. Similar to Met the shoulder is the result of formation of N-centered radicals with lower g-factor and only α protons polarized at high field.

CIDNP kinetics

To clarify the origin of the effects that are responsible for CIDNP generation in the system under study, kinetic measurements at pH 6.7, 11.3, and 13.3 were performed. The results of the measurements are shown in Figs. 6.1.7 and 6.1.8. At a pH above 9.6, the signal of the δ protons is overlapping with an emissive signal, and the enhanced absorption of the side product superimposes the low-field component of the signal of the γ protons (Fig. 6.1.1 left, trace c). Thus, at pH 11.3 and 13.3 only the signal of the α proton was evaluated.

The kinetic curves obtained at pH 6.7 (Fig. 6.1.7) show a fast decay of CIDNP in time. The decay rate becomes faster when the concentration of the amino acid is increased. This behavior is typical for degenerate electron exchange (DEE) (Chapter 1.1) and it is a clear

evidence that this process takes place in the bulk. By transient optical experiments the absorbance of the dimeric sulfur radical cations with the maximum at 408 nm is well characterized.[164] It should be mentioned that DEE reaction is not suitable for optical detection because it does not lead to any change in the absorption spectrum, but it is well suited for investigation by time-resolved CIDNP techniques. Also in time-resolved EPR (CIDEP) spectra observed for the photoreaction of triplet 9,10-anthraquinone-2-sulfonic acid (AQS) with methionine in neutral aqueous solution[173] the dimeric sulfur radical cations were detected with hyperfine splitting corresponding to six and four protons and assigned to the δ and γ protons (a_δ=0.712 mT, a_γ= 0.566 mT). Based on these data the fast decay of the CIDNP signal can be attributed to the following DEE:

$$^{*}\left[H_3C(R)S^{+}\therefore S(R)CH_3\right] + S(R)CH_3 \xleftrightarrow{Kex} {}^{*}H_3C(R)S + \left[H_3C(R)S^{+}\therefore S(R)CH_3\right] \quad (6.1.1)$$

Here $H_3C(R)S$ denotes the methionine molecule and the asterisk denotes dynamic nuclear polarization.

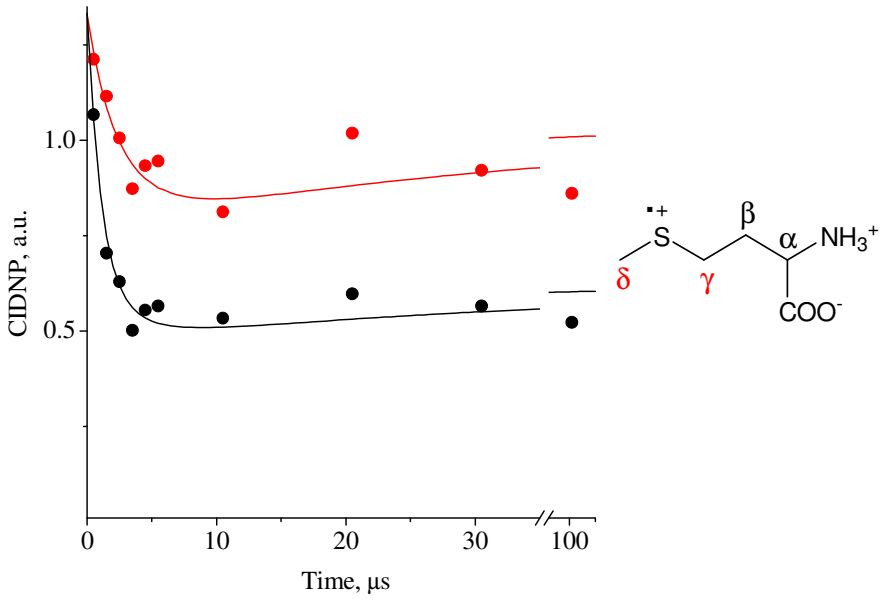

Figure 6.1.7. ^{1}H CIDNP kinetics of the photoreaction between Met and CBP observed for the γ protons at a pH of 6.7 and a concentration of Met of 1.1 mM (red), and 2.2 mM (black). The lines were calculated according to the procedure described in the text. For the values of the parameters used, see the text.

On the other hand the concentrations of methionine used in the present investigation were one order of magnitude lower than in the EPR measurements.[173] The lower concentration leads to less probable formation of dimers, so the degenerate electron exchange between the

monomeric S-centered radical of Met and Met in diamagnetic state shown in reaction scheme (6.1.1) can not be excluded:

$$^{*}H_3C(R)S^{\bullet+} + S(R)CH_3 \xleftrightarrow{Kex} {}^{*}H_3C(R)S + H_3C(R)S^{\bullet+} \qquad (6.1.2)$$

Another fact supporting the existence of process (6.1.2) rather than (6.1.1) is that the CIDNP field dependence in neutral solution shows formation of the monomer radical of Met. However, it can not be excluded that both DEE processes (6.1.1) and (6.1.2) can take place during the radical reaction at the same time.

The numerical simulations of the CIDNP kinetics were done using the approach described in Chapter 1.1 and is shown in Fig. 6.1.7 by the solid line. As it will be shown further below, the degenerate electron exchange can be included by introducing the term $k_{ex}CP(R)$ into (1.1.4) and (1.1.5). It describes the transfer of radical polarization, $P(R)$, from the paramagnetic to the diamagnetic species with concentration C.

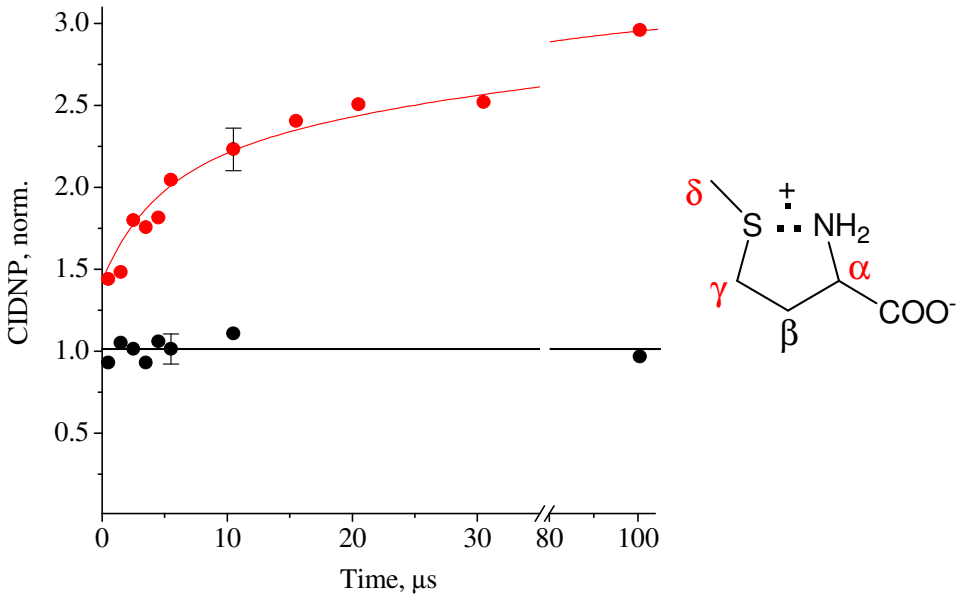

Figure 6.1.8. ^{1}H CIDNP kinetics of the photoreaction between Met and CBP observed for the α proton at pH 11.3 (black), and pH 13.3 (red). The lines were calculated according to the procedure described in the text. For the values of the parameters used, see the text.

At a pH of 11.3 the CIDNP of the α proton of Met is constant in time (Fig. 6.1.10, black), in full accordance with the fast decarboxylation rate reported for the cyclic Met radical (5×10^{6} s^{-1}),[184,185] which allows only geminate polarization to be formed. A remarkably growing CIDNP kinetics is obtained at pH 13.3 (Fig. 6.1.10, red). At pH values between 11.3 and 13.3 a

monotonous increase of CIDNP at 100 μs relative to that at zero delay with a growing intensity of the geminate polarization is observed (not shown).

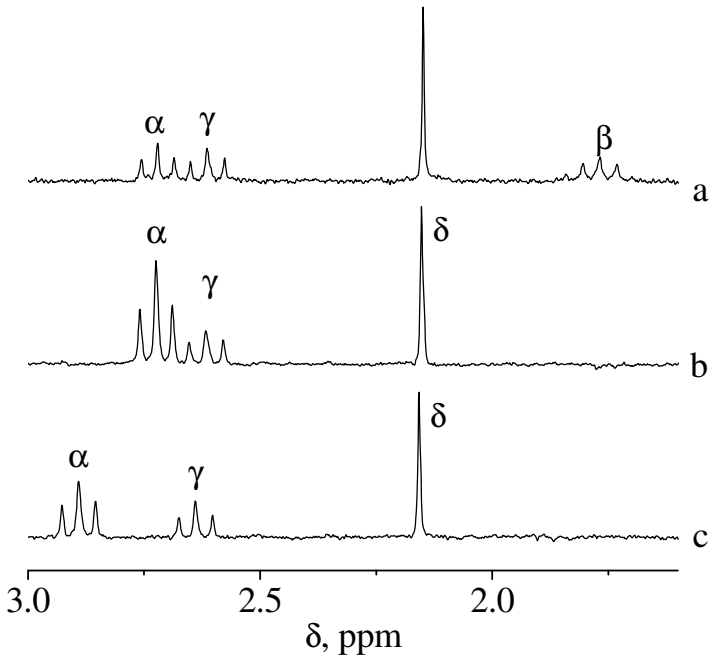

Figure 6.1.9. ^{1}H NMR spectrum of MTPA at pH 12.6 (a). ^{1}H CIDNP spectra obtained in the photoreaction of MTPA and CBP immediately after the laser pulse at pH 12.6 (b), and 11.0 (c). NMR spectrum and CIDNP spectra are scaled independently.

The obtained results allows to propose the degenerate electron exchange as the reason responsible for the deviation of the CIDNP pH dependence from the titration curve in Ref. 158. The similarity of the CIDNP pH dependence to chemical shift dependence is base on an assumption that the polarization is proportional to the concentration of the diamagnetic precursors. While it is true for the geminate polarization as can be seen in Fig. 6.1.2, the steady state polarization is strongly attenuated by the exchange reaction (6.1.1 or 6.1.2). The degree of cancellation is determined by the concentration of the protonated Met molecule but is independent of the deprotonated Met concentration. Hence, no proportionality on the precursor concentration is expected for steady state polarization. Indeed, at a pH well below p$K_{a,}$ 100% of the Met molecules can participate in the exchange reaction, whereas only 50% are available at pH 9.6. Thus, as the pH decreases, the stationary CIDNP value of γ and δ protons formed in the "open form" of Met decreases, hence the ratio of stationary polarizations of α and γ protons of Met increases beyond the value expected for the normal titration curve. No interconversion

among three forms of Met radical is needed to explain the observed stationary CIDNP pH dependence especially with the fact that the geminate polarization pH dependence does not deviate from the titration curve (Fig. 6.1.2). An additional argument against the scheme introduced in Ref. 158 is the pK_a value of the amino group of the "open form" Met cation radical, that is stated to be 8.5.[158] The characteristic time τ_d of deprotonation can be expressed via the ionization constant K_a and the protonation rate constant k_p (~10^{10} $M^{-1}s^{-1}$): $\tau_d = K_a^{-1} \times k_p^{-1}$, which is 30 ms at p$K_a$=8.15. This time constant is too big to have equilibrium conditions established during the lifetime of the radicals, which under the conditions of CIDNP experiments can hardly be longer than 0.1 ms.

The decarboxylation of Met radical at basic solution masks other types of radical reactions. In order to gain more insight into the radical reactions of methionine at these pH values that lead to the observed CIDNP effects the ^{1}H CIDNP in the reaction of the prototype of Met, 3-(methylthio)propylamine (MTPA) were explored. It does not contain the carboxyl group and therefore has a lifetime of its cyclic radical that is not limited by the fast decarboxylation reaction. MTPA is used as a model compound for unraveling the redox chemistry in sulfur-containing amino acids and peptides, therefore the kinetics and structural properties of the cyclic radical formed from MPTA in aqueous solution are well characterized.[186]

The CIDNP spectra taken for two different pH values at zero time delay between laser pulse and NMR pulse are presented in Fig. 6.1.9. The pH dependence of geminate CIDNP detected in photoreactions of MTPA with different dyes is shown in Fig. 6.1.12. The CIDNP patterns at zero delay closely resemble in all their peculiarities those of methionine: polarization is detected for the α, γ, and δ protons, but not for the β protons. No polarization is detected for MTPA with CBP below the pK_a of the amino group, 10.5,[186] indicating that no reaction takes place between the triplet excited CBP and protonated MTPA. Polarization of both, α and γ protons, first grows with increasing pH with pK_a = 10.5, and at higher pH the direction of CIDNP amplitude change for these two types of protons becomes opposite, similar to that obtained for Met. In addition, the CIDNP of MTPA in the reaction with another sensitizer, AQS was checked. AQS was used before in a time-resolved CIDEP study of methionine cation radicals.[173] In the photoreaction of AQS with MTPA CIDNP of MTPA was found in the whole pH range studied (5 < pH < 13). The pH-dependence of the geminate CIDNP amplitude for the α protons is shown in Fig. 6.1.12 by triangles. It is seen that after passing through a maximum at around pH=11.5 the CIDNP of the α protons decreases at higher pH. The corresponding pH dependence for the γ

protons (not shown) starts from a non-zero value below pK_a and is qualitatively the same as obtained for Met and CBP (cf. Fig. 6.1.2).

The CIDNP kinetics obtained at different pH for the α and γ protons (Fig. 6.1.10) has the following peculiarities: a monotonic decay with a pH-independent decay rate is detected for the γ protons, while the influence of pH is seen in the attenuation of the geminate CIDNP amplitude in accordance with the pH dependence in Fig. 6.1.12 (red circles). In Fig. 6.1.10, an almost coinciding kinetics obtained at pH 11.0 and 12.6 is shown by red, respectively. Furthermore, the kinetics of the γ protons is independent of the concentration of MTPA. For the α protons, the CIDNP kinetics changes from a monotonic decay at pH 11 to an initial rise followed by a slight decrease at pH 12 and 12.6.

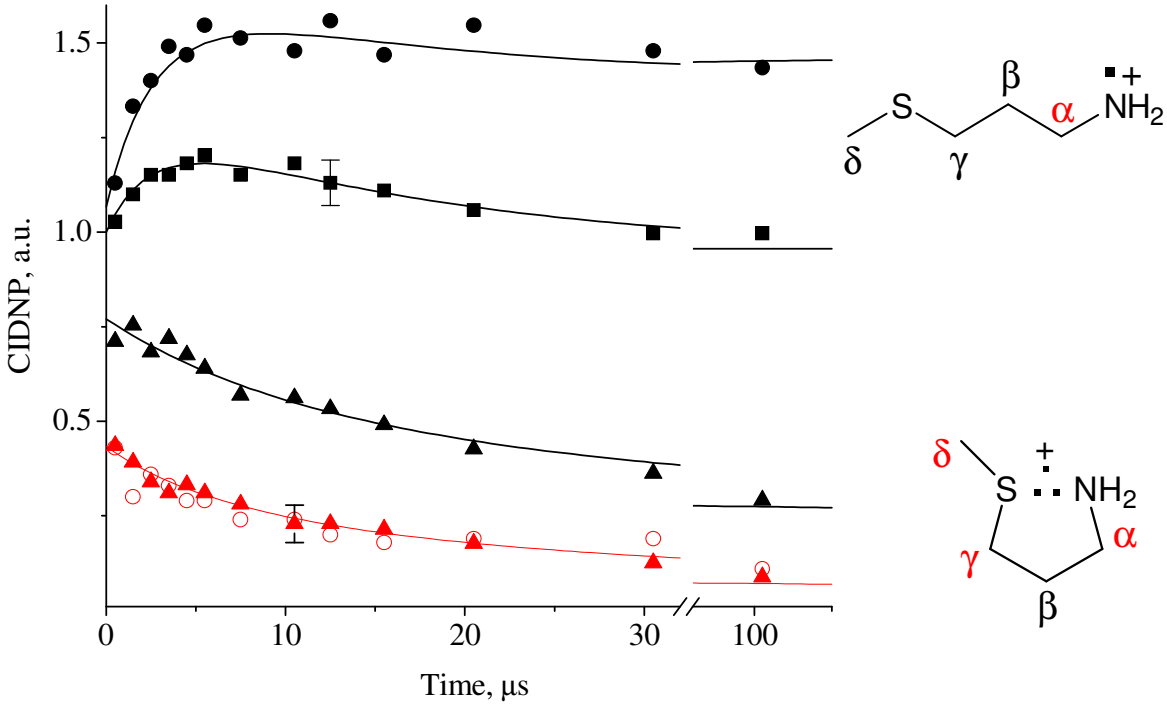

Figure 6.1.10. ^{1}H CIDNP kinetics obtained in photoreactions of MTPA and CBP for α protons at pH 12.6 (black circles), pH 12.0 (black squares), pH 11.0 (black triangles), and for γ protons at pH 12.6 (open red circles), and pH 11.0 (red triangles). The lines were calculated according to the procedure described in the text. For the values of the parameters, see the text.

That the kinetics of the γ protons stays invariant with pH provides as conclusion that only one sort of species is responsible for the formation of CIDNP for these protons. Based on the previous studies, it is concluded that this species is the cyclic cation radical, which is formed

very fast from the "open form" S-centered cation radical. The kinetics of the γ protons seen here differs significantly from that detected earlier in reversible radical reactions, which is usually characterized by an initial growth and subsequent decay to a stationary value. Since the CIDNP kinetics is not affected by the variation of concentration of MTPA, it can be concluded that the degenerate electron exchange is not operative for the cyclic cation radical. The decay rate of the CIDNP kinetics at pH 11.0 nearly coincides for the α and γ protons indicating that it does not depend on the paramagnetic T_1 that is expected to be different for these protons. This result supports the hypothesis about the low efficiency of CIDNP formation in the bulk for radical pairs containing the cyclic radical. This hypothesis is based on the assumption of fast conformational changes that modulate the magnitude and the sign of hyperfine interaction constants in radical **II** of MTPA. This hypothesis is supported by the ESR spectrum of MTPA that becomes wide and structureless at pH~10.5.[173]

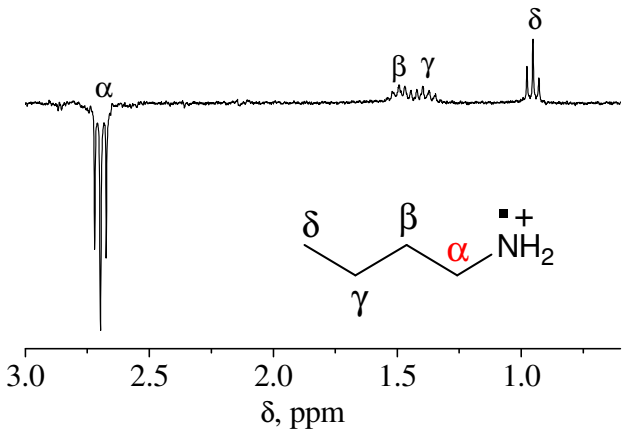

Figure. 6.1.11. ^{1}H NMR spectrum obtained during light irradiation of the solution containing 3 mM of N-butylamine and 0.5 mM of AQS, pH 12.2.

The CIDNP kinetics for the α protons of MTPA gives evidence for CIDNP formation from several sources. The opposite behavior in the CIDNP amplitude change for the α protons obtained in reactions with different dyes suggests that the aminium cation radical is formed in the system under study. While in the photo reaction of CBP with MTPA in Fig. 6.1.9 the α protons are positively polarized, in the reaction of AQS with N-butylamine (Fig. 6.1.11) it is seen that the α protons are negatively polarized. The β, γ and δ protons do not carry any dynamic polarization, but have the same intensity as in the thermally polarized NMR spectrum without irradiation (not shown). This observation is in accordance with the spin density distribution as it is expected for the primary aminium cation radical**.** According to Kaptein's rules, (eq 1.1.2)[23] the

sign of the geminate polarization of a given nucleus for the case of a triplet precursor is determined by the sign of difference of g-factors in RP and the sign of the hyperfine coupling constant. The g-factors of the radical species are: $g(NR_2^{\bullet+})=2.0035$,[187] $g(CBP^{\bullet-})=2.0033$ (*vide supra*), $g(AQS^{\bullet-})=2.0039$;[188] therefore, $\Delta g=(g_1-g_2)$ for the aminium radical has the opposite sign in the pairs with radicals originating from CBP as compared to AQS. Thus, enhanced absorption is formed for the α protons in the pair with $CBP^{\bullet-}$, and emission in the pair with $AQS^{\bullet-}$.

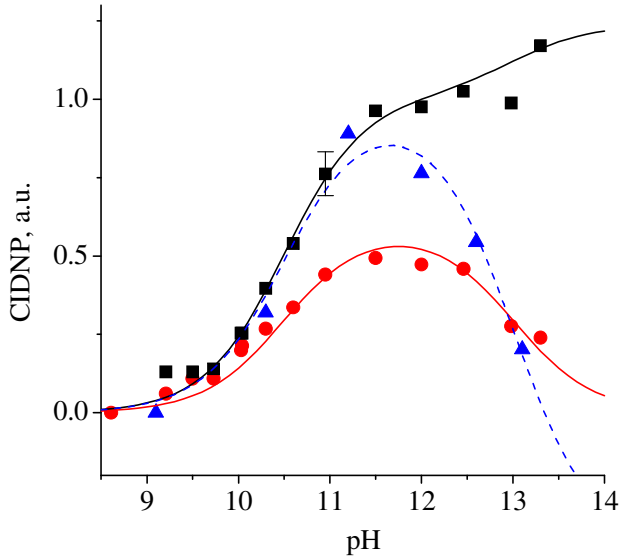

Figure 6.1.12. pH dependence of ^{1}H CIDNP obtained in the photoreaction of MTPA and CBP immediately after the laser pulse for the α protons of MTPA (black squares), and for the γ protons of MTPA (red circles), and in the photoreaction of MTPA and AQS immediately after the laser pulse for the α-protons of MTPA (blue triangles). The lines were simulated according to eq. (6.1.3) with the following parameters: p_1=0, p_2=0, q=10 (fitting to red circles); p_1=0, p_2=1.2, q=10 (fitting to black squares); p_1=0, p_2= −0.45, q=10 (fitting to blue triangles).

The aminium radical cation does not contribute to the CIDNP of the γ protons of MTPA. The fact that the polarization of these protons drops for pH>11.5 (Fig. 6.1.12) provides further evidence that there are two competitive channels of the oxidative quenching reaction, one being the formation of the S-centered cation radical followed by its fast cyclization to the cyclic radical, and the other channel being electron transfer from nitrogen with aminium radical cation formation. The efficiency of the second channel is pH-dependent. The aminium cation radical

does not form the cyclic species, otherwise the geminate polarization of γ protons would not decrease with pH.

The dependence of the geminate CIDNP on the pH obtained for protons of the two compounds, Met and MTPA, was simulated using the following equation:

$$P \sim p_1 \times \frac{10^{-pH}}{10^{-pK_a}+10^{-pH}} + \frac{10^{-pK_a}}{10^{-pK_a}+10^{-pH}} \times \left(\frac{1}{1+10^{pH-14+pK_b}} + p_2 \times \frac{10^{pH-14+pK_b}}{1+10^{pH-14+pK_b}} \right) \qquad (6.1.3)$$

Here, pK_a is the ionization constant of diamagnetic molecule. The first term describes CIDNP originating from the molecule with a charged amino group, while CIDNP from its conjugated base is associated with polarization described by the second term. In the parentheses, the first and the second term reflect the share contribution to CIDNP from cyclic and aminium radicals, respectively. The pK_b determines the relative contributions of the two above mentioned channels of quenching at a given pH and represent ionization constant of some reactive intermediate. The CIDNP enhancement factor for the cyclic radical was taken as a unity, p_1 and p_2 are the enhancement factors for the "open form" S-centered radical and the aminium radical relative to the cyclic radical, respectively.

For the γ protons of MTPA (red circles in Fig. 6.1.11), p_1 and p_2 were taken as zero; the best fit for the pH dependence was obtained at pK_b=1 (the second fitting parameter was the scaling factor). For the α protons of MTPA with CBP, p_1=0 and pK_b=1 were used obtained from simulation of the γ protons, and the best fit was reached at p_2=1.2. With AQS as photosensitizer, p_2= −0.5 was used. In a similar way, the pH dependence of CIDNP for the α proton of Met was simulated (Fig. 6.1.4). The following parameters for Met were found from the simulations p_1=0, p_2=1.9, pK_b=1.

From the CIDNP kinetic measurements it follows that the aminium radical formed as a result of oxidative quenching from nitrogen undergoes fast deprotonation to form the neutral aminyl radical, otherwise degenerate electron exchange between the aminium cation radical and the neutral MTPA would lead to a decaying CIDNP kinetics, in contrast to the observation.

The results of the present CIDNP investigation of the radical reactions of L-methionine (Met) and its model compounds obtained can be summarized in the reaction scheme given in Fig. 6.1.13. The structures of 3-(methylthio)propylamine (MTPA) correspond to R=H on the left hand side of Fig. 6.1.13, while the structures with R=COO^{-} refer to Met.

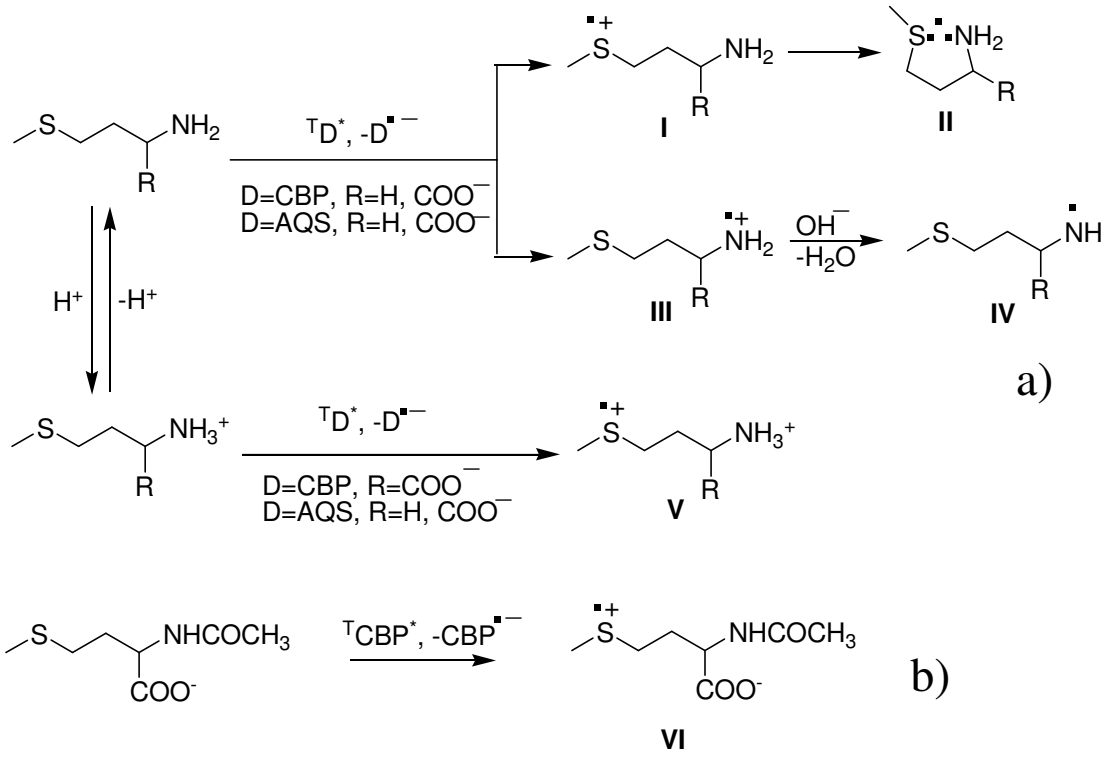

Figure 6.1.13. Reaction scheme of the Met and MTPA (a) with photo excited CBP and AQS and NMet (b) with CBP.

The Met quenches triplet states of CBP at a diffusion controlled rate with a high yield of the cyclic (**II**) and "open form" (**V**) radicals.[164] For Met the condition for degenerate exchange (6.1.1) or (6.1.2) is met at a pH below the pK_a. Another reducing quenching mechanism that operates in basic conditions and therefore is important for the photochemistry of methionine is the electron transfer from the nonbonding electron pair at the nitrogen to the triplet sensitizer leading to the radical **III** (Fig. 6.1.13). This quenching mechanism was first proposed for photooxidation of methionine and related compounds in 1975[189] and was recently found to be responsible for the main channel of the reaction of CBP with aliphatic amino acids.[181] The evidence for this comes from the emergence of the $CBP^{\bullet-}$ radical anion on the nanosecond time-scale after photo-excitation. Although for about 30 years an array of circumstantial investigations were done the formation of an aminium cation radical of sulfur containing amino acids has not received much attention so far.[153,155,190] The primary aminium radical is one of the main species involved in the oxidative damage of proteins. Up to now, due to the lack of a chromophore group in the radical **III** that precludes it from detection by transient optical absorption, this reducing mechanism for methionine was not taken into account in numerous publications on the photochemistry of methionine related compounds.[164,165,167-172,191-193]

To describe the CIDNP kinetics, the set of differential equations described in Chapter 1.1 weas used. Eqs. (1.1.3-5) were modified in order to take into account decarboxylation and degenerate electron exchange and look in the following way:

$$R(t) = \frac{R_0}{1+k_t R_0 t} \tag{6.1.4}$$

$$R_1(t) = \frac{e^{-k_d t} R_0}{1+k_t R_0 t} \tag{6.1.5}$$

$$\frac{dP(R)}{dt} = -k_t P(R)R - k_t \beta R R_1 - \frac{P(R)}{T_1} - k_{ex} C P(R) - k_d P(R) \tag{6.1.6}$$

$$\frac{dP(Pr)}{dt} = k_t P(R)R + k_t \beta R R_1 + k_{ex} C P(R) \tag{6.1.7}$$

Here R_0, $R(t)$, $R_1(t)$, $P(Pr)$, k_t, T_1 and $\beta=\gamma P^G/R_0$ have the same meaning as in Eqs. (1.1.3-5). R_1 is the concentration of cyclic Met radicals, $k_{ex}CP(R)$ describes the transfer of polarization from paramagnetic to diamagnetic species with concentration C in the degenerate electron exchange, k_d is the decarboxylation rate constant.

The kinetics of CIDNP of the protons of MTPA at pH 11 that is formed only in the radical with the cyclic structure was simulated using the following parameters: $R_0k_t=1.0\times10^5$ s^{-1}, $k_d=0$, $k_{ex}=0$, α protons: $T_{1,c}=600$ μs, $\gamma_c=0.2$; γ protons: $T_{1,c}=150$ μs, $\gamma_c=0.6$ (here, subscript "c" refers to the cyclic structure). The kinetics of the α protons at pH > 11 is treated as a superposition of two contributions, one originating from the cyclic structure with the weight χ and the other with the weight (1-χ) originating from the "open form" N-centered radical, being aminium **III** at the geminate stage and subsequently converted into aminyl radical **IV**. The different contributions of the radicals to CIDNP formation at the geminate and homogeneous stage is taken into account by adjusting the parameter γ to a value different from 3. The parameters for the nuclear polarization formed in the cyclic radical ($T_{1,c}$, γ_c) were taken from the fit at pH 11. The value χ at a given pH was calculated as $\frac{1}{1+10^{pH-14+pK_b}}$ with the pK_b value obtained from the best fit of the dependence of geminate CIDNP on pH by eq. (6.1.3). The parameter R_0k_t was increased by 30% up to 1.3×10^5 s^{-1} since at pH 11 only 76% of MTPA molecules are deprotonated at the amino group and contribute to the quenching reaction, making it is less efficient than at pH 12 and 12.6 where almost 100% of MTPA molecules participate in the quenching reaction that would result in an increased radical pair concentration. The following parameters correspond to the best-fit simulation shown in Fig. 6.1.10: $T_{1,N}=25$ μs, pH

12: γ_N =11, χ=0.91; pH 12.6: γ_N=6.4, χ=0.72 (here, subscript "N" denotes the common attribute of the radicals **III** and **IV**). The fact that γ_N>3 indicates that CIDNP formation is more efficient in the aminyl than in the aminium radical. This is reasonable since the g-factor of the aminyl radical is 2.0049 and thus the term $\Delta g B_0$ at B_0=4.7 T closer to the condition of maximum CIDNP in comparison with the aminium radical having g=2.0035.

It was not possible to fit the kinetics at pH 12.0 and 12.6 with a single value of γ_N. That probably indicates that deprotonation of aminium radical **III** is accelerated by OH^-, and that at pH 12.6 radical deprotonation already takes place at times <0.5μs, the lower limit of the time resolution.

The possibility of direct formation of the aminyl radical **IV** via deprotonation of the cyclic form **II** with the rate constant k_{-H} was checked by incorporating the corresponding terms into the set of eqs 6.1.4-6.1.7. A value of k_{-H} equal to or smaller than 5×10^3 s^{-1} had no influence on the simulation of the CIDNP time-dependence. The quality of the fit, however, deteriorated as k_{-H} was increased above 1×10^4 s^{-1}. Thus, it can be concluded that deprotonation of the cyclic radical **II** does not take place on the time scale of CIDNP formation.

For the α proton of methionine, the cyclic radical **II** gives a constant contribution to the CIDNP kinetics because of the high decarboxylation rate constant prohibiting the cancellation of polarization. For consistency, the CIDNP kinetics shown in Fig. 6.1.10 by open symbols was simulated using the following parameter set: $T_{1,N}$=13 μs, $T_{1,c}$=150 μs, $R_0k_t=8\times10^4$ s^{-1}, $k_d=5\times10^6$ s^{-1}, γ_N=3, γ_c=0.6, χ=0.33, k_{ex}=0.

The best fit of the exchange-type kinetics obtained for the γ protons at pH 6.9 with two concentrations of Met was achieved using eqs. 6.1.4-6.1.7 with the following parameters: $T_{1,S}$=8.5 μs, $R_0k_t=1.1\times10^5$ s^{-1}, $k_{ex}=3.4\times10^8$ $M^{-1}s^{-1}$. The value of degenerate electron exchange constant of Met is in the range of that for histidine,[24] tyrosine[194] and tryptophan.[195] The difference of the two curves is determined only by the change of parameter *C,* that is the concentration of the starting compound Met (1.1 mM - red symbols, 2.2 mM - black symbols in Fig. 6.1.7). The description of the exchange-type reaction by eqs. 6.1.6 and 6.1.7 is suitable for both reactions: the charge transfer reaction between the cationic radical dimer and the diamagnetic monomer and the degenerate electron exchange reaction between radical and diamagnetic monomer according to the theoretical results obtained for low viscosity solution.[196]

6.2 Met-Gly, Gly-Met dipeptides

The present study is a continuation of exploring the properties of short-lived intermediates formed during photo-oxidation of small methionine and glycine containing peptides by CIDNP methods. The dipeptides Gly-Met and Met-Gly are combinations of a methionine (Met) residue and glycine (Gly), the simplest amino acid among the 20 amino acids,. The aim of this study is to derive the dependence of the radical properties on the position of Met in the peptide chain and influence of the peptide bond. It is important to check whether CIDNP of the Met residue can be used for determining the accessibilities of residues on the protein surface. The detailed reaction scheme will be established below (Fig. 6.2.10). In Fig. 6.2.10 and below, the indices **a** and **b** refer to an acid and its conjugated base, respectively, for all species.

As it was shown in the previous chapter**,** the protonation state of the amino group (pK_a value is 8.2 for **I** and 7.6 for **II**[197]) plays a key role in the photolytical reactions. The oxidation mechanism for the peptides Met-Gly and Gly-Met proposed in Ref. 170 is electron transfer from their sulfur atom; below the pK_a of amino group for both dipeptides (**Ia** and **IIa**) S-centered radicals (**IIIa** and **VIa**) are formed; above the pK_a the reported[170] oxidized form of Met-Gly (**IIb)** is the cyclic radical with an S-N bond (**VII**), whereas for the oxidized form of Gly-Met (**Ib**) only the "open form" radical (**IIIb)** was observed.[170] No indication for fast decarboxylation of the radicals produced from the methionine-containing peptides, Gly-Met or Met-Gly, was detectable.[170] Since the terminal amino group in the dipeptide Met-Gly belongs to the Met residue, the oxidation mechanism of Met-Gly is expected to closely resemble that known for the free amino acid methionine (Met) and its analogue 3-methyl-thiopropylamine (MTPA).[186]

Transient radicals in the photo-oxidation of Gly-Met

Fig. 6.2.1 shows representative NMR spectra of Gly-Met and CIDNP spectra obtained for the reaction of Gly-Met with CBP in neutral (pH 7.3, **Ia**) and basic solution (pH 12, **Ib**). For the methionine residue, in the whole pH range explored ($6 < pH < 13.5$) nuclear polarization was detected only for the protons in the γ and δ positions, but not for the α position. The CIDNP kinetics obtained for the γ and δ protons coincided with each other for both peptides in all cases except for the individual scaling amplitude; therefore, only the kinetic data for the δ protons are shown in Figs. 6.2.2, 6.2.5, 6.2.7 because they have the highest signal intensity. The polarization of these protons in **I** decays in time, with the decay being accelerated when the concentration of the peptide is increased. Fig. 6.2.2 shows the kinetic data obtained for **Ia** and **Ib**. At a fixed concentration of Gly-Met, the shape of the CIDNP kinetics for these protons was found to be

pH-independent. The polarization pattern and the kinetics are similar to those detected for the S-centered radical of free Met. From the observations it can be concluded that at the methionine residue only the S-centered radical **III** is formed in neutral and in basic solution (**IIIa** and **IIIb**, respectively), and that it participates in degenerate electron exchange with the corresponding parent peptide, **Ia** or **Ib**. The higher the concentration is, the faster is the exchange and the smaller is the polarization detected at long delay τ. If the cyclic radical species were formed at the methionine residue, no degenerate electron exchange would be detected. The close similarity of the two kinetic curves, as found for constant peptide concentration below and above the pK_a of the amino group allows us to conclude that the protonation state of the amino group does not affect the kinetic and magnetic resonance parameters of the "open form" S-centered radicals of Gly-Met (**IIIa** and **IIIb)**.

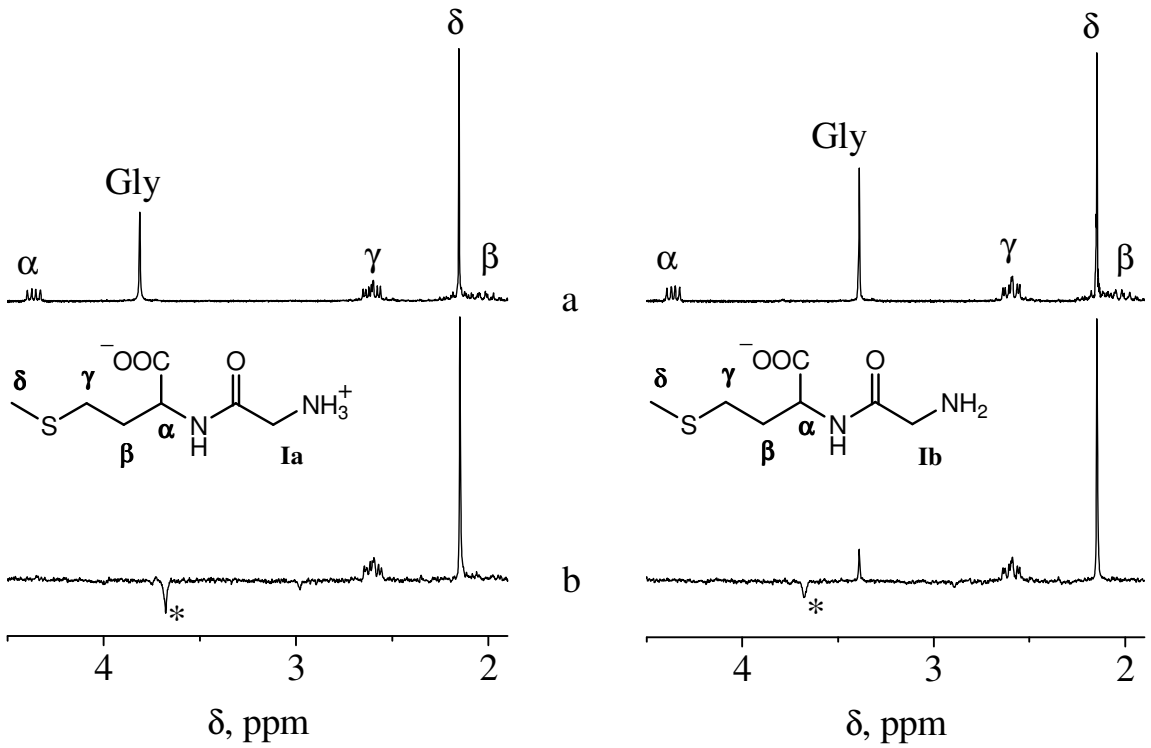

Figure 6.2.1. a) 200 MHz ^{1}H NMR spectrum and chemical structures of Gly-Met at pH 7.3 (left) and 12.0 (right). b) Aliphatic region of 200 MHz ^{1}H CIDNP spectra, obtained in the photoreaction of CBP and Gly-Met at pH 7.3 (left) and 12.0 (right) with a detecting RF-pulse of 4 μs (a and b). Asterisks denote the signals of side products.

Polarization of the α protons of the glycine moiety was detected only at pH values above the pK_a of the amino group. The inset in Fig. 6.2.2 shows the kinetic data obtained for the

α protons of glycyl in **Ib**. The strong increase of polarization with time is qualitatively in agreement with the results obtained for the corresponding protons at the N-terminus of glycylglycine.[198] For the glycine residue oxidation leads to formation of the primary aminium radical **IV**. It takes place only at pH values above the pK_a of the amino group. The net polarization of the glycyl residue at zero delay was lower than the polarization detected for the δ protons by a factor of about 0.07. Because of the low signal-to-noise ratio a quantitative analysis of the kinetic data for this signal was not performed. The growing of glycine polarization with time allows to conclude that the amimium radical **IV** deprotonates very fast with the formation of the aminyl radical **V**; otherwise a fast decay of the CIDNP kinetics would be expected, which is determined by degenerate electron exchange that takes place between the parent molecule and its electron deficient derivative, as it is for the S-centered radicals. This observation is in full accordance with the data obtained for Gly-Gly.[198]

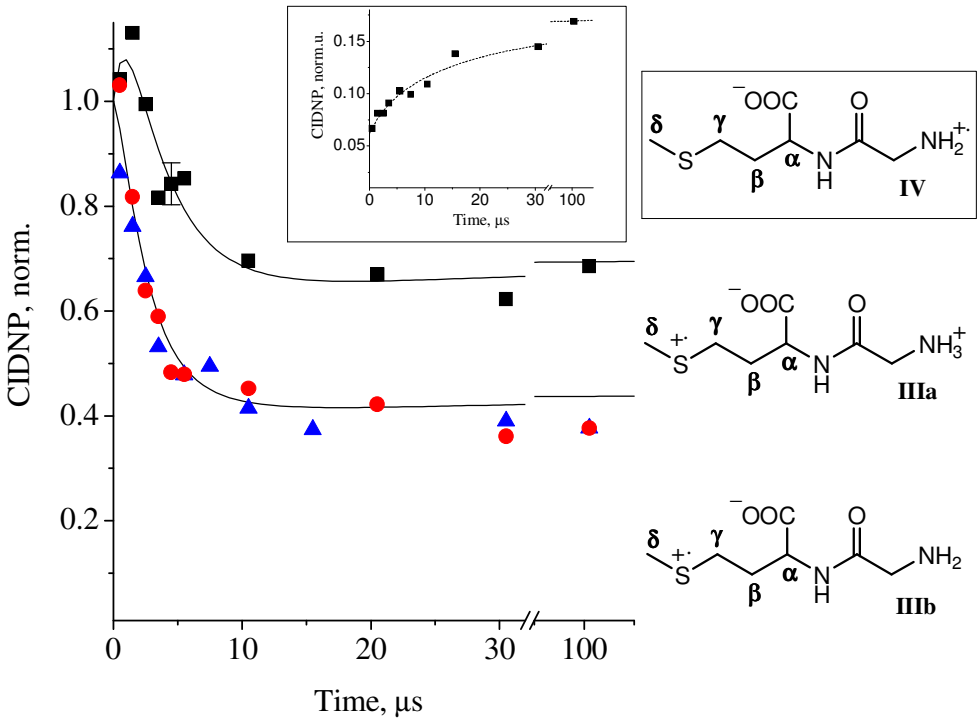

Figure 6.2.2. Photoreaction of CBP and Gly-Met. ^{1}H CIDNP kinetics of the δ protons of the Met residue: black squares - pH 7.3, 1.5 mM Gly-Met; red circles - pH 7.3, 3.0 mM Gly-Met; blue triangles - pH 12.0, 3.0 mM Gly-Met. Solid lines – model simulations for radical **III** with the parameters of simulation listed in Table 6.2.1. Inset: ^{1}H CIDNP kinetics of the α protons of the Gly residue at pH 12.0. Dashed line in the inset is not a simulation, but serves only as guide for the eye.

To describe the CIDNP kinetics the set of equations (6.1.4-6.1.7) was used. The parameters for fitting the two kinetic data sets obtained at two different concentrations of the peptide for the polarization of the δ and γ protons formed in **IIIa** and **IIIb** were R_0k_t, T_1, k_{ex} and the vertical scaling factor. The best fit was obtained at $R_0k_t=3.0\times10^5$ s^{-1}, $T_1=10$ μs, $k_{ex}=2.0\times10^8$ $M^{-1}s^{-1}$. The numerical values of the parameters are very close to those found for the S-centered radical of the free amino acid methionine.

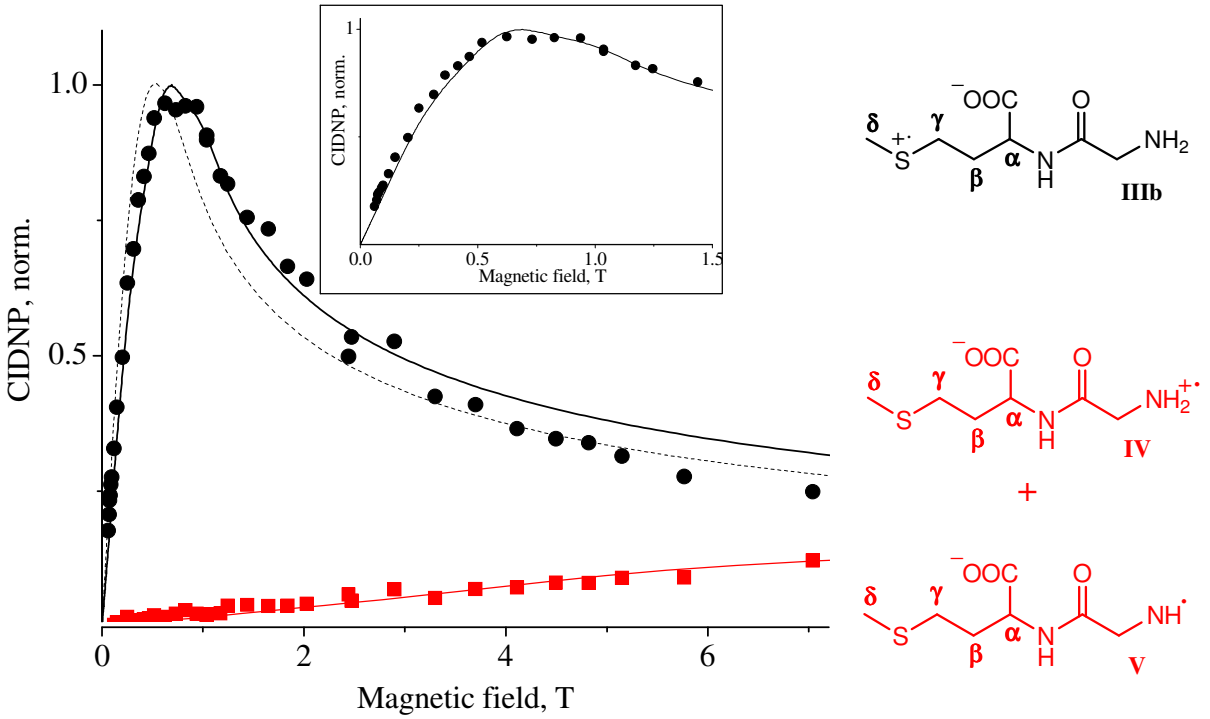

Figure 6.2.3. ^{1}H CIDNP field dependences, obtained in the photoreaction of CBP and Gly-Met at pH 12.0. Black circles - δ protons of the methionine residue; red squares - α protons of the glycine residue. The solid line fitted to circles shows CIDNP simulation for the "open form" sulfur radical (**III**) of the methionine residue. The solid line fitted to squares shows the linear combination of contributions to CIDNP from two radical pairs with the relative contribution of 20% and 80% for the pair containing the aminium radical (**IV**) and the aminyl radical (**V**), respectively. The parameters of simulations are listed in Table 6.2.1. Dashed lines: simulation for the $\left[H_3C(R)S\therefore S(R)CH_3\right]^+$ structure; see text for details.

The field dependence of CIDNP of Gly-Met is shown in Fig. 6.2.3 with the relative intensities of experimental points in this figure corresponding to those in the CIDNP spectra. The same holds true for Figs 6.2.5 and 6.2.8. The CIDNP data obtained for the protons in the γ and δ positions of the methionine residue show a well pronounced maximum at around 0.7 T. The

magnetic field at the CIDNP maximum coincides with that for the "open form" sulfurs-centered radical derived from the free amino acid (Fig. 6.1.4) and N-acetylmethionine (Fig. 6.1.5).

Here the numerical simulation of the CIDNP field dependence was restricted to the high field part of the field dependence using the simulation approach described in Chapter 1.1. With the g-factor and the HFI constants of the anion radical of benzophenone listed in the Table 6.2.1 two calculations of the CIDNP magnetic field dependence were performed, in order to find out whether the S-centered radicals form dimers with the diamagnetic molecule or stay in monomeric form. In the first calculation (showed by the dashed lines in Fig. 6.2.3), a HFI of 0.565 mT was considered for each of the 4 protons in γ position and 0.71 mT for each of the 6 protons in δ position as found for the dimeric structure of the free amino acid and the corresponding radical with a three-electron S-S bond as observed by ESR.[173] In the second calculation, the HFC for the monomeric Met cation radical was taken into account with twice as large HFC values. The maximum of CIDNP calculated for the monomeric radical coincides well with the experimental data shown in Figure 6.2.3, whereas the maximum of CIDNP calculated for the S-S dimeric structure is located at the much lower magnetic field of 0.52 T. Therefore a major contribution of dimers to CIDNP is ruled out. The same was found out for the free amino acid methionine (Chapter 6.1).

For the glycyl residue the polarization grows with increasing magnetic field; here, the CIDNP maximum is not reached in the field range available. The field dependence was simulated as the sum of the CIDNP from aminium and aminyl radicals with 20% and 80% contributions, respectively. These numbers were estimated as contributions from geminate and F-pair CIDNP to the resulting stationary value with the parameters for the glycine residue determined from calculation of the CIDNP kinetics of Gly-Gly.[198] However, since the field dependence is rather featureless and has low intensity in the available magnetic field range, the simulation has mainly an illustrative character.

Thus the collection of the results described above gives strong evidence for the photo-oxidation pathways of Gly-Met as shown in Fig. 6.2.10 including the formation of three different radicals (**IIIb, IV** and **V**) in basic solution and of the S-centered radical **IIIa** in neutral solution. The behavior of the Gly-Met and radical intermediate structures are similar to that observed for N-acetylmethionine in Chapter 6.1.

Transient radicals in the photo-oxidation of Met-Gly

The change of residue order in the dipeptide has strong influence on the CIDNP pattern. The NMR spectra of Met-Gly (**II**) together with the corresponding CIDNP spectra are shown in

Fig. 6.2.4. As a first difference to Gly-Met no polarization was detected for the glycine residue at any pH. This is in agreement with the absence of polarization for the residue at the C-terminus of Gly-Gly.[198]

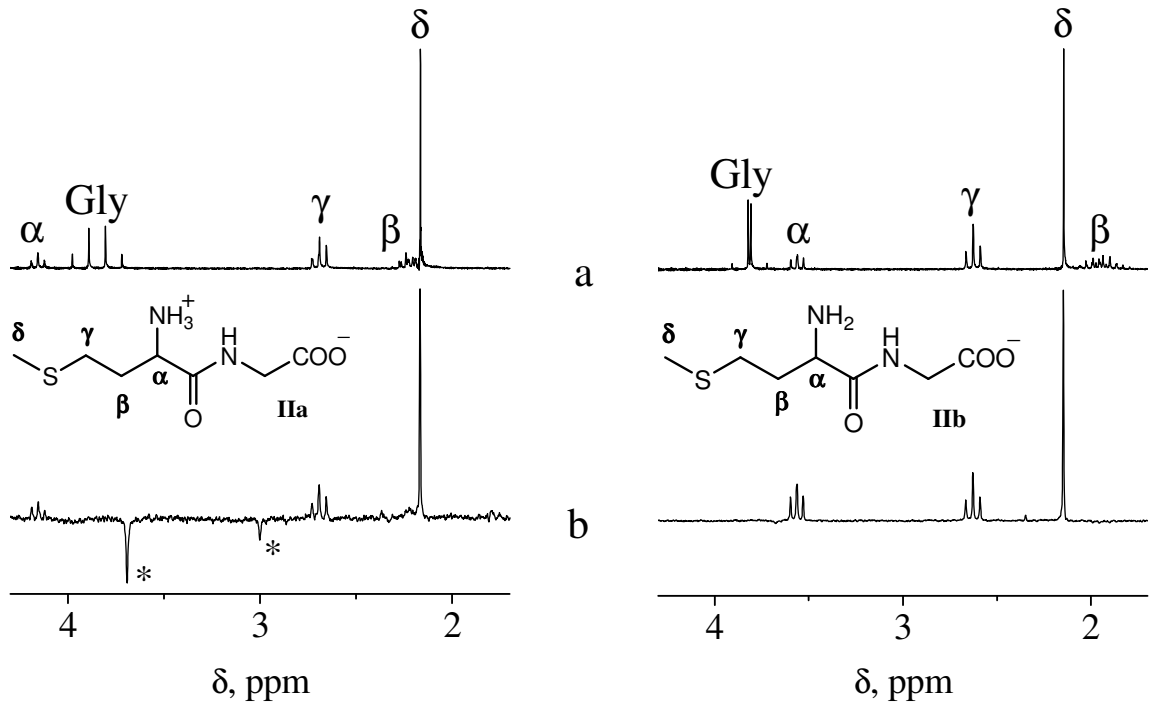

Figure 6.2.4. a) 200 MHz ^{1}H NMR spectrum and chemical structures of Met-Gly at pH 6.2 (left) and 12.0 (right). b) Aliphatic region of 200 MHz ^{1}H CIDNP spectra, obtained in the photoreaction of CBP and Met-Gly at pH 6.2 (left) and 12.0 (right) with a detecting RF-pulse of 4 μs.

The CIDNP kinetic data for the methionine residue depend significantly on the protonation state of the terminal amino group as in case of free amino acid. The kinetic data of the δ and γ protons at fixed concentration do not depend on the pH at values higher than the pK_a of the amino group (only the kinetic data of the δ protons at the lowest and the highest pH values of 9.1 and 12.6 are shown in Fig. 6.2.5). In contrast, the kinetics of the α proton varies with pH. At pH 9.1 the kinetics obtained for the α proton of the methionine residue is the same as that found for the γ and δ protons. They closely resemble the behavior characteristic for cyclic radicals with a two-center three-electron bond between the nitrogen and sulfur atoms as it was described for MTPA in the Chapter 6.1. The decay of polarization with time indicating a low efficiency of polarization formation is the characteristic feature of such a cyclic radical.

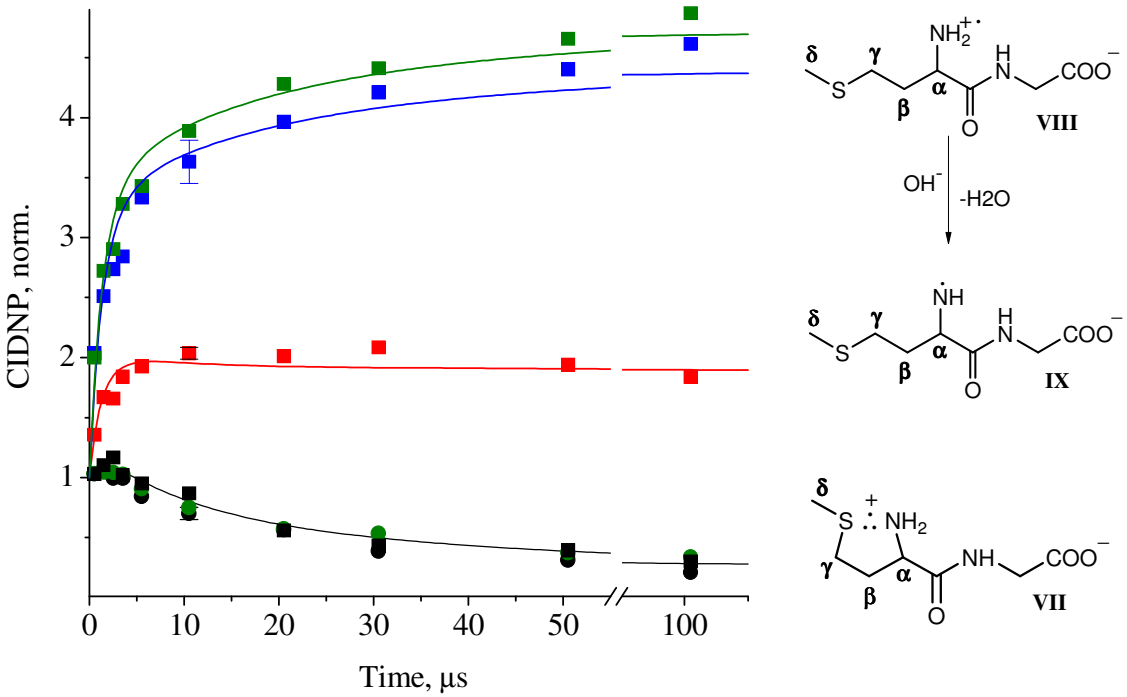

Figure 6.2.5. ^{1}H CIDNP kinetics of the δ protons of Met-Gly (**II**), obtained in the photoreaction of CBP and 3 mM Met-Gly: δ protons – black circles (pH 9.1), green circles (pH 12.6); α proton - black squares (pH 9.1), red squares (pH 11.3), blue squares (pH 12.0), green squares (pH 12.6). Solid lines – model simulations (see text) with the parameters of simulation listed in Table 6.2.1.

The CIDNP kinetics obtained at pH 11.3, 12.0 and 12.6 is shown in Fig. 6.2.5 by red, blue and green color, respectively. With increasing pH the CIDNP kinetics for the α proton turns from a decaying to a growing curve. The signal growth of the α proton is similar to that observed for the polarization of the α protons of the glycine residue of Gly-Met (Fig. 6.2.8), Gly-Gly[198] and MTPA (Fig. 6.1.10). Thus, differences between the CIDNP kinetics of the α proton and that of the γ, δ protons can be explained by adding contributions from two radical species, namely aminium (**VIII**) and aminyl (**IX**) radicals (Fig. 6.2.5)**,** to the polarization of the α proton of the methionine residue.

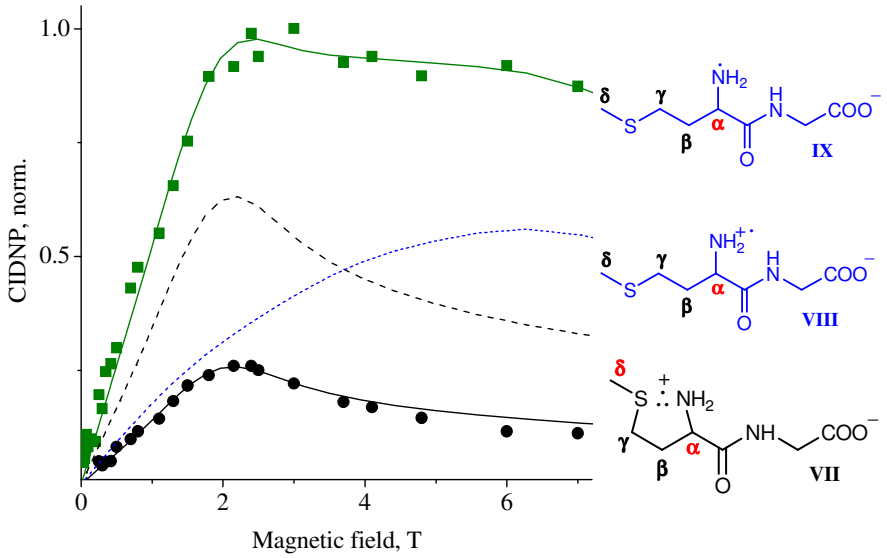

Figure 6.2.6. ^{1}H CIDNP field dependences of the methionine residue in the photoreaction of CBP and Met-Gly (**IIb**) at pH 12.5. Black circles - δ protons; green squares - α proton of the methionine residue. CIDNP calculated for radicals pairs consisting of the anion radical of $CBP^{\bullet-}$ and the cyclic radical (**VII**) (black solid line: fitting to circles; black dashed line: same, only scaled a factor of 2.5); blue short dashed line: total CIDNP resulting from pairs of $CBP^{\bullet-}$ with aminium (**VIII**) and with aminyl (**IX**) radicals (with contributions 20% and 80%, respectively); green solid line: fitting to squares by the sum of dashed and short dashed lines with optimized amplitudes.

The comparison of the CIDNP field dependences detected for the α proton and the γ, δ protons of the methionine residue in the dipeptide Met-Gly (**IIb**) at pH 12.0 is shown in Fig. 6.2.6. For the δ protons the field dependence of CIDNP has its maximum at 2.4 T and is in good agreement with the simulation for a pair with the cyclic radical (**VII**) having the same parameters as obtained for the corresponding cyclic radical of the free amino acid in Chapter 6.1. The field dependence of the α proton has a complex structure which is not in accordance with the simulation for the cyclic radical. The well pronounced shoulder at the high field part of the field dependence is attributed to the contribution from two radical pairs containing nitrogen centered radicals. The field dependence of CIDNP for the α proton of the methionine residue was simulated as the sum of polarization from the cyclic (**VII**) and the nitrogen centered radicals (**VIII** and **IX**). The latter contribution was taken with a fixed ratio (4:1) of the two radical pairs, with aminium (**VIII**) and aminyl (**IX**) radicals, as it was done for Gly-Met (*vide supra*). The best

fit shown in Fig. 6.2.6 was obtained at 80% contribution of the cyclic radical (**VII**) and 20% from the two N-centered radicals.

The CIDNP kinetics observed for the δ protons of Met-Gly (**IIa**) at pH 6.2 is shown in Fig. 6.2.7 for a peptide concentration of 1.5 mM and 3 mM. The CIDNP kinetic data obtained for the δ protons at pH values lower than the pK_a of the amino group do not reflect the kinetics that are typical for degenerate electron exchange, as it was detected for Gly-Met and shown in Fig. 6.2.3. Instead, a fast decay is followed by a relatively slow decay. The latter is typical for CIDNP originating from a cyclic radical, and thus it was assumed that the sulfur-centered cation-radical **VIa** undergoes deprotonation to **VIb** on the microsecond time scale, the latter species being transformed into the cyclic radical **VII** (Fig. 6.2.7).

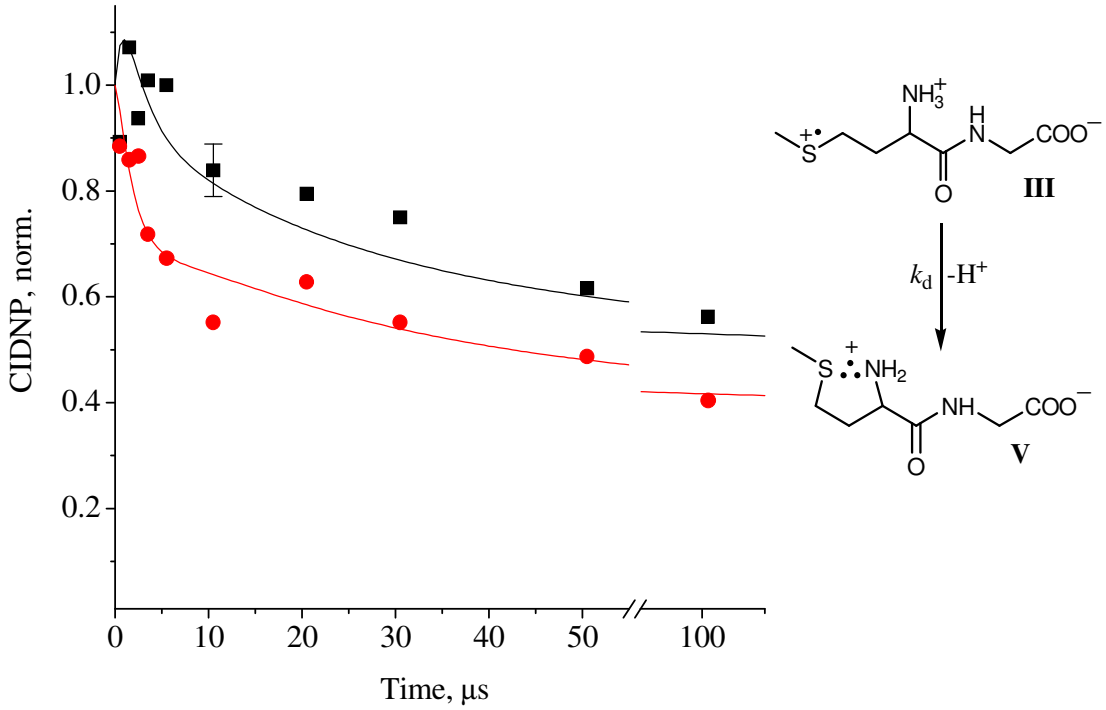

Figure 6.2.7. ^{1}H CIDNP kinetics of the δ protons of Met-Gly at variable concentration, obtained in the photoreaction of CBP and Met-Gly at pH 6.2. Squares - 1.5 mM Met-Gly; circles - 3.0 mM Met-Gly. Solid lines – model simulations (see text) with the parameters of simulation listed in Table 6.2.1. Top: reaction of deprotonation of **VIa** to the cyclic radical (**VII**).

The CIDNP kinetics of the δ and γ protons was simulated using the approach described in above applying equations (6.2.4-6.2.7) in the whole pH range. At a pH higher than the pK_a of the amino group, the CIDNP kinetics for the α protons was treated as a superposition of two contributions, one originating from the reactions of cyclic radicals (with the share χ), and

another one (with the share 1-χ) from the reactions of nitrogen centered radicals being aminium at the geminate stage and aminyl at the homogeneous stage of the process. The difference in magnetic resonance parameters between the radicals participating in the geminate and homogeneous stages (aminium **VIII** and aminyl **IX**, respectively) was taken into account by using for the parameter γ a value different from 3, the value that is characteristic when no transformation of the radical and therefore no change of magnetic resonance parameters takes place. In the same way it has been already earlier described the CIDNP kinetics in photoreactions of Met in Chapter 6.1 Using Adrian's model, the efficiency of CIDNP formation for the α proton formed in the following two triplet radical pairs was calculated: (i) the pair consisting of the anion radical of $CBP^{\bullet-}$ and the aminium radical; and (ii) the pair consisting of the anion radical of $CBP^{\bullet-}$ and the aminyl radical. The level of polarization formed in the second radical pair was found to be 3.9 times higher than that formed in the first pair, resulting in γ=11.

When modeling the CIDNP kinetics originating from the reactions of the cyclic radical (kinetic data for the α proton at pH 9.1, and for the δ protons at any pH above pK_a of the amino group), a decent fit is possible with parameter sets varying over a wide range – from $R_0k_t=5\times10^4$ s^{-1}, T_1=1000 μs, γ=0 to $R_0k_t=5\times10^5$ s^{-1}, T_1=100 μs, γ=2.7. No unique solution can be found; however, the range of the parameters can be narrowed by fitting the polarization of the α proton. A simultaneous fit for all data sets for the α proton in the range of pH>pK_a was performed. The general fitting procedure applied to fit the kinetics of the α proton at pH 11.3, 12.0, and 12.6 was the following: from the whole mentioned range a representative number of parameter sets that fit the kinetics of the cyclic structure were selected. Then each of the calculated kinetics with a share χ_i was added to the kinetics calculated for the nitrogen centered radicals (**VIII** and **IX**) keeping the parameter R_0k_t fixed. The fitting parameters were χ (at each pH), T_1 of the aminyl radical, the ratio of polarization per radical pair created in the pairs of aminium and cyclic radicals, and the vertical scaling factor. This procedure was iterated until a satisfactory fit for all experimental data was found. The final parameter set is: $R_0k_t=3.0\times10^5$ s^{-1}, T_1(**IX**)=7 μs, T_1(**VII**)=300 μs, γ(**VII**) =1.6, the ratio of polarization formed per pair of the aminium and the cyclic radicals =1.5, γ(**IX**)=11 (calculated), χ=0.83 (pH 11.3), χ=0.50 (pH 12.0), χ=0.45 (pH 12.6).

For simulating the data obtained at pH values below the pK_a of the amino group the general approach was modified to take into account the radical transformation. It was assumed that deprotonation of **VIa** immediately leads to the formation of the cyclic radical (Fig. 6.2.7). The concentrations R_1 of the "open form" **VIa** and R_2 of the cyclic radicals **VII** are as follows:

$$R_1(t) = \frac{R_0 e^{-k_d t}}{1 + k_t R_0 t} \tag{6.2.1}$$

$$R_2(t) = \frac{R_0(1 - e^{-k_d t})}{1 + k_t R_0 t} \tag{6.2.2}$$

$$\frac{dP(R_1)}{dt} = -k_t P(R_1)R - k_t \beta_1 R R_1 - \frac{P(R_1)}{T_1^{R_1}} - k_{ex} C P(R_1) - k_d P(R_1) \tag{6.2.3}$$

$$\frac{dP(R_2)}{dt} = -k_t P(R_2)R - k_t \beta_2 R R_2 - \frac{P(R_2)}{T_1^{R_2}} + k_d P(R_1) \tag{6.2.4}$$

$$\frac{dP(Pr)}{dt} = k_t(P(R_1) + P(R_2))R + k_t \beta_1 R R_1 + k_t \beta_2 R R_2 + k_{ex} C P(R_1) \tag{6.2.5}$$

where k_d is the rate constant of the deprotonation reaction (Fig. 6.2.7). The main difference of the present case with respect to equations (6.2.1-6.2.3) is that the polarizations in the cyclic $P(R_1)$ and in the "open form" $P(R_2)$ radicals are coupled via the term $k_d P(R_1)$ describing the polarization transfer in the deprotonation reaction. The polarization of the product, $P(Pr)$, was considered to be the sum of the polarizations formed in the cyclic and the "open form" radicals. Accordingly three differential equations (6.2.3-6.2.5) instead of two (6.1.6-6.1.7) were solved simultaneously.

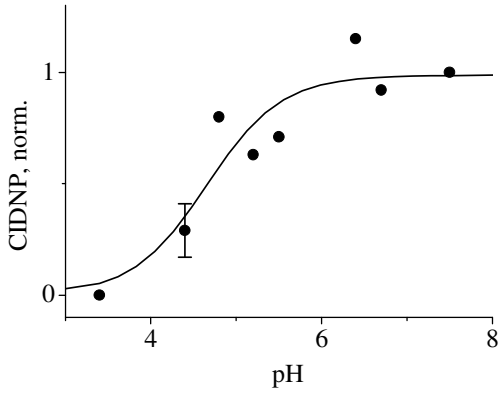

Figure 6.2.8. pH dependence of CIDNP intensity for the α proton of the Met residue of Met-Gly, obtained in the photoreaction of Met-Gly with 3,3′,4,4′-benzophenone-tetracarboxylic acid.

In order to minimize the number of fitting parameters, several values found previously for Gly-Met were used, namely T_1(**VI**)=10 μs, k_{ex}=2.0×10^8 M^{-1}s^{-1}, assuming that these parameters do not vary significantly for the "open form" radical of Met-Gly; T_1(**VII**)=300 μs, γ(**VII**)=1.6 were taken as found for the cyclic structure at a pH above the pK_a of the amino group. The only fitting parameter besides the scaling factor was the deprotonation rate constant

k_d. The best fit was obtained at $k_d=1.8\times10^5$ s^{-1}; no adjustment of the parameters mentioned above was necessary.

Using the obtained deprotonation rate constant and a typical value of the protonation rate constant $k_p=10^{10}$ $M^{-1}s^{-1}$, one can estimate the corresponding pK_a value: $K_a=k_d/k_p=1.8\times10^{-5}$ M, i.e. pK_a=4.7.

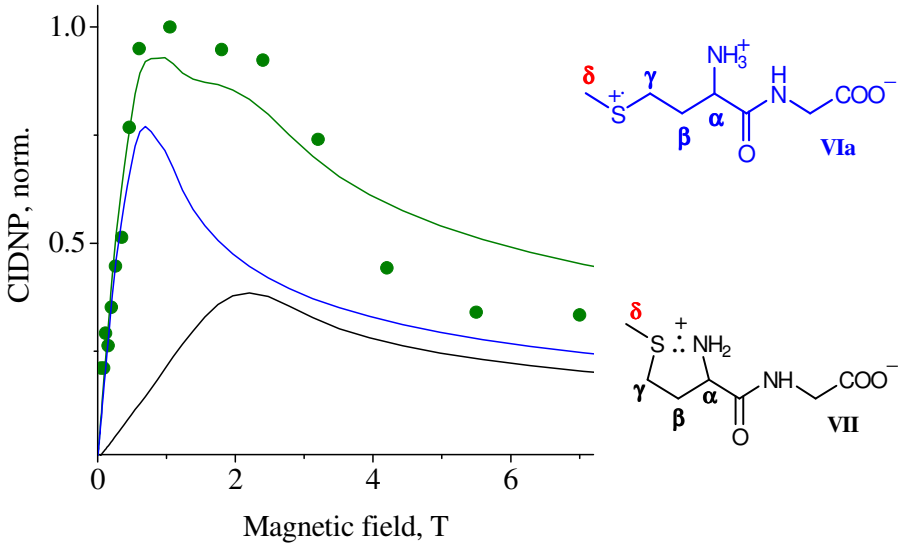

Figure 6.2.9. ^{1}H CIDNP field dependences of the δ protons of the methionine residue in the photoreaction of CBP and Met-Gly at pH 6.2. Green line is sum of polarizations originating from two radicals: the "open form" S-centered radical (blue line) and the cyclic radical (black line). Simulation parameters of the methionine radicals are listed in the Table 6.2.1.

The presence of the reaction (Fig. 6.2.7) is also confirmed by observation of polarization at the α position for pH values much lower (pH 6.2, Fig. 6.2.6) than the pK_a of the amino group (pK_a=7.6). Since the solubility of CBP under acidic conditions is too low to provide the optical density necessary for quantitative analysis, the photosensitizer analog of CBP with four carboxylic groups 3,3′,4,4′-benzophenone-tetracarboxylic acid was used to detect the CIDNP for the α proton of the methionyl residue of Met-Gly in the range 3.5 < pH < 7.5 where it has higher solubility. The corresponding data obtained at zero delay after the laser pulse are shown in Fig. 6.2.8. Fitting of the experimental data for the pH dependence of CIDNP curve resulted in pK_a=4.7±0.3. The coincidence of this value with the value calculated from the kinetic data is taken as further evidence for the reliability of time-resolved CIDNP to provide kinetic information about transformation processes of elusive radical species.

The involvement of both, the cyclic radical and the "open form" S-centered radicals of Met-Gly in the reaction at pH 6.2 was confirmed by the dependence of the polarization on the

external magnetic field. The field dependence for CIDNP of the δ protons (Fig. 6.2.9) is characterized by the broader width (at half maximum) and the somewhat more protracted maximum than it is expected for each individual radical of the residue as shown in Fig. 6.2.9 by the blue and black lines. The data for CIDNP of the δ protons were fitted as a superposition of the field dependences of the polarizations formed in the cyclic and the "open form" sulfur radicals with 50% contribution of each species. The parameters were taken from the corresponding radicals of the free amino acid and are listed in the Table 6.2.1.

The results of the present CIDNP investigation of the radical reactions of Met-Gly and Gly-Met can be summarized in the reaction scheme given in Fig. 6.2.10.

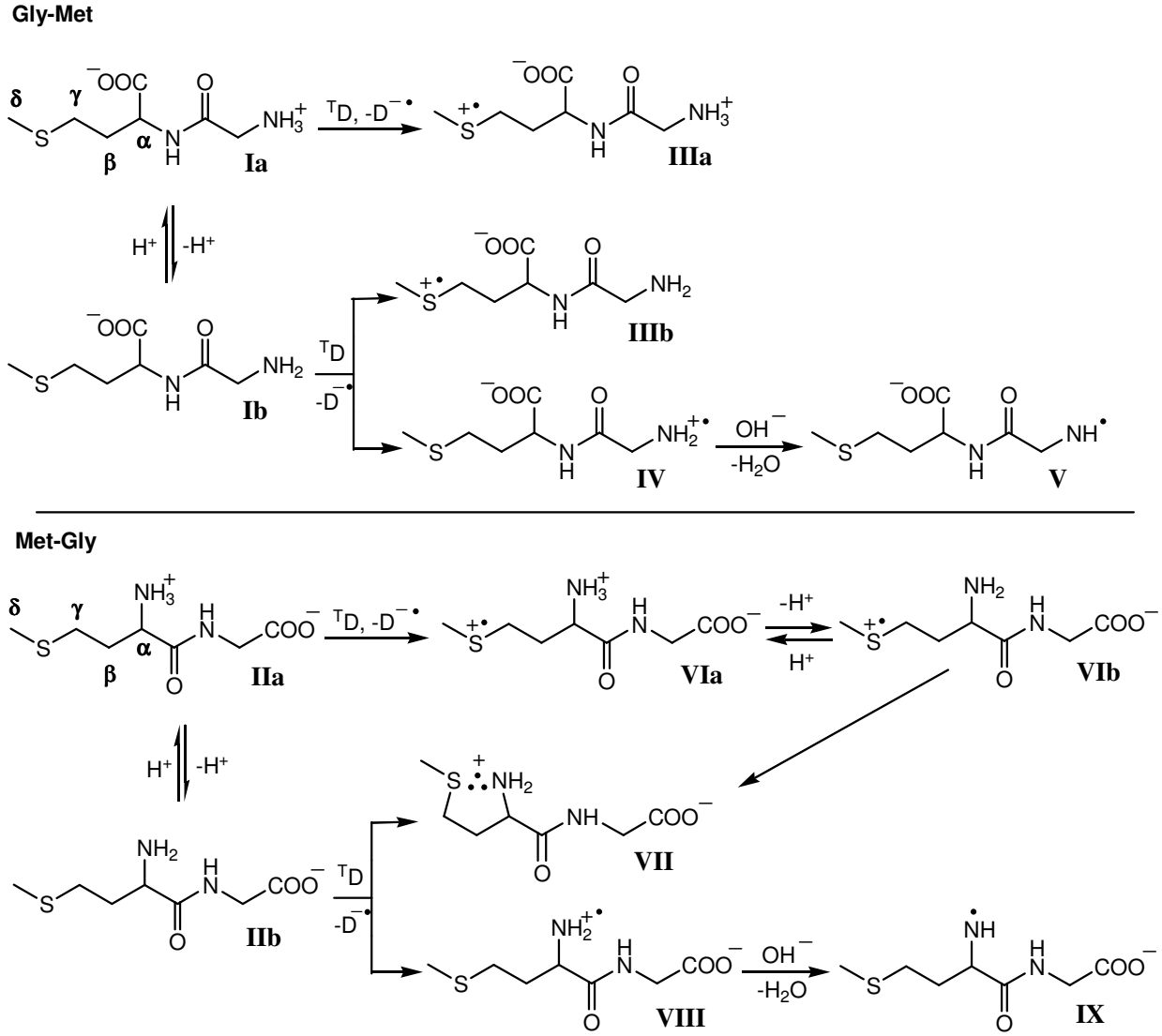

Figure 6.2.10. Reaction scheme of the Gly-Met and Met-Gly with photo excited CBP.

Table 6.2.1. Parameters of the radicals used in the simulation of CIDNP kinetics and CIDNP field dependences.

Radical	T_1, μs	k_{ex}, $M^{-1}s^{-1}$	γ	g-factor	HFI constants, mT
III	10	2.0×10^8	2.8	2.01012[173]	1.42 (3H, δ), 1.13 (2H, γ)[173]
IV	n/a[a]	n/a[a]	n/a[a]	2.0036[199]	1.87 (N), 0.344 (2D), 3.75 (2H)[199]
V	n/a[b]	n/a[b]	n/a[b]	2.0044[200]	1.36 (N), 0.35 (D), 4.35 (2H)[200]
VI	10	2.0×10^8	2.8	2.01012[173]	1.42 (3H, δ), 1.13 (2H, γ)[173]
VII	300	0	1.6	2.0064	0.7 (3H, δ), 0.8 (2H, γ), 1.0 (1H, α), 2.0(N)
VIII	n/a[a]	n/a[a]	n/a[a]	2.0036[199]	1.87 (N), 0.344 (2D), 3.75 (H)[199]
IX	7	0	11	2.0044[200]	1.36 (N), 0.35 (D), 4.35 (H)[200]
CBP$^{-\bullet}$	n/a[b]	n/a[b]	n/a[b]	2.0033[183]	0.29 (4H), 0.11 (4H), 0.35 (1H)[183]

[a] The radical lifetime is much shorter than the time resolution of the CIDNP experiment.

[b] Kinetics is not simulated because of insufficient S/N ratio.

The parameter $R_0k_t=3.0\times10^5$ $M^{-1}s^{-1}$ used in all cases.

Summary and conclusions

The Chapters 6.1 and 6.2 describe the results of a comprehensive time-resolved and field dependent CIDNP study of the reactions of methionine, 3-(methyl)thiopropylamine, N-acetylmethionine, Met-Gly and Gly-Met with 4-carboxybenzopheone, 3-carboxybenzopheone, 3,3′,4,4′-benzophenone-tetracarboxylic acid and 9,10-anthraquinone-2-sulfonate in aqueous solution at different pH (6.7-13.3). Time-resolved and field dependent CIDNP techniques were applied to study radical intermediates.

The obtained results give clear evidence that two oxidative quenching mechanisms formally attributed to electron abstraction from sulfur and nitrogen atoms are operative in reactions with excited triplet states of suitable acceptor molecules. Thus, the structure of the methionine radical cations derived from the free amino acid or the dipeptides depends on the pH. After electron transfer from the sulfur atom to the triplet excited dye molecule two structures of the radical cation having different distributions of spin density are formed. At pH values above the pK_a of the amino group, the Met radical cation exists in a cyclic form with a two-center, three-electron bond between the nitrogen and sulfur atoms, whilst in solutions below pK_a the Met radical cation has a “open form” structure. The same behavior is observed for 3-

(methylthio)propylamine. The results obtained for N-acetylmethionine indicate formation of only the S-centered "open form" radical in neutral and basic solutions. The comparison of the TR-CIDNP results with literature data obtained by steady state CIDNP measurements casts doubt on the hypothesis that interconversion between three types of methionine cation radicals occurs. Instead a competitive channel for oxidative quenching of the triplet sensitizer by direct electron transfer from the nitrogen atom leading to formation of the aminium radical cation was revealed that is operative in strongly basic solution. The study of the CIDNP kinetics formed in the photoreaction of 3-(methylthio)propylamine and methionine at strongly basic condition shows a much higher efficiency of polarization formation in the aminyl radical than in the two other species, the aminium and cyclic radicals.

In case of the dipeptides the reactions are more complex. Gly-Met form S-centered radicals at all pH whereas the Met-Gly only at a pH below 4.5. At a pH above 4.7 a cyclic radical with a two center, three-electron bond between the N and S atoms is formed for the case of Met-Gly, but not for Gly-Met. In neutral solution at a pH above 4.5 but below the pK_a of the amino group Met-Gly forms first S-centered radicals which undergoe deprotonation on the microsecond scale with formation of the cyclic radical. In basic solution (pH>11) the existence of a channel of oxidative quenching via electron transfer from the lone electron pair of nitrogen of the amino group was revealed for both Met and Gly allowing to suggest that it is a common feature of all amino acids and proteins. The CIDNP kinetics of Met-Gly and Gly-Met showed that in basic solution the aminium radical deprotonates on the sub-microsecond time scale forming the aminyl radical.

The time-resolved CIDNP measurements also allow demonstrating the crucial influence of the degenerate electron exchange between cationic radicals (or dimers) and diamagnetic molecules on the intensity of the CIDNP signals in the pH range below the pK_a of the amino group of methionine. The rate constant for the electron exchange was obtained. The kinetics of the polarization in the 3-(methylthio)propylamine chosen as a model compound to study magnetic resonance properties in cyclic five-membered ring radicals allows to determine the paramagnetic nuclear relaxation time T_1 for α and γ protons and to show that protons in the vicinity of the nitrogen have a much faster relaxation than the other protons. Kinetic parameters were also obtained for both dipeptides in neutral and basic solutions.

The high sensitivity of the CIDNP field dependence with respect to changes in Δg results in high accuracy of the parameters obtained and makes the analysis of CIDNP very suitable for characterizing short lived paramagnetic reaction intermediates. Polarization transfer among coupled protons in low field complicates the analysis of the field dependences, however,

comparison of the experimental results with model calculations of the CIDNP field dependences allowed to obtain the g-factor of the cyclic radical and check the g-factor of the "open form" radical of the methionine, N-acetylmethionine and dipeptides cation radicals. In addition it showed that generation of CIDNP of S-centered radicals occurs in their monomer form.

The polarization of the Gly residue is formed only when it is located at the N-terminus of the protein. The position of the Met residue, whether it at the N-terminus, the C-terminus or in the middle of the protein, can be derived from the polarization pattern: the α proton is polarized only at the N-terminus and not polarized in the other cases.

The results presented here demonstrate that the time-resolved CIDNP technique is very suitable for characterizing short-lived paramagnetic reaction intermediates, whereas it has to be emphasized that only the polarization observed within the first microsecond after the photo-excitation arises solely from recombination of geminate radical pairs. Thus, any attempts to get quantitative information about the geminate evolution of radicals from CIDNP spectra detected at continuous irradiation of the sample are fault-prone. Important consequences for CIDNP of protein residues are in particular that not only geminate factors, such as surface accessibility determine the CIDNP amplitude, but also effects of neighboring groups, of N vs C terminal have to be taken into account. As it was demonstrated not only aromatic amino acid residues give CIDNP, but at the N terminus other residues, such as Gly, also become polarized. Moreover, the protonation state of the diamagnetic and paramagnetic species plays a major role. The direct application of CIDNP method to complex peptides may lead to erroneous conclusions, therefore, systematic studies on peptides of increasing complexity are necessary first.

7. Conclusions and outlook

Nuclear magnetic resonance (NMR) experiments on hyperpolarized multi-spin molecules in low viscosity solutions were performed at variable magnetic field in the range between 0.1 mT and 7 T. For the first time such experiments were done using high spectral resolution and fast field variation with a well controlled time profile. For this a novel experimental setup was used utilizing transfer of a probehead loaded with the sample between two field positions. Considerable modifications of the NMR spectrometer were necessary to obtain the field stability at the detection position (7 T) that is desired for the high resolution. In particular a probehead was constructed using material with compensated magnetic susceptibility and a reduced fraction of metal as a prerequisite for achieving high resolution (0.3 Hz line width) at fast field switching (<0.3 s).

Spectral resolution of about 10^{-9} is an indispensable requirement of liquid state nuclear magnetic resonance spectroscopy. It allows investigation of the physicochemical properties of molecules with atomic resolution and a wealth of information unrivaled by other methods. High spectral resolution is essential particular for the detection of multiplet effects of hyperpolarization as they are generated in the course of parahydrogen induced polarization (PHIP). In this case the net polarization is zero and, thus, without high resolution no polarization can be detected (see Chapter 4). To describe the field dependent spectral pattern it was only necessary to consider the scalar coupling among spins and their Zeeman interaction together with the effects of field switching. In this respect it is compulsory to take into account the exact time profile of the field variation for precise simulation of the results. With this approach the polarization of ring protons of ethylbenzene during parahydrogenation was detected for the first time showing the existence of polarization transfer among protons in the molecule in fields below 0.3 T.

Such a polarization transfer was shown to occur from originally polarized nuclei to other ones in the field range when scalar coupling among spins is comparable to their difference in Larmor frequency. In such a case the energy states describing the nuclear spin system have a collective character in contrast to the high field limit when the states can be written as a product of individual spin functions. The re-distribution of polarization results from mixing the states and interconversion between spin coherence and polarization by rapid field variation. Coherences are generally expected to appear in the nuclear spin density matrix after sudden changes of the Hamiltonian and to disappear after a dephasing time T_2. For example, no coherences were observed after parahydrogenation because of the long reaction period. However, the presence of

the coherences could be confirmed in experiments with exact timing control of both hyperpolarization generation and field variation. For this purpose chemically induced dynamic nuclear polarization (CIDNP) is particularly suitable because initiation by a laser flash provides the desired time resolution. The generation of hyperpolarization occurs in course of a fast radical photo-reaction. Oscillations in the polarization are detected when the delay between laser irradiation and the field switch is stepwise increased. The period of the oscillations is equal to the inverse spin-spin coupling, J^{-1}. Accordingly, the rate of polarization transfer is ~ J^{-1} in the beginning of the oscillation, and thus much faster than any stochastic process such as cross-relaxation that usually is seen responsible.

The effect of strong coupling manifests itself also in spin relaxation when it is measured at variable field. The longitudinal relaxation times detected for individual nuclei in strongly coupled spin systems tend to be equal as long as the spin state relaxes as a whole, giving rise to stepwise features in their relaxation dispersion data. In addition, oscillatory contributions can be observed in relaxation measurements when sudden field variation is used. These effects have to be taken into account when trying to separate field dependent and independent relaxation mechanisms. In addition, site specific influence of paramagnetic additives in the solution on the relaxation dispersion of the solute was found. It was possible to separate the paramagnetic effect from the strong coupling effect. The site specific paramagnetic influence may be useful in studying metal organic molecules e.g. active sites of proteins.

The strong coupling of spins in low field is not the only effect of their scalar coupling. In multi-spin systems level anti-crossings among spin states with the same total spin projection, I_z, are frequently present in fields up to several Tesla. In these level crossing fields, the entanglement of spin states can become particular pronounced and give rise to sharp maxima and minima in both, relaxation dispersion curves, and in the field dependence of hyperpolarization. Occurrence of such features is shown to be crucially dependent on the timing of each step in the field-cycling experiment.

To utilize hyperpolarization for providing structural and dynamic information on the molecular systems it is often necessary to transfer the polarization to specific target nuclei and preserve it from the relaxation. Coherent polarization transfer studied here that uses strong coupling of the spins occurs with the rate of reciprocal scalar coupling that is faster than typical relaxation processes in low viscosity solutions. In a large molecule where relaxation is usually faster the residual non-averaged dipole-dipole interactions can play the same role as scalar coupling in polarization transfer. The dipole-dipole interaction can reach several kHz and, thus, successfully compete with relaxation. Coherent polarization transfer can also be used for hetero-

nuclear polarization transfer although the magnetic field strength must be much lower than that used here. A more promising way is using the field of level anti-crossings which can reach several Tesla. PHIP experiments were shown demonstrating that the homo-nuclear polarization transfer among spins can be more efficient at level crossings fields (50 mT) than at the lowest available field. For preservation of the hyperpolarization the long-lived states generated by lowering magnetic field can be used.

In another set of experiments coherent motion of electronic spins was successfully applied in Overhauser-type dynamic nuclear polarization (DNP) experiments for the optimization of hyperpolarization. Here nuclear polarization is formed as result of driving the electronic spin system of paramagnetic additives away from thermal equilibrium by pumping of EPR transitions and subsequent cross-relaxation. In comparison to cw pumping mode the application of short strong π–pulses can substantially reduce the power losses caused by dielectric absorption of the solvent. This experimental protocol allows one to get close to the maximum achievable polarization enhancement at a small duty cycle and, consequently, low power deposition. Moreover, in case of a complex EPR spectrum of the stable radical one can increase the B_1 field and invert several components in the spectrum at once and, thus, get a drastic increase in the enhancement. An obvious future extension is the use of complex pulse sequences designed by algorithms of optimum control theory[201] for inverting the whole EPR spectrum.

In addition to characterizing the polarization transfer, the photo-CIDNP technique was applied to gain understanding of the underlying photo-physics and -chemistry of light induced radical reactions. This is demonstrated in Chapter 6, which deals with the analysis of short-lived radicals of methionine containing molecules. Time-resolved measurements allowed to separate primary and secondary reaction stages and to determine the reaction rates as well as the nuclear relaxation time at the radical stage. Because of the high spectral resolution site-specific information on the spin density distribution in the radicals was achieved. From these data information about the structure of the radicals and the way of their formation was obtained. At ambient conditions in aqueous solutions these species are too short-lived to be registered by EPR. On the other hand they do not have an absorption band to be detected by optical spectroscopy. Despite the fact that the low field part of the CIDNP field dependences is too complex to be analysed quantitatively so far, the combination of time-resolved and field dependent CIDNP methods in high field allowed for the identification of the radicals and determination of their structure. Moreover, the magnetic resonance parameters of the radicals (g-factor, hyperfine interaction constants) were derived.

Formation of four types of the methionine containing molecule radicals were observed depending on the pH of the aqueous solution and on the dye molecule. Moreover, the pH of aqueous solution influences the branching of the radical formation not only through the protonation state of the precursor but also through the reaction intermediates. In addition to the well known sulfur-centered radical of methionine for the first time nitrogen-centered radicals of the amino acids and peptides were observed which could not be detected by other methods. The detection of the nitrogen-centered radical of glycine residue may be an indication that in basic solution any amino acid at the N-terminus forms such radicals and gives CIDNP. The investigation of the peptides showed that effects of neighboring groups, of N vs C terminal, have to be taken into account causing important consequences for CIDNP studies of protein residues. In particular, not only geminate factors, such as surface accessibility determine the CIDNP amplitude. Thus, the results show that before going to protein studies it is necessary to get further information on small peptides.

The hyperpolarization method is still in its infancy and, thus, has to be explored in more detail. The investigations described here dealing with hyperpolarization and ways of its utilization already showed that exploitation of the scalar spin-spin couplings and coherences can contribute to hyperpolarization as an analytical tool and as a way of enhancing the sensitivity of nuclear magnetic resonance.

Curriculum Vitae

For reasons of data protection, Curriculum Vitae is not published in the online version.

Publications

In parts, this work has been published in the following contributions:

Papers:

(1) Korchak, S. E.; Ivanov, K. L.; Yurkovskaya, A. V.; Vieth, H.-M. *Structure and magnetic resonance parameters of the cation-radicals of methionine as studied by the CIDNP magnetic field dependence*; ARKIVOC **2004**, 121-31.

(2) Morozova, O. B.; Korchak, S. E.; Sagdeev, R. Z.; Yurkovskaya, A. V. *Time-Resolved Chemically Induced Dynamic Nuclear Polarization Studies of Structure and Reactivity of Methionine Radical Cations in Aqueous Solution as a Function of pH*; Journal of Physical Chemistry A **2005**, *109*, 10459-66.

(3) Ivanov, K. L.; Miesel, K.; Yurkovskaya, A. V.; Korchak, S. E.; Kiryutin, A. S.; Vieth, H.-M. *Transfer of CIDNP Among Coupled Spins at Low Magnetic Field*; Applied Magnetic Resonance **2006**, *30*, 513-34.

(4) Korchak, S. E.; Ivanov, K. L.; Yurkovskaya, A. V.; Vieth, H.-M. *Para-hydrogen induced polarization in multi-spin systems studied at variable magnetic field*; Physical Chemistry Chemical Physics **2009**, *11*, 11146 - 56.

(5) Morozova, O. B.; Korchak, S. E.; Vieth, H.-M.; Yurkovskaya, A. V. *Photo-CIDNP Study of Transient Radicals of Met-Gly and Gly-Met Peptides in Aqueous Solution at Variable pH*; Journal of Physical Chemistry B **2009**, *113*, 7398-406.

(6) Korchak, S. E.; Kiryutin, A. S.; Ivanov, K. L.; Yurkovskaya, A. V.; Grishin, Y. A.; Zimmermann, H.; Vieth, H.-M. *Low-Field, Time-Resolved Dynamic Nuclear Polarization with Field Cycling and High-Resolution NMR Detection*; Applied Magnetic Resonance **2010**, *37*, 515-37.

Conferences:

1. Korchak, S.; Morozova, O.; Ivanov, K.; Yurkovskaya, A.; Vieth, H.-M., *CIDNP of transient methionine cation radicals: structure, magnetic resonance parameters and kinetics*, Spin Chemistry Meeting 2005, 9th International Symposium on Spin and Magnetic Field Effects in Chemistry and Related Phenomena, Oxford, 2005.
2. Korchak, S.E.; Ivanov, K.L.; Yurkovskaya, A.V.; Vieth, H.-M., *Structure and Magnetic Resonance Parameters of the Cation-Radicals of Methionine as Studied by the CIDNP Magnetic Field Dependence*, Poster/Abstract: Verhandl. DPG (VI), 40 2/ CPP 30.13 p.123, 2005.

3. Ivanov, K.; Korchak, S.; Miesel, K.; Vieth, H.-M.,; Yurkovskaya, A., *Characterisation of short-lived reaction intermediates by CIDNP and its variation with the external magnetic field*, Spin Chemistry Meeting 2005, 9th International Symposium on Spin and Magnetic Field Effects in Chemistry and Related Phenomena, Oxford, 2005.
4. Korchak, Sergey, *Radicals of biomolecules studied by nuclear spin polarization*, Triple-symposium of GK 788 on "Hydrogen bonding and hydrogen transfer", Halle, 2006.
5. Vieth, H.-M.; Morozova, O. B.; Korchak, S. E.; Ivanov, K. L.; Yurkovskaya, A. V., *CIDNP studies of structure and reactivity of methionine radical cations*. XX International symposium on reactivity of ion-radicals, Rome, Italy, 2. - 6. Juli 2006, S. P19.
6. Miesel, K.; Ivanov, K.L.; Yurkovskaya, A.V.; Korchak, S.E.; Kiryutin, A.S.; Vieth, H.-M., *Coherent transfer of CIDNP in biologically important molecules at low magnetic field* XXII International Conference on Magnetic Resonance in Biological Systems, Göttingen, Germany, 20. – 25. August, 2006, S. 212.
7. Ivanov, K.L.; Korchak, S.E.; Miesel, K.; Vieth, H.-M.; Yurkovskaya, A.V.; *Quantitative CIDNP of Biomolecules*, XXII International Conference on Magnetic Resonance in Biological Systems, Göttingen, Germany, 20. – 25. August 2006, S. 39
8. Kiryutin, A.S.; Korchak, S.E.; Ivanov, K.L.; Vieth, H.-M.; Yurkovskaya, A.V., *Dynamic Polarization and Relaxation in Systems of Coupled Nuclear Spins*, International Symposium on Modern Problems of Chemical Physics, Kazan, Russia, 31. Oktober – 4. November 2006.
9. Yurkovskaya, A.V.; Ivanov, K.L.; Korchak, S.E.; Kiryutin, A.S.; Vieth, H.-M., *Re-distribution of hyperpolarization infield cycling NMR experiments with high resolution detection*, The 5th Conference on Field Cycling NMR Relaxometry, Torino, Italy, May 30-June 3, 2007, p. O2.
10. Miesel, K.; Ivanov, K.L.; Yurkovskaya, A.V.; Korchak, S.E.; Kiryutin, A.S.; Vieth H.-M.; *Influence of spin-spin couplings on longitudinal relaxation dispersion*, The 5th Conference on Field Cycling NMR Relaxometry, Torino, Italy, May 30-June 3, 2007, p. O15
11. Ivanov, K. L.; Yurkovskaya, A. V.; Korchak, S. E.; Kiryutin, A. S.; Miesel, K.; Vieth H.-M., *Influence of spin-spin couplings on T_1 relaxation dispersion*, The International conference Zavoysky -100 "Modern developments of magnetic resonance". Kazan, September 24-29 2007, p. 30
12. Korchak, S.E.; Ivanov, K.L.; Yurkovskaya, A.V.; Vieth, H.-M., *Photo CIDNP redistribution and T1 relaxation of histidine at variable magnetic field*, Spin Chemistry Meeting 2007, 10th International Symposium on Spin and Magnetic Field Effect in Chemistry and Related phenomena, Venice, Italy, 18-21, June 2007, P19, p.65

13. Miesel, K.; Ivanov, K.L.; Yurkovskaya, A.V.; Korchak, S.E.; Kiryutin, A.S.; Vieth, H.-M., *Coherent transfer of hyper-polarization due to strong coupling of spins*, 11th Chianti Workshop on Magnetic Resonance "Methods for biomolecular magnetic resonance", Vallombrosa (Florence), Italy, June 3-8, 2007, p. 88
14. Ivanov, K.L.; Korchak, S.E.; Yurkovskaya, A.V.; Vieth, H.-M., *Effects of spin-spin couplings on photo-CIDNP re-distribution and T1-relaxation dispersion of histidine*, 11th Chianti Workshop on Magnetic Resonance "Methods for biomolecular magnetic resonance", Vallombrosa (Florence), Italy, June 3-8, 2007, p.70
15. Morozova, O.B.; Korchak, S.E. ; Yurkovskaya, A.V., *Photo-Oxidation of Methionine and 3-Methyl-Thiopropylamine Studied by Time-Resolved CIDNP*, CECP 2008 "Central European Conference on Photochemistry", Bad Hofgastein, Austria, February 10-14, 2008, poster P43, p. 89.
16. Vieth, H.-M.; Morozova, O.B.; Korchak, S.E.; Yurkovskaya, A. V., *CIDNP Studies of Structure and Reactivity of Methionine Radical Cations in the Dipeptides Met-Gly and Gly-Met*, Bad Hofgastein, Austria, February 10-14, 2008, poster P44, p. 90.
17. Korchak, S.; Ivanov, K.; Köchling, T.; Yurkovskaya, A.; Vieth, H.-M., *Biological NMR Spectroscopy: Hyperpolarization at Variable Field*, Poster/Abstract: Verhandl. DPG (VI), 43 1/ BP 26.15 p.62 (2008)
18. Köchling, T.; Ivanov, K.; Korchak, S.; Yurkovskaya, A.; Vieth, H.-M., *Magnetic Relaxation Dispersions of Biomolecules: Effects of Field-Cycling*, Poster/Abstract: Verhandl. DPG (VI), 43 1/ BP 26.14 p.62 (2008)
19. Ivanov, K.; Köchling, T.; Korchak, S.; Yurkovskaya, A.; Vieth, H.-M., *Effects of Field-Cycling on Hyperpolarization and Relaxation Dispersion*, Poster/Abstract: The 49th ENC (Experimental Nuclear Magnetic Resonance Conference), M-T 189, March 9-14, 2008, Asilomar Conference Center, Pacific Grove, CA, USA
20. Korchak, S.; Ivanov, K.; Yurkovskaya, A.; Vieth, H.-M., *Para-hydrogen induced nuclear spin polarization at variable magnetic field*, Poster/Abstract: Verhandl. DPG (VI), 44 5/ CPP 15.6 p.85 (2009)
21. Köchling, T.; Hörner, G.; Korchak, S.; Yurkovskaya, A.; Vieth, H.-M., *CIDNP as a tool for determining the structure and magnetic resonance parameters of transient radicals of biomolecules*, Poster/Abstract: Verhandl. DPG (VI), 44 5/ CPP 16.14 p.89 (2009)
22. Morozova, O.; Korchak, S.; Vieth, H.-M.; Yurkovskaya, A, *Photo-CIDNP study of transient radicals of Met-Gly and Gly-Met peptides*, Talk/Abstract: Verhandl. DPG (VI), 44 5/ CPP 37.11 p.114 (2009)

23. Ivanov, K.L.; Korchak, S.E.; Yurkovskaya, A.V.; Vieth,H.-M.; *Para-Hydrogen Induced Polarization Effects Studied at Variable Magnetic Field*, Poster/Abstract: The 50th ENC (Experimental Nuclear Magnetic Resonance Conference), M-T 189, March 29-April 4, 2009, Asilomar Conference Center, Pacific Grove, CA, USA
24. Morozova, O.; Vieth, H.-M.; Yurkovskaya, A., *Possibilities of time-resolved CIDNP in protein research*, Poster/Abstract: The 50th ENC (Experimental Nuclear Magnetic Resonance Conference), M-T 189, March 29-April 4, 2009, Asilomar Conference Center, Pacific Grove, CA, USA
25. Morozova, O.; Korchak, S.; Vieth, H.-M.; Yurkovskaya, A., *Photo-CIDNP study of transient radicals of Gly-Gly, Met-Gly and Gly-Met peptides,* Poster/Abstract: The 50th ENC (Experimental Nuclear Magnetic Resonance Conference), M-T 189, March 29-April 4, 2009, Asilomar Conference Center, Pacific Grove, CA, USA
26. Korchak, S.; Morozova, O.; Vieth, H.-M.; Yurkovskaya, A., *Photo-Oxidation of Gly-Gly, Met-Gly and Gly-Met Peptides Studied by CIDNP*, 4th European Young Investigator Conference 2009, Slubice, Poland, O-11
27. Köchling, T.; Hörner, G.; Korchak, S.; Yurkovskaya, A.; Vieth, H.-M., *CIDNP as a Tool to Determine Magnetic Resonance Parameters and Structure of Radicals in Biomolecules*, 4th European Young Investigator Conference 2009, Slubice, Poland, P-12
28. Ivanov, K.; Korchak, S.; Yurkovskaya, A.; Vieth, H.-M., *Para-Hydrogen Induced Polarization in Multi-spin Systems Studied at Variable Magnetic Field*, Spin Chemistry Meeting 2009 11th International Symposium on Spin and Magnetic Field Effects in Chemistry and Related Phenomena, Brock University, St. Catharines, Ontario, Canada.
29. Korchak, S.E.; Köchling, T.; Hörner, G.; Ivanov, K.L.; Yurkovskaya, A.V.; Vieth, H.-M., *Dynamic Polarization and T_1 Relaxation Dispersion Studied by Field Cycling NMR with High Resolution*, Spin Chemistry Meeting 2009 11th International Symposium on Spin and Magnetic Field Effects in Chemistry and Related Phenomena, Brock University, St. Catharines, Ontario, Canada.
30. Korchak, S.; Morozova, O.; Vieth, H.-M.; Yurkovskaya, A., *Investigation of Transient Radicals of Met-Gly and Gly-Met Peptides by Photo-CIDNP*, Spin Chemistry Meeting 2009 11th International Symposium on Spin and Magnetic Field Effects in Chemistry and Related Phenomena, Brock University, St. Catharines, Ontario, Canada. Poster.

Acknowledgements

Author is grateful to following persons in their help concerning this PhD work:

Prof. Dr. Hans-Martin Vieth, for providing the guidance and opportunity to join his group.

Dr. Alexandra V. Yurkovskaya, for giving her advices and guidance to achieve this thesis.

Dr. Konstantin L. Ivanov, for his great collaboration.

Dr. Alexey S. Kiryutin, for his experimental work together with me.

Dipl. Talea Köchling, for her experimental work together with me.

Dr. Olga B. Morozova, for her collaboration in methionine studies.

Dipl. Matthias Seurig, for his help in design of the probehead for field-cycling setup.

Dr. Achim Gädke, for his help concerning DAMARIS.

Sebastian John, for his programming of the additions to DAMARIS for controlling stepping motor and magnetic field.

To all employee of mechanical and electronic workshop of FU-Berlin, for their help in production of the mechanical and electronic parts of the probeheads and field cycling parts.

Bibliography

(1) Salikhov, K. M.; Molin, Y. N.; Sagdeev, R. Z.; Buchachenko, A. L. *Spin Polarization and Magnetic Effects in Chemical Reactions*; Elsevier, Amsterdam, 1984.

(2) Natterer, J.; Bargon, J. *Parahydrogen induced polarization*; Progress in Nuclear Magnetic Resonance Spectroscopy **1997**, *31*, 293-315.

(3) Adams, R. W.; Aguilar, J. A.; Atkinson, K. D.; Cowley, M. J.; Elliott, P. I. P.; Duckett, S. B.; Green, G. G. R.; Khazal, I. G.; Lopez-Serrano, J.; Williamson, D. C. *Reversible Interactions with para-Hydrogen Enhance NMR Sensitivity by Polarization Transfer*; Science **2009**, *323*, 1708-11.

(4) Happer, W. *Optical Pumping*; Reviews of Modern Physics **1972**, *44*, 169 - 249

(5) Goodson, B. M. *Nuclear Magnetic Resonance of Laser-Polarized Noble Gases in Molecules, Materials, and Organisms*; Journal of Magnetic Resonance **2002**, *155*, 157-216.

(6) Pietrass, T. *Optically polarized ^{129}Xe in magnetic resonance techniques*; Magnetic Resonance Review **2000**, *17*, 263-337.

(7) Stehlik, D.; Vieth, H.-M. *Mechanism of the photochemical hydrogen transfer reaction in doped fluorene crystals*; Molecular Crystals and Liquid Crystals **1983**, *93*, 83-93.

(8) Stehlik, D.; Vieth, H.-M. *Time evolution of electron-nuclear cross-polarization in radiofrequency induced optical nuclear spin polarization (RF-ONP)*; In *Pulsed Magnetic Resonance: NMR, ESR, Opt.*; Bagguley, D. M. S., Ed.; Oxford University Press, Oxford, 1992, p 446-77.

(9) Jeffries, C. D. *Dynamic Nuclear Orientation*; Interscience, New York, 1963.

(10) Hausser, K. H.; Stehlik, D. *Dynamic Nuclear Polarization in Liquids*; In *Advances in Magnetic Resonance*; Waugh, J. S., Ed.; Academic Press Inc., New York, 1968; Vol. 3, p 79-139.

(11) Borghini, M.; De Boer, W.; Morimoto, K. *Nuclear dynamic polarization by resolved solid-state effect and thermal mixing with an electron spin-spin interaction reservoir*; Physics Letters A **1974**, *48A*, 244-6.

(12) Hartmann, S. R.; Hahn, E. L. *Nuclear Double Resonance in the Rotating Frame*; Physical Review **1962**, *128*, 2042-53.

(13) Pelupessy, P.; Chiarparin, E. *Hartmann-Hahn Polarization Transfer in Liquids: An Ideal Tool for Selective Experiments*; Concepts in Magnetic Resonance **2000**, *12*, 103-24.

(14) Carravetta, M.; Johannessen Ole, G.; Levitt Malcolm, H. *Beyond the T1 limit: singlet nuclear spin states in low magnetic fields*; Physical Review Letters **2004**, *92*, 153003.

(15) Möbius, K.; Savitsky, A.; Schnegg, A.; Plato, M.; Fuchs, M. *High-field EPR spectroscopy applied to biological systems: characterization of molecular switches for electron and ion transfer*; Physical Chemistry Chemical Physics **2005**, *7*, 19-42.

(16) Bittl, R.; Kay, C. W. M.; Weber, S.; Hegemann, P. *Characterization of a flavin radical product in a C57M mutant of a LOV1 domain by electron paramagnetic resonance*; Biochemistry **2003**, *42*, 8506-12.

(17) Teutloff, C.; Pudollek, S.; Kessen, S.; Broser, M.; Zouni, A.; Bittl, R. *Electronic structure of the tyrosine D radical and the water-splitting complex from pulsed ENDOR spectroscopy on photosystem II single crystals*; Physical Chemistry Chemical Physics **2009**, *11*, 6715-26.

(18) Bargon, J.; Fischer, H.; Johnsen, U. *Nuclear magnetic resonance emission lines during fast radical reactions. I. Recording methods and examples*; Zeitschrift für Naturforschung, Teil A: Astrophysik, Physik und Physikalische Chemie **1967**, *22*, 1551-5.

(19) *Chemically Induced Magnetic Polarization*; Muus, L. T.; Atkins, P. W.; McLauchlan, K. A.; Pedersen, J. B., Eds.; D. Reidel, Dordrecht, 1977.

(20) Nagakura, S.; Hayashi, H.; Azumi, T. *Dynamic Spin Chemistry*; Kodansha and John Wiley&Sons co-publication, Tokyo and New York, 1998.

(21) *Chemically Induced Magnetic Polarization*; Lepley, A. R.; Closs, G. L., Eds.; John Wiley&Sons, New York, 1973.

(22) Adrian, F. J. *Role of Diffusion-Controlled Reaction in Chemically Induced Nuclear-Spin Polarization II. General Theory and Comparison with Experiment*; Journal of Chemical Physics **1971**, *54*, 3912-17.

(23) Kaptein, R. *Simple Rules for Chemically Induced Dynamic Nuclear Polarization*; Journal of the Chemical Society: Chemical Communications **1971**, 732-3.

(24) Tsentalovich, Y. P.; Morozova, O. B.; Yurkovskaya, A. V.; Hore, P. J.; Sagdeev, R. Z. *Time-Resolved CIDNP and Laser Flash Photolysis Study of the Photoreactions of N-Acetyl Histidine with 2,2'-Dipyridyl in Aqueous Solution*; Journal of Physical Chemistry A **2000**, *104*, 6912-6.

(25) Morozova, O. B.; Kiryutin, A. S.; Sagdeev, R. Z.; Yurkovskaya, A. V. *Electron Transfer between Guanosine Radical and Amino Acids in Aqueous Solution. 1. Reduction of Guanosine Radical by Tyrosine*; Journal of Physical Chemistry B **2007**, *111*, 7439-48.

(26) Vollenweider, J.-K.; Fischer, H.; Hennig, J.; Leuschner, R. *Time-resolved CIDNP in laser flash photolysis of aliphatic ketones. A quantitative analysis*; Chem. Phys. Letters **1985**, *97*, 217-34.

(27) Vollenweider, J.-K.; Fischer, H. *Absolute chemically induced nuclear polarizations and yields from geminate radical pair reactions. A test of high-field radical pair theories*; Chemical Physics **1988**, *124*, 333-45.

(28) Dvinskikh, S. V.; Yurkovskaya, A. V.; Vieth, H.-M. *A Time-Resolved Stimulated Nuclear Polarization Study of Biradicals in Low Magnetic Field*; Journal of Physical Chemistry **1996**, *100*, 8125-30.

(29) Bagryanskaya, E. G.; Grishin, Y. A.; Sagdeev, R. Z.; Molin, Y. N. *CIDNP-detected ESR of short-lived radical pairs in solutions*; Chemical Physics Letters **1985**, *114*, 138-42.

(30) Carver, T. R.; Slichter, C. P. *Polarization of nuclear spins in metals*; Physical Review **1953**, *92*, 212-13.

(31) Ardenkjaer-Larsen, J. H.; Fridlund, B.; Gram, A.; Hansson, G.; Hansson, L.; Lerche, M. H.; Servin, R.; Thaning, M.; Golman, K. *Increase in signal-to-noise ratio of > 10,000 times in liquid-state NMR*; Proceedings of the National Academy of Sciences USA **2003**, *100*, 10158-63.

(32) Golman, K.; Olsson, L. E.; Axelsson, O.; Mansson, S.; Karlsson, M.; Petersson, J. S. *Molecular imaging using hyperpolarized ^{13}C*; British Journal of Radiology **2003**, *76*, S118-27.

(33) Mansson, S.; Johansson, E.; Magnusson, P.; Chai, C.-M.; Hansson, G.; Petersson, J. S.; Stahlberg, F.; Golman, K. *^{13}C Imaging-A New Diagnostic Platform*; European radiology **2006**, *16*, 57-67.

(34) Maly, T.; Debelouchina, G. T.; Bajaj, V. S.; Hu, K.-N.; Joo, C.-G.; Mak-Jurkauskas, M. L.; Sirigiri, J. R.; van der Wel, P. C. A.; Herzfeld, J.; Temkin, R. J.; Griffin, R. G. *Dynamic nuclear polarization at high magnetic fields*; Journal of Chemical Physics **2008**, *128*, 052211/1-/19.

(35) Barnes, A. B.; De Paëpe, G.; van der Wel, P. C. A.; Hu, K. N.; Joo, C. G.; Bajaj, V. S.; Mak-Jurkauskas, M. L.; Sirigiri, J. R.; Herzfeld, J.; Temkin, R. J.; Griffin, R. G. *High-Field Dynamic Nuclear Polarization for Solid and Solution Biological NMR*; Applied Magnetic Resonance **2008**, *34*, 237-63.

(36) Prisner, T.; Köckenberger, W. *Dynamic Nuclear Polarization: New Experimental and Methodology Approaches and Applications in Physics, Chemistry, Biology and Medicine*; Applied Magnetic Resonance **2008**, *34*, 213-8.

(37) Höfer, P.; Carl, P.; Guthausen, G.; Prisner, T.; Reese, M.; Carlomagno, T.; Griesinger, C.; Bennati, M. *Studies of Dynamic Nuclear Polarization with Nitroxides in Aqueous Solution*; Applied Magnetic Resonance **2008**, *34*, 393-8.

(38) Müller-Warmuth, W.; Meise-Gresch, K. *Molecular motions and interactions as studied by dynamic nuclear polarization (DNP) in free radical solutions.*; In *Advances in Magnetic Resonance*; Waugh, J. S., Ed.; Academic Press, New York, 1983; Vol. 11, p 1-45.

(39) Potenza, J. *Measurement and applications of dynamic nuclear polarization*; Advances in Molecular Relaxation Processes **1972**, *4*, 229-354.

(40) McCarney, E. R.; Armstrong, B. D.; Kausik, R.; Han, S. *Dynamic Nuclear Polarization Enhanced Nuclear Magnetic Resonance and Electron Spin Resonance Studies of Hydration and Local Water Dynamics in Micelle and Vesicle Assemblies*; Langmuir **2008**, *24*, 10062-72.

(41) Armstrong, B. D.; Han, S. *Overhauser Dynamic Nuclear Polarization To Study Local Water Dynamics*; Journal of the American Chemical Society **2009**, *131*, 4641-7.

(42) Khramtsov, V. V.; Grigor'Ev, I. A.; Foster, M. A.; Lurie, D. J.; Nicholson, I. *Biological applications of spin pH probes*; Cellular and Molecular Biology **2000**, *46*, 1361-74.

(43) Grucker, D.; Guiberteau, T.; Eclancher, B. *Oximetry by Dynamic Nuclear Polarization*; Magnetic Resonance in Medicine **1995**, *34*, 219-26.

(44) Halse, M. E.; Callaghan, P. T. *A dynamic nuclear polarization strategy for multi-dimensional Earth's field NMR spectroscopy*; Journal of Magnetic Resonance **2008**, *195*, 162-8.

(45) Farkas, A. *Orthohydrogen, Parahydrogen and Heavy Hydrogen*; Chembridge University Press, London, 1935.

(46) Duckett, S. B.; Sleigh, C. J. *Applications of the parahydrogen phenomenon: A chemical perspective*; Progress in Nuclear Magnetic Resonance Spectroscopy **1999**, *34*, 71-92.

(47) Goldman, M.; Jóhannesson, H.; Axelsson, O.; Karlsson, M. *Hyperpolarization of ^{13}C through order transfer from parahydrogen: A new contrast agent for MRI*; Magnetic Resonance Imaging **2005**, *23*, 153-7.

(48) Vasos, P. R.; Comment, A.; Sarkar, R.; Ahuja, P.; Jannin, S.; Ansermet, J. P.; Konter, J. A.; Hautle, P.; Van Den Brandt, B.; Bodenhausen, G. *Long-lived states to sustain hyperpolarized magnetization*; Proceedings of the National Academy of Sciences of the United States of America **2009**, *106*, 18469-73.

(49) Warren, W. S.; Jenista, E.; Branca, R. T.; Chen, X. *Increasing Hyperpolarized Spin Lifetimes Through True Singlet Eigenstates*; Science **2009**, *323*, 1711-4.

(50) Canet, D.; Bouguet-Bonnet, S.; Aroulanda, C.; Reineri, F. *About Long-Lived Nuclear Spin States Involved in Para-Hydrogenated Molecules*; Journal of the American Chemical Society **2007**, *129*, 1445-9.

(51) Carravetta, M.; Levitt, M. H. *Theory of long-lived nuclear spin states in solution nuclear magnetic resonance. I. Singlet states in low magnetic field*; Journal of Chemical Physics **2005**, *122*, 214505/1-/14.

(52) Pravica, M. G.; Weitekamp, D. P. *Net NMR alignment by adiabatic transport of para-hydrogen addition products to high magnetic field*; Chemical Physics Letters **1988**, *145*, 255-8.

(53) Eisenschmid, T. C.; Kirss, R. U.; Deutsch, P. P.; Hommeltoft, S. I.; Eisenberg, R.; Bargon, J.; Lawler, R. G.; Balch, A. L. *Para Hydrogen Induced Polarization in Hydrogenation Reactions*; Journal of the American Chemical Society **1987**, *109*, 8089-91.

(54) Aime, S.; Gobetto, R.; Reineri, F.; Canet, D. *Polarization transfer from para-hydrogen to heteronuclei: Effect of H/D substitution. The case of AA'X and $A_2A_2'X$ spin systems*; Journal of Magnetic Resonance **2006**, *178*, 184-92.

(55) Johansson, E.; Olsson, L. E.; Månsson, S.; Petersson, J. S.; Golman, K.; Ståhlberg, F.; Wirestam, R. *Perfusion Assessment With Bolus Differentiation: A Technique Applicable to Hyperpolarized Tracers*; Magnetic Resonance in Medicine **2004**, *52*, 1043-51.

(56) Jóhannesson, H.; Axelsson, O.; Karlsson, M. *Transfer of para-hydrogen spin order into polarization by diabatic field cycling*; Comptes Rendus Physique **2004**, *5*, 315-24.

(57) Kuhn, L. T.; Bommerich, U.; Bargon, J. *Transfer of Parahydrogen-Induced Hyperpolarization to ^{19}F*; Journal of Physical Chemistry A **2006**, *110*, 3521-6.

(58) Aime, S.; Gobetto, R.; Reineri, F.; Canet, D. *Hyperpolarization transfer from parahydrogen to deuterium via carbon-13*; Journal of Chemical Physics **2003**, *119*, 8890-6.

(59) Reineri, F.; Viale, A.; Giovenzana, G.; Santelia, D.; Dastru, W.; Gobetto, R.; Aime, S. *New Hyperpolarized Contrast Agents for ^{13}C-MRI from Para-Hydrogenation of Oligooxyethylenic Alkynes*; Journal of the American Chemical Society **2008**, *130*, 15047-53.

(60) Vinogradov, E.; Grant, A. K. *Hyperpolarized long-lived states in solution NMR: Three-spin case study in low field*; Journal of Magnetic Resonance **2008**, *194*, 46-57.

(61) Ivanov, K. L.; Yurkovskaya, A. V.; Vieth, H.-M. *Coherent transfer of hyperpolarization in coupled spin systems at variable magnetic field*; Journal of Chemical Physics **2008**, *128*, 154701/1-/13.

(62) Miesel, K.; Ivanov, K. L.; Yurkovskaya, A. V.; Vieth, H.-M. *Coherence transfer during field-cycling NMR experiments*; Chemical Physics Letters **2006**, *425*, 71-6.

(63) Miesel, K.; Ivanov, K. L.; Köchling, T.; Yurkovskaya, A. V.; Vieth, H.-M. *Field-Cycling Effects on Dynamic Nuclear Polarization*; Applied Magnetic Resonance **2008**, *34*, 423-37.

(64) Korchak, S. E.; Ivanov, K. L.; Yurkovskaya, A. V.; Vieth, H.-M. *Para-hydrogen induced polarization in multi-spin systems studied at variable magnetic field*; Physical Chemistry Chemical Physics **2009**, *11*, 11146 - 56.

(65) Ivanov, K. L.; Miesel, K.; Yurkovskaya, A. V.; Korchak, S. E.; Kiryutin, A. S.; Vieth, H.-M. *Transfer of CIDNP Among Coupled Spins at Low Magnetic Field*; Applied Magnetic Resonance **2006**, *30*, 513-34.

(66) De Kanter, F. J. J.; Kaptein, R. *CIDNP transfer via nuclear dipolar relaxation and spin-spin coupling*; Chemical Physics Letters **1979**, *62*, 421-6.

(67) Günther, H. *NMR spectroscopy, Chapter 5*; 2nd ed.; John Wiley &Sons, New York, 1994.

(68) Ivanov, K. L.; Vieth, H.-M.; Miesel, K.; Yurkovskaya, A. V.; Sagdeev, R. Z. *Investigation of the magnetic field dependence of CIDNP in multi-nuclear radical pairs. Part II. Photoreaction of tyrosine and comparison of model calculation with experimental data*; Physical Chemistry Chemical Physics **2003**, *5*, 3470-80.

(69) Schäublin, S.; Wokaun, A.; Ernst, R. R. *The creation of off-diagonal elements in chemically induced dynamic nuclear polarization experiments*; Chemical Physics **1976**, *14*, 285-93.

(70) Schäublin, S.; Wokaun, A.; Ernst, R. R. *Pulse Techniques Applied to Chemically Induced Dynamic Nuclear Polarization*; Journal of Magnetic Resonance **1977**, *27*, 273-302.

(71) Salikhov, K. M. *Creation of spin coherent states in the course of chemical reactions*; Chemical Physics Letters **1993**, *201*, 261-4.

(72) Kimmich, R.; Anoardo, E. *Field-cycling NMR relaxometry*; Progress in Nuclear Magnetic Resonance Spectroscopy **2004**, *44*, 257-320.

(73) Bertini, I.; Luchinat, C.; Parigi, G. *^{1}H NMRD profiles of paramagnetic complexes and metalloproteins*; Advances in Inorganic Chemistry **2005**, *57*, 105-72.

(74) Canet, D. *General theory of nuclear relaxation*; Advances in Inorganic Chemistry **2005**, *57*, 3-40.

(75) Fasano, M. *Biological applications of relaxometry*; Chimica e l'Industria (Milan, Italy) **2001**, *83*, 89.

(76) Venu, K.; Sastry, V. S. S. *Smectic order fluctuations and nematic phase stability - nuclear magnetic relaxation dispersion studies*; Solid State Physics, Proceedings of the DAE Solid State Physics Symposium, 42nd, Kalpakkam, India, Dec. 20-24, 1999 **2000**, 15-21.

(77) Kothe, G.; Stohrer, J. *Nuclear spin relaxation and molecular motion in liquid crystals*; NATO ASI Series, Series C: Mathematical and Physical Sciences **1994**, *431*, 195-206.

(78) Roberts, M. F.; Cui, Q.; Turner, C. J.; Case, D. A.; Redfield, A. G. *High-Resolution Field-Cycling NMR Studies of a DNA Octamer as a Probe of Phosphodiester Dynamics and Comparison with Computer Simulation*; Biochemistry **2004**, *43*, 3637-50.

(79) Bertini, I.; Gupta, Y. K.; Luchinat, C.; Parigi, G.; Schlörb, C.; Schwalbe, H. *NMR Spectroscopic Detection of Protein Protons and Longitudinal Relaxation Rates between 0.01 and 50 MHz*; Angewandte Chemie International Edition **2005**, *44*, 2223-5.

(80) Luchinat, C.; Parigi, G. *Collective Relaxation of Protein Protons at Very Low Magnetic Field: A New Window on Protein Dynamics and Aggregation*; Journal of the American Chemical Society **2007**, *129*, 1055-64.

(81) Clarkson, R. B. *Blood-Pool MRI Contrast Agents: Properties and Characterization*; Topics in Current Chemistry **2002**, *221*, 201-35.

(82) Redfield, A. G. *The theory of relaxation processes*; Advances in Magnetic Resonance **1966**, *1*, 1-32.

(83) Wagner, S.; Dinesen, T. R. J.; Rayner, T.; Bryant, R. G. *High-Resolution Magnetic Relaxation Dispersion Measurements of Solute Spin Probes Using a Dual-Magnet System*; Journal of Magnetic Resonance **1999**, *140*, 172-8.

(84) Roberts, M. F.; Redfield, A. G. *Phospholipid bilayer surface configuration probed quantitatively by ^{31}P field-cycling NMR*; Proceedings of the National Academy of Sciences of the United States of America **2004**, *101*, 17066-71.

(85) Roberts, M. F.; Redfield, A. G. *High-Resolution ^{31}P Field Cycling NMR as a Probe of Phospholipid Dynamics*; Journal of the American Chemical Society **2004**, *126*, 13765-77.

(86) Ivanov, K.; Yurkovskaya, A.; Vieth, H.-M. *High resolution NMR study of T1 magnetic relaxation dispersion. I. Theoretical considerations of relaxation of scalar coupled spins at arbitrary magnetic field*; Journal of Chemical Physics **2008**, *129*, 234513/1-/12.

(87) *The DAMARIS project user page and documentation* http://damaris.berlios.de/.

(88) Gädke, A.; Rosenstihl, M.; Schmitt, C.; Stork, H.; Nestle, N. *DAMARIS – A flexible and open software platform for NMR spectrometer control*; Diffusion Fundamentals **2007**, *5*, 6.1-6.9.

(89) Delsuc, M. A.; Lallemand, J. Y. *Improvement of Dynamic Range in NMR by Oversampling*; Journal of Magnetic Resonance **1986**, *69*, 504-7.

(90) Jacobsen, N. E. *NMR Spectroscopy Explained: Simplified Theory, Application and Examples for Organic Chemistry and Structural Biology*; John Wiley&Sons Inc, New Jersey, 2007.

(91) Wider, G. *Elimination of Baseline Artifacts in NMR Spectra by Oversampling*; Journal of Magnetic Resonance **1990**, *89*, 406-9.

(92) Moskau, D. *Application of Real Time Digital Filters in NMR Spectroscopy*; Concepts in Magnetic Resonance (Magnetic Resonance Engineering) **2002**, *15*, 164-76.

(93) Ramsey, N. F.; Pound, R. V. *Nuclear Audiofrequency Spectroscopy by Resonant Heating of the Nuclear Spin System*; Physical Review **1951**, *81*, 278-9.

(94) Kimmich, R. *Field Cycling in NMR Relaxation Spectroscopy: Applications in Biological, Chemical and Polymer Physics*; Bulletin of Magnetic Resonance **1980**, *1*, 195-218.

(95) Kimmich, R. *NMR-Tomography, Diffusometry, Relaxometry*; Springer, Heidelberg, 1997.

(96) Noack, F. *NMR field-cycling spectroscopy: principles and applications*; Progress in Nuclear Magnetic Resonance Spectroscopy **1986**, *18*, 171-276.

(97) Redfield, A. G. *Pure Nuclear Electric Quadrupole Resonance in Impure Copper*; Physical Review **1963**, *130*, 589-95.

(98) Redfield, A. G.; Fite, W.; Bleich, H. *Precision High Speed Current Regulators for Occasionally Switched Inductive Loads*; Review of Scientific Instruments **1968**, *39*, 710.

(99) Stohrer, M.; Noack, F. *Molecular motion in solid odd-numbered paraffin $C_{19}H_{40}$: Proton spin relaxation spectroscopy from 5.8 kHz to 86 MHz*; Journal of Chemical Physics **1977**, *67*, 3729-38.

(100) Job, C.; Zajicek, J.; Brown, M. F. *Fast field-cycling nuclear magnetic resonance spectrometer*; Review of Scientific Instruments **1996**, *67*, 2113-22.

(101) Bagryanskaya, E. G.; Grishin, Y. A.; Avdievich, N. I.; Sagdeev, R. Z.; Molin, Y. N. *Studies of various mechanisms of nuclear polarization due to a resonant high-frequency field in radical reactions*; Chemical Physics Letters **1986**, *128*, 162-7.

(102) Hore, P. J.; Winder, S. L.; Roberts, C. H.; Dobson, C. M. *Stopped-Flow Photo-CIDNP Observation of Protein Folding*; Journal of the American Chemical Society **1997**, *119*, 5049-50.

(103) Bielecki, A.; Zax, D. B.; Zilm, K. W.; Pines, A. *Zero-field NMR and NQR spectrometer*; Review of Scientific Instruments **1986**, *57*, 393-403.

(104) Redfield, A. G. *Shuttling device for high-resolution measurements of relaxation and related phenomena in solution at low field, using a shared commercial 500 MHz NMR instrument*; Magnetic Resonance in Chemistry **2003**, *41*, 753-68.

(105) Grosse, S.; Gubaydullin, F.; Scheelken, H.; Vieth, H.-M.; Yurkovskaya, A. V. *Field Cycling by Fast NMR Probe Transfer: Design and Application in Field-Dependent CIDNP Experiments*; Applied Magnetic Resonance **1999**, *17*, 211-25.

(106) Grosse, S. *CIDNP-Untersuchungen an photoinduzierten Radikalpaar-Reaktionen mit Feldzyklisierung im Magnetfeldbereich von 0 bis 7 Tesla*; PhD Thesis, Freie Universität Berlin, 2000.

(107) Seurig, M. *Entwurf und Konstruktion eines magnetisch neutralen Probenkopfes für Messungen der chemisch induzierten dynamischen Kernspinpolarisation mit schneller Feldzyklisierung*; Diploma Thesis, Technische Fachhochschule Berlin, University of Applied Sciences, 2005.

(108) Schäublin, S.; Höhener, A.; Ernst, R. R. *Fourier Spectroscopy of Nonequilibrium States, Application to CIDNP, Overhauser Experiments, and Relaxation Time Measurements*; Journal of Magnetic Resonance **1974**, *13*, 196-216.

(109) Mispelter, J.; Lupu, M.; Briguet, A. *NMR Probeheads for Biophysical and Biomedical Experiments. Theoretical Principles and Practical Guidelines*; Imperial College Press, London, 2006.

(110) Kiryutin, A. S.; Ivanov, K. L.; Morozova, O. B.; Yurkovskaya, A. V.; Vieth, H. M.; Pirogov, Y. A.; Sagdeev, A. R. Z. *TR-CIDNP as Tool for Quantitative Analysis of Hyperfine Couplings in Elusive Radicals*; Doklady Physical Chemistry **2009**, *428*, 183-8.

(111) Kiryutin, A.; Ivanov, K.; Yurkovskaya, A.; Vieth, H.-M. *High-resolution study of nuclear magnetic relaxation dispersion of purine nucleotides: Effects of spin-spin coupling*; Solid State Nuclear Magnetic Resonance **2008**, *34*, 142-9.

(112) Landolt-Börnstein. *Magnetic Properties of Free Radicals*; Springer Verlag, Berlin, Heidelberg, and New York, 1977.

(113) Günther, H. *NMR spectroscopy*; 2nd ed.; John Wiley &Sons New York, 1994.

(114) Kowalewski, J.; Mäler, L. *Nuclear spin relaxation in liquids: Theory, experiments, and applications*; CRC Press, Boca Raton, Fla. , 2006.

(115) Pearson, H.; Gust, D.; Armitage, I. M.; Huber, H.; Roberts, J. D.; Stark, R. E.; Vold, R. R.; Vold, R. L. *Nuclear Magnetic Resonance Spectroscopy: Reinvestigation of Carbon-13 Spin-Lattice Relaxation Time Measurements of Amino Acids*; Proceedings of the National Academy of Sciences of the United States of America **1975**, *72*, 1599-601.

(116) Blomberg, F.; Maurer, W.; Rüterjans, H. *Nuclear Magnetic Resonance Investigation of ^{15}N-labeled Histidine in Aqueous Solution*; Journal of the American Chemical Society **1977**, *99*, 8149-59.

(117) Bertini, I.; Luchinat, C.; Parigi, G.; Pierattelli, R. *NMR Spectroscopy of Paramagnetic Metalloproteins*; ChemBioChem **2005**, *6*, 1536-49.

(118) Bertini, I.; Gupta, Y. K.; Luchinat, C.; Parigi, G.; Schlörb, C.; Schwalbe, H. *NMR Spectroscopic Detection of Protein Protons and Longitudinal Relaxation Rates between 0.01 and 50 MHz*; Angewandte Chemie, International Edition **2005**, *44*, 2223-5.

(119) Luchinat, C.; Parigi, G. *Collective Relaxation of Protein Protons at Very Low Magnetic Field: A New Window on Protein Dynamics and Aggregation*; Journal of the American Chemical Society **2007**, *129*, 1055-64.

(120) Anoardo, E.; Bonetto, F.; Kimmich, R. *Apparent low-field spin-lattice dispersion in the smectic-A mesophase of thermotropic cyanobiphenyls*; Physical Review E **2003**, *68*, 022701.

(121) Nakano, A.; Inagaki, F.; Tasumi, M.; Miyazawa, T. *^{1}H spin-lattice Relaxation Times of Imidazole and $_{L}$-Histidine Treated with a Metal-chelating Resin*; Journal of the Chemical Society, Chemical Communications **1976**, 232-3.

(122) Grosse, S.; Yurkovskaya, A. V.; Lopez, J.; Vieth, H.-M. *Field Dependence of Chemically Induced Dynamic Nuclear Polarization (CIDNP) in the Photoreaction of N-Acetyl Histidine with 2,2'-Dipyridyl in Aqueous Solution*; Journal of Physical Chemistry A **2001**, *105*, 6311-9.

(123) Ivanov, K. L.; Lukzen, N. N.; Vieth, H. M.; Grosse, S.; Yurkovskaya, A. V.; Sagdeev, R. Z. *Investigation of the magnetic field dependence of CIDNP in multinuclear radical pairs. 1. Photoreaction of histidine and comparison of model calculation with experimental data*; Molecular Physics **2002**, *100*, 1197-208.

(124) Schaefer, T.; Penner, G. H.; Sebastian, R. *^{1}H nuclear magnetic resonance and molecular orbital studies of the structure and internal rotations in ethylbenzene*; Canadian Journal of Chemistry **1987**, *65*, 873-7.

(125) Giernoth, R.; Huebler, P.; Bargon, J. *Intermediate Product-Catalyst Complexes in the Homogeneous Hydrogenation of Styrene Derivatives with Parahydrogen and Cationic Rh^{1} Catalysts*; Angewandte Chemie, International Edition **1998**, *37*, 2473-5.

(126) Harthun, A.; Giernoth, R.; Elsevier, C. J.; Bargon, J. *Rhodium- and palladium-catalyzed proton exchange in styrene detected in situ by para-hydrogen induced polarization*; Chemical Communications **1996**, 2483-4.

(127) Harthun, A.; Selke, R.; Bargon, J. *Proof of a Reversible, Pairwise Hydrogen Transfer during the Homogeneously Rhodium(I)-Catalyzed Hydrogenation of α,β-Unsaturated Carbonic Acid Derivatives with In Situ NMR Spectroscopy and Parahydrogen*; Angewandte Chemie, International Edition in English **1996**, *35*, 2505-7.

(128) Dunne, J. P.; Blazina, D.; Aiken, S.; Carteret, H. A.; Duckett, S. B.; Jones, J. A.; Poli, R.; Whitwood, A. C. *A combined parahydrogen and theoretical study of H_2 activation by 16-electron d^8 ruthenium(0) complexes and their subsequent catalytic behaviour*; Dalton Transactions **2004**, 3616-28.

(129) Blazina, D.; Dunne, J. P.; Aiken, S.; Duckett, S. B.; Elkington, C.; McGrady, J. E.; Poli, R.; Walton, S. J.; Anwar, M. S.; Jones, J. A.; Carteret, H. A. *Contrasting photochemical*

and thermal reactivity of $Ru(CO)_2(PPh_3)(dppe)$ towards hydrogen rationalized by parahydrogen NMR and DFT studies; Dalton Transactions **2006**, 2072-80.

(130) Duckett, S. B.; Wood, N. J. *Parahydrogen-based NMR methods as a mechanistic probe in inorganic chemistry*; Coordination Chemistry Reviews **2008**, *252*, 2278-91.

(131) Jonischkeit, T.; Bommerich, U.; Stadler, J.; Woelk, K.; Niessen, H. G.; Bargon, J. *Generating long-lasting 1H and 13C hyperpolarization in small molecules with parahydrogen-induced polarization*; Journal of Chemical Physics **2006**, *124*, 201109/1-/5.

(132) *Dynamic Nuclear Polarization: New Experimental and Methodology Approaches and Applications in Physics, Chemistry, Biology and Medicine*; Applied Magnetic Resonance **2008**, *34*.

(133) Un, S.; Prisner, T.; Weber, R. T.; Seaman, M. J.; Fishbein, K. W.; McDermott, A. E.; Singel, D. J.; Griffin, R. G. *Pulsed dynamic nuclear polarization at 5 T*; Chemical Physics Letters **1992**, *189*, 54-9.

(134) Alecci, M.; Lurie, D. J. *Low Field (10 mT) Pulsed Dynamic Nuclear Polarization*; Journal of Magnetic Resonance **1999**, *138*, 313-9.

(135) Kobzar, K.; Skinner, T. E.; Khaneja, N.; Glaser, S. J.; Luy, B. *Exploring the limits of broadband excitation and inversion pulses*; Journal of Magnetic Resonance **2004**, *170*, 236-43.

(136) Kobzar, K.; Skinner, T. E.; Khaneja, N.; Glaser, S. J.; Luy, B. *Exploring the limits of broadband excitation and inversion: II. Rf-power optimized pulses*; Journal of Magnetic Resonance **2008**, *194*, 58-66.

(137) Rozantsev, E. G. *Free Nitroxide Radicals*; Plenum Press, New York, 1970.

(138) Korchak, S. E.; Kiryutin, A. S.; Ivanov, K. L.; Yurkovskaya, A. V.; Grishin, Y. A.; Zimmermann, H.; Vieth, H.-M. *Low-Field, Time-Resolved Dynamic Nuclear Polarization with Field Cycling and High-Resolution NMR Detection*; Applied Magnetic Resonance **2010**, *37*, 515-37.

(139) Solomon, I. *Relaxation Processes in a System of Two Spins*; Physical Review **1955**, *99*, 559-65.

(140) Robinson, B. H.; Haas, D. A.; Mailer, C. *Molecular Dynamics in Liquids: Spin-Lattice Relaxation of Nitroxide Spin Labels*; Science **1994**, *263*, 490-3.

(141) Lukzen, N. N.; Petrova, M. V.; Koptyug, I. V.; Savelov, A. A.; Sagdeev, R. Z. *The generating functions formalism for the analysis of spin response to the periodic trains of RF pulses. Echo sequences with arbitrary refocusing angles and resonance offsets*; Journal of Magnetic Resonance **2009**, *196*, 164-9.

(142) Lukzen, N. N.; Savelov, A. A. *Analytical derivation of multiple spin echo amplitudes with arbitrary refocusing angle*; Journal of Magnetic Resonance **2007**, *185*, 71-6.

(143) Ernst, R. R.; Bodenhausen, G.; Wokaun, A. *Principles of Nuclear Magnetic Resonances in One and Two Dimensions* Clarendon Press Oxford, 1978.

(144) Ernst, R. R.; Anderson, W. A. *Application of Fourier Transform Spectroscopy to Magnetic Resonance*; Review of Scientific Instruments **1966**, *37*, 93-102.

(145) Prandolini, M. J.; Denysenkov, V. P.; Gafurov, M.; Endeward, B.; Prisner, T. F. *High-Field Dynamic Nuclear Polarization in Aqueous Solutions*; Journal of the American Chemical Society **2009**, *131*, 6090-2.

(146) Armstrong, B. D.; Han, S. *A new model for Overhauser enhanced nuclear magnetic resonance using nitroxide radicals*; Journal of Chemical Physics **2007**, *127*, 104508/1-/10.

(147) Tseitlin, M.; Dhami, A.; Quine, R. W.; Rinard, G. A.; Eaton, S. S.; Eaton, G. R. *Electron Spin T_2 of a Nitroxyl Radical at 250 MHz Measured by Rapid-Scan EPR*; Applied Magnetic Resonance **2006**, *30*, 651-6.

(148) Kaptein, R.; Dijkstra, K.; Nicolay, K. *Laser photo-CIDNP as a surface probe for proteins in solution*; Nature **1978**, *274*, 293-4.

(149) Hore, P. J.; Broadhurst, R. W. *Photo-CIDNP of biopolymers*; Progress in Nuclear Magnetic Resonance Spectroscopy **1993**, *25*, 345-402.

(150) Redfield, C.; Dobson, C. M.; Scheek, R. M.; Stob, S.; Kaptein, R. *Surface accessibility of aromatic residues in human lysozyme using photochemically induced dynamic nuclear polarization NMR spectroscopy*; FEBS Letters **1985**, *185*, 248-52.

(151) Wirmer, J.; Kühn, T.; Schwalbe, H. *Millisecond Time Resolved Photo-CIDNP NMR Reveals a Non-Native Folding Intermediate on the Ion-Induced Refolding Pathway of Bovine α-Lactalbumin*; Angewandte Chemie, International Edition **2001**, *40*, 4248-51.

(152) Dobson, C. M.; Hore, P. J. *Kinetic studies of protein folding using NMR spectroscopy*; Nature Structural Biology **1998**, *5*, 504-7.

(153) Vogt, W. *Oxidation of methionyl residues in proteins: tools, targets, and reversal*; Free Radical Biology & Medicine **1995**, *18*, 93-105.

(154) Schöneich, C. *Redox Processes of Methionine Relevant to β-Amyloid Oxidation and Alzheimer's Disease*; Archives of biochemistry and biophysics **2002**, *397*, 370-6.

(155) Schöneich, C. *Methionine oxidation by reactive oxygen species: reaction mechanisms and relevance to Alzheimer's disease*; Biochimica et Biophysica Acta **2005**, *1703*, 111-9.

(156) Stob, S.; Kaptein, R. *Photo-CIDNP of the amino acids*; Photochemistry and Photobiology **1989**, *49*, 565-77.

(157) Lyon, C. E.; Lopez, J. J.; Cho, B.-M.; Hore, P. J. *Low field CIDNP of amino acids and proteins: characterization of transient radicals and NMR sensitivity enhancement*; Molecular Physics **2002**, *100*, 1261-9.

(158) Goez, M.; Rozwadowski, J. *Reversible Pair Substitution in CIDNP: The Radical Cation of Methionine*; Journal of Physical Chemistry A **1998**, *102*, 7945-53.

(159) Goez, M.; Rozwadowski, J.; Marciniak, B. *CIDNP spectroscopic observation of (S-N)+ radical cations with a two-center three-electron bond during the photooxidation of methionine*; Angewandte Chemie, International Edition **1998**, *37*, 628-30.

(160) Morozova, O.; Yurkovskaya, A.; Tsentalovich, Y.; Sagdeev, R. *Time-resolved CIDNP study of protein-related molecules*; RIKEN Review **2002**, *44*, 131-3.

(161) Morozova, O. B.; Yurkovskaya, A. V.; Tsentalovich, Y. P.; Forbes, M. D. E.; Hore, P. J.; Sagdeev, R. Z. *Time resolved CIDNP study of electron transfer reactions in proteins and model compounds*; Molecular Physics **2002**, *100*, 1187-95.

(162) Stob, S.; Scheek, R. M.; Boelens, R.; Kaptein, R. *Photo-CIDNP study of the interaction between lac repressor headpiece and lac operator DNA*; FEBS Letters **1988**, *239*, 99-104.

(163) Glasoe, P. K.; Long, F. A. *Use of glass electrodes to measure acidities in deuterium oxide*; Journal of Physical Chemistry **1960**, *64*, 188-90.

(164) Bobrowski, K.; Marciniak, B.; Hug, G. L. *4-Carboxybenzophenone-Sensitized Photooxidation of Sulfur-Containing Amino Acids. Nanosecond Laser Flash Photolysis and Pulse Radiolysis Studies*; J. Am. Chem. Soc. **1992**, *114*, 10279-88.

(165) Bobrowski, K.; Hug, G. L.; Marciniak, B.; Kozubek, H. *4-Carboxybenzophenone-Sensitized Photooxidation of Sulfur-Containing Amino Acids in Alkaline Aqueous Solutions. Secondary Photoreactions Kinetics*; J. Phys. Chem. **1994**, *98*, 537-44.

(166) Marciniak, B.; Bobrowski, K.; Hug, G. L. *Quenching of Triplet Sates of Aromatic Ketones by Sulfur-Containing Amino Acids in Solution. Evidence for Electron Transfer*; Journal of Physical Chemistry **1993**, *97*, 11937-43.

(167) Bobrowski, K.; Schöneich, C.; Holcman, J.; Asmus, K.-D. *$^{\bullet}$OH radical Induced Decarboxylation of Methionine-containing Peptides. Influence of Peptide Sequence and Net Charge*; Journal of the Chemical Society, Perkin Transactions 2 **1991**, 353-62.

(168) Schöneich, C.; Pogocki, D.; Wisniowski, P.; Hug, G. L.; Bobrowski, K. *Intramolecular Sulfur-Oxygen Bond Formation in Radical Cations of N-Acetylmethionine Amide*; Journal of the American Chemical Society **2000**, *122*, 10224-5.

(169) Hug, G. L.; Marciniak, B.; Bobrowski, K. *Acid-Base Equilibria Involved in Secondary Reactions Following the 4-Carboxybenzophenone Sensitized Photooxidation of Methionylglycine in Aqueous Solution. Spectral and Time Resolution of the Decaying $(SN)^+$ Radical Cation*; Journal of Physical Chemistry **1996**, *100*, 14914-21.

(170) Hug, G. L.; Marciniak, B.; Bobrowski, K. *Sensitized photo-oxidation of sulfur-containing amino acids and peptides in aqueous solution*; Journal of Photochemistry and Photobiology A: Chemistry **1996**, *95*, 81-8.

(171) Marciniak, B.; Hug, G. L.; Bobrowski, K.; Kozubek, H. *Mechanism of 4-Carboxybenzophenone-Sensitized Photooxidation of Metionine-Containing Dipetides and Tripeptides in Aqueous Solution*; Journal of Physical Chemistry **1995**, *99*, 13560-8.

(172) Hug, G. L.; Bobrowski, K.; Kozubek, H.; Marciniak, B. *pH effects on the photooxidation of methionine derivatives by the 4-carboxybenzophenone triplet state*; Nukleonika **2000**, *45(1)*, 63-71.

(173) Yashiro, H.; White, R. C.; Yurkovskaya, A. V.; Forbes, M. D. E. *Methionine Radical Cation: Structural Studies as a Function of pH Using X- and Q-Band Time-Resolved Electron Paramagnetic Resonance Spectroscopy*; Journal of Physical Chemistry A **2005**, *109*, 5855-64.

(174) Goez, M.; Rozwadowski, J.; Marciniak, B. *CIDNP Spectroscopic Observation of (SN) Radical Cation with a Two-Centered Three-Electron Bond During the Photooxidation of Methionine*; Angew. Chem. Int. Edit. **1998**, *37*, 628-30.

(175) Goez, M.; Rozwadowski, J. *Reversible Pair Substitution in CIDNP: The Radical Cation of Metionine*; Journal of Physical Chemistry **1998**, *102*, 7945-53.

(176) Naito, A.; Akasaka, K.; Hatano, H. *Dimer cation radicals of N-acetyl methionine: ESR and ENDOR studies*; Molecular Physics **1981**, *44*, 427-43.

(177) Bobrowski, K.; Marciniak, B.; Hug, G. L. *4-Carboxybenzophenone-Sensitized Photooxidation of Sulfur-Containing Amino Acids. Nanosecond Laser Flash Photolysis and Pulse Radiolysis Studies*; Journal of American Chemical Society **1992**, *114*, 10279-88.

(178) Kiryutin, A. S.; Morozova, O. B.; Kuhn, L. T.; Yurkovskaya, A. V.; Hore, P. J. *^1H and ^{13}C Hyperfine Coupling Constants of the Tryptophanyl Cation Radical in Aqueous Solution from Microsecond Time-Resolved CIDNP*; Journal of Physical Chemistry B **2007**, *111*, 11221-7.

(179) Rozwadowski, J. *Sensybilizowane fotoutlenianie zwiazkow organicznych zawierajacych atom siarki (II) w roztworach*, Adam Mickiewicz University, 1996.

(180) Hiller, K. O.; Masloch, B.; Göbl, M.; Asmus, K. D. *Mechanism of the $OH^\bullet$ Radical Induced Oxidation of Methionine in Aqueous Solution*; Journal of the American Chemical Society **1981**, *103*, 2734-43.

(181) Hug, G. L.; Bonifačić, M.; Asmus, K.-D.; Armstrong, D. A. *Fast Decarboxylation of Aliphatic Amino Acids Induced by 4-Carboxybenzophenone Triplets in Aqueous Solutions. A Nanosecond Laser Flash Photolysis Study*; Journal of Physical Chemistry B **2000**, *104*, 6674-82.

(182) Säuberlich, J.; Beckert, D. *Photoionization of Benzophenonecarboxylic Acids in Two-Photon Process. A Fourier Transform EPR Study*; Journal of Physical Chemistry **1995**, *99*, 12520-4.

(183) Säuberlich, J.; Brede, O.; Beckert, D. *Photoionization of Benzophenone Carboxylic Acids in Aqueous Solution. A FT EPR and Optical Spectroscopy Study of Radical Cation Decay*; Journal of Physical Chemistry **1996**, *100*, 18101-7.

(184) Asmus, K.-D.; Göbl, M.; Hiller, K.-O.; Mahling, S.; Mönig, J. *S:.N and S:.O Three-electron-bonded Radicals and Radical Cations in Agueous Solutions*; Journal of the Chemical Society, Perkin Transactions 2 **1985**, 641-6.

(185) Davies, M. J.; Gilbert, B. C.; Norman, R. O. C. *Electron-spin resonance studies. Part 64. The hydroxyl radical-induced decarboxylation of methionine and some related compounds*; Journal of the Chemical Society, Perkin Transactions 2: Physical Organic Chemistry (1972-1999) **1983**, 731-8.

(186) Tripathi, G. N. R.; Tobien, T. *The Intramolecular Sulfur-Nitrogen Bond in Aqueous 3-(Methylthio)propylamine Radical Cation*; Journal of Physical Chemistry A **2001**, *105*, 3498-504.

(187) Landolt-Boernstein. *Magnetic Properties of Free Radicals*; Springer Verlag, Berlin, Heidelberg, and New York, 1977.

(188) Vuolle, M.; Makela, R. *Electron Spin Resonance, ENDOR and TRIPLE Resonance of some 9,10-Anthraquinone and 9,10-Anthraquinol Radicals in Solution*; Journal of the Chemical Society, Faraday Transactions 1 **1987**, *83*, 51-5.

(189) Cohen, S. G.; Ojanpera, S. J. *Photooxidation of Methionine and Related Compounds*; J. Am. Chem. Soc. **1975**, *97*, 5633-4.

(190) Lassmann, G.; Kolberg, M.; Bleifuss, G.; Gräslund, A.; Sjöberg, B.-M.; Lubitz, W. *Protein thiyl radicals in disordered systems: A comparative EPR study at low temperature*; Physical Chemistry Chemical Physics **2003**, *5*, 2442-53.

(191) Marciniak, B.; Bobrowski, K.; Hug, G. L. *Quenching of Triplet Sates of Aromatic Ketones by Sulfur-Containing Amino Acids in Solution. Evidence for Electron Transfer*; J. Phys. Chem. **1993**, *97*, 11937-43.

(192) Marciniak, B.; Bobrowski, K.; Hug, G. L.; Rozwadowski, J. *Photoinduced Electron Transfer between Sulfur-Containing Carboxylic Acids and the 4-Carboxybenzophenone Triplet State in Aqueous Solution*; Journal of Physical Chemistry **1994**, *98*, 4854-60.

(193) Hug, G. L.; Bobrowski, K.; Kozubek, H.; Marciniak, B. *Photo-oxidation of Methionine-containing Peptides by the 4-Carboxybenzophenone Triplet State in Aqueous Solution. Competition Between Intramolecular Two-centered Three-electron bonded $(S:.S)^+$ and $(S:.N)^+$ Formation*; Photochemistry and Photobiology **2000**, *72*, 1-9.

(194) Tsentalovich, Y. P.; Morozova, O. B. *Laser flash photolysis and time resolved CIDNP study of photoreaction of 2,2'-dipyridyl with N-acetyltyrosine in aqueous solutions*; Journal of Photochemistry and Photobiology, A: Chemistry **2000**, *131*, 33-40.

(195) Tsentalovich, Y. P.; Morozova, O. B.; Yurkovskaya, A. V.; Hore, P. J. *Kinetics and mechanism of the photochemical reaction of 2,2'-dipyridyl with tryptophan in water: Time-resolved CIDNP and laser flash photolysis study*; Journal of Physical Chemistry A **1999**, *103*, 5362-8.

(196) Morozov, V. A.; Ivanov, K. L.; Lukzen, N. N. *Theoretical treatment of ion-molecular charge transfer reactions involving dimer radical ions*; Physical Chemistry Chemical Physics **2003**, *5*, 2360-8.

(197) Lyons, A. Q.; Pettit, L. D. *Formation Constants of Silver(I) Complexes of Some Sulfur-containing Dipeptides and Valylvaline*; Journal of the Chemical Society, Dalton Transactions **1984**, 2305-8.

(198) Morozova, O. B.; Yurkovskaya, A. V. *Aminium Cation Radical of Glycylglycine and its Deprotonation to Aminyl Radical in Aqueous Solution*; Journal of Physical Chemistry B **2008**, *112*, 12859-62.

(199) Danen, W. C.; Rickard, R. C. *Nitrogen-Centered Free Radicals, IV. An Electron Spin Resonance Study of Transient Dialkylaminium Radical Cations*; Journal of the American Chemical Society **1972**, *94*, 3254-6.

(200) Tarabek, P.; Bonifacic, M.; Beckert, D. *Photooxidation of Glycylglycine. Two-Channel Reaction Mechanism as Studied by Time-Resolved FT EPR*; Journal of Physical Chemistry A **2004**, *108*, 3467-70.

(201) Pomplun, N.; Heitmann, B.; Khaneja, N.; Glaser, S. J. *Optimization of electron-nuclear polarization transfer*; Applied Magnetic Resonance **2008**, *34*, 331-46.